Identification of Neurotrypsin-dependent Changes in Synapses and the Hippocampus Proteome

DISSERTATION

zur

Erlangung der naturwissenschaftlichen Doktorwürde

(Dr. sc. nat.)

vorgelegt der

Mathematisch-naturwissenschaftliche Fakultät

der

UNIVERSITÄT ZÜRICH

von

Pascal Walther

von

Wohlen (BE)

Promotionskomitee

Prof. Dr. Peter Sonderegger (Vorsitz und Leitung)

Prof. Dr. Ruedi Aebersold

Dr. Detlev Boison

Zürich 2007

Die vorliegende Arbeit wurde von der Mathematisch-naturwissenschaftlichen Fakultät der Universität Zürich auf Antrag von Prof. Dr. Peter Soneregger und Prof. Dr. Heinz Gehring als Dissertation angenommen.

Abbreviations

2DE	2D gel electrophoresis
aa	amino acid
ACN	acetonitrile
AD	Alzheimer's disease
AMPA	α-amino-3-hydroxy-5-methylisoxazole-4- propionic acid
α-CCA	α-cyano-4-hydroxycinnamic acid
AK	adenosine kinase
ASAPRatio	automated statistical analysis of protein abundance ratio
CHAPS	3-[(3-Cholamidopropyl)dimethylammonio]-1-propanesulfonate
CID	collision-induced dissociation
CNS	central nervous system
DAB	diaminobenzidine tetrahydrochloride
DTT	DL-Dithiothreitol
EAAT2	excitatory amino acid transporter 2
ECM	extracellular matrix
EDTA	ethylenediaminetetraacetic acid
EtOH	ethanol
ER	endoplasmatic reticulum
Erk	extracellular regulated kinase
ESI-MS	electrospray ionization mass spectrometry
FT ICR	Fourier transform ion cyclotron resonance
GO	gene ontology
GFAP	glial fibrillary acidic protein
GluR2	glutamate receptor 2
Grp	glucose-regulated protein
GS	glutamine synthetase
HEPES	4-(2-hydroxyethyl)-1-piperazineethanesulfonic acid
hNT	human neurotrypsin
HRP	horseradish peroxidase
ICAT	isotope-coded affinity tag
IEF	isoelectric focusing
IgG	immunoglobulin
IPG	immobilized pH gradient
kDa	kilo Dalton
KO	knock-out
L-LTP	late long-term potentiation
LTD	long term depression
μLC	microcapillary liquid chromatography
MALDI-TOF	matrix-assisted laser disorption/ionization time-of-flight
MAPK	mitogen-activated protein kinase
MPT	minimal probability threshold
mNT	mouse neurotrypsin
MetOH	methanol
m/z	mass-to-charge ratio

NMJ	neuromuscular junction
NMDAR	*N*-methyl-D-aspartic acid receptor
PAR	protease-activated receptor
PBS	phosphate buffered saline
PAK1	p21-activated kinase 1
PCR	polymerase chain reaction
PKC	protein kinase C
PSD	post-synaptic density
PVDF	polyvinylidene fluoride
ppm	parts per million
RF	radio frequency
RP	reversed phase
SDS-PAGE	sodium dodecyl sulfate polyacrylamide gel electrophoresis
SCX	strong cation exchange
SIC	single ion chromatogram
TAMRA	carboxytetramethylrhodamine
TBS	Tris buffered saline
TCEP	tris(2-carboxyethyl)phosphine hydrochloride
TFA	triflouracetic acid
tPA	tissue-type plasminogen activator
uPA	urokinase-type plasminogen activator
VDAC	voltage-dependent anion channel

Table of contents

Summary

Neurotrypsin is a multi-domain serine peptidase expressed in the developing and adult nervous system. Based on expression analysis we hypothesized that neurotrypsin is implicated in processes such as memory formation and learning. A four base-pair deletion in the human gene causes non-syndromic mental retardation. Recently the synapse organizer agrin, a large extracellular proteoglycan, was identified as a specific substrate for neurotrypsin both, in vitro and in vivo. Neurotrypsin cleaves agrin at two positions resulting in the generation of three products. Two fragments, the C-terminal 22-kDa LG3 domain and the 90-kDa intermediate fragment, are enriched in supernatants and soluble fractions and are therefore thought to be released into the ECM where they might freely diffuse. Probably the N-terminal fragment remains associated to the plasma membrane. No cleavage products are found in the neurotrypsin knock-out mice, suggesting an exclusive catalytic processing of agrin by neurotrypsin. Furthermore, it was shown by Hilgenberg et al. that the C-terminal LG3 fragment released after the cleavage can bind to the a3 subunit of Na+/K+-ATPase and is therefore capable to inactivate the ion pump and trigger a downstream signaling cascade, thereby regulating presynaptic excitability. However, the molecular function of the proteolytic cleavage and the fate of the newly generated fragments remain to be shown. To shed light on the molecular function and cellular processes that are affected by neurotrypsin activity we performed a quantitative protein profiling. We compared the protein composition of hippocampi and synapses from whole brains from wild-type with neurotrypsin-overexpressing mice. We mainly found changed proteins that are involved in exo- and endocytosis of synaptic vesicles, reorganization of the cytoskeleton, cell adhesion, termination of synaptic signaling, and energy metabolism. For example, we showed that the expression level of the synaptic protein kinase α-CaMK II was reduced in transgenic mice by about 10%. We found elevated levels of proteins such as PAK1, Cdc42, and p21-Rac, all of which regulate actin cytoskeleton polymerization and/or depolymerization. Moreover, the cell adhesion molecules L1 and NrCAM were decreased in soluble fractions by 20%. Changed abundance was also found for EAAT2 and glutamine synthetase, both of which were down regulated in membrane fractions by 25%. Finally, expression levels of PKC-α and -ε were decreased by 40%, whereas MAPK1 was increased by 20 – 40%. These results support the notion that neurotrypsin, together with agrin, is a crucial factor in synapse organization and they provide the basis for further studies demonstrating a functional role of neurotrypsin in synaptic signal transmission.

Zusammenfassung

Neurotrypsin ist eine Multi-Domänen Serin Peptidase, welche am stärksten in dem sich entwickelnden und im adulten Nervensystem exprimiert ist. Basierend auf Expressionsanalysen geht man davon aus, dass Neurotrypsin in Gedächtnisbildung und Lernprozessen involviert ist. Eine Deletion von vier Basen im menschlichen Gen ruft eine schwere geistige Behinderung hervor. Kürzlich wurde gezeigt, dass Agrin, bekannt als grosses extrazelluläres Proteoglykan und als Organisator von Synapsen, ein spezifisches Substrat für Neurotrypsin ist. Neurotrypsin spaltet Agrin an zwei Positionen und generiert so drei neue Agrin-Fragmente. Zwei davon, nämlich die C-terminale 22-kDa LG3-Domäne und das mittlere 90-kDa grosse Fragment, waren in Zellüberständen und löslichen Fraktionen angereichert. Demzufolge werden sie in die extrazelluläre Matrix abgegeben und sind darin möglicherweise frei diffusionsfähig. Wahrscheinlich bleibt der N-terminale Teil mit der Plasmamembran assoziert. In der Neurotrypsin knock-out Maus wurden bisher keine Agrin Spaltprodukte gefunden, was sehr für eine einzigartige katalytische Proteolyse von Agrin durch Neurotrypsin spricht. Zudem konnte kürzlich von Hilgenberg et al. gezeigt werden, dass die LG3-Domäne nach ihrer Freisetzung an die α3 Untereinheit der Na^+/K^+-ATPase binden kann und somit via dieser Ionenpumpe eine nachgeschaltete Signalkaskade auslöst, welche schliesslich die präsynaptische Reizbarkeit steuert. Allerdings kennt man bis heute weder die molekulare Funktion dieser Interaktion noch das Schicksal der daraus entstehenden Produkte. Um über die molekularen Funktionen und zellulären Porzesse, welche durch die Aktivität von Neurotrypsin in Gang gesetzt werden, Aufschluss zu geben, wurde ein quantitatives Proteinprofil erstellt. Wir verglichen die Proteinzusammensetzung von Hippocampi und von gereinigten Synapsen aus dem Gesamtgehirn aus wildtyp Mäuse mit Neurotrypsin überexprimierenden Mäusen. Dabei wurden vor allem Proteine gefunden die in der Exo- und Endozytose von synaptischen Vesikeln, Neuorganisierung des Zytoskeletts sowie Zelladhäsion, der Beendigung von synaptischen Signalen und Energiemetabolismus involviert sind. Zum Beispiel konnten wir zeigen, dass der Grad der Expression von α-CaMK II in den trangsenen Tieren um etwa 10% reduziert ist. Wir fanden eine erhöhte Expression von PAK1, Cdc42 und p21-Rac, Proteine, die alle die Polymerisierung und Depolymerisierung des Aktin Zytoskeletts regulieren. Des weiteren waren die Zelladhäsionsmoleküle L1 und/oder NrCAM in der löslichen Fraktion 20% herunter reguliert. Relativ veränderte Proteinmengen konnten auch für EAAT2 und die Glutamin Synthetase gezeigt werden. Die beiden waren etwa 25% weniger häufig in den Membranfraktionen der transgenen Tieren. Zu guter Letzt war die Expression von PKC-α and -ε um 40% herunter und die von MAPK1 um 20 – 40% herauf reguliert. Diese Resultate unterstützen die Hypothese, dass Neurotrypsin, zusammen mit Agrin, wichtige Faktoren sind, die für die Organisation von Synapsen witchtig sind, und zur sogenannten synaptischen Plastizität wesentlich dazu beitragen. Des Weiteren bieten sie die molekulare Grundlage für zukünftige Studien, welche die funktionelle Rolle von Neurotrypsin in der synaptischen Signalübermittlung aufzeigen sollen.

1. Introduction

1.1 Proteolytic enzymes

A fundamental condition for life is that organisms are provided with enzymes that are able to catalyze chemical reactions efficiently and selectively. Without catalysis chemical reactions such as hydrolytic cleavage could not occur on a useful time scale, and thus could not support life.

One important class of enzymes is the class of hydrolases and among them the hydrolases of peptide bonds, the peptidases. They form the subclass 3.4 of the enzyme classification (EC) system, the internationally recognized scheme for the classification and nomenclature of all enzymes. Since the EC system places each peptidase in one of just 13 subclasses, it inevitably pools together peptidases that are very different. About 1992, N. D. Rawlings and A.J. Barret started to develop a new form of classification system for peptidases, grouping them in a way that reflects structural features and evolutionary relationships. In 1996 the system was published on the world wide web as the *MEROPS* database (URL: http://www.merops.sanger.co.uk).

The *MEROPS* database uses a hierarchical, structure-based classification of peptidases. On the basis of similarities in amino acid sequence each peptidase is assigned to a family, and families that are thought to be homologous are grouped together in a clan (Rawlings et al., 2006). The residue of the catalytic centre that mediates the nucleophilic attack on the peptide bond or the metal ion required for catalytic activity defines the classification: At present, 39 different clans and 183 families are registered; 14 aspartic peptidase families (A), 60 cysteine peptidase families (C), 1 glutamic peptidase family (G), 53 families of metallo peptidases (M), 42 serine peptidase families (S), 4 threonine peptidase families (T) and 9 families of unknown catalytic type (U). The importance of peptidases and their inhibitors is illustrated by the fact that ~2% of all genes encode peptidases and their homologs in all kinds of organisms, and that there are over 550 putatively active peptidases in the human genome.

1.1.1 Serine peptidases

Almost one-third of all peptidases are classified as serine peptidases. They are named after their nucleophilic serine residue at the active site. Four different families of serine peptidases are known with 'classic' catalytic triads consisting of histidine, asparagine, and serine. The prototypic serine peptidases of the four families are chymotrypsin (S1), subtilisin (S8), carboxypeptidase Y (S10), and Clp protease (S14). The major difference among them is the order of the amino acid residues from the catalytic triad. To date the members of these families represent by far the vast majority of all known serine peptidases. The remainder of the serine peptidases bear 'novel' catalytic triads or dyads including Ser–His–Glu, Ser–His/Lys, His–Ser–His, and N-terminal Ser.

Serine peptidases can be found in eukaryotes, prokaryotes, archae, and viruses. They are involved in physiological processes including digestion, hemostasis, apoptosis, cell proliferation, reproduction, synaptic plasticity, and immune responses. Even cascades of sequential activation of serine peptidases are known, e.g. in the blood coagulation, where they were first observed and characterized complement fixation, matrix remodeling, and differentiation. These diverse biological processes demand a wide variety of specificities, ranging from digestive peptidases that cleave after a hydrophobic or positively charged residues to proteases that recognize a five amino acid stretch or even hydrolyze a single protein only. Specificity can often be presumed

from the topology of the substrate binding sites and the exosites, whose conformation often have striking consequences on the rates of proteolytic kinetics.

1.1.2 S1 family peptidases and their catalytic mechanism

Based on the nomenclature of chymotrypsin numbering the structure of the S1 family peptidases, also called chymotrypsin-like peptidases, is generally divided into catalytic, substrate recognition and zymogen activation domains. In addition to the proteolytic function, many serine peptidases are also modular proteins containing non-catalytic regulatory domains.
The catalytic triad spans the active site cleft, with the Ser_{195} on one side and the Asp_{102} and the His_{57} on the other side. The catalytic triad is part of an extensive hydrogen-bonding network (Fig. 1.1). The oxyanion hole is formed by the backbone NHs of the amide bond of Gly_{193} and Ser_{195}. These atoms form a pocket of positive charges that activates the carbonyl carbon of the scissile peptide bond and stabilizes the negatively charged oxyanion of the tetrahedral intermediate. Figure 1.1 shows schematically the mechanism of the proteolytic cleavage of peptide bonds. To hydrolyze a peptide bond, all peptidases must overcome three obstacles: i) Amide bonds are generally very stable due to electron donation from the amide nitrogen to the carbonyl. Thus, peptidases usually activate the amide bond via the interaction of the carbonyl oxygen of the substrate with the main chain NHs of Gly_{193} and Ser_{195}. Only now comes the nucleophilic attack of the Ser_{195} oxygen on the carbonyl carbon. Assisted by His_{57}, acting as a general base, a tetrahedral intermediate is formed. The resulting His_{57}-H^+ is stabilized by a hydrogen bond to Asp_{102}, and the oxyanion of the tetrahedral intermediate is stabilized by an interaction with the main chain NHs of the oxyanion hole. ii) Amines are poor leaving groups, thus peptidases protonate the amine prior to expulsion: His_{57}-H^+ protonates the leaving amine and the tetrahedral intermediate collapses with the expulsion of $R'NH_2$, the new N-terminal portion of the cleaved polypeptide chain, resulting in the acylenzyme intermediate. The leaving group will be replaced by water from the solvent. iii) But H_2O is a poor nucleophile; serine peptidases first activate H_2O via a His_{57} activates water and the water molecule undergoes a nucleophilic attack to the carbon of the acylenzyme to form a second tetrahedral intermediate. The deacylation of the acylenzyme is essentially the reversal of the previous steps. The second tetrahedral intermediate collapses, by the release of the carboxylate product (the new C-terminal portion of the cleaved polypeptide chain) to yield the active enzyme. As the reaction proceeds, changes in bonding and charges at the scissile bond will propagate to more remote enzyme – substrate interactions and vice versa (Hedstrom, 2002).

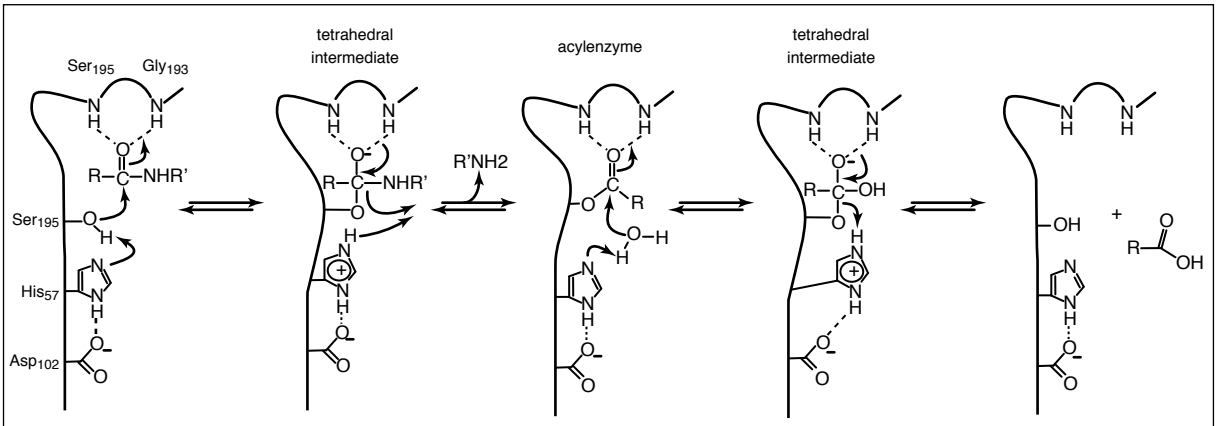

Figure 1.1 The catalytic mechansim of chymotrypsin-like serine peptidases

1.2 Peptidases are capable to modulate brain function

Peptidases and their natural inhibitors have been implicated in both physiological and pathophysiological processes in the central nervous system (CNS). They are involved in almost every aspect of neuronal development. Some are crucial for cell proliferation, neuronal migration, neurite outgrowth and path finding, synaptogenesis and synaptic plasticity. Others are required for neuronal death, tumor growth and invasion. They also contribute to a variety of neuropathologies, including neurodegenerative diseases (e.g. Alzheimer's disease (AD), Parkinsons's disease), demyelination diseases (e.g. multiple sclerosis), brain tumors and cerebral ischemia, hemorrhagic stroke, and epileptic seizures.

Four major classes of peptidase are present in the CNS. Those are the (1) *serine peptidases*, with the well-known members tPA, plasmin, thrombin, and neuropsin. Many different S1 family serine peptidases, peptidase receptors, and specific inhibitors are expressed in the brain (Table 1.1); (2) *matrix metalloproteases* (MMPs), which consist of more than 20 members that all require Zn^{2+} for their enzymatic activity; (3) *aspartic peptidases*, such as the lysosomal peptidases cathepsins; and (4) *cysteine peptidases*, which include 14 caspases involved in distinct steps of the apoptotic pathway, as well as the intracellular active calpains.

A measurement for the persistent increase in the synaptic strength that last for minutes to several days is called long-term potentiation (LTP). It is widely accepted being one of the major mechanisms by which memory is formed and stored in the brain. Several peptidases are involved in the regulation of LTP (Fig. 1.2). From studies with transgenic animals lacking or overexpressing one or the other peptidase it was suggested that functional redundancy or compensation among different members and their inhibitors do exist. Normally, specific inhibitors tightly regulate peptidase activity to prevent disastrous proteolysis. Imbalances in the catalytic activity of peptidases and their inhibitors compromises neural homeostasis and can result in neuropathological changes.

The following sections provide an overview of the functional mechanisms through which some of the peptidases contribute to the physiological and pathophysiological processes in the CNS.

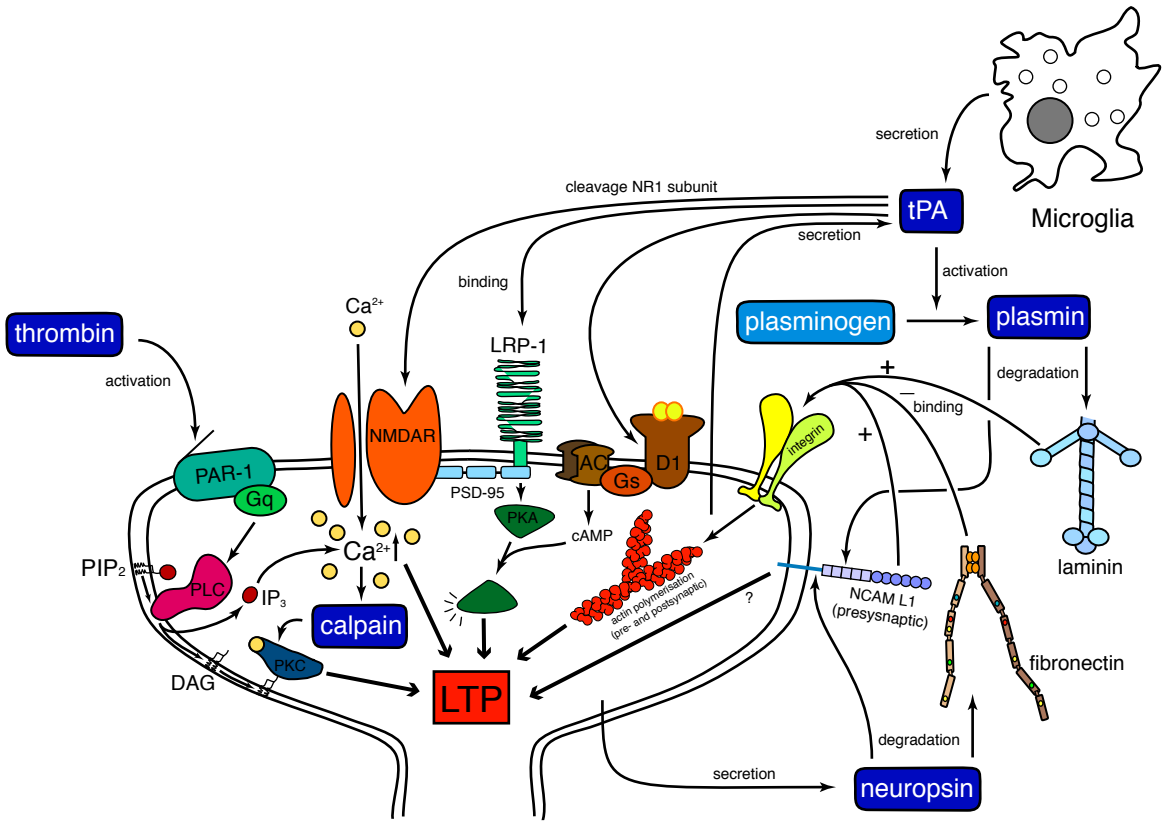

Figure 1.2 Schematic representation of peptidases involved in long-term potentiation (LTP).
AC: adenylate cyclase; AMPAR: α-amino-3-hydroxy-5-methylisoxazole-4-propionic acid receptor; D1: Dopamine 1-like receptor; DAG: diacylglycerol; IP3: inositol 1,4,5-triphosphate; LRP-1: low-density lipoprotein receptor-related protein-1; NCAM L1: neural cell adhesion molecule L1; NMDAR: N-methyl-D-aspartic acid receptor; PAR-1: protease-activated receptor 1; PIP2: phosphatidylinositol (4,5)-bisphosphate; PLC: phospholipase C; PKA: cAMP-dependent kinase A; PKC: protein kinase C; PSD-95: postsynaptic density protein 95.

1.2.1 Plasminogen activators play a crucial role in the CNS

Plasminogen activators (PAs) are best known for their thrombolytic action to dissolve blood clots in the vasculature. They specifically cleave the Arg-Val bond in plasminogen. Plasmin is then able to digest fibrin polymers. In addition to that, plasmin has a wide spectrum of substrates in the CNS, including extracellular matrix (ECM) proteins, such as fibronectin and laminin.
Two types of plasminogen activators (PAs) are known: tissue-type plasminogen activator (tPA) and urokinase-type plasminogen activator (uPA). They are encoded by two different genes and share similar enzymology, but differ in their domain organization and properties of the non-catalytic regions (Vassalli et al., 1991) (Fig. 1.3). In the normal CNS, tPA is the predominant PA whereas uPA is more relevant in the context of brain tumor biology (Levicar et al., 2003; Mohanam et al., 1994).

1.2.1.1 Tissue-type plasminogen activator

tPA is a secreted S1 serine peptidase that converts plasminogen to proteolytically active plasmin. Structurally, tPA consists of an N-terminal fibronectin type I domain (FN1), followed by an epidermal growth factor-like domain (EGF), two kringle domains (KR), and a C-terminal

catalytic domain consisting of Ser, His and Asp residues (Fig. 1.3). The presence of multiple non-catalytic domains is critical in mediating protein-protein and cell-cell interactions. For instance, tPA binds to fibrin with high affinity and subsequently has an increased affinity to plasminogen. This interaction leads to an elevated catalytic efficiency on the activation of plasminogen between 100 and 1000-fold. Hence, poorly active tPA is released, binds to fibronectin or laminin and is subsequently potentiated to activate plasminogen. However, the single chain, almost fully active enzyme, can further be processed into a two-chain, fully active form. The cleavage occurs proximal to the protease domain after Arg_{310} and is catalyzed by plasmin, kallikreins or factor Xa. tPA chains A and B are linked via an interchain disulfide bond.

Within the CNS, the spatial and temporal localization of tPA presents a candidate modulator of neurotransmission (Table 1.1). Upon neural activity tPA the transcript is regulated as an immediate-early gene (Qian et al., 1993). Both intracellular tPA protein and mRNA deposits have been localized to the synapse and various depolarizing agents promote exocytosis of tPA from neuronal stores (Gualandris et al., 1996). Moreover, its synthesis is increased in processes such as synaptic plasticity, motor learning and seizures (Qian et al., 1993; Seeds et al., 1995). On the other hand, tPA is also involved in pathological events, such as excitotoxic cell death. It was observed that genetic deficiency of tPA (Tsirka et al., 1995; Tsirka et al., 1997) and infusion of the specific inhibitor neuroserpin (Yepes et al., 2002) results in a significant resistance to cell death induced either by direct injection of an excitotoxin or by generation of a seizure. In cerebral ischemia, tPA seems to have both beneficial (Marler and Goldstein, 2003) and deleterious (Wang et al., 1998) effects. Early after onset of cerebral ischemia the associated neuronal depolarization *in vivo* leads to an increased secretion of tPA from neurons and microglial cells, followed by a compensatory expression of neuroserpin. If the ischemic insult is prolonged, the effect of tPA overcomes the balancing action of its inhibitor, and the unopposed neurotoxic effect results in cell death (Yepes et al., 2000). Most likely an abnormal high level of tPA-mediated plasmin activity induces the neurotoxic lesions, thereby acting on non-fibrinogenic substrates to compromise cell viability. It is very important to better understand the function of tPA, because recombinant tPA is now used as treatment for occlusive stroke due to its ability to dissolve fibrin clots and to allow reperfusion of ischemic brain areas (del Zoppo et al., 1997; Hacke et al., 1995; Wardlaw et al., 1997). However, in animal models, administered tPA can penetrate brain tissue (Wang et al., 1998) and thus therapeutic thrombolytic treatment with tPA could have fatal consequences due to the production of excessive plasmin, which may elicit neuronal cell death. Another pathological situation where the tPA-plasmin system has been suggested to play a role is AD (Selkoe, 2001). *In vitro* experiments have shown that amyloid-ß (Aß) peptide can stimulate tPA activity, resulting in plasmin generation and subsequent Aß degradation (Kingston et al., 1995; Ledesma et al., 2000; Tucker et al., 2000). Recently, the contribution of the tPA-plasmin system in the clearance of Aß has also been shown *in vivo* (Melchor et al., 2003). These data suggest that tPA, through plasmin generation, could have beneficial effects for AD treatment.

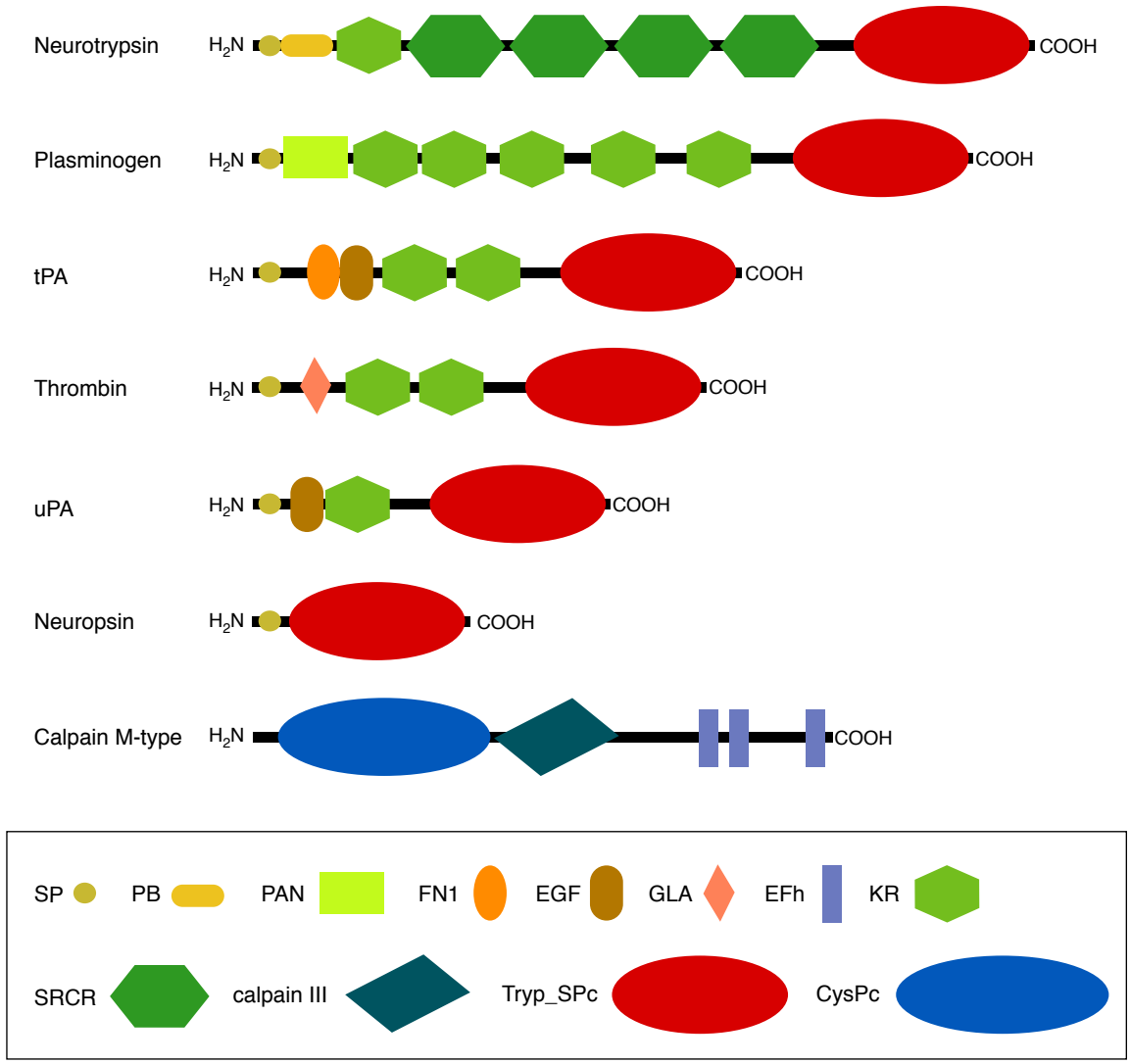

Figure 1.3 Comparison of the domain structure of neurotrypsin, plasminogen, tPA, thrombin, uPA, neuropsin and calpain M-type.
SP: Signal peptide; PB: Proline-rich basic segment, might mediate binding to components of cell surface and ECM; PAN: Apple domain, 6 conserved cysteines forming three disulphide bonds. Binds to kininogen, factor XIIa, factor IX, platelets, and heparin; FN1: Fibronectin type I domain, in tPA together with the EGF-like domain is involved in fibrin-binding; EGF: Epidermal grwoth factor-like domain is a repeat pattern involving a number of conserved Cys residues, thought to be important for its recognition by receptors and other molecules. Frequently found in extracellular proteins; GLA:Vitamin K-dependent carboxylation/gamma-carboxyglutamic domain. Responsible for the high-affinity binding of Ca^{2+}; EFh: EF-hand, Ca^{2+}-binding motif that occurs at least in pairs. EF-hands undergo a conformational change upon Ca^{2+}-binding; KR: Kringle domain, are triple-looped, disulfide cross-linked domains found in a varying number of copies, in some serine peptidases and plasma proteins. Thought to play a role in binding mediators, such as phospholipids and other proteins, and in the regulation of proteolytic activity; SRCR: Scavanger receptor cysteine-rich domain, disulphide rich extracellular domains. Found in several extracellular receptors and may be involved in protein-protein interactions; CalpainIII: Calpain large subunit, with currently unknown function. Calpains participate in intracellular signaling pathways mediated by Ca^{2+}-ions; Tryp_SPc: Trypsin-like serine peptidase with the catalytic traide Ser, Asp, His; Cys_Pc: Calpain-like thiol protease family (peptidase family C2). Ca^{2+}-activated by the large subunit.

Table 1.1: Peptidases and peptidase inhibitors in the CNS

Protein	Expression in the nervous system	Function in the nervous system	Known substrates, inhibitors, interactions
*Plasmin	Hippocampus, cerebellum, and the cerebral cortex, neural	LTP, cell migration, neurite outgrowth, excitotoxic cell death, neuroprotection	Laminin, fibrin, fibronectin, MMPs, proteoglycans collagenases, thrombospondin, F-spondin, N-CAM L1
*tPA	Hippocampus, hypothalamus, cerebellum, amygdala, and sympathetic nerves, nucleus accumbens, neural and glial	LTP, cell migration, neurite outgrowth, excitotoxic cell death, neuroprotection	Plasminogen, NR1, MMP-9
*uPA	Subiculum, entorhinal cortex, CA1, dentate gyrus, ventral tegmental area, neural	Cell adhesion and migration, degradation of ECM, addiction, growth and invasion of tumors	Plasminogen, MMP-2, uPAR
*Thrombin	Dentate gyrus, CA1 – CA3, cerebellum, olfactory bulb, cortex	Cytoprotective, apoptotic, proliferative	PARs, Protein C
Neuropsin	CA1 – CA3, amygdala	Activity-dependent neural plasticity, LTP	N-CAM L1, casein, fibronectin, gelatin, collagen, fibrinogen, kininogen, tPA
Neurotrypsin	Hippocampus, amygdala, olfactory bulb, neocortex layer V and VI, brain stem, spinal cord, DRG	Synaptic plasticity	Agrin
*Activated protein C	Cerebral cortex, hippocampus, cerebellum, neural	Anti-inflammatory, anti-apoptotic, neuroprotective	Factors Va and VIIIa
Kallikrein-6	Spinal cord, hippocampus, substantia nigra, and basal ganglia, oligondendrocytic, neural	Demyelination	Myelin-associated (α-MOG), fibronectin, laminin
Granzyme B	Cerebral cortex, hippocampus and diencephalon, forebrain and hypothalamus	Apoptosis, immune response	Caspases-3, -7, -9, -10
*PAR-1	Piriform cortex, nucleus accumbens, neocortex, hypothalamus, amygdala, hippocampus, cerebellum	Protease activated receptor, G-protein coupled seven-transmembrane receptor	Thrombin
*uPAR	Subiculum, entorhinal cortex, CA1, dentate gyrus, neural	GPI-anchored receptor	uPA
*Thrombomodulin	Vasculature of CNS	Type I transmembrane receptor, neuroprotective	Thrombin
*PAI-1	Hypothalamus, brain blood vessels, cortex, hippocampus, amygdala	Peptidase inhibitor, KA-mediated seizure	tPA, uPA, plasmin, LRP1
Neuroserpin	Axons of dorsal root ganglia	Serine peptidase inhibitor, dementia, neuroprotection, neurite outgrowth	Plasmin, tPA
Protease nexin-1	Brain blood vessels, cerebral cortex, astroglial	Peptidase inhibitor, neurite outgrowth, neural development	Thrombin, LRP

*also present in blood coagulation/fibrinolysis pathway

1.2.1.2 Urokinase-type plasminogen activator

uPA is a S1 serine peptidase first isolated from the urine. It exists either as a 54 kDa monomer or as a homodimer linked by an interchain disulfide bridge (Fig. 1.3). uPA is a member of the plasminogen activation system, which facilitates nerve regeneration by digesting adhesive cell contacts and by activation of other peptidases, thereby initiating a proteolytic cascade. The expression level of uPA seems to be much lower than that of tPA (Meiri et al., 1994). Both tPA and uPA activate some MMPs, either indirectly via plasminogen activation or directly, such as the uPA activation of MMP-2 (Siconolfi and Seeds, 2003). It is synthesized as a proenzyme with little or no activity and can be activated by various peptidases, including its immediate substrate plasmin, generating a positive feedback loop of self-activation (Levicar et al., 2003). It has been clearly shown that a specific glycosylphosphatidyl-inositol (GPI)-anchored receptor for uPA (uPAR) is expressed on the surface of many cell types (Roldan et al., 1990) (Table 1.1). The uPA-uPAR interaction occurs between the EGF-like domain of uPA and the N-terminus of the receptor with high specificity and affinity. The interaction induces conformational changes in uPAR, which is then able to bind plasmin(ogen), integrin, and the ECM protein vitronectin. This multi protein complex formation facilitates local proteolysis, ECM degradation, and eventually neurite outgrowth or cell migration. Considering the necessity of cell movement and tissue invasion during tumor progression it is not surprising that uPA-uPAR is closely related to the growth and dissemination of various tumors, including those originating in the brain (Mohanam et al., 1994; Schmitt et al., 1997). Both mRNA and protein levels of uPA and uPAR are dramatically enriched in malignant brain tumors (Kinder et al., 1993; Landau et al., 1994). High levels of uPAR and uPA activity correlate with cellular degradation of the ECM, cell migration, and Matrigel invasion in a dose-dependent manner. Therefore, blocking the uPA-uPAR interaction is being targeted as a novel strategy to inhibit growth and spread of malignant brain tumors that are refractory to conventional therapy (Reuning et al., 2003). E.g. down regulation of uPAR by antisense RNA or blockage of uPA-uPAR interaction by specific ligands inhibits glioblastoma cell migration *in vitro* and *in vivo* (Mohan et al., 1999; Mohanam et al., 2002). However, given the fact that uPA and uPAR are synthesized by many cell types throughout the body and are critical in maintaining ECM turnover, it is conceivable that nonspecific inhibition might have harmful consequences.

1.2.2 tPA modulates neurotransmission and synaptic plasticity

Via proteolytic remodelling of cell-cell and cell-matrix molecules and non-proteolytic mechanisms tPA is engaged in the formation of LTP, neurite outgrowth, cell migration, and microglia activation. Several lines of evidence indicate multiple mechanisms by which tPA could exert its modulatory effect on neurotransmission and synaptic plasticity.

1.2.2.1 tPA interacts with NMDA receptors

Controversial evidence suggests that tPA might be involved in the modulation of NMDA receptor (NMDAR) function. A physical interaction between tPA and the glutamate receptor NR1 subunit was demonstrated. The tPA cleavage, which could enhance NMDA-evoked rise in free intracellular calcium ($\Delta[Ca^{2+}]_i$), was localized to the C-terminal side of Arg_{260} of the NR1 subunit (Fernandez-Monreal et al., 2004; Liot et al., 2004; Nicole et al., 2001) (Fig. 1.4, left). A role for plasmin in tPA-mediated NR1 proteolysis was considered unlikely because incubation of recombinant NR1 with plasmin led to complete degradation (Fernandez-Monreal et al.,

2004; Matys and Strickland, 2003). The specific tPA-NR1 interaction was defined from embryonic neuronal cultures, whereas others, utilizing lysates from adult mouse brain, failed to detect the tPA-mediated cleavage of NR1 (Kvajo et al., 2004; Liu et al., 2004; Matys and Strickland, 2003). Furthermore, the fact that co-immunoprecipitation of tPA with NR2B but to a lesser extent with NR1 was observed in three month old wild-type mice (Pawlak et al., 2005a) strongly suggests that the type of action of tPA on NMDA receptor subunits depends on the developmental stage. However, direct evidence that NR1 cleavage has an electrophysiological consequence is lacking. Since $\Delta[Ca^{2+}]_i$ is not a reflection of NMDA-mediated excitatory postsynaptic current (EPSCs), it is conceivable that the potentiation of $\Delta[Ca^{2+}]_i$ by tPA may lie downstream of other receptor-mediated signaling events. This hypothesis is emphasized by the fact that in primary hippocampal neurons tPA promotes a proteolytic-independent activation of the Erk1/2 signal transduction pathway through NMDA receptors, possibly NR2B, G proteins and PKC. The activation of this signaling pathway results in glycogen synthetase kinase 3 (GSK3) activation, a process that requires de novo protein synthesis, and leads to tau hyperphosphorylation, microtubule destabilization and apoptosis. Similar effects are produced by amyloid aggregates in a tPA-dependent manner. Consistently, it was shown that tPA co-localizes with amyloid-rich areas, activated Erk1/2 and phosphorylated tau in senile plaques of AD human brains (Medina et al., 2005).

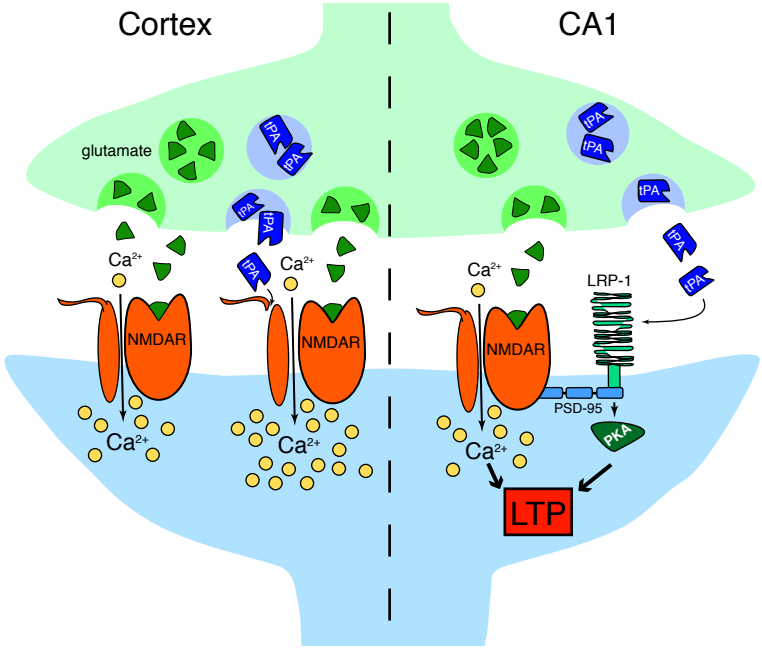

Figure 1.4 Mechanism by which tPA influences glutamatergic transmission.
Left: tPA cleavage of the glutamate receptor NR1 subunit increases NMDAR-dependent Ca^{2+}-flux and excitotoxic cell death. **Right:** Lipoprotein receptor-related protein 1 (LRP-1) is tethered to the NMDA receptor via PSD-95. tPA facilitates NMDAR-dependent late-LTP at the CA1 synapse by binding to LRP-1 and transducing a signal that elevates PKA levels. For simplicity, only the exocytosis of tPA from presynaptic stores is depicted. However, tPA stores within the postsynapse have also been demonstrated.

1.2.2.2 tPA induces late-LTP through the association with LRP-1

Extracellular tPA activity is controlled by neuroserpin and plasminogen activator inhibitor (PAI)-1. It is targeted to cell surfaces by association with Annexin II and lipoprotein receptor-related protein (LRP)-1. LRP-1 is a member of the low-density lipoprotein receptor (LDLR) family of endocytic receptors. LRP-1 is widely expressed throughout the CNS where it mediates the signaling and catabolism of many ligands. Indeed, LRP-1 endocytoses free tPA as well as inhibitory complexes tPA:PAI-1 (Makarova et al., 2003). Mice deficient in tPA ($tPA^{-/-}$) exhibit a selective reduction in late LTP (L-LTP) in hippocampal slices in both the Schaffer collateral-CA1

and mossy fiber-CA3 pathways (Huang et al., 1996). Application of tPA restored L-LTP along the CA1 pathway and increased protein kinase A (PKA) activity (Zhuo et al., 2000). Interestingly, co-application of tPA together with the LDLR ligand blocker receptor-associated protein, RAP, ablated both the restoration of L-LTP and the activation of PKA. Although other LDLR family members are crucial for LTP, LRP-1 is the most intriguing in this respect given its known association with tPA. In addition, other LRP-1 ligands – α-2-macroglobulin, lactoferrin, apoε4 – can also modulate NMDA receptor-evoked $\Delta[Ca^{2+}]_i$ (Qiu et al., 2003). To this end, LRP-1 is tethered to the NMDA receptor via postsynaptic density protein 95, PSD-95, in an activity-dependent manner (May et al., 2004). Altogether, free tPA and tPA:LRP-1 complexes are ideally suited to be NMDA receptor modulators (Fig. 1.4).

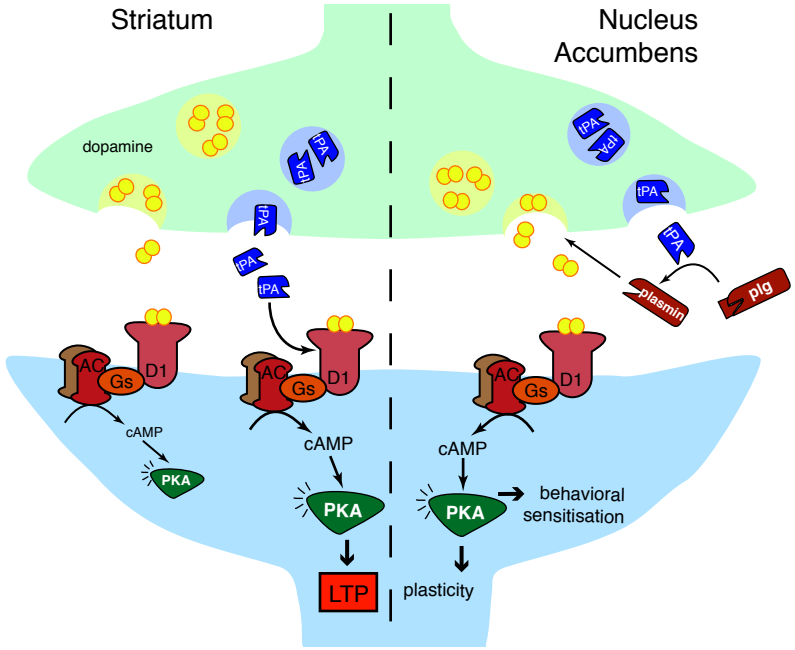

Figure 1.5 Mechanism by which tPA influences dopaminergic transmission.
The D1 class of dopamine receptors couples to Gs protein and elevates cAMP/PKC levels upon activation of adenylate cyclase (AC). **Left:** In the striatum, tPA-/- mice have impaired D1receptor-mediated signaling that impedes corticostriatal LTP induction. **Right:** In the nucleus accumbens, tPA-mediated generation of plasmin triggers dopamine release upon morphine injection. This underlies the plasticity-related behavioral sensitization brought on by morphine administration.

1.2.2.3 tPA facilitates late-LTP via the dopaminergic system

The striatum is heavily innervated by dopaminergic neurons. Dopamine is a slow-acting neuromodulatory transmitter that exerts its effect on two classes of receptors: D1-like receptors that couple to G_s proteins and elevate cAMP and D2-like receptors that couple to G_i proteins and suppress cAMP. Substantial evidence for tPA involvement in dopaminergic transmission has been obtained in the synaptic plasticity paradigms of LTP and drug addiction. Despite unaltered physiological and pharmacological EPSPs, $tPA^{-/-}$ mice showed impairment in corticostriatal LTP (Centonze et al., 2002). Mimicking D1-receptor activation by an elevation of cAMP could restore LTP. It was therefore postulated that tPA facilitates D1-mediated signaling. In addition a reduced level of D2 receptor was found in $tPA^{-/-}$ striatum, which seems to reflect an adaptation to attenuated high levels of cAMP and activated PKA (Fig. 1.5, left). Nevertheless, whether and how tPA acts on D1 receptor signaling and thus elevates the level of postsynaptic cAMP remains to be shown. Connections between tPA and dopaminergic transmission in LTP has also been made along the CA1 and CA3 circuits (Huang et al., 1996). These two forms of hippocampal LTP can also be evoked by the pharmacological elevation of cAMP. However, in $tPA^{-/-}$ mice, LTP induced by D1 agonist was abolished in CA1, and forskolin, a cAMP agonist could also reduce

L-LTP in CA3. Huang and colleagues speculated that dopamine-induced rise in cAMP might initiate immediate-early gene tPA that dramatically facilitates L-LTP in the hippocampus. In line with LTP being a molecular correlate for learning and memory, formation of cognitive deficits in striatum-dependent but not in hippocampus-dependent tasks have been documented. Hence, the dopamine-dependent deficiencies in hippocampal L-LTP in $tPA^{-/-}$ mice may have an impact on behavioral processes such as anxiety and addiction and cannot be translated into deficits in spatial learning and memory.

1.2.2.4 tPA is involved in drug addiction

Drug abuse triggers cellular and behavioral changes that are long lasting, experience dependent, and strengthened by repetition. Synaptic plasticity is a crucial event that takes place in drug addiction. Furthermore, psychomotor stimuli, such as cocaine, morphine, and amphetamines are known to rely on dopaminergic transmission. It is therefore not surprising that tPA plays a prominent role in drug abuse. Morphine treatment altered the tPA expression via the generation of plasmin-induced dopamine release in the nucleus accumbens (NAcc) (Nagai et al., 2004) (Fig. 1.5, right). However, the plasmin-sensitive target remains unknown. Morphine-induced conditioned place preference and hyperlocomotion were significantly reduced in $tPA^{-/-}$ and $plasminogen^{-/-}$ ($plg^{-/-}$) mice, being accompanied by a loss of dopamine release in the NAcc. Either exogenous tPA or plasmin reversed the defect of dopamine release and hyperlocomotion in tPA-/- mice. These findings demonstrate a function of the tPA-plasmin system in regulating dopamine release, which is involved in the rewarding effects of morphine.

Taken together, tPA is a multifaceted modulator of neuronal transmission and synaptic plasticity by both proteolytic and non-proteolytic type of action. As a peptidase it is capable to cleave two known important substrates in the brain: NR1 to alter ion channel properties and plasminogen to degrade ECM molecules. tPA can increase cell surface receptor activity and trigger intracellular signaling cascades, such as PKA and MAPK. Further, tPA can act as a ligand of LRP-1 in order to be desensitized and thereby facilitating NMDA receptor-dependent L-LTP in CA1. It can interact in an as yet unknown manner with D1-like receptors and increase L-LTP in the striatum. Generally, tPA is accepted as crucial factor in the CNS but unidentified non-plasminogen substrates for tPA as well as the precise mechanism through which tPA exerts its function on dopaminergic transmission, LTP, and memory formation remain to be determined.

1.2.3 Plasminogen in the brain – a versatile peptidase activated by tPA and uPA

Plasminogen is the zymogen of S1 serine peptidase plasmin. It is a 92 kDa glycoprotein consisting of seven structural domains: a N-terminal preactivation peptide (PAN), five KR domains, and a C-terminal catalytic domain. (Fig. 1.3). The multiple kringle domains are crucial for substrate recognition, membrane association, and inhibitor binding (Syrovets and Simmet, 2004). Plasmin can be cleaved and activated by both tPA and uPA, as well as by kallikrein and several coagulation factors. The activation of plasminogen occurs at the Arg_{561}–Val_{562} peptide bond. This cleavage gives rise to a two-chain protein linked by a disulfide bond. Plasmin is an important enzyme present in blood that degrades many blood plasma proteins, most notably fibrin clots. Apart from fibrinolysis, plasmin proteolyses proteins in various other systems:

it activates collagenases, some mediators of the complement system and weakens the wall of the Graafian follicle, leading to ovulation. It cleaves fibrin, fibronectin, thrombospondin, laminin and von Willebrand factor and can activate MMPs. Plasmin also mediates the release of the guidance molecule F-spondin from the ECM (Tzarfaty-Majar et al., 2001). Furthermore, a 150 kDa neural cell adhesion molecule (N-CAM) L1 fragment released by plasmin could stimulate cell migration (Mechtersheimer et al., 2001). In contrast to the dual cellular source of tPA in the CNS, plasminogen is exclusively synthesized by neurons with highest expression in the hippocampus, cerebellum, and the cerebral cortex (Tsirka et al., 1997; Zhang et al., 2002) (Table 1.1). Thus in the CNS, plasmin acts as a downstream effector of tPA in processes such as cell migration, neurite outgrowth and synapse elimination. In this respect it was demonstrated that the tPA/plasmin system induces mossy fiber sprouting. The chondroitin sulfate proteoglycan phosphacan, an ECM component associated with inhibition of neurite outgrowth, was identified as one physiological target of plasmin (Wu et al., 2000). Unexpectedly, mice lacking tPA displayed decreased mossy fiber outgrowth but $plg^{-/-}$ mice showed normal mossy fiber outgrowth. This strongly suggests that tPA functions both through a plasmin-depended and a plasmin-independent pathway to mediate mossy fiber reorganization. Another chondroitin sulfate proteoglycan, NG2, which inhibits neurite outgrowth, can bind to the kringle domains of plasminogen and enhances plasmin generation by uPA (Goretzki et al., 2000). Consequently, the plasminogen activator/plasmin system works in concert to promote ECM degradation and remodeling (Lijnen, 2001).
On the other hand the tPA/plasmin system also promotes excitotoxic cell death. This action is dependent on the proteolytic activity of plasmin, which can degrade laminin, an early step in the neuronal death pathway. The $plg^{-/-}$ mice exhibit decreased microglial migration to the site of excitotoxic cell death and are more resistant to excitotoxic injuries (Chen and Strickland, 1997; Tsirka et al., 1997). Furthermore, repeated stress can impair hippocampal function. Both pre- and postsynaptic effects of chronic stress result in a reduction in the number of NMDAR and dendritic spines in the CA1 region. Strikingly, the stress-induced decrease in NMDA receptors coincides spatially with sites of plasminogen activation. Consistent with this, $tPA^{-/-}$ and $plg^{-/-}$ mice are protected from stress-induced decrease in NMDAR and reduction in dendritic spines (Pawlak et al., 2005b). On the other hand, plasmin seems to be neuroprotective in the case of AD. As mentioned above, the tPA/plasmin proteolytic cascade accelerates Aß degradation and inhibits Aß-induced neurodegeneration (Melchor et al., 2003). The opposing roles of plasmin in neuronal survival versus death emphasize the functional complexity of this peptidase that is determined by particular cellular settings and various stimuli.

1.2.4 Thrombin is involved in brain development

Thrombin is a secreted S1 serine peptidase that cleaves peptide bonds after Arg and Lys, converts fibrinogen to fibrin and activates factors V, VII, VIII, XIII and, in complex with thrombomodulin, protein C. It is heavily involved in blood coagulation and tissue repair of many different origins. Prothrombin is composed of an N-terminal gamma carboxyglutamic acid-rich (GLA) domain that is responsible for high affinity binding of Ca^{2+} ions, followed by two KR domains and a C-terminal trypsin-like serine protease domain (Fig. 1.3). Prothrombin is activated on the surface of phospholipid membranes, which bind the N-terminus of prothrombin as well as factors Va and Xa in a Ca^{2+}-dependent manner. The activity of factor Xa is greatly enhanced by binding to factor Va. Factor Xa removes the activation peptide of prothrombin including the second

KR domain and cleaves the remaining part into light and heavy chains. Prior to its activation by factor Xa thrombin itself can cleave the N-terminal fragment of prothrombin including the GLA and the first KR domain. The activation process starts slowly because factor V has to be activated by the initially small amounts of thrombin.
Apart from other tissues prothrombin mRNA was also detected in the brain and in cell lines of neuronal and glial origin (Dihanich et al., 1991) (Table 1.1).

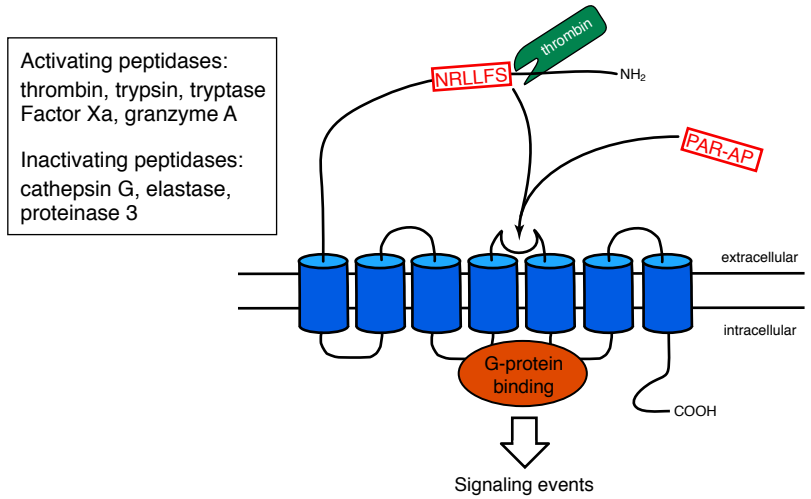

Figure 1.6 Activation of Protease-Activated Receptor 1 (PAR-1).
Following irreversible proteolytic cleavage of PAR a new N-terminus is unmasked (SFLLRN) acting as a tethered ligand that can interact with the extracellular loop 2 of the receptor. A synthetic peptide derived from the N-terminal sequence of PAR-1 (PAR-AP) is able to activate the receptor in the absence of peptidases. Different peptidases may act on the extracellular N-terminus, either exposing the tethered ligand to activate, or disabling the tethered ligand to inactivate PARs by cleaving at a site downstream of the tethered ligand sequence. The intracellular loops 2 and 3 have been proposed to play a role in G protein coupling for PAR-1.

1.2.4.1 Proteolytic activation of thrombin receptors

Protease-activated receptors (PARs) belong to the superfamily of G protein-coupled receptors (GPCRs). The central step of human PAR-1 activation by peptidases is the specific cleavage of the extracellular N-terminus of the receptor after Arg_{41}, unmasking a new N-terminus (SFLLRN) that functions as a tethered ligand and binds intramuscularly to the receptor. By this new interaction with the extracellular loop 2 a signal is transduced intracellular via G proteins. G_q is associated to intracellular loops 2 and 3 (Hollenberg and Compton, 2002) and $G_{12/13}$ was shown to bind to the cytosolic C-terminal tail of PAR-1 (Pai et al., 2001). Synthetic PAR-activating peptide (PAR-AP) that mimic the tethered ligand can also activate PARs (Fig. 1.6).
Until now four members of the PAR family have been identified. PAR-1, -3 and -4 are considered as thrombin receptors, while PAR-2 is activated by serine proteases other than thrombin, such as trypsin and mast cell tryptase. Two thrombin interaction sites have been proposed on hPAR-1: one is the cleavage site, and the other one is between residue 53 and 64 and is involved in the thrombin anion-binding exosite (Rydel et al., 1991). Apart from thrombin other peptidases such as Factor Xa, tissue factor/factor VIIa complex, granzyme A, and trypsin can activate PARs as well. Although, PARs are constitutively activated by proteolysis, they are rapidly desensitized by a variety of mechanisms, including phosphorylation and internalization through coated pits (Brass et al., 1994; Ishii et al., 1994). Furthermore, PARs can also be inactivated by peptidases

such as cathepsin G and thermolysin, which are capable of cleaving within the tethered ligand (Ubl and Reiser, 2000; Ubl et al., 2000).
It is now widely accepted that activated thrombin signals through the family of protease-activated receptors (PARs). Four different thrombin receptors have found to be widely distributed in brain tissue. PAR-1, -2, -3 and -4, which are expressed in neuronal cells at various densities in numerous brain regions (Striggow et al., 2001), have also been identified in glial cell culture (Wang et al., 2002a) (Table 1.1). The co-expression suggests distinct functions or cross-talk among the PAR family members. Ample evidence point to the idea that thrombin changes the morphology of neurons and astrocytes, induces glial cell proliferation, and even exerts, depending on the concentration, either apoptotic or cytoprotective effects on neural cells.

1.2.4.2 Thrombin elicits proliferative and pathophysiological changes in the brain

One of the most pronounced effects of thrombin is the induction of morphological changes in neural cells (Gebbink et al., 1997; Jalink and Moolenaar, 1992; Pai and Cunningham, 2002; Turnell et al., 1995) and astrocytes (Grabham and Cunningham, 1995; Majumdar et al., 1998). Both the application of PAR-AP and thrombin causes a rapid neurite retraction in neuronal cells and a reversal of stellation in astrocytes. These processes rely on cytoskeletal rearrangements that in turn require induction of specific signaling pathways activated through PAR. The downstream signaling cascades involved here are discussed later in this work. However, a well-controlled balance between thrombin and its inhibitors is essential to regulate neuronal connections through the modulation of neurite outgrowth. Moreover, thrombin has been shown to potentiate NMDAR responses in CA1 pyramidal cells (Gingrich et al., 2000). It is known to enhance neural growth factor (NGF) and endothelin-1, and to induce astrocyte proliferation (Ehrenreich et al., 1993; Grabham and Cunningham, 1995; Neveu et al., 1993). Furthermore, thrombin has been reported to induce secretion of Aß precursor in astrocytes (Davis-Salinas et al., 1994). Notably, at low concentrations thrombin promotes cell survival, while at high concentrations it induces apoptosis, e.g. thrombin significantly protected hippocampal neurons against ischemic insults but caused degeneration at high concentrations *in vivo* and *in vitro* (Striggow et al., 2000). The finding that PARs are expressed in microglia cells also suggests that thrombin might be a mediator of brain inflammation. First, thrombin stimulates proliferation of microglial cells and second, thrombin leads to the release of the cytokines tumor necrosis factor-α (TNF-α), interleukin-6 (IL-6), interleukin-12 (IL-12), the chemokine KC, and the soluble TNF-α receptor II (Moller et al., 2000; Suo et al., 2002). Conversely, another group found no increase in IL-6 and TNF-α secretion. However, they found a PAR-1-induced release of the chemokine GRO (growth-regulated oncogene)/CINC-1 (cytokine-induced neutrophil chemoattractant-1) that was mainly mediated by c-Jun N-terminal kinase (JNK) activation and preserved astrocytes from toxic insults. Importantly, a specific JNK inhibitor significantly abolished the protective action of PAR-1 (Wang et al., 2006). PAR agonists provoked and thrombin inhibitors blocked all these effects on astrocytes and neurons. The different physiological roles of PAR-2, -3, and -4 are still not clear. However, the fact that PAR-4 activation requires high concentrations of thrombin (Xu et al., 1998) raises the possibility that the deleterious effects of high thrombin concentrations may be mediated by PAR-4.

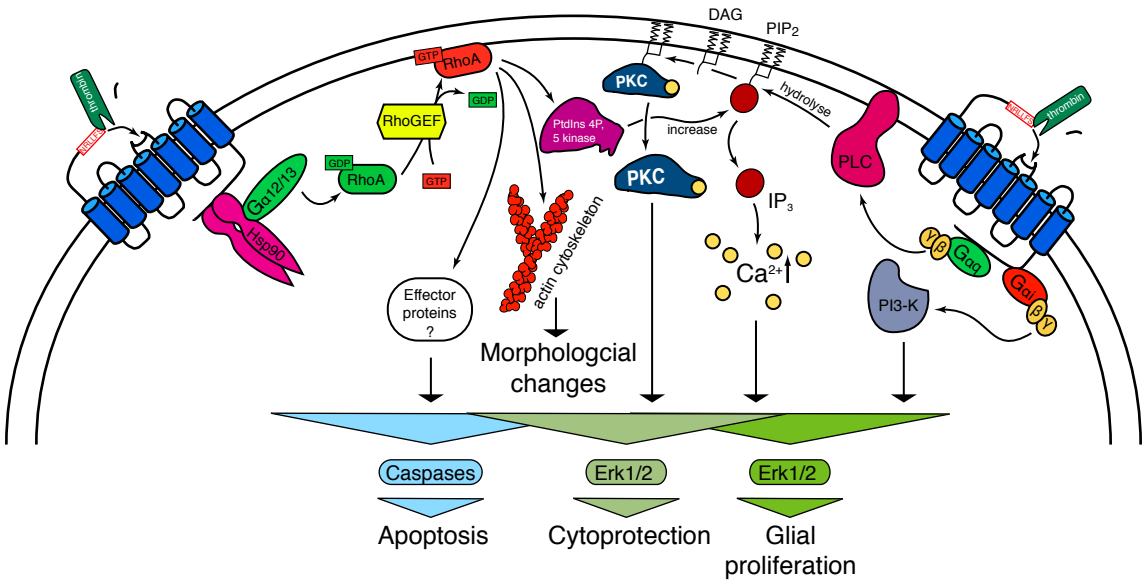

Figure 1.7 Thrombin-induced signaling events via PAR-1 activation in the brain.
Activated PAR-1 may couple to $G_{12/13}$ with association of Hsp90, leading to activation of RhoA. Subsequently, activated RhoA translocates to the membrane where it can transduce a signal through downstream factors to the actin cytoskeleton. Potential effector proteins of RhoA involved in both cytoprotective and toxic effects include phosphatidylinositol 4-phosphate 5-kinase (PtdIns 4P, 5 kinase), which in turn increases available PIP_2. PAR-1 coupled to G_q activates PLC to produce DAG and IP_3 from PIP_2, resulting in Ca^{2+}-mobilization and activation of PKC. As a Ser/Thr kinase, PKC has been implicated in protection and apoptosis. However, it is still necessary to define the links upstream of caspases released for apoptosis and extracellular signal-regulated kinase 1/2 (Erk1/2) activation for neuroprotection. In astrocytes however, activation of PAR-1 results in the activation of both G_i/G_0 and G_q, mediating activation of Erk1/2 cascades leading to proliferation. PI3-K: phosphatidylinositol 3-kinase.

1.2.4.3 Activated PAR-1 signaling in the CNS

Depending on the cell type PAR-1 activation by thrombin is coupled to heterotrimeric G proteins including G_i, $G_{12/13}$, and G_q. Subsequent intracellular events involve activation of phospholipase C (PLC), generation of inositol triphosphate (IP_3) and diacylglycerol (DAG), followed by intracellular increase of Ca^{2+} concentration and protein kinase C (PKC) activation. Non-receptor tyrosine kinases Src and focal adhesion kinase (FAK) are phosphorylated in response to thrombin. Ras and Ras-related protein Rho are also implicated in thrombin-induced response. Moreover, the activation of phosphatidylinositol 3-kinase (PI3-kinase) and MAPK by thrombin stimulation as been observed as well (Macfarlane et al., 2001) (Fig 1.7). Thrombin induced cellular shape changes like neurite retraction or reversal of stellation in astrocytes, do not underlay the same signaling pathways. In mammalian cells it is the highly conserved Rho family of small GTPases that plays a key role in signal transduction pathways, which link plasma membrane receptors to the reorganization of the actin cytoskeleton, resulting in neurite retraction. Specifically, the cytoskeletal effects of thrombin appear to be mediated by the $G_{12/13}$ subunits that act upstream of RhoA. The signals are believed to be transduced by Rho-specific guanine nucleotide exchange factors (Rho-GEFs) Lbc and p115 (Majumdar et al., 1998). Heat shock protein 90 (Hsp90) might help to couple $G_{12/13}$ to the PAR cytoplasmic C-terminus (Pai et al., 2001) (Fig. 1.7).

The signaling pathway underlying thrombin-induced astrocyte proliferation mainly takes place through PAR-1 (Wang et al., 2002b). Thrombin stimulates Erk1/2 phosphorylation in a time- and concentration-dependent manner. This effect can be fully mimicked by the specific activation

peptide PAR-AP. The stimulation is mainly transduced via two branches: 1) the G_i-mediated PI3-kinase branch, and 2) the G_q - PLC/Ca^{2+} - PKC pathway (Fig. 1.7).
Furthermore, thrombin can evoke phosphorylation of proline-rich tyrosine kinase (Pyk2), a linker between GPCRs and Erk1/2 activation via PAR-1 (not shown). Pyk-2 links PAR-1-dependent increase in cytosolic Ca^{2+}. PKC activation initiates MAPK pathway by recruiting the adaptor protein growth factor receptor-bound protein 2 (Grb2) (Wang and Reiser, 2003). In addition, an involvement of Hsp27 and Erk1/2 in the neuroprotective effects was also shown (Xi et al., 2001; Xi et al., 1999). Finally, activation of both PAR-1 and PAR-2 resulted in the release of the GRO/CINC-1, but PAR-2-induced GRO/CINC-1 release was independent of PKC, PI3-kinase and Erk1/2 activation. However, these three kinases were involved in PAR-1-induced GRO/CINC-1 release. Despite such differences between PAR-1 and PAR-2 signaling, JNK was identified in both signaling pathways to play a pivotal role. It was demonstrated that different JNK isoforms mediated GRO/CINC-1 secretion, when it was induced by either PAR-1 or PAR-2 activation (Wang et al., 2007). Taken together, these data suggest that PAR-1 and PAR-2 have overlapping functions, but can activate separate pathways under certain conditions to rescue neural cells from cell death.
As mentioned earlier, in hippocampal neurons and astrocytes, thrombin has been shown to exhibit both beneficial and harmful effects in a concentration dependent manner. Similar profiles are involved in protective and apoptotic functions, e.g. involvement of tyrosine kinases, Ser/Thr kinases, RhoA, and the cytoskeleton (Donovan and Cunningham, 1998; Donovan et al., 1997). For the induction of the apoptotic pathway a continual presence of thrombin was beyond doubt more important than high concentrations *per se*. Hence, it was suggested that in both responses the same pathway is activated. The cell death pathway, however, may result from an over-activation of PAR-1 and over-activation of the connected pathway. Additionally, caspase-3 and caspase-1 were activated following PAR-1 stimulation to initiate apoptosis (Smirnova et al., 1998).
Taken together it is now apparent that activation of PARs by thrombin does not always produce the same pattern of cellular responses. Irrespective of the endeavor to push the understanding of the thrombin-signaling forward, it will be of great importance to study the activation mechanism for converting prothrombin into thrombin in brain under physiological conditions in more detail. Similarly, there is little knowledge about the function of PAR-2, -3, and -4 in neurons. Independent of the missing pieces in the puzzle, the mediators, including thrombin activation, involved in the signaling cascades might be potential targets for treatment of brain injury and diseases.

1.2.5 Neuropsin – a neural activity-dependent serine peptidase

The *neuropsin* gene, also called *kallikrein-8*, is encoded in a gene cluster as a member of the big kallikrein-like multigene family in humans (Yoshida et al., 1998). It is a simple S1 serine peptidase with an apparent M_r of 30 kDa that is composed of one polypeptide chain containing 260 amino acids (Chen et al., 1995) (Fig. 1.3). There is no characteristic domain other than a serine protease domain. Proneuropsin has a predicted signal peptide and is secreted via both regulated and constitutive pathways (Chen et al., 1995; Oka et al., 2002). In the hippocampal CA1-3 subfields and amygdala, the gene shows activity dependent expression evoked by neuronal stimuli such as epilepsy or LTP. The non-active proneuropsin protein is stored in extracellular spaces, probably in the synaptic cleft and remains inactive until stimulation (Shimizu et al., 1998). Indeed,

increased neural activity triggered the rapid, transient activation of the zymogen of neuropsin in an NMDA-dependent manner. Inhibition of the MAPK, PKA, PKC or CaMK II signaling pathway indicated that the activation of neuropsin may lie downstream of one of these generic signaling cascades (Matsumoto-Miyai et al., 2003). In addition, various concentrations of recombinant neuropsin resulted in a dose-dependent increase of the amplitude of the tetanic stimulation-induced early phase of LTP (E-LTP) via its proteolytic action (Komai et al., 2000). The brief increase (< 30 min) in neuropsin activity following neural potentiation of excitatory presynapses in CA1 immediately processed the extracellular domain of L1 resulting in a freely diffusible extracellular fragment of 180 kDa. Subsequently, the magnitude of Schaffer collateral E-LTP is diminished (Matsumoto-Miyai et al., 2003). In spite of the marked changes L1 immunoreactive synapses, neuropsin null-mutant mice exhibited no significant impairment in hippocampal LTP (Davies et al., 2001). This speaks in favor of the fact that other peptidases such as plasmin also proteolyse N-CAM L1 and thus can compensate for the absence of neuropsin. Ankyrins and syntenin-1 bind to the cytoplasmic tail of N-CAMs and thus serve as adaptors that link cell adhesion molecules to the cytoskeleton. Thus, the cleavage of L1 by neuropsin may induce a dynamic rearrangement of the submembrane cytoskeleton and membrane protein clustering to induce changes in the synaptic morphology.

1.2.6 Calpains act in the pre- and postsynaptic boutons

Calpains, Ca^{2+}-dependent cysteine peptidases that act intracellular, are expressed as proenzymes that undergo autocatalytic processing to yield the mature form. Two ubiquitous calpains, μ-calpain and m-calpain, are highly expressed in the CNS. Calpain substrates such as membrane receptors, postsynaptic density proteins, kinases, and phosphatases are localized intracellularly. It has been shown that calpain has direct proteolytic activity on NMDAR 2 (NR2) subunits and thus modulates the NMDAR function and turnover (Guttmann et al., 2001). PSD-95 clustering and direct association of NR2A to PSD-95 mediate the blockade of calpain-induced cleavage of NR2A (Dong et al., 2004). Moreover, several lines of evidence suggest that calpain activation in the synapse is necessary for LTP. Fodrin cleavage by calpain causes increased LTP putatively through the insertion of NMDAR into the post-synaptic membrane (Lynch and Baudry, 1984). The molecular mechanism however, how calpain activity induces LTP, remains to be determined. Furthermore, both long-term depression (LTD) and cleavage of protein kinase C (PKC) -ζ are prevented by calpain inhibitors (Hrabetova and Sacktor, 1996). Calpain-mediated proteolytic cleavage of PKC-ζ gives rise to constitutively active PKM resulting in burst firing in dopaminergic neurons (Liu et al., 2007). In addition, glutamate receptor-interacting protein (GRIP) is also a substrate of calpains. Calpain activation results in the disruption of GRIP binding to the GluR2 subunit of AMPA receptors. Because GRIP has been proposed to function as an AMPA receptor-targeting and stabilizing protein, degradation of GRIP and disruption of AMPA receptor anchoring are likely to play important roles in the structural and functional reorganization accompanying synaptic modifications in LTP and LTD (Lu et al., 2001).
It is obvious that the calpains are the only peptidases addressed in this work that do not belong to the S1 peptidase family. Nevertheless, it exemplifies the enormous diversity by which peptidases in general exert their functions in the brain.

1.3 Neurotrypsin – a brain specific extracellular serine peptidase

Using RT-PCR, Gschwend et al. searched for novel serine peptidases that are expressed in the nervous system. Degenerated primers complementary to the conserved region around the His/Ser residues of the catalytic triad of known serine peptidases, such as trypsin, tPA, uPA or thrombin were used. The approach resulted in the cloning of a novel murine cDNA, which encodes a multidomain trypsin-like serine peptidase with a unique domain composition. Since it exhibits a highly intriguing neuronal expression pattern in the adult murine nervous system, it was termed neurotrypsin (Gschwend et al., 1997). Neurotrypsin is the peptidase under investigation in this work.

The structural composition deduced from the amino acid sequence revealed a multidomain protein of 761 amino acids with a typical C-terminal S1 type serine protease domain (PD). N-terminally it starts with a putative signal peptide for secretion, followed by a proline-rich basic (PB) segment and one kringle domain. In case of human there are four (Proba et al., 1998), and in case of mouse and rat there are three scavenger receptor cysteine-rich (SRCR) domains. In fact, the first copy of the SRCR domains (exons 2 – 3) is missing in the murine protein. Since all other species tested so far bear four intact SRCR domains, the rodent lineage must have lost exons 2 and 3 during evolution. The functional consequences, however, are not known (Xu and Su, 2005). The next region is the zymogen activation (ZA) site that is located proximal to the C-terminal PD with the conserved catalytic triad of serine peptidases (Fig. 1.3). To gain proteolytic activity, an activation cleavage, similar to tPA, must occur at the ZA site that separates the protein into two chains that are connected by a disulfide bond. This activation cleavage is in all probability carried out by furin, a member of the subtilisin superfamily. Furin is a ubiquitous Ca^{2+}-dependent endopeptidase active within the constitutive secretory pathway and capable to cleave at Arg-X-Lys/Arg-Arg motifs. Thus, neurotrypsin is most likely activated during its secretion. The non-catalytic domains are thought to mediate binding of neurotrypsin to cell surfaces or ECM molecules, navigating the peptidase to its site of action or bring it into proximity to its substrates.

1.3.1 Neurotrypsin is a trypsin-like serine peptidase

An alignment of the amino acid sequence classifies neurotrypsin into the S1 family of trypsin-like serine peptidases (Fig. 1.8). The sequences of chymotrypsin, trypsin, neurotrypsin, tPA and uPA are shown. In the chymotrypsin index, His_{57}, Asp_{102}, and Ser_{195} form the catalytic triad and residues 189 – 195, 214 – 220, and 225 – 228 form the primary substrate-binding pocket called S1 binding pocket. Residues 185 – 188 and 221 – 224 form two loops near the S1 pocket, called L1 and L2, respectively (Fig. 1.8). Catalytic mechanisms of trypsin and chymotrypsin as well as of the other serine peptidases are similar, but their substrate specificities are different. Trypsin favors cleavage after basic residues like lysine and arginine; chymotrypsin favors aromatic residues like phenylalanine, tyrosine, and tryptophan (Vajda and Szabo, 1976). The S1 binding pocket in trypsin and chymotrypsin are almost identical in primary sequences and backbone tertiary structures (Fig. 1.8). An important difference is that residue 189 is a negatively charged Asp in trypsin and a polar Ser in chymotrypsin. This residue lies at the bottom of the S1 binding pocket and determines different S1 pocket chemical properties. It was once used to explain the different substrate specificity of trypsin and chymotrypsin (Steitz et al., 1969; Vajda and Szabo, 1976). But the mechanism is not that simple. Mutation of Asp_{189} in trypsin (D189S) did not change the substrate specificity from trypsin-like to chymotrypsin-like (Graf et al., 1988; Hedstrom,

1996; Hedstrom et al., 1992); instead the enzyme just lost its activity. And mutation of S189D in chymotrypsin did not convert its specificity into that of trypsin either (Venekei et al., 1996). When the two loops L1 and L2 of trypsin were replaced by those of chymotrypsin in addition to the D189S mutation, the new protein showed an increase of chymotrypsin activity up to 1000-fold against the D189S mutant alone. These experiments imply that in addition to the S1 substrate-binding pocket, loop regions of trypsin and chymotrypsin have significant effect on enzyme activity and substrate specificity.

A significant finding important for the development of trypsin-like serine peptidase inhibitors is that considerable specificity can be achieved at the S1 pocket alone (Katz et al., 2000; Yang et al., 1990; Zeslawska et al., 2000). Despite the high structural similarity in the S1 binding site of trypsin-like serine peptidases, these sites are differentiated from one another by two important features that can be targeted for selectivity development of inhibitors – their depth, and the identity of residue 190 (Fig. 1.8). Simple amidine inhibitors tend to be selective for Ser_{190} peptidases (uPA, trypsin, neurotrypsin, and factor VIIa) rather than Ala_{190} peptidases (tPA, thrombin, and factor Xa), because of an additional hydrogen bond between the amidine and $O\gamma_{Ser190}$ in the former class (Katz et al., 2000).

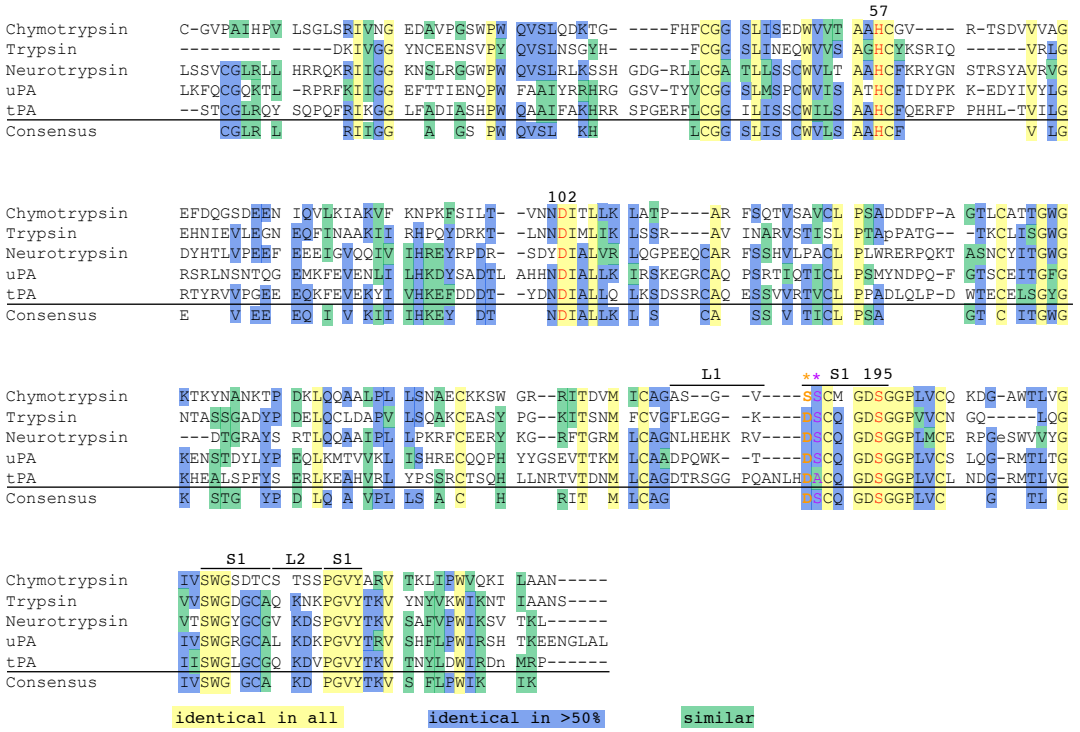

Figure 1.8 Sequence alignment of human neurotrypsin catalytic domain with other serine peptidases.
The alignment shows the sequence similarities of chymotrypsin, trypsin, neurotrypsin, uPA and tPA in chymotrypsin numbering. The alignment is grouped into three categories: i) identical amino acid residues in all serine peptidases are highlighted in yellow, ii) the residues, which are identical in more than 50% are shown in blue, and iii) green indicates similarities in chemical properties of the amino acid residues. Substrate-binding pocket S1 and two loops L1and L2 are displayed above the sequences. The amino acids of the catalytic triad are shown in red. Ser189 and Asp189 in the S1 pocket of chymotrypsin and trypsin, respectively, are important determinants for substrate specificity (orange asterisk). Ser190 or Ala190 define two different classes of trypsin-like serine proteases (magenta asterisk). This residue strongly influences the conformation of the S1 substrate binding pocket and thus may change the substrate specificity of the peptidase.

1.3.2 The role of neurotrypsin in the CNS – some evidence for a function in synaptic plasticity

Northern blot analysis of neurotrypsin mRNA isolated from liver, intestine, spleen, lung, brain, and cerebral cortex of adult mice revealed strongest signals in the brain and lungs, whereas only small quantities were detected in the intestine and spleen. No neurotrypsin transcripts were found in the liver. The expression of neurotrypsin mRNA in the CNS of adult mouse brain was studied in more detail by *in situ* hybridization. In the nervous system mRNA was confined to neurons. In the forebrain, labeling was exclusively detected in distinct subsets of neurons of the cortex, the hippocampus, the amygdala, and the olfactory bulb (Figs. 1.9a – c). Neurotrypsin mRNA in the neocortex was most intensive in neurons of layers V and VI (Fig. 1.9b). In the hippocampus, neurotrypsin expression was strongest in the subiculum and in pyramidal cells of the CA1 region (Fig. 1.9c). Moderate expression was observed in granule cells of the dentate gyrus. In addition, there was strong expression in neurons from the brain stem motor nuclei (Figs. 1.9d and e) and the motor columns of the spinal cord (Fig. 1.9f). Expression of neurotrypsin mRNA was also found in the peripheral nervous system. In the dorsal root ganglia (DRG) a subpopulation of neurons expressed neurotrypsin mRNA (not shown) (Gschwend et al., 1997). The expression of neurotrypsin mRNA in the mouse during prenatal and postnatal development was examined for different brain regions (Wolfer et al., 2001). Neuronal expression of neurotrypsin mRNA correlates best with periods of target invasion and maturation of synaptic contacts (Fig. 1.10). Together with the ongoing expression in the adult CNS, there is substantial support for the idea that neurotrypsin is involved in synaptic plasticity both during synapse formation and maintenance. In conjunction with its structural homologies to PAs and the anatomical distribution led us come to the prediction that the extracellular proteolytic action of neurotrypsin subserves structural reorganization processes. Immunoelectron microscopy on adult human brain sections revealed that neurotrypsin is located in presynaptic nerve endings, in particular close to the presynaptic membrane lining the synaptic cleft. Furthermore, a genetic analysis of four mentally retarded and four healthy siblings disclosed that a mutation in the *neurotrypsin* gene is associated with cognitive impairment and low IQ (<50) in the four affected individuals. The 4-base pair deletion results in a truncated form of neurotrypsin, missing the catalytic domain. The data emphasize the crucial role of neurotrypsin for synaptic proteolysis in higher brain function, the ablation of it leading to non-syndromic mental retardation (Molinari et al., 2002).

In order to investigate the functional role for neurotrypsin in more detail transgenic mice overexpressing neurotrypsin were generated (Fig 5.1). Observations of brush-like structures in the diaphragm immunostained for neurofilament revealed a degenerated nerve innervation of the end-plate band and deficient synapse formation. A similar phenotype has been found in agrin$^{-/-}$ mouse (Gautam et al., 1996), which lead to the assumption that neurotrypsin can proteolytically process agrin.

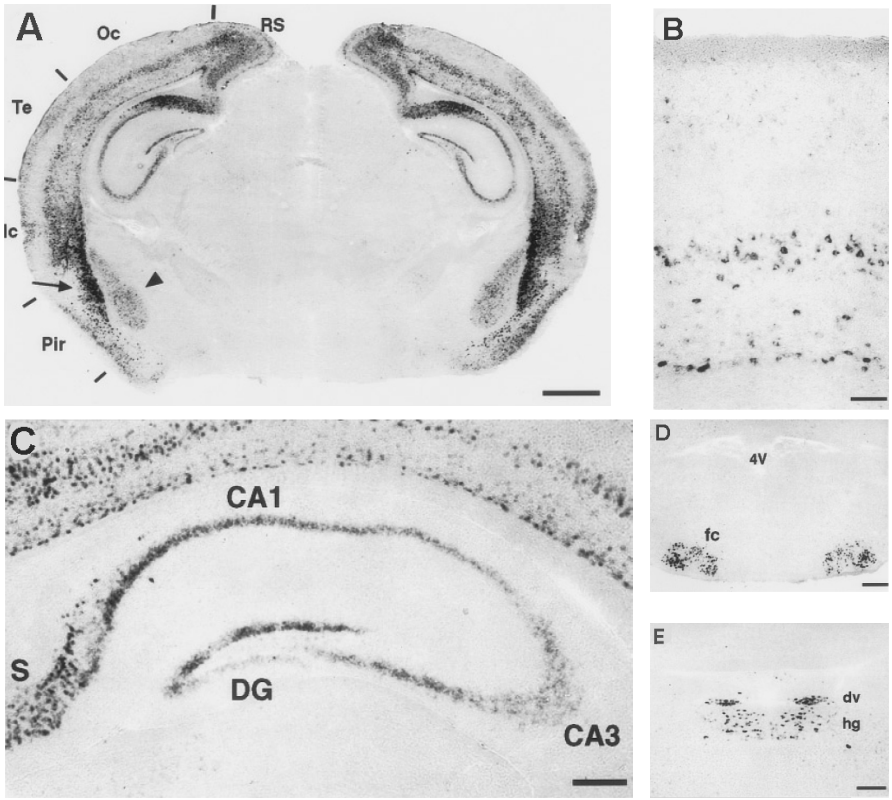

Figure 1.9 In situ hybridization for neurotrypsin transcripts in adult mouse brain.
(A) Labeling is seen in distinct layers throughout the neocortex (Te, temporal cortex; Oc, occipital cortex) with a more widespread labeling in the transition zones between iso- and allocortex (Ic, insular cortex; RS, retrosplenial cortex). In the allocortex, labeling is detected in the piriform cortex (Pir), with a strong signal in the endopiriform nucleus (arrow), and in the hippocampal formation. Neurotrypsin expression is also seen in the lateral amygdala (arrowhead). Bar, 1 mm. **(B)** Coronal section of the parietal cortex. Large positive neurons are seen in the lower half of layer V. In layer VI, positive cells are found throughout the layer. Weak labeling is associated with cells scattered in layers II and III. No mRNA is detected in layers I and IV. Bar, 100 µm. **(C)** Coronal section of the hippocampus. Labeling is detected in neurons of the subiculum (S), in pyramidal neurons of CA1 and CA3, and in granule neurons of the dentate gyrus (DG). Bar, 300 µm. (D) Coronal section of the pons. Labeling is seen in neurons of the facial nucleus (fc). Bar, 500 µm. (E) Coronal section of the medulla. Labeling in neurons of the dorsal motor nucleus of dorsal vagus (dv) and the hypoglossal nucleus (hg). Bar, 300 µm. (F) Cross-section of the cervical spinal cord. Large cells are labeled in the motor columns (arrowheads). Labeling is also detected in the DRG (arrow). Bar, 300 µm. (4V) Forth ventricle.

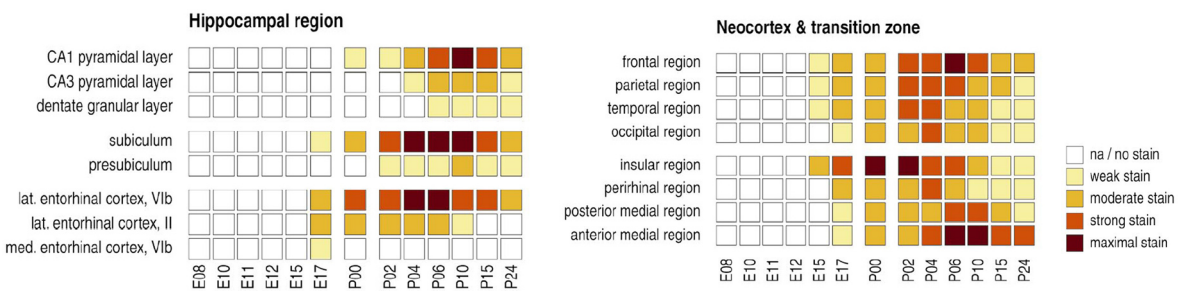

Figure 1.10 Time course of neurotrypsin mRNA expression in neural tissues during pre- and postnatal development.
Columns represent developmental stages. Rows represent cell populations, regions, or tissues. The shading pattern of each box indicates the average signal intensity, assigned to one of the four staining levels listed in the legend. E: embryonic stage, P: postnatal.

1.3.3 Cleavage of agrin by co-expression with neurotrypsin in cell culture and *in vivo* in the hippocampus

The finding that neurotrypsin overexpression in mice showed a brush-like structure in the diaphragm resembling the phenotype of agrin $^{-/-}$ lead to the hypothesis that agrin is a substrate for neurotrypsin *in vivo*. To test this hypothesis, agrin and neurotrypsin were co-expressed in HeLa cells and supernatants and cell lysates were immunoblotted with antibodies raised against the 90-kDa agrin intermediate fragment and the C-terminal laminin globular domain 3 (LG3 domain), respectively. When membrane-bound TM-agrin-y^4z^8 was expressed alone and the cell lysate was immunoblotted, a smeary signal was detected above 250 kDa, whereas in the supernatant the signal was absent (Fig. 1.11a). However, Western blotting of the supernatant after 48h of co-expression of TM-agrin-y^4z^8 and neurotrypsin, three bands were detected. The upper band represents the 112- kDa C-terminal fragment after the α-cleavage, the intermediate 90 kDa band, is the fragment resulting after cleavage at both, the α- and the β-sites, and the lower band is the very C-terminal LG3 domain produced by the β-cleavage (Fig. 1.11a, c). In fact, upon cleavage by neurotrypsin the C-terminal agrin fragments were released into the supernatant. The cell lysate was negative for agrin immunodetection, indicating a complete processing of agrin. The membrane bound N-terminal part of agrin could not be detected due to inexistent antibodies against this part of the protein. Even more convincing evidence for a specific proteolytic-dependent interaction of neurotrypsin with agrin is given by the following experiment (Fig. 1.11a): Co-expression of agrin with an inactive form of neurotrypsin, where Ser_{825} was mutated to an Ala (S/A), and subsequent immunoblotting resulted in the detection of the full-length agrin in the cell lysate as if neurotrypsin was absent. Consequently, no cleavage product in the supernatant was found either. A similar pattern for the agrin bands was found *in vivo* in the hippocampus homogenate (Fig. 1.11b). The cleavage products were enriched in transgenic samples and absent in the KO, whereas full-length agrin was reduced in transgenic, and accumulated in KO samples. The amino acid sequence of the α- (PIER | ASCY) and β-cleavage site (LVEK | SVGD) were determined by N-terminal sequencing (Fig. 1.11c) (Reif et al., 2007). So far, no other homologous cleavage site was found in any target sequences of other potential substrates. The cleavages are presumed to take place at the neuromuscular junction (NMJ) as well as in the CNS. Two findings suggest a very high specificity of neurotrypsin for substrate recognition and cleavage of agrin. Firstly, the fact that the basic residues Arg or Lys at P1 and acidic Glu at the P2 positions of agrin are highly conserved and thus, point mutations to alanine basically abolished cleavage. Secondly, typical serine protease inhibitors, such as aprotinin, leupeptin, and (4-amidinophenyl) methanesulfonyl fluoride (APMSF), as well as specific inhibitors for trypsin, plasmin, uPA and thrombin could not or only very little affect the proteolytic activity of neurotrypsin. Furthermore, sequence alignments do not imply neurotrypsin activation cleavage on other serine peptidases such as plasminogen, uPA, tPA, or prothrombin. It is believed that substrate diversity is limited and no participation in ECM degradation through plasminogen activation cascade is implicated. It is assumed that neurotrypsin catalytically processing of agrin is restricted to extracellular areas of the brain in close vicinity to synapses. Finally, very recent data suggest a neuronal activity- dependent release of neurotrypsin into the synaptic cleft (unpublished data). Nevertheless, the scope of neurotrypsin function in the CNS is far from being fully disclosed. For instance, a direct interaction of neurotrypsin with agrin is yet to be shown *in vivo*. And, neurotrypsin catalytic or non-catalytic activity has not been coupled to any of the generic signaling pathways to elicit cellular responses. Altogether, this data speak in favor of the fact that the neurotrypsin – agrin interaction is highly specific.

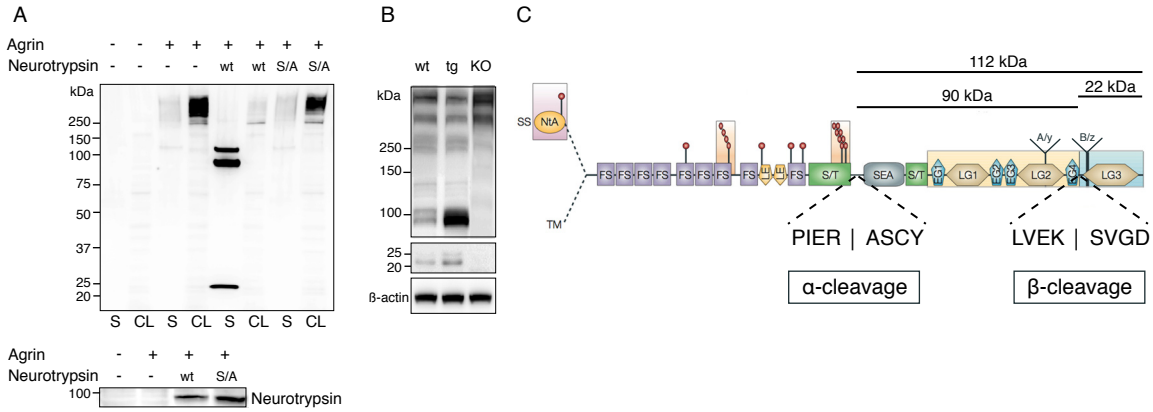

Figure 1.11 Neurotrypsin cleaves agrin at two positions in vitro and in vivo.
(A) In vitro digestion of agrin by co-expression with neurotrypsin in HeLa cells. Agrin and wild-type (wt) or inactive (S/A) neurotrypsin were coexpressed for 48h. Supernatants (S) and cell lysates (CL) were immunoblotted with R132, directed against the 90-kDa fragment, together with R139, directed against the laminin globular domain 3 (LG3 domain), antibodies. Uncleaved membrane-bound full-length agrin expressed alone was detected in the CL. Co-expression with neurotrypsin resulted in the secretion of three agrin C-terminal agrin fragments. In S, one band represents the 112-kDa and the other the 90-kDa fragment. The lower band represents the LG3 domain. Full-length agrin in the cell lysate is fully digested and thus has vanished. S/A neurotrypsin could not cleave agrin, resulting in the detection of full-length agrin in the CL. The lower panel shows the presence of wt and S/A neurotrypsin in the co-expression detected with G93 (The Western blot was kindly provided by R. Reif and S Sales). **(B)** In vivo cleavage of agrin in the hippocampus homogenate. A similar pattern for agrin processing is observed. The upper panel is incubated with R132 antibody. Full-length agrin is detected in three distinct major bands above 250 kDa. The signals in transgenic (tg), primarily the two upper bands, are slightly reduced as compared to wild-type (wt) littermates. Consequently, there is an accumulation of the 90-kDa cleavage product in tg. Only a little effect is observed for the 112-kDa fragment. For the knock-out (KO) the upper two full-length agrin bands are most prominent, whereas the lowest one is very weak. No cleavage product, neither of 112 kDa nor for the 90 kDa, is detectable. The middle panel, incubated with R139, reveals an augmentation of the LG3domain in tg. KO is devoid of the C-terminal cleavage product. The lower panel shows the loading control with β-actin. **(C)** A schematic representation of the agrin domain structure. Indicated above the diagram are the calculated molecular masses of agrin cleavage products as a consequence of neurotrypsin activity. The cleavage sites were determined by N-terminal sequencing. The α-cleavage site is PIER | ASCY, at which the cleavage occurs after the Arg, resulting in a C-terminal 112-kDa fragment. The β-cleavage site is LVEK | SVGD. Here, the hydrolysis occurs after the Lys, resulting in C-terminal 22-kDa fragment consisting of the LG3 domain including the z-site. Upon cleavage at both sites the 90-kDa middle fragment is produced.

1.4 Agrin – an extracellular matrix heparan sulfate proteoglycan

Agrin was purified from the basal lamina from the synapse-rich electric organ of the pacific electric ray *Torpedo californica* in 1987 (Nitkin et al., 1987). Over a decade later the 'agrin hypothesis', which postulates that agrin is a nerve-derived trophic factor responsible for the assembly of the postsynaptic apparatus at the neuromuscular junction, has been confirmed. First, agrin-deficient mice do not form functional postsynaptic structures and die perinatally (Gautam et al., 1996). And second, agrin could activate synapse-specific gene expression and establish fully functional and mature synapses on innervated rodent muscles in non-synaptic regions (Bezakova et al., 2001; Jones et al., 1997).

1.4.1 Alternative splicing of agrin

In all species in which agrin has been identified, the gene encodes a protein of more than 2000 amino acids with a predicted molecular mass of 225 kDa (Fig. 1.11). The extensive N- and O-linked glycosylation of the N-terminal half increases the apparent molecular mass of agrin to ~600 kDa. At least three of the O-linked carbohydrate attachment sites serve as docking sites for heparan sulfate glycosaminoglycan (HS-GAG) side chains and assign agrin to the family

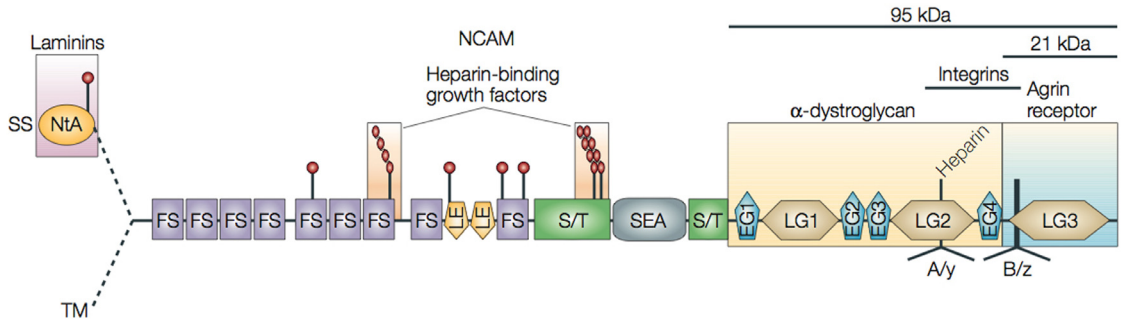

Figure 1.12 Schematic representation of agrin.
The structural domains, the sites of alternative mRNA splicing, and the binding regions of some of the most important partners for agrin are illustrated. The signal sequence (SS) and amino (N)-terminal agrin domain (NtA) are present in an agrin isoform that is localized to the NMJ. These two regions are responsible for the secretion of agrin (SS) and the binding to laminins in the basal lamina (NtA). The alternatively spliced type II transmembrane segment (TM) of agrin anchors this isoform at places that are devoid of basal laminae such as the ECM of the brain. The N-terminal half of agrin is highly glycosylated at Ser/Thr (S/T) attachment sites. These regions are involved in binding to NCAM L1 and heparin-binding growth factors. The C-terminal 95 kDa, a part of agrin is fully active in AChR aggregation and contains binding sites for α-dystroglycan, heparin some integrins and an as yet unidentified agrin receptor. The four amino acid-long insert at the A/y site is encoded by a separate exon. Similarly, the different inserts at the B/z site of 8, 11, and 19 amino acid are also encoded by separate exons. The most C-terminal 21-kDa LG3 domain is sufficient to induce AChR aggregation although at much lower potency. Its activity requires the eight amino acid insert. FS, follistatin-like domain; LE, laminin EGF-like domain; LG, laminin globular domain; SEA, sperm protein enterokinase and agrin domain.

of heparan sulfate proteoglycans (Tsen et al., 1995). Two different agrin isoforms resulting from alternative mRNA splicing are known (Fig. 1.11). One isoform encodes a cleaved signal sequence (SS) followed by the N-terminal agrin (NtA) domain (SS-NtA). The other isoform contains a shorter amino terminus with a type II transmembrane (TM) domain (TM-agrin). They affect the association of agrin to either the ECM, as only SS-NtA-agrin isoform can bind to laminins, or the membrane (TM-agrin) (Burgess et al., 2000; Neumann et al., 2001). Both isoforms can additionally be alternatively spliced in at least two more positions, which are known as the A/y and B/z sites (A and B and y and z are used to denote the sites in chicken or mammals, respectively). The splice sites are located in the C-terminal laminin-globular (LG) domains LG2 and LG3, respectively (Fig. 1.11). Splicing at the y-site gives rise to protein variants that can contain 0 or 4 amino acids. Insertion of 4 amino acids is required for heparin binding and modulates the binding of agrin to α-dystroglycan (Gesemann et al., 1996; Hopf and Hoch, 1996). On the other hand, splicing at the z-site (agrin-z^+) results in the insertion of 0, 8, 11 or 19 (8+11) amino acids. Inserts at the z-site are crucial for agrin-induced acetylcholine receptor (AChR) aggregation (Burgess et al., 1999). Interestingly, splicing at this site is regulated in a tissue-specific manner. The main source for the 'active' agrin form (agrin-z^+) is neuronal, including motoneurons. Transcripts from all other non-neuronal cells, except adult Schwann cells, encode 'inactive' agrin-z^-.

1.4.2 Agrin is an important organizer of the neuromuscular junction

Although, binding of NtA-agrin to laminins in the basal lamina of the NMJ is essential for maintaining the postsynaptic apparatus *in vivo*, the AChR-aggregating activity of agrin is retained in a soluble, 95 kDa fragment of the C-terminal part. Surprisingly, a 21 kDa fragment of agrin-z^+ that consists of the LG3 domain (LG3-z^+) still induces the maximal number of AChR aggregates *in vitro*, albeit with several-hundred-fold lower potency than full-length agrin or the 95 kDa fragment (Gesemann et al., 1995). This implies that agrin-z^+ interacts with its receptor through the LG3-z^+ domain. The 95 kDa agrin fragment binds to α-dystroglycan and activates the

muscle-specific receptor tyrosine kinase (MuSK). Originally, α-dystroglycan was proposed to be a functional agrin receptor that mediates downstream signaling leading to AChR aggregation (Bowe et al., 1994; Campanelli et al., 1994; Gee et al., 1994). But, α-dystroglycan also binds to the agrin-z^- with high affinity. Conversely, LG3-z^+ does not bind to α-dystroglycan. (Gesemann et al., 1996; Hopf and Hoch, 1996; Sugiyama et al., 1994). And the NMJ is formed even in the absence of α-dystroglycan (Cote et al., 1999; Grady et al., 2000; Jacobson et al., 2001) although their morphology is altered. Thus, α-dystroglycan does not seems to be involved in the primary formation of postsynaptic structures, although it might be involved in their consolidation. MuSK, on the other hand, is crucial for agrin-triggered signaling at the NMJ. MuSK-deficient mice lack any postsynaptic specializations at the nerve–muscle contact and die perinatally, as do agrin-deficient mice (DeChiara et al., 1996). Cultured myotubes devoid of MuSK do not aggregate AChR in response to agrin, and the ability of myotubes to aggregate AChRs recovers after MuSK expression is restored (Herbst et al., 2002). Agrin-z^+, but not agrin-z^-, induces MuSK phosphorylation and, as observed for AChR aggregation, the minimal activation fragment comprises the LG3-z^+ domain (Glass et al., 1996). Nevertheless, no direct interaction for agrin with neither MuSK nor AChR was shown. Thus, differentiated muscle cells contain yet another entity that functions as an 'agrin receptor', the identity of which is unknown until now.

1.4.3 The function of agrin in the brain

In addition to motor neurons, agrin mRNA has been detected in embryonic rat and chicken brains and in adult marine ray, suggesting that this molecule may also be involved in the formation of synapses between neurons. Northern blot and *in situ* hybridization indicated that agrin mRNA is expressed predominantly by neurons broadly distributed throughout the adult CNS. All four agrin-z transcripts are expressed in the adult CNS. z^0, z^8, and z^{19} were broadly expressed, z^{11} was detected only in the forebrain. Both the level of expression and the pattern of the alternative splice variants are differentially regulated in the brain (O'Connor et al., 1994). Notably, the structure with the highest agrin immunoreactivity in the brain is the microvasculature, in which agrin could bind to α-dystroglycan and laminin, and thus, stabilize the specialized basal lamina, which builds the blood–brain barrier. Furthermore, an increase in agrin protein levels precedes synaptogenesis in cultured hippocampal neurons. This increase in agrin expression is accompanied by its extracellular deposition along the distal third of the axon (Ferreira, 1999). The organizing role of agrin at the NMJ and its expression pattern in the brain indicate that it might orchestrate synaptogenesis in the entire nervous system. Indeed, agrin is important in regulating the formation of cholinergic interneuronal synapses in the superior cervical ganglion (SCG). Here, agrin-deficient embryos show a mismatch between pre- and postsynaptic structures and have defective synaptic transmission (Gingras et al., 2002). Importantly, soluble agrin-z^+ (but not agrin-z^-) restored the wild-type phenotype in cultured agrin-deficient SCGs. Agrin expressed in the SCG is TM-agrin (Gingras and Ferns, 2001) and could affect synaptogenesis through MuSK, which is expressed in neural tissue (Ip et al., 2000). The suppression of agrin expression in cultured hippocampal neurons by antisense oligonucleotide treatment resulted in the impairment of dendritic development and the formation of fewer synapses than in non-treated or sense treated neurons (Bose et al., 2000; Ferreira, 1999).

Agrin could function as a signaling molecule that interacts with a receptor other than MuSK. For instance, Hilgenberg (Hilgenberg et al., 1999; Hilgenberg and Smith, 2004) proposed that in neurons agrin signals via a receptor tyrosine kinase, which is coupled to the immediate-early

gene *c-fos*. The expression of *c-fos* was induced by agrin in a concentration-dependent and saturable manner. They further suggested that agrin binding to its receptor is associated with a rise in intracellular Ca^{2+}, a ubiquitous second messenger capable of mediating a wide range of intracellular effects such as activation of CaMK II or MAPK. The agrin-induced increase in intracellular Ca^{2+} is characterized by an initial release from intracellular stores, supplemented by an extracellular influx through voltage-gated calcium channels and was indistinguishable when agrin-z^+ or-z^- were applied. Consequently, the same group recently presented the α3 subunit of the Na^+/K^+-ATPase (NKA) as a neuronal receptor for agrin (Hilgenberg et al., 2006). They showed that the C-terminal agrin released after cleavage could bind and inhibit the ion pump activity and thus regulate presynaptic excitability. An increase in intracellular Na^+ due to an impaired NKA function depolarizes synaptic membranes and triggers Ca^{2+} influx through voltage-gated channels. Finally, increased cytoplasmic Ca^{2+} activates CaMK II and other Ca^{2+} effectors known to regulate a variety of synaptic functions such as neurotransmitter release and neurotransmitter receptor turnover.

To analyze the function of agrin in neurite outgrowth, TM-agrin was clustered on neurons using anti-agrin antibodies (Annies et al., 2006). On axons and dendrites from mouse hippocampal neurons anti-agrin antibodies induced a dose and time-dependent formation of numerous filopodia-like processes within minutes. These data provide evidence for a specific role of TM-agrin in shaping the cytoskeleton of neurites. In agreement with this, overexpression of TM-agrin caused the formation of filopodia on neurites of hippocampal neurons cultured for 1–6 days and increased Cdc42 activation (McCroskery et al., 2006). Conversely, suppression of agrin expression by siRNA reduced the number of filopodia. The N-terminal half of agrin was necessary for the induction of filopodia. By positively regulating filopodia in developing neurons, TM-agrin may influence the pattern of neurite outgrowth and synapse formation by increasing their initiation and stability.

In cultured agrin-deficient neurons, glutamatergic and GABAergic synapses still form (Serpinskaya et al., 1999). Moreover, electrophysiological analysis demonstrates that functional GABAergic synapses form between mutant neurons (Li et al., 1999). The frequency and amplitude of miniature postsynaptic glutamatergic and GABAergic currents are similar in mutant and age-matched wild-type neurons in culture. These results demonstrate that neuron-specific agrin is not required for the formation and early development for functional synaptic contacts between CNS neurons, and suggest that mechanisms of interneuronal synaptogenesis are distinct from those regulating synapse formation at the NMJ. Hence, synapses still form in the absence of agrin, albeit their stabilization seems to be agrin-dependent. Similarly, targeting any single molecule that has been implicated to have a function *in vitro* in synaptogenesis does not severely compromise the formation of synapses in the brain *in vivo*. It is therefore conceivable that several signaling systems provide compensatory mechanisms at central synapses. Such functional redundancy could also explain why synapses still form in the brain of agrin-deficient mice.

1.5 Mass spectrometry and protein analysis

Proteomics generally deals with the large-scale determination of cellular function directly at the protein level. Mass spectrometry (MS) has increasingly become the method of choice for the analysis of complex protein samples. MS-based proteomics is made possible by the availability of gene and genome sequence databases and technical and conceptual advances in many areas, most notably the discovery and development of protein ionization methods, as recognized by the 2002 Nobel prize in chemistry.

MS was restricted for a long time to small and thermostable compounds because of the lack of effective techniques to softly ionize and transfer the ionized molecules from the condensed phase into the gas phase without excessive fragmentation. In the late 1980s two techniques were developed that dramatically changed this situation and made polypeptides accessible to MS analysis — electrospray ionization (ESI) (Fenn et al., 1989) and matrix assisted laser desorption/ionization (MALDI) (Karas and Hillenkamp, 1988). Today mass spectrometers are used either to measure simply the molecular mass of a polypeptide or to determine additional structural features including the amino acid sequence and posttranslational modifications. In the former case, single-stage mass spectrometers are used, acting essentially as balances to weigh molecules. In the latter case, after the initial mass determination of precursor ions has occurred, specific ions are selected and subjected to fragmentation through collision-induced dissociation (CID). In such experiments, referred to as tandem mass spectrometry (MS/MS), detailed structural features of the peptides can be inferred from the analysis of the masses of the resulting fragments. In the context of proteomics, the key parameters for a mass analyzer are sensitivity, resolution, mass accuracy and the ability to generate information-rich ion mass spectra from peptide fragments (CID spectra). There are four basic types of mass analyzer currently used in proteomics research. These are the ion trap, time-of-flight (TOF), quadrupole or linear ion trap and Fourier transform cyclotron (FT-MS) analyzers. These mass spectrometers can be stand-alone or, in some cases, put together in tandem to take advantage of the strengths of each other (Fig. 1.12).

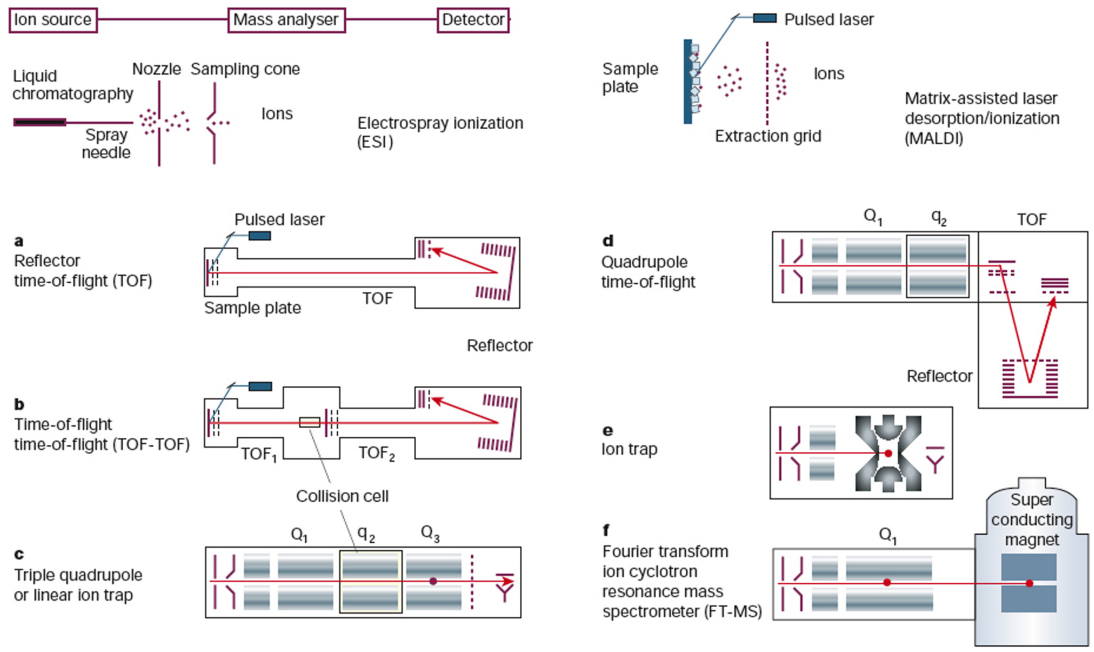

Figure 1.13 Mass spectrometers used in proteome research.
The left and right upper panels depict the ionization and sample introduction process in electrospray ionization (ESI) and matrix-assisted laser desorption/ionization (MALDI). The different instrumental configurations (a–f) are shown with their typical ion source. **a)** In reflector time-of-flight (TOF) instruments, the ions are accelerated to high kinetic energy and are separated along a flight tube as a result of their different velocities. The ions are turned around in a reflector, which compensates for slight differences in kinetic energy, and then impinge on a detector that amplifies and counts arriving ions. **b)** The TOF-TOF instrument incorporates a collision cell between two TOF sections. Ions of one mass-to-charge (m/z) ratio are selected in the first TOF section, fragmented in the collision cell, and the masses of the fragments are separated in the second TOF section. **c)** Quadrupole mass spectrometers select by time-varying electric fields between four rods, which permit a stable trajectory only for ions of a particular desired m/z. Again, ions of a particular m/z are selected in a first section (Q1), fragmented in a collision cell (q2), and the fragments are separated in Q3. In the linear ion trap, ions are captured in a quadruple section, depicted by the red dot in Q3. They are then excited via resonant electric field and the fragments are scanned out, creating the tandem mass spectrum. **d)** The quadrupole TOF instrument combines the front part of a triple quadruple instrument with a reflector TOF section for measuring the mass of the ions. **e)** The (three-dimensional) ion trap captures the ions, fragments ions of a particular m/z, and then scans out the fragments to generate the tandem mass spectrum. **f)** The FT-MS instrument also traps the ions, but does so with the help of strong magnetic fields. The figure shows the combination of FT-MS with the linear ion trap for efficient isolation, fragmentation and fragment detection in the FT-MS section.

1.5.1 Quadrupole ion trap vs. Fourier transform ion cyclotron mass spectrometry

The quadrupole ion trap (QIT) mass spectrometer was developed in parallel with the quadrupole mass analyzer by the Nobel prize winning mass spectrometry pioneer, Wolfgang Paul. His work in the early 1950's lead to the development of the basic parameters of today's benchtop instruments, however it took breakthroughs in design at Finnigan (MAT) in the 1980's to make the QIT-MS the simple to use practical instrument it is today. Commercial QIT instruments are today very amenable being coupled to ESI and MALDI ionization as well as to liquid chromatography.
The ions, produced in the source of the instrument, enter into the trap through the inlet and are trapped through action of the three hyperbolic electrodes: the ring electrode and the entrance and exit endcap electrodes. The ions are trapped in the space between these three electrodes by (alternating current) AC ~1 MHz and (direct current) DC, non-oscillating, static electric fields. The ring electrode radio frequency (RF) potential, an AC potential of constant

frequency but variable amplitude, produces a 3D quadrupolar potential field within the trap. This traps the ions in a stable oscillating trajectory. The exact motion of the ions is dependent on the voltages applied and their individual mass-to-charge (*m*/z) ratios. For detection of the ions, the potentials are altered to destabilize the ion motions resulting in ejection of the ions through the exit endcap. The ions are usually ejected in order of increasing *m*/z by a gradual change in the potentials. This 'stream' of ions is focused onto the detector of the instrument to produce the mass spectrum. The very nature of trapping and ejection makes a quadrupolar ion trap especially suited to performing MS^n experiments in structural elucidation studies. It is possible to selectively isolate a particular *m*/z in the trap by ejecting all the other ions from the trap. Fragmentation of this isolated precursor ion can then be induced by CID experiments. The isolation and fragmentation steps can be repeated a number or times and is only limited by the trapping efficiency of the instrument. MS^5 experiments are fairly routine with this set-up as is the coupling of liquid chromatography to perform LC-MS^n studies (March 2000).

Fourier transform ion cyclotron resonance (FT-ICR) mass spectrometry is a type mass spectrometer for determining the mass-to-charge ratio (m/z) of ions based on the cyclotron frequency of the ions in a fixed magnetic field (Fig. 1.12f). In the basic FT-MS instrument, the ions are generated in the source as usual and then pass through a series of pumping stages at increasingly high vacuum. When the ions enter the cell (ion trap) pressures are in the range of 10^{-10} to 10^{-11} mBar with temperatures close to absolute zero. The cell is located inside a spatial uniform static superconducting high field magnet cooled by liquid helium and liquid nitrogen. When the ions pass into the magnetic field they are bent into a circular motion in a plane perpendicular to the field by the Lorentz Force (see equation 1, below). They are prevented from processing out of the cell by the trapping plates at each end. The frequency of rotation of the ions is dependent on their *m*/z ratio (equation 2). At this stage, no signal is observed because the radius of the motion is very small. A RF pulse achieves excitation of each individual ion across the excitation plates of the cell. Each individual excitation frequency will couple with the ions natural motion and excite them to a higher orbit where they induce an alternating current between the detector plates. The frequency of this current is the same as the cyclotron frequency of the ions and the intensity is proportional to the number of ions. When the RF goes off resonance for that particular *m*/z value, the ions drop back down to their natural orbit (relax) and the next *m*/z packet is excited. Although the RF sweep is made up of a series of stepped frequencies, it can be considered as all frequencies simultaneously. These results in the measurement of all the ions in one go producing a complex frequency *vs*. time spectrum containing all the signals – the free induction decay (FID). Deconvolution of the FID by FT methods results in the deconvoluted frequency *vs*. intensity spectrum, which is then converted to the mass *vs*. intensity spectrum (the mass spectrum) by equation 3. Due to the ion-trap nature of FT-MS, it is possible to measure the ions without destroying them; this enables further experiments to be performed on the ions. The most common of these would be some kind of fragmentation study (MS/MS) for structural elucidation experiments.

(1) $\mathbf{F} = zv \times \mathbf{B}$

(2) $\omega_c = \frac{z\mathbf{B}}{2\pi m}$

(3) $m/z = \frac{\mathbf{B}}{2\pi\omega_c}$

- **F** is the Lorentz Force observed by the ion when entering the magnetic field
- **B** is the magnetic field strength (constant)
- v is the incident velocity of the ion
- ω_c is the induced cyclotron frequency
- *m* is the mass of the ion
- z is the charge on the ion

FT-ICR mass spectrometry is a very high-resolution technique in that masses can be determined with very high accuracy. Mass accuracy of better than 2 ppm with external calibration is common for most applications. Many applications of FT-ICR MS use this mass accuracy to help determine the composition of molecules based on accurate mass. Another place where FT-ICR MS is useful is in dealing with complex peptide mixtures since the resolution (narrow peak width) allows the signals of two ions of similar m/z to be detected as distinct ions. A maximum resolution of better than 500,000 can be achieved. Peptides with multiple charges can be produced by electrospray ionization. These peptides contain a distribution of isotopes that produce a series of isotopic peaks, which can be resolved by ICR. FT-ICR MS differs significantly from other mass spectrometry techniques in that the ions are not detected by hitting a detector such as an electron multiplier but only by passing near detection plates. Additionally the masses are not resolved in space or time as with other techniques but only in frequency. Thus, the different ions are not detected in different places as with sector instruments or at different times as with time-of-flight instruments but all ions are detected simultaneously over some given period of time.
The technique of ICR-MS was first published in the 1950's where it was demonstrated for the measurement of very small mass differences at very high precision by Hipple JA. The technique remained a largely academic tool until the application of FT methods by Alan Marshall and Melvin Comisarow in the early 1970's when it has become more widely used (Comisarow and Marshall, 1996).

1.5.2 Interpretation of MS/MS spectra

In mass spectrometry, CID is a mechanism by which molecular ions are fragmented in the gas phase. The ions are usually accelerated by some electrical potential to high kinetic energy in the vacuum of a mass spectrometer and then allowed to collide with neutral gas molecules (often helium, nitrogen or argon). In the collision some of the kinetic energy is converted into internal energy, which results in bond breakage and the fragmentation of the molecular ion into smaller fragments. These fragment ions can then be analyzed by a mass spectrometer. The fragment ions produced by CID are used for several purposes. Partial or complete structural determination can be achieved. Another use is in simply achieving more sensitive and specific detection. CID is used as part of tandem mass spectrometry for many experiments in proteomics. The CID mass spectra of peptides are very well suited for the determination of their amino acid sequence.
In a triple quadrupole mass spectrometer there are three quadrupole mass analyzers. The first quadrupole termed "Q1" can act as a mass filter that transmits a selected ion and accelerates it towards "q2" which is termed a collision cell (Fig. 1.12c). The pressure in q2 is higher and the ions collide with neutral gas in the collision cell and fragments by CID. The fragments are

then accelerated out of the collision cell and enter Q3, which scans through the mass range, analyzing the resulting fragments (as they hit a detector). This produces a mass spectrum of the CID fragments from which structural information or identity can be gained.
CID spectra in proteomics usually derive from tryptic peptides. It is generally accepted that usable CID spectra can only be obtained from peptides of less than 2 – 3 kDa, and trypsin produces peptides of this size or smaller. It seems that the easiest spectra to interpret are those generated from doubly charged precursors, where the resulting fragment ions mostly are singly charged with only a few doubly charged fragments. Doubly charged precursors also fragment such that most of the peptide bonds break with comparable frequency, increasing the likelihood to derive a complete sequence. Another reason for using trypsin proteolysis has to do with the desirability of placing basic residues, notably lysine and arginine, at the C-terminus of a peptide. It is a general observation that in low energy CID the presence of an arginine in the middle of a peptide will often result in the absence of fragmentations at several contiguous peptide bonds adjacent to the arginine. By putting the basic residues at the C-terminus, peptides fragment in a more predictable manner throughout the length of the peptide is achieved.

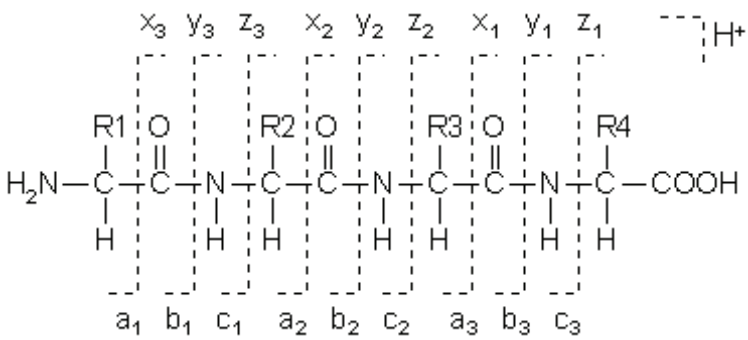

Figure 1.14 Sequence ions generated by collision induced dissociation (CID).
Fragments will only be detected if they carry at least one charge. If this charge is retained on the N terminal fragment, the ion is classed as either a, b or c. If the charge is retained on the C terminal, the ion type is either x, y or z. A subscript indicates the number of residues in the fragment.

The types of fragment ions observed in a CID spectrum depend on many factors including primary sequence, the amount of internal energy, how the energy was introduced, charge state, etc. The accepted nomenclature for fragment ions was first proposed by Roepstorff and Fohlman (Roepstorff and Fohlman, 1984), and subsequently modified by Johnson *et al.* (Johnson et al., 1987). Low energy CID of peptides results in a limited number of fragment ions. The key sequence-specific fragment ions are the y-type and b-type ions, and both of these can lose water (18.011u) or ammonia (17.027u). Usually, the y-type and b-type ions are more abundant than their corresponding losses of water or ammonia (Fig. 1.13). In addition to losing water or ammonia, the b-type ions can also lose CO (27.995 u) to give the so-called a-type ion, although these ions seem to occur most commonly for the lower mass fragments containing two, three, or four of the N-terminal residues. The prototypical CID spectrum of a tryptic peptide using a triple quadrupole contains a continuous series of y-type ions. The b-type ions are usually seen only at lower masses below the precursor m/z value and contain only a few of the N-terminal amino acids. Ion trap CID data of tryptic peptides is a bit different in that one often finds a continuous series of both b-type and y-type ions throughout the spectrum. This difference in intensity of b-type ions compared to triple quadrupoles is presumably due to precursor ions falling out of resonance with the excitation frequency in the trap. Once the molecule breaks

apart in the trap it ceases to undergo further fragmentations. This is in contrast to quadrupole collision cells where fragment ions continue to bump into neutral gas atoms with higher collision energy. Presumably, b-type ions are less stable than y-type ions, and when they form in a triple quadrupoles further collisions involving these fragments cause them to break down into smaller bits.
The bonds N-terminal to a proline residue seem to be particularly labile, whereas the bond on the C-terminal side is not. For peptides containing proline(s) this has the effect of producing a pattern where a y-type series of ions may have a particularly abundant y-type ion due to cleavage on the N-terminal side of proline, but the y-type ion resulting from cleavage on the C-terminal side of proline has a much reduced abundance or is sometimes absent. A similar phenomenon may be observed for peptides containing glycine, where the cleavage on the C-terminal side results in ions of reduced abundance (partially extracted from http://www.abrf.org/ResearchGroups/MassSpectrometry/EPosters/ms97quiz/SequencingTutorial.html).

1.5.3 MS analysis of partially purified proteins

Virtually every mass spectrometry–based proteomic workflow consists of three distinct stages: (i) Protein samples are isolated from their biological source and optionally fractionated. The final protein sample is then digested and the resulting peptide sample is further fractionated. (ii) The peptides are subjected to qualitative and optionally to quantitative MS analysis. (iii) The large data sets generated are analyzed by suitable software tools to deduce the amino acid sequence and, if applicable, the quantity of the proteins in a sample. The peptide identity is assigned to the CID spectra through database searching (Baldwin, 2004). A subsequent statistical analysis of the search results is critical to ensure confidence in the identifications (Keller et al., 2002). Using subcellular fractionation in combination with multi-dimensional mass spectrometry a lot of effort has been taken to determine proteomes of diverse organisms, organelles, body fluids, such as the cerebral spinal fluid (Pan et al., 2007; Yuan and Desiderio, 2005; Zhang et al., 2005a; Zhang et al., 2005b) and urinary (Adachi et al., 2006), and even protein complexes (Husi et al., 2000). For the large-scale analysis of yeast proteome, tryptic peptides of different fractions of *S. cerevisiae* whole cell-lysates were loaded onto a biphasic microcapillary column packed with strong cation exchange (SCX) and reverse-phased (RP) materials (Washburn et al., 2001). The column was directly coupled to a Finnigan LCQ ion trap mass spectrometer and peptides were first displaced from the SCX to the RP by a salt gradient followed by elution from the RP into the MS. The tandem mass spectra acquired were correlated to theoretical mass spectra generated from protein or DNA databases by the SEQUEST algorithm (Eng et al., 1994). A total of 1,484 proteins were detected and identified. Categorization of the hits demonstrated the ability of this technology to detect and identify proteins rarely seen in proteome analysis, including low abundance proteins like transcription factors and protein kinases. In addition, 131 proteins with three or more predicted transmembrane domains were detected. Furthermore, the high throughput protein profiling of another frequently used model organism, *C. elegans*, resulted in the identification of 1616 proteins, including 110 secreted and 242 transmembrane proteins (Mawuenyega et al., 2003). Very recently a high-quality catalog of the proteome of *Drosophila Melanogaster* was published (Brunner et al., 2007). They identified 63% of the predicted *D. Melanogaster* proteome by detecting 9124 proteins from 498000 redundant and 72281 distinct peptide identifications. This was achieved by combining sample diversity, multidimensional biochemical fractionation and analysis-driven experimentation feedback loops. The collection

of the data was guided by statistical analysis of prior data.
In addition subcellular fractions were subjected to MS-based proteome analysis. To investigate the protein composition of the postsynaptic density (PSD), synaptosomal preparations were enriched from brain homogenates by differential and density gradient centrifugation followed by an extraction with 0.5% Triton-X 100. Proteins were then separated by SDS-PAGE and the in-gel digested gel slices were analyzed by either MALDI-TOF (Walikonis et al., 2000) or LC-ESI-MS (Peng et al., 2004). Over 370 different proteins that copurified with the PSD structure and thirteen phosphorylated sites from eight proteins were discovered. These proteins were classified into numerous functional groups, revealing crucial information about the molecular diversity in the PSD, and provided a basis for further studies on the molecular mechanisms of synaptic function and plasticity. Moreover, molecules associated with or inserted into the synaptic plasma membrane were identified using analogous techniques (Stevens et al., 2003). In general, the analysis of organelles with proteomic methods is an active field of research, and significant progress has been made in defining the proteomes of multiple organelles. Hence, organelles and other large cellular structures have been analyzed, (e.g. plasma membrane, ER, lipid rafts, mitochondria, exosomes, clathrin-coated vesicles, lysosomes, centrosome/spindle poles, midbodies, cytoskeleton, phagosomes, peroxisomes, Golgi, nuclear pores, nucleolus, nuclear envelope (Yates et al., 2005)).
To dig deeper into even smaller entities of multi-protein structures, constituents of protein complexes were investigated by MS. So far, the number and identities of proteins in each subunit of the 80S ribosomes from *S. cerevisiae* have been determined primarily by isolating the ribosomal particles, electrophoretically separating the proteins and sequencing the proteins by Edman degradation. The effort of several groups was needed to estimate that the yeast 80S ribosome complex contains 78 different proteins present at unimolar amounts (32 proteins in the 40S and 46 in the 60S subunits). Now, multi-dimensional mass spectrometry was applied to isolated ribosomes resulting in the identification of 75 of the 78 predicted ribosomal proteins and of one novel protein component (YMR116p) of the yeast and human 40S subunit (Link et al., 1999). Another fundamental study that reveals the protein composition of the NMDA receptor-signaling (NRC) complex underscores the tremendous potential of multi-dimensional LC-ESI-MS/MS. The receptor complex was isolated from mouse forebrain extracts using covalently coupled NR1 immunoaffinity resins, immunoprecipitation with NR1 specific antibody, and peptide-affinity chromatography with a hexapeptide of the NR2B C-terminus (Husi et al., 2000). The NRC comprised 77 proteins organized into receptor, adaptor, signaling, cytoskeletal and novel proteins, of which 30 are known from binding studies and another 19 participate in NMDAR signaling. NMDAR and metabotropic glutamate receptor subtypes were linked to cadherins and L1 cell-adhesion molecules in complexes lacking AMPA receptors. These neurotransmitter–adhesion receptor complexes were bound intracellularly to kinases, phosphatases, GTPase-activating proteins and Ras with effectors including components of the MAPK pathway.

1.5.4 Strategies for quantitative peptide analysis

To add a quantitative dimension to peptide LC-MS/MS experiments, the technique of stable-isotope labeling has been applied. This method makes use of the fact that pairs of chemically identical analytes of different stable-isotope composition can be differentiated in a mass spectrometer thanks to their mass difference. The ratio of signal intensities for such analyte pairs accurately indicates the abundance ratio for the two analytes (Fig. 1.14). To this end,

stable-isotope tags have been introduced to proteins via metabolic labeling using heavy salts or amino acids (Conrads et al., 2002), enzymatically via transfer of ^{18}O from water to peptides (Mirgorodskaya et al., 2000; Yao et al., 2001), or via chemical reactions using isotope-coded affinity tags (ICAT) or similar reagents (Gygi et al., 1999b; Zhou et al., 2002). Post-isolation chemical isotope tagging of proteins is currently the most versatile and most commonly used labeling method. An attractive feature of this approach is that the selectivity of the labeling reactions can be used to direct the isotopes and attached affinity tags to specific functional groups or protein classes, thus enabling their selective isolation and analysis. So far, isotope-tagging chemistries have been described that are specific for sulphhydryl groups (Gygi et al., 1999b; Zhou et al., 2002), amino groups (Munchbach et al., 2000), the active sites for serine (Liu et al., 1999) and cysteine hydrolases (Greenbaum et al., 2000), for phosphate ester groups (Oda et al., 2001; Zhou et al., 2001) and for *N*-linked carbohydrates (Zhang et al., 2003). Recently, a method called 'stable-isotope labeling with amino acids in cell culture', or SILAC, has been described (Ong et al., 2002). In this method, one cell state is metabolically labeled with light and the other with heavy form of a particular amino acid, for example, ^{13}C-labeled arginine. Potentially all peptides can be labeled and the absence of any chemical steps make the method easy to apply as well as compatible with multistage purification procedures.

In summary, quantitative proteomics provide a tool for the identification and quantification of hundreds and thousands of proteins from complex mixtures simultaneously. Despite the high sensitivity of the today's mass spectrometers, a detailed validation of the enormous amount of data acquired is needed. Nonetheless, proteomics is a useful technique for high throughput profiling of protein regulation and screening for candidate molecules in a perturbed system.

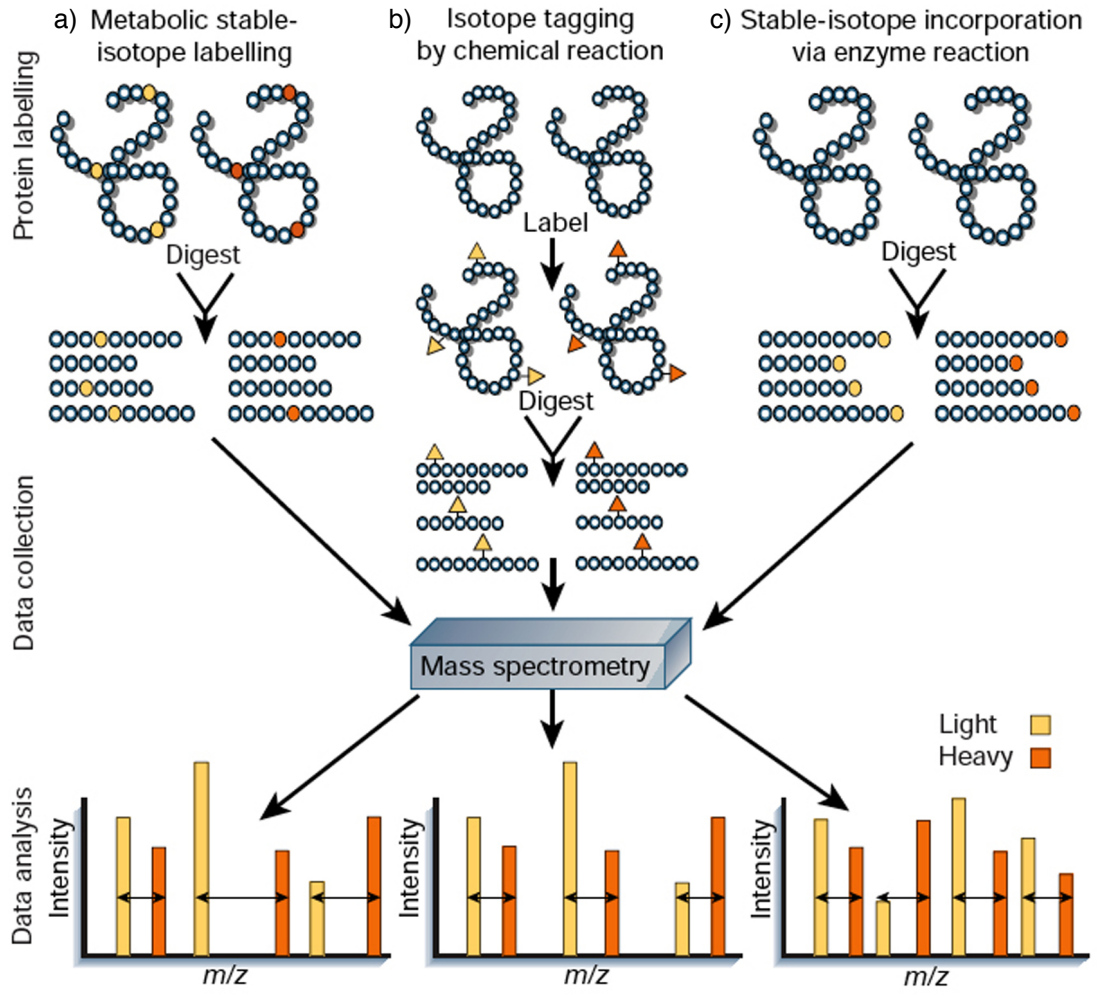

Figure 1.15 Schematic representation of methods for stable-isotope protein labeling for quantitative proteomics. **A)** Proteins are labeled metabolically by culturing cells in media that are isotopically enriched (for example, containing ^{15}N salts, or ^{13}C-labeled amino acids or isotopically depleted. **B)** Proteins are labeled at specific sites with isotopically encoded reagents. The reagents can also contain affinity tags, allowing for the selective isolation of the labeled peptides after protein digestion. The use of chemistries of different specificity enables selective tagging of classes of proteins containing specific functional groups. **C)** Proteins are isotopically tagged by means of enzyme-catalyzed incorporation of ^{18}O from ^{18}O water during proteolysis. Each peptide generated by the enzymatic reaction carried out in heavy water is labeled at the C-terminus. In each case, labeled proteins or peptides are combined, separated and analyzed by mass spectrometry and/or tandem mass spectrometry for the purpose of identifying the proteins contained in the sample and determining their relative abundance. The patterns of isotopic mass differences generated by each method are indicated schematically. The mass difference of peptide pairs generated by metabolic labeling is dependent on the amino acid composition of the peptide and is therefore variable. The mass difference generated by enzymatic ^{18}O incorporation is either 4 Da or 2 Da, making quantitation difficult. The mass difference generated by chemical tagging is one or multiple times the mass difference encoded in the reagent used.

1.5.5 Isotope-coded affinity tag (ICAT)

Protein labeling with isotope-coded affinity tags (ICAT) followed by tandem mass spectrometry allows sequence identification and accurate quantification of proteins in complex mixtures (Fig. 1.15). It has been applied to the analysis of global protein expression changes in yeast (Gygi et al., 1999b; Smolka et al., 2001), to identify protein changes in subcellular fractions comparing the PSD proteome from rat forebrain and cerebellum, identifying the alterations in protein expression in the synaptic plasma membrane of hippocampal PSD proteins after morphine administration (Cheng et al., 2006; Moron et al., 2007; Prokai et al., 2005). Components of

protein complexes were compared such as RNA polymerase II pre-initiation complex (PIC) and a control sample or the protein composition of different subtypes of 20S proteasome subunits were determined (Ranish et al., 2003; Schmidt et al., 2006). And protein secretion and body fluids were analyzed quantifying proteins from the urinary of mice deficient in factor H or comparing human cerebrospinal fluid (CSF) from aged vs. young individuals and from patients with AD vs. healthy individuals (Braun et al., 2006; Zhang et al., 2005a; Zhang et al., 2005b). The method is suitable for large-scale analysis of complex samples including whole proteomes and allows quantitative analysis of proteins. The ICAT approach is based on two principles. First, a short sequence of contiguous amino acids from a protein (e.g. trypsinized peptides of 5–25 residues) contains sufficient information to identify that unique protein. Second, pairs of peptides tagged with the light and heavy ICAT reagents, respectively, are chemically identical and therefore serve as ideal mutual internal standards for accurate quantification. In MS, the ratios between the peaks intensities of the lower and upper mass of the pairs provide an accurate measure of the relative abundance of the peptides (and hence the proteins) in the original sample pools. This is because the MS intensity response to a given peptide is independent of the isotopic composition of the ICAT reagents. The data of this report provide the first comprehensive proteomic profiling of a transgenic mouse line using the ICAT technology.

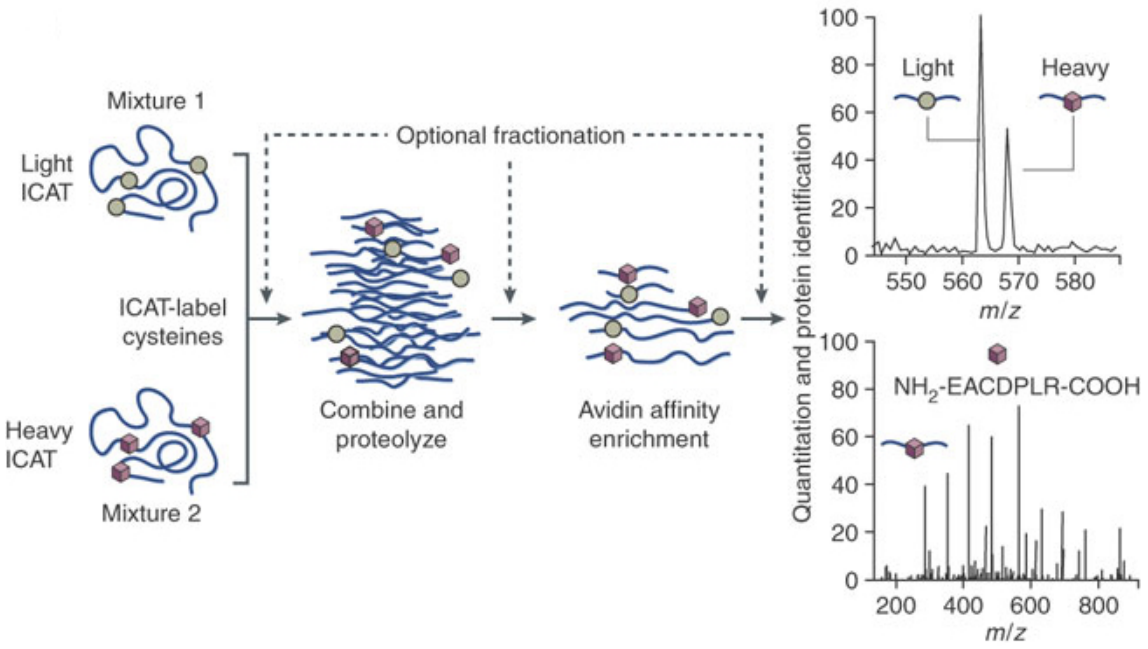

Figure 1.16 The ICAT strategy for identifying and quantifying differential protein expression.
Two protein mixtures representing two different samples are treated with the isotopically light and heavy ICAT reagents, respectively; an ICAT reagent is covalently attached to each cysteinyl residue in every protein. Proteins from sample 1 are shown in green, and proteins from sample 2 are shown in blue. The protein mixtures are combined and proteolyzed with trypsin to peptides, and ICAT-labeled peptides are isolated utilizing the biotin tag. These peptides are separated by microcapillary high-performance liquid chromatography. A pair of ICAT-labeled peptides is chemically identical and is easily visualized because they essentially co-elute. There is a 9 Da mass difference measured in a scanning mass spectrometer (4.5 mass-to-charge (m/z) units difference for a doubly charged ion). The ratios of the original amounts of proteins from the two samples are strictly maintained in the peptide fragments. The relative quantification is determined by the ratio of the peptide pairs. Every other scan is devoted to fragmenting and then recording sequence information about an eluting peptide (tandem mass spectrum). Computer searching of the recorded sequence information against large protein databases identifies the protein.

2. Aim of this work

The focus of the group where this work was performed is to characterize the function of neurotrypsin proteolytic and non-proteolytic activity in the brain and the NMJ. In a screen for trypsin-like serine peptidases, neurotrypsin mainly was found in the nervous system. Spatial and temporal distribution suggested a role for neurotrypsin in processes such as synaptic plasticity that is generally accepted to be involved in learning and memory. As mentioned earlier agrin is a substrate for neurotrypsin but the functional role of the cleavage and the molecular fate of the resulting fragments are as yet unknown. Consequently, no generic downstream signaling pathway could be assigned to the agrin cleavage. Furthermore, despite of the conspicuous non-catalytic domains neither additional substrates nor other proteolytic-independent binding partners of neurotrypsin could be found.

This study was performed to shed light on the molecular function of neurotrypsin proteolytic and non-proteolytic activity using a quantitative proteomic analysis. To this end transgenic mice overexpressing neurotrypsin under the control of the brain specific promotor Thy-1.2 were generated and synaptosomes as well as hippocampal subcellular fractions of transgenic mice were compared with their wild-type litter mates. For the proteomic profiling two complementary approaches were chosen. Firstly, peptides of the two states were labeled with either light or heavy isotope-coded affinity tags (ICAT) followed by fractionation and affinity purification and subsequent measurement by LC-ESI-MS. The acquired CID spectra were cross-correlated with theoretical spectra to identify peptide sequences, which in turn were assigned to specific proteins. Relative quantification of each protein (ICAT light wild-type versus ICAT-heavy transgenic samples) was calculated using Automated Statistical Analysis on Protein Ratio (ASAP Ratio) and XPRESS software that both reconstructed ion chromatograms for the peptide ions measured. Secondly, proteins were fractionated and then separated by two-dimensional polyacrylamide gel electrophoresis (2DE). Spot intensities from wild-type and transgenic mice were compared using Proteomweaver and differentially regulated spots were excised and identified by MALDI TOF-TOF mass spectrometry.

Computer based analysis and manual inspection of the high throughput data put forth a set of proteins with changed abundance ratios. Finally, candidate proteins whose expression profile has been changed due to either direct or indirect interaction with neurotrypsin were validated by Western blot or immunohistochemical analysis.

3. Results

3.1 Neurotrypsin in the mouse brain

3.1.1 Neurotrypsin is expressed in synaptosomes and the hippocampus

The expression of neurotrypsin in human brain was found in presynaptic nerve endings of cortical synapses (Molinari et al., 2002). Immunogold localization at synapses with affinity-purified antibodies raised against the proteolytic domain of neurotrypsin showed exclusive labeling of presynaptic terminals in the region lining the synaptic cleft, the active zone. In addition, due to the signal peptide for secretion and multiple non-catalytic domains, well known from other secreted peptidases, neurotrypsin is possibly released into the synaptic cleft and remains associated with membrane bound pre- or postsynaptic components or the ECM within the cleft.

3.1.1.1 Isolation of synaptosomes

To investigate the expression level of neurotrypsin and to search for changes in protein expression in neurotrypsin-overexpressing mice by isotope-coded affinity tag (ICAT) technology, synaptosomes were isolated from whole brain homogenate of P20 and P40 mice (Fig. 3.1a). Synaptosomes are isolated synapses produced by subcellular fractionation of brain tissue. They are formed during mild disruption. Shearing forces cause the nerve endings to break off and by subsequent resealing of the membranes, synaptosomes are generated (Turner AJ, 1997). They contain the complete presynaptic terminal, including the synaptic cleft, synaptic vesicles, mitochondria and the attached postsynaptic density (PSD). Synaptosomes retain the morphological features and chemical composition of the synaptic boutons (Fig. 3.1b). Apart from the fact that synaptosomes represent a highly specialized subcellular fraction, they also include impurities, e.g. cell debris, intracellular organelles such as nuclei, Golgi, ER or lysosomes, and more pronounced, components of astroglial origin. However, synaptosomes are preferentially isolated from whole brain homogenate of adolescent and adult mice while endogenous neurotrypsin expression in the developing CNS. E.g. the diencephalon and the cerebellum are largely devoid of staining (Wolfer et al., 2001). Depending on the neuronal tissue, the expression is strongest in late embryonic stages and stays high until postnatal day 15 (P15) after birth and seems to decline during adolescence. Therefore, we decided also to analyze a more defined area of the brain, the hippocampus, which is known to express high levels of neurotrypsin starting from P4 to P10.

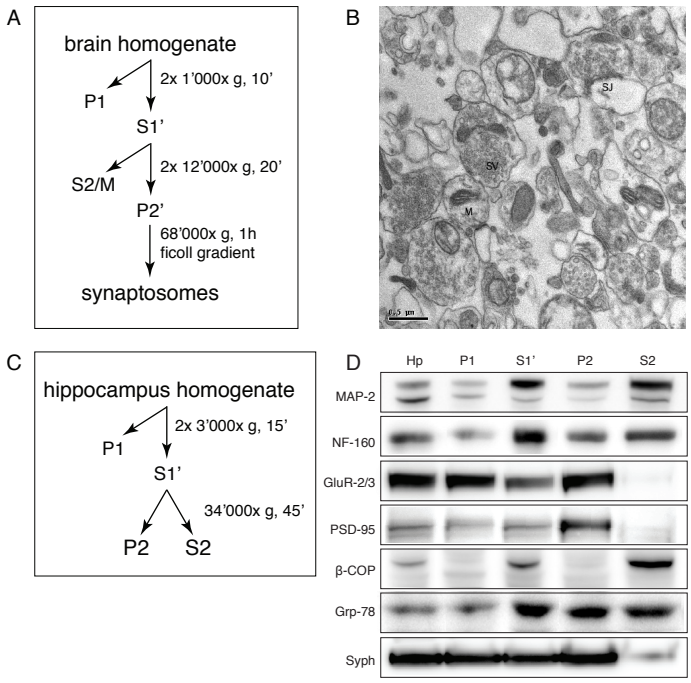

Figure 3.1 Isolation of synaptosomes and subcellular fractionation of the hippocampus.
(A) Schematic diagram of the preparation of synaptosomes. Synaptosomes are obtained after homogenization and subcellular fractionation of brain tissue. The fractionation involves differential and density-gradient centrifugation to separate synaptosomes from nuclei (P1), cell debris (S2), and mitochondria (M). **(B)** Representative electron micrograph of isolated synaptosomes. Pre- and postsynaptic components, mitochondria, as well as impurities are present in the sample. SV, synaptic vesicle; SJ, synaptic junction; M, mitochondira (Schrimpf et al., 2005). **(C)** Subcellular fractionation of the hippocampus using three centrifugation steps results in a pelletous (P2) and a soluble fraction (S2). **(D)** Marker protein analysis of the hippocampus fractions. Pre- and postsynaptic markers synaptophysin, glutamate receptors 2 and 3 (GluR-2/3), and postsynaptic density protein-95 (PSD-95) are enriched in P2 as opposed to S2. Dendritic microtubule-associated protein-2 (MAP-2) and Golgi specific β-COP are accumulated in S1' and S2. Neurofilament-NF-160 and ER protein Grp-78 are distributed likewise in S1', P2, and S2. Hp: hippocampus homogenate.

3.1.1.2 Subcellular fractionation of the hippocampus

Hippocampi of P10 mice were dissected and subjected to subcellular fractionation (Fig 3.1c). Cell debris and nuclei were removed by two repetitive centrifugation steps at 1'000x g. The resulting supernatant S1' was further subdivided with a 34'000x g centrifugation step into a pelletous fraction P2 and a soluble fraction S2. In order to characterize the hippocampal fractions, marker proteins were immunoblotted (Fig. 3.1d). Striking evidence suggests that P2 very much resembles the synaptosomes. Presynaptic synaptophysin and postsynaptic markers glutamate receptors 2 and 3 (GluR2/3) as well as postsynaptic density protein-95 (PSD-95) were heavily enriched in P2 as opposed to S2. Obviously, also cytosolic proteins like microtubule-associated protein 2 (MAP2), neurofilament-160 (NF-160), and the ER-marker Grp-78 were present in P2, indicating that P2 was contaminated with extra synaptic molecules. S2 was virtually devoid of GluR 2/3, PSD-95, and synaptophysin, whereas MAP2 and the Golgi-marker β-COP were strongly, and NF-160 was slightly enriched. Grp-78 was evenly distributed when comparing P2 and S2. Altogether, conspicuous data demonstrate that S2 mainly consists of soluble cytosolic proteins, whereas P2 includes more membranous or membrane associated molecules. Importantly, all forthcoming studies in this report, comparing wild-type with transgenic animals, were either performed with synaptosomes of P20 and P40 mice or with hippocampal subcellular fractions S2 and P2 of P10 mice.

3.1.1.3 Detection of neurotrypsin in wild-type and overexpressing mouse lines

Until now, neurotrypsin protein has not been detected in mouse CNS. In order to detect neurotrypsin we used, two polyclonal antibodies G87 and G93 raised against the protease domain (PD) of human neurotrypsin (hNT) and against the full-length (fl) protein of mouse neurotrypsin (mNT), respectively. Synaptosomes were isolated from a pool of whole brains of P12 – P15 wild-

type and human neurotrypsin-overexpressing transgenic mice (M491S). Brain homogenates, supernatant S2, and synaptosomes were loaded onto a SDS-PAGE and immunodetected with G93 antibody. Endogenous mNT with a calculated molecular mass of 84.1 kDa was found in equal amounts in wild-type and transgenic mice and evenly distributed among the fractions (Fig. 3.2a, arrowhead). This is a contradictory finding to the immunogold labeling for neurotrypsin previously performed in our laboratory, which showed an accumulation of gold particles in the presynaptic active zone (Molinari et al., 2002). Yet the signal was absent in the brain homogenate of the neurotrypsin knock-out (KO) mice. The human transgene though with a M_r: 97.0 kDa, was enriched in the transgenic samples (3.2a, asterisk), indicating an overexpression of hNT. The background signal in the wild-type samples running exactly at the same size was also seen in the KO, suggesting that an unspecific band was recognized by G87. PSD-95 was used as a loading control and to show an enrichment of synaptic components in the synaptosomes.
In addition, neurotrypsin expression was also probed by immunoblot assay in the hippocampal fractions comparing wild-type and transgenic M494 mice, using G87. Here, endogenous full-length protein was enriched in pelletous fraction P1, and particularly in P2 (Fig. 3.2b, arrowhead). The transgenic full-length hNT was also strongest in P2 and basically absent in S2 (Fig. 3.2b, asterisk). Interestingly, the antibody also recognized the unspecific band in the hippocampus, but to a lesser extent as opposed to the synaptosomes. On the one side, native PD was highly abundant in P1 and in P2 of wild-type samples (Fig. 3.2b, PD). On the other hand, an accumulation of exogenous PD in P1 of transgenic samples was not observed. Anyhow, there is strong evidence for an induction of human neurotrypsin expression in the hippocampus, since in all other fractions, although weakly, an increased signal for full-length protein and PD was found in transgene samples. Taken together, these data suggest a moderate overexpression of hNT in the transgenic mouse lines M491S and M494. Furthermore, a generic accumulation of endogenous neurotrypsin in synaptosomes was not found. Instead, full-length endogenous neurotrypsin was enriched in P2 fractions of the hippocampus, whereas the PD was enriched in P1.

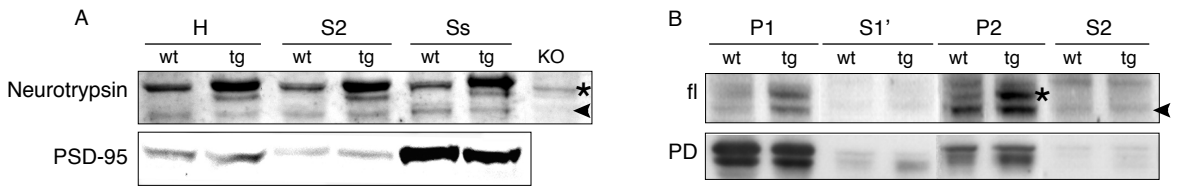

Figure 3.2 Neurotrypsin expression in synaptosomes and the hippocampus of wild-type and transgenic mice. **(A)** Detection of neurotrypsin in brain homogenate (H), supernatant 2 (S2), and synaptosomes (Ss) of P12 - P15 wild-type (wt) and M491S transgenic (tg) mice with G93 antibody raised against full-length mouse neurotrypsin. The double band represents the human neurotrypsin overexpressed in transgenic samples (asterisk). The lower band is endogenous mouse neurotrypsin, which is absent in the neurotrypsin knock-out (KO) mouse (arrowhead). PSD-95 immunoblot confirms the enrichment of postsynaptic elements in synaptosomes (the picture was kindly provided by A. Stephan). **(B)** Both the endogenous mouse (arrowhead) and the overexpressed human (asterisk) full-length (fl) form of neurotrypsin are enriched in the pelletous fractions P1 and P2 of the hippocampus. Similarly, the protease domain (PD) is more abundant in P1 and P2, compared to the soluble fractions S1' and S2. The signals for exogenous full-length protein and PD are enriched in transgenic samples (M494).

3.2 Neurotrypsin cleaves agrin in cell culture and in the CNS

3.2.1 Agrin processing by neurotrypsin in synaptosomes and in the hippocampus

In the CNS the type II transmembrane form of agrin-$y^4z^{-/+}$ is predominant (Neumann et al., 2001). To test whether agrin is enriched in synaptosomes, protein extracts of whole brain homogenate (H), supernatant S2, and synaptosomes (Ss) from M491S were loaded on a 4 – 12% NuPAGE gel in equal amounts and immunoblotted with R132 antibody raised against the 90-kDa agrin fragment and R139 antibody against the LG3 domain (Fig. 3.4a). In contrast to the smeary full-length agrin signal from the cell culture assay, agrin full-length protein was resolved in three distinct bands above 250 kDa. It might well be that they represent different glycosylation forms of agrin. Compared to transgenic samples the uppermost band was strongest mainly in wild-type synaptosomes. Interestingly, it was this particular form of agrin that disappeared in the transgenic samples. Here again, the most outstanding change was observed in synaptosomes, suggesting a preferential cleavage of the fully glycosylated form of full-length agrin. Furthermore, the 90-kDa cleavage product was accumulated in wild-type S2 as compared to wild-type H and wild-type Ss, indicating a release into the ECM of the fragment after cleavage. Without controversy, the fragment was enriched in every transgenic sample, implying an increased cleavage by neurotrypsin. Similar observations were made for the LG3 domain, which was strongest in the S2 fraction when comparing wild-type samples. (Fig. 3.4a).

Western blotting of hippocampal subcellular fractions homogenates revealed a similar picture of the agrin fragment distribution using R132 and R139 antibodies (Fig. 3.3b and 3.4b – d). In wild-type samples three distinct agrin full-length bands were detected all of which appeared above 250 kDa. In M494 transgenic mice, the intensity of the lowest band of the three was similar to wild-type, while the upper two were seemingly reduced. Surprisingly, exactly these two upper bands of agrin were by far the most abundant ones in the KO samples, whereas the lowest band was weaker (Fig. 3.3b). Consequently, neurotrypsin might preferentially cleave the upper full-length agrin forms also in the hippocampus. Comparing the various fractions of wild-type hippocampal fractions, a different distribution of agrin full-length variants was observed. While in the pelletous fraction P1, which mainly consists of nuclei and heavy membranous compartments like ER, the putatively immature forms of agrin were strongly represented, the situation had completely changed in supernatant S1 and pelletous fraction P2. Mainly in P2, the potentially fully glycosylated form of agrin was enriched, whereas in soluble fraction S2, composed of cytosolic molecules and light membranous structures like Golgi, all agrin full-length forms were more or less evenly distributed. These findings indicate that during secretion, agrin might run through a maturation process that ends with a fully glycosylated form that is most susceptible to neurotrypsin cleavage. In wild-type, both the 112-kDa and the 90-kDa intermediate agrin fragments were produced in equal amounts, whereas in the transgenes the production of the 90-kDa fragment was increased due to excessive proteolytic activity at the α- and β-cleavage sites. In the KO however, no cleavage product was found at all (Fig. 3.4b and c). The same observations were made for the immunodetection of the LG3 domain. Stronger signals were detected in the hippocampus of neurotrypsin-overexpressing mice as compared to wild-type littermates. No LG3 domain was found in the neurotrypsin KO (Fig. 3.4b and c). In the control line S/A 785, overexpressing an inactive variant of neurotrypsin, no differences

were found comparing wild-type and transgene (Fig. 3.4d). Moreover, a comparison of the 104 and 90-kDa fragments as well as the LG3 domain among the subcellular fractions, showed an enrichment of the signals in S2 wild-type, suggesting a release of the cleavage products from heavy membranous structures such as the synaptic plasma membrane (Fig. 3.4b – d). These data provide evidence supporting the hypothesis that agrin is specifically cleaved by neurotrypsin *in vivo*. In neurotrypsin-overexpressing mice an accumulation of the agrin cleavage products and a decline of the potentially fully glycosylated mature full-length agrin form was demonstrated. In addition, due to the lack of neurotrypsin activity in the KO, there is first of all no production of any cleavage product, and second of all an accumulation of the uncleaved full-length agrin forms. Noticeable the most susceptible agrin variant to neurotrypsin cleavage is enriched in P2. Nevertheless, the fate of the cleavage products remains to be shown.

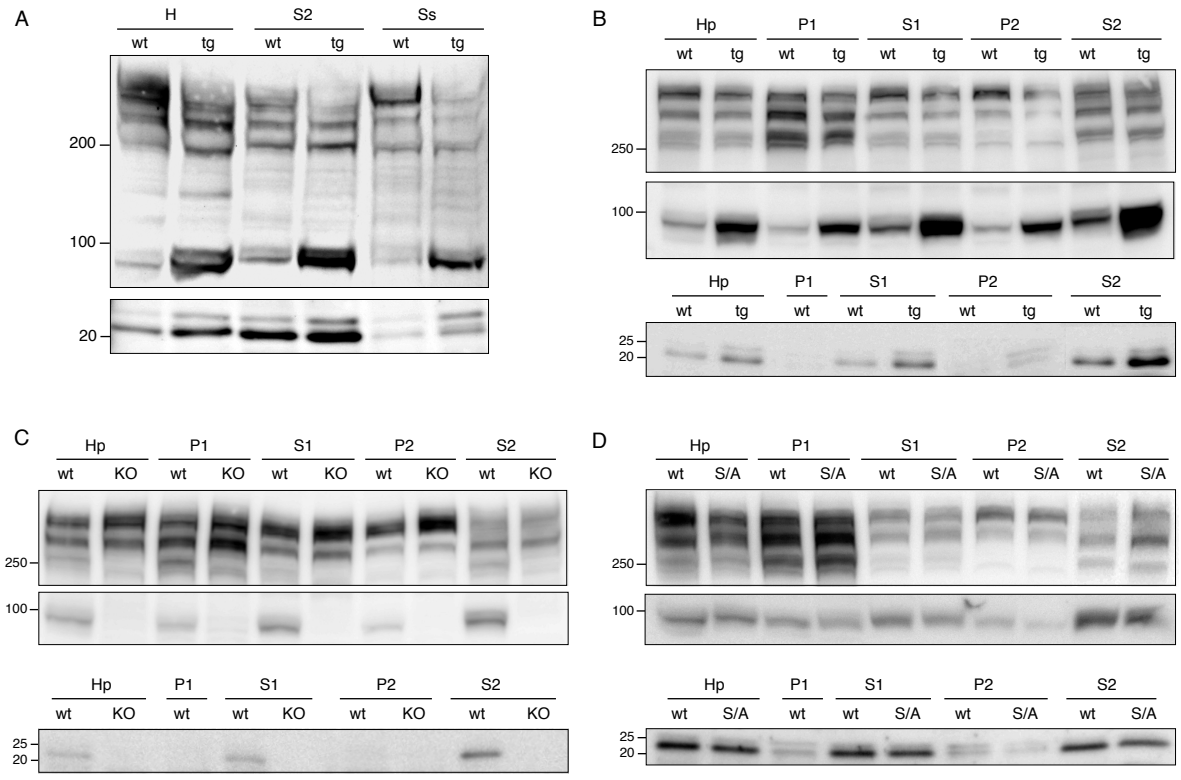

Figure 3.3 Agrin processing by neurotrypsin in synaptosomes and in the hippocampus.
(A) Immunoblot with R132 antibody against the 90-kDa fragment of whole mouse brain homogenate (H), supernatant 2 (S2), and synaptosomes (Ss) detects three major agrin full-length bands. Comparing wild-type (wt) and transgenic (tg) samples the uppermost band is strongest in wt Ss and S2. The 90-kDa fragment of agrin is enriched in the tg samples (upper panel). Consequently, when R139 antibody, directed against the laminin globular domain 3 (LG3) is used the signal is also enriched in tg (lower panel). The Western blot was kindly provided by A. Stephan. **(B)** An immunoblot of M494 hippocampus homogenate (Hp) and its subcellular fractions using R132 antibody detects three full-length agrin bands (upper panel). In the supernatant 1 (S1), and pelletous fraction 2 (P2), the upper band is most prominent and is processed most intensively, when comparing wt and tg. Otherwise, the three bands in pellet 1 (P1) and soluble fraction 2 (S2) are evenly distributed. In wt, the strongest enrichment of the 90-kDa agrin fragment is seen in S2 (middle panel). An increase in the cleavage product is clearly observed in tg samples. Strong evidence for an increased cleavage of agrin in tg is the fact that the LG3 domain (lower panel) is also increased. The fragment can hardly be detected in wt P1 and P2, whereas it is enriched in S2. **(C)** In the neurotrypsin knock-out mouse (KO) the distribution of agrin full-length protein is similar to (B), but as expected, a decline of the upper band is not observed (upper panel). In addition, absolutely no signal is seen for the 90-kDa (middle panel) and the LG3domain (lower panel). **(D)** An immunoblot of agrin from control mice overexpressing a proteolytic inactive form of neurotrypsin (S/A) shows no increase of agrin cleavage products, when comparing wt and tg. The distribution of agrin full-length bands is as described above.

3.3 Proteomic profiling of synaptosomes and the hippocampus comparing wild-type and transgenic mice

In the search for neurotrypsin-dependent differences in protein regulation, proteomic profiling using isotope-coded affinity tags (ICAT) and mass spectrometry was performed. Samples from wild-type mice were compared with samples from transgenic mice overexpressing neurotrypsin under the control of the Thy-1.2 promotor. The mouse lines used in this study was M491S and M494. Synaptosomes from wild-type and transgenic P20 and P40 mice as well as hippocampus fractions S2 and P2 of P10 mice have been processed.

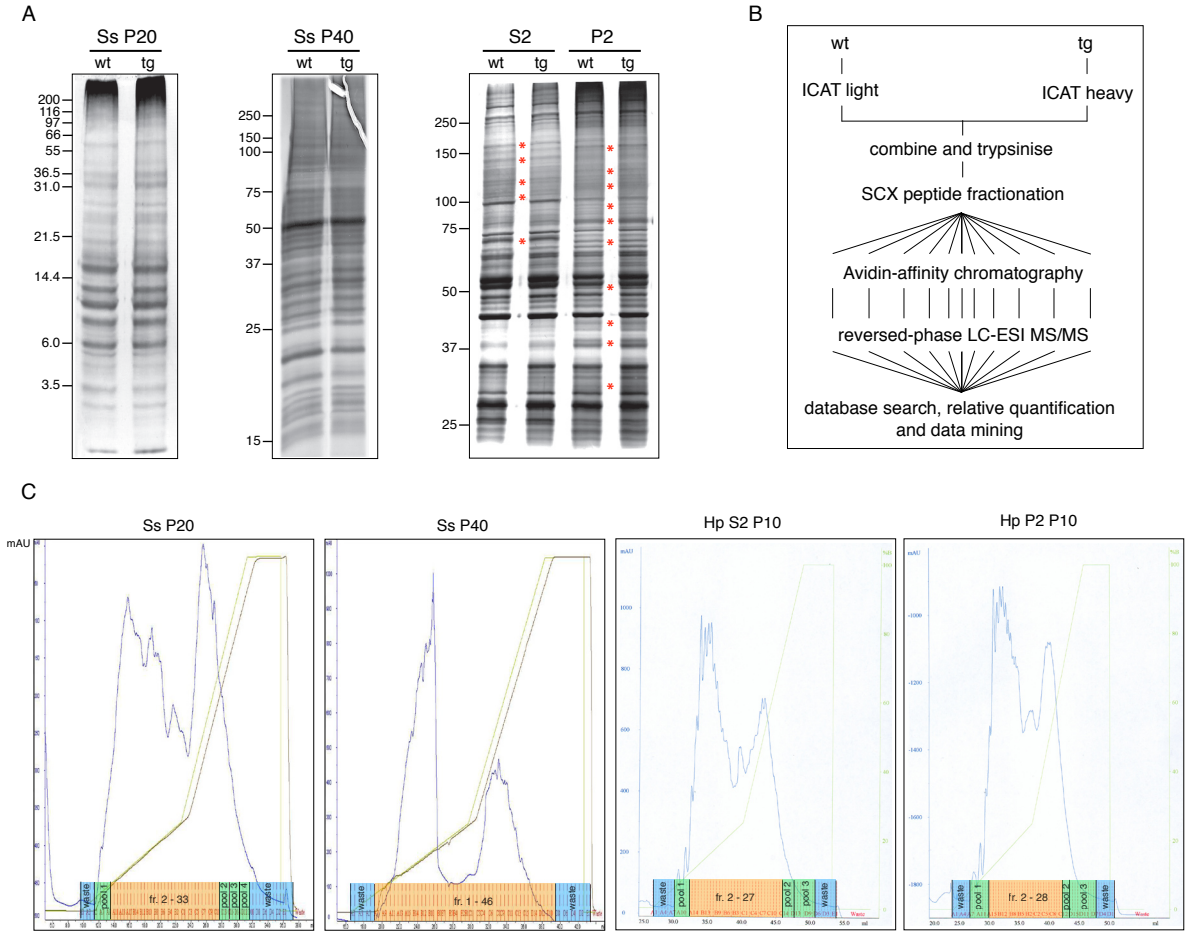

Figure 3.4 Sample preparation for quantitative proteome analysis using isotope-coded affinity tags (ICAT). **(A)** Before ICAT labeling protocol was conducted, the samples were separated on a gel and stained with silver. Equal amounts of wild-type (wt) and transgenic (tg) synaptosomes (Ss) isolated from P20 and P40 whole mouse brain were loaded on an SDS-PAGE (left panels), and hippocampal supernatant 2 (S2) and pellet 2 (P2) fractions of P10 mice were loaded on a 4 - 12% NuPAGE gel (right panel). Differences, comparing S2 and P2, are highlighted with red asterisks. **(B)** Schematic diagram of the ICAT labeling protocol. Protein extracts derived from wt mice were isotopically labeled with ICAT light while ICAT heavy was used for tg samples. The two samples were combined and trypsin digested. Thereafter the complex peptide mixture was fractionated with a strong cation exchange-column (SCX) followed by avidin-affinity purification of each individual fraction. Subsequent measurement of the ICAT labeled, cysteine-containing peptides was performed, with reversed-phase liquid-chromatography electrospray ionization tandem mass spectrometry (RP-LC-ESI-MS/MS). Peptide sequences were determined and protein assignment was performed by database searching using SEQUEST and Mascot search engines. Relative quantification was computed with Automated Statistical Analysis on Protein Ratio (ASAPRatio) and XPRESS software. Finally, data mining was carried out. **(C)** SCX elution profiles of Ss P20 and P40 and S2and P2 from P10 are depicted. Fractions (fr.) shaded in blue were discarded, fractions in green were pooled, and those in orange were collected individually for avidin-affinity purification.

3.3.1 Sample validation for the proteomic profiling

After the proteins had been isolated, they were loaded on a gel and stained with silver to estimate the quality of the sample. Equal amounts of synaptosomes from wild-type and transgenic P20 mice were loaded on a reducing 12% SDS-PAGE and stained with silver. Synaptosomes from P40 mice were loaded equally on a reducing 10% SDS-PAGE (Fig. 3.5a, left and middle). Both showed a typical ladder-like separation of proteins from low to high molecular masses. Comparable staining intensity was observed comparing wild-type with transgenic samples. For the hippocampal fractions a 4 – 12% NuPAGE gel was used to separate the proteins from S2 and P2. Equal amounts of proteins from wild-type and transgenic samples were stained (Fig. 3.5a, right). The band pattern of wild-type and transgenic S2 and P2 were the same. Differences were only found when lanes from S2 were compared with lanes from P2, pointing out different protein compositions of the two (asterisk).

3.3.2 Isotope-coded affinity tag (ICAT) labeling and multidimensional peptide separation

The ICAT method involved the following sequential steps (Fig. 3.5b): (1) The side chains of cysteinyl residues in a reduced protein sample representing one state, here wild-type, were derivatized with the isotopically light form of the cleavable ICAT reagent. The equivalent groups in a sample representing a second state, here transgenic, were derivatized with the isotopically heavy reagent (mass difference between light and heavy is 9 Da). (2) The two samples were combined and enzymatically cleaved by trypsin to generate peptide fragments, some of which are tagged with ICAT. (3) The complex peptide mixture was fractionated using strong cation exchange (SCX) chromatography (Fig. 3.5c). Highly similar elution profiles were observed for all samples processed. The difference in the elution chromatogram of P40 synaptosomes might be due to the fact that originally less amount of protein was used as compared to the other approaches. (4) The tagged (cysteine-containing) peptides were isolated by avidin-affinity chromatography. (5) Finally, the isolated peptides were separated and analyzed by reversed-phase microcapillary liquid chromatography electrospray ionization tandem mass spectrometry (RP-μLC-ESI-MS/MS). In this last step automated multistage MS determined both the quantity and sequence identity of the proteins from which the tagged peptides originated. This was achieved by measuring the signal intensities of peptides eluting from the RP-column in the MS mode to determine the relative quantities for pairs of peptide ions of identical sequence tagged with the isotopically light or heavy form. They differ in mass by the mass differential encoded by the ICAT reagent (9 Da). Peptide sequence information was generated by selecting peptide ions of a particular mass-to-charge (m/z) ratio for CID in the mass spectrometer, operating in the MS/MS mode (Gygi et al., 1999a; Gygi et al., 1999c; Link et al., 1997). Using sophisticated computer search algorithms SEQUEST and Mascot search engines (Eng et al., 1994; Perkins et al., 1999), the resulting CID spectra were automatically correlated with sequence databases to identify the protein from which the peptide originated. Combination of the results generated by MS and MS/MS analyses of ICAT-labeled peptides therefore determined the relative quantities as well as the sequence identities of the components of the protein mixture.

3.3.3 Quantitative proteome analysis of synaptosomes from P20 and P40 mice using the ICAT method

Synaptosomes from whole mouse brain of P20 and P40 wild-type and transgenic mice overexpressing neurotrypsin were isolated. Equal amounts of synaptosomal proteins (for P20 M491S mouse line 0.65 mg protein for each wild-type and transgene, and for P40 M494 mouse line 1 mg protein for each was used) from wild-type (light) and transgene (heavy) were labeled with cleavable ICAT and prepared for the analysis by RP-μLC-ESI-MS/MS. In total, 36 avidin-affinity purified SCX fractions for P20 and 46 fractions for P40 mice were measured by a classical ion trap mass spectrometer, LCQ Deca XP. The mass spectrometer operated in a dual mode in which it alternated between one survey scan and three MS/MS scans. In the survey scan mode relative quantities of precursor ions were measured and in the MS/MS scans sequential information was collected. Typical base peak chromatogram of SCX fractions showed ICAT-labeled peptides eluting from the RP column by increasing concentration of acetonitrile. An expanded view of an ICAT pair was monitored from a survey scan at the retention time indicated with a red line (Fig. 3.6a and b). The monoisotopic peak of the light variant of the precursor ion with a m/z ratio of 1084.83 was more abundant than the monoisotopic peak of the heavy labeled peptide. Co-elution and a detected mass difference of 4.5 U implied that the two ions represent a pair of doubly charged ICAT-labeled peptides of identical sequence (a mass difference of 9 Da with a charge state of two). By the reconstruction of the single ion chromatograms (SIC) for doubly and triply charged ions the relative quantities of the precursor ions were determined. The contour of the respective peaks was integrated using Automated Statistical Analysis of Protein Ratio (ASAPRatio) (Li et al., 2003). The ASAPRatio program computes the peptide ratio in two substeps: (1) Abundance ratios of the peptides with corresponding precursor masses in different charge states (2+: 1.618; 3+: 1.63) were first grouped together to calculate an abundance ratio (1.627 ± 0.257) (Fig. 3.6c). (2) Abundance ratios of the peaks in different RP-chromatographic fractions (1.527 ± 0.258 and 3.503 ± 0.314) were then merged to calculate the unique peptide ratio (1.537 ± 0.142) (Fig. 3.6d). However, the main function of the ASAPRatio program is to evaluate an abundance ratio for each protein identification in an LC-ESI-MS/MS experiment. If a single peptide was identified for a protein, the corresponding unique peptide ratio and its associated error were passed on as the protein abundance ratio and its error. Frequently however, more than one unique peptide was identified for the same protein. In this case, statistical methods for weighted samples were applied to calculate the protein abundance ratio and its associated standard deviation from all of its corresponding unique peptide ratios. Thus, the unique peptide ratios (3.003 ± 2.224 and 1.537 ± 0.142) were weighted by their errors. The result of this step was a protein abundance ratio of 1.55 ± 0.224 for the identified protein, of which two different peptides have been identified and quantified (Fig. 3.6c). The CID spectrum derived by the fragmentation of the precursor ion with m/z 1084.83 provides enough information to deduce the amino acids sequence of the peptide (Fig. 3.6e). Fragment ions in the spectrum represent mainly single-event cleavage of peptide bonds resulting in sequence information recorded from both the N and C termini simultaneously. The one-letter code for encountered amino acids is LTDFGFCAGITPEQSKR. Database searching with this spectrum identified a peptide allocated to p21-activated kinase (PAK1).

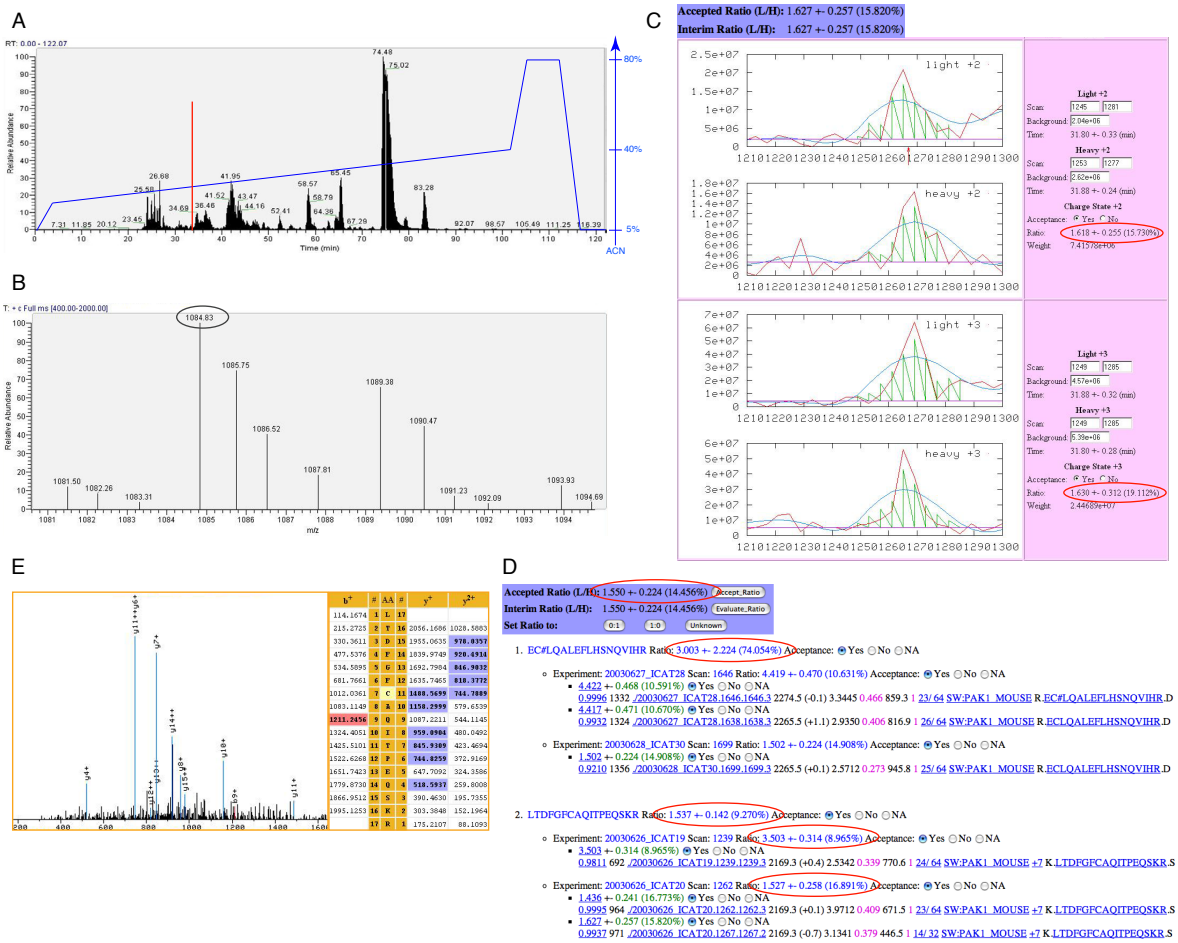

Figure 3.5 Mass spectrometry with synaptosomes using isotope-coded affinity tagging (ICAT).
(A) A representative elution chromatogram of a strong cation exchange (SCX) fraction from P20 synaptosomes after avidin-affinity purification measured with 3D ion trap mass spectrometer LCQ Deca. The acetonitrile (ACN) gradient, eluting the peptides from the reversed-phase column is indicated in blue. The red line marks the retention time (RT) of the ICAT-pair depicted in (B). **(B)** A zoom into a survey scan showing a pair of ICAT-labeled peptides of identical sequence with a monoisotopic mass-to-charge (m/z) ratio of 1084.83 for the light and for the heavy variant of 1089.38. The difference in m/z of 4.55 U reveals that doubly charged precursor ions are depicted here. The peak with m/z 1084.83 was captured in the ion trap for collision-induced dissociation (CID) resulting in a MS/MS spectrum. **(C)** A reconstructed single-ion chromatogram (SIC) computed with Automated Statistical Analysis of Protein Ratio (ASAPRatio) for the precursor ions measured in (B). The elution profiles in the upper panel are derived from doubly charged light and heavy labeled peptide. The areas used for calculating the abundance ratio of 1 : 1.618 are in green. The lower panel depicts the SIC from triply charged ICAT-pair with a calculated abundance ratio of 1.63. The ratios of the doubly and triply charged peptides are averaged and weighted by the corresponding spectrum intensities to obtain the peptide light:heavy ratio and its error of 1.627 ± 0.257. The red arrow points at the precursor ion selected for MS/MS, the red line is the raw signal, blue is the Savitzky-Golay smoothened signal, and the magenta line is the background noise subtracted from the spectrum. On the right are the start and end scan numbers, the background intensities, and the retention time of the light and heavy peptides, the acceptance, the abundance ratios, and the weight of the charge state. **(D)** Screen shot of accepted protein ratio (1.550 ± 0.224) calculated by ASAPRatio. Abundance ratios of peaks from the same peptide in different chromatographic fractions, e.g. 1.527 ± 0.258 and 3.503 ± 0.314, were grouped to calculate the unique peptide ratio of 1.537 ± 0.142. The unique peptide ratios were weighted by their errors, resulting in the protein abundance ratio of 1.55 ± 0.224. **(E)** SEQUEST program searched the acquired CID spectra against the database. This tandem mass spectrum was assigned to the peptide with amino acid sequence LTDFGFCAGITPEQSKR. The highlighted 'C' indicates a fragment ion with an ICAT-modification attached to the cysteinyl residue. This peptide in turn is allocated to Ser/Thr-protein kinase PAK 1.

3.3.3.1 Data filtering with Peptide- and ProteinProphet (I)

PeptideProphet was used to assess the validity of peptide assignments (Keller et al., 2002). Sensitivity and error rates for peptide identifications in the experiments with P20 and P40 synaptosomes were computed with PeptideProphet. For both an error rate of 5% was chosen, from which a minimal probability threshold of 0.58 for P20 and 0.63 for P40 arose. From a total of 8500 peptides in P20 and 5018 in P40, 7687 (sensitivity of 90.4%) and 4021 (sensitivity of 83.7%) correctly estimated peptides passed the filter (Fig. 3.7). Proteins were filtered using ProteinProphet, a statistical model for computing probabilities for a protein being present in a sample (Nesvizhskii et al., 2003). Only proteins with a probability ≥ 0.95 were allowed to pass the filter. Totally, 690 proteins from P20 animals and 462 proteins from P40 animals were present. Sensitivities and error rates of protein identifications as a function of minimum protein probability were computed. False positive identifications in both P20 and P40 were estimated at 2 proteins per sample (Fig. 3.7).

PeptideProphet

P20

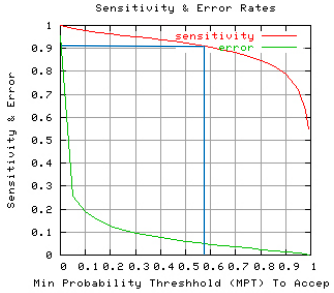

P40

Protein Prophet

min_prob	sens	err	# corr	# incorr
1.00	0.681	0.000	576	0
0.99	0.737	0.001	623	1
0.98	0.776	0.001	656	1
0.97	0.791	0.002	669	1
0.96	0.805	0.003	681	2
0.95	0.813	0.003	688	2
0.90	0.859	0.007	727	5
0.80	0.907	0.016	767	12
0.70	0.931	0.025	787	20
0.60	0.948	0.033	802	27
0.50	0.957	0.041	809	35
0.40	0.973	0.059	823	52
0.30	0.988	0.084	836	77
0.20	1.000	0.113	846	108
0.10	1.000	0.113	846	108
0.00	1.000	0.689	846	1874

min_prob	sens	err	# corr	# incorr
1.00	0.603	0.000	353	0
0.99	0.686	0.001	401	0
0.98	0.723	0.002	423	1
0.97	0.747	0.003	437	1
0.96	0.763	0.004	446	2
0.95	0.786	0.005	460	2
0.90	0.820	0.008	480	4
0.80	0.874	0.018	511	9
0.70	0.900	0.027	527	15
0.60	0.919	0.038	538	21
0.50	0.938	0.052	549	30
0.40	0.960	0.077	562	47
0.30	0.981	0.110	574	71
0.20	1.000	0.152	585	105
0.10	1.000	0.152	585	105
0.00	1.000	0.776	585	2027

Figure 3.6 PeptideProphet and ProteinProphet analysis for synaptosomes of P20 and P40 mice.
Sensitivity and error plots from PeptideProphet. In P20 mice an estimated number of 8500 peptides were correctly identified. With an error rate of 5% the number of correctly identified peptides is reduced to 7687 with a minimal probability threshold (MPT) of 0.58. In P40 mice merely 5018 correctly identified peptides were found in the whole dataset. Filtering with an error rate of 5% resulted in an estimated number of correctly identified peptides of 4201 with a MPT of 0.63. ProteinProphet predicted a total number of correct protein entries of 846 for P20 and of 585 for P40. An MPT of 0.95 was set. For P20 mice, 690 proteins passed the filter with an error rate of 0.3%. 462 proteins with an error rate of 0.5% passed the filter in P40 mice.

3.3.4 Quantitative proteomic profiling of the hippocampus from P10 mice using ICAT

Hippocampi dissected from P10 wild-type and transgenic M494 mice were homogenized and centrifuged to produce soluble fraction S2 and pelletous fraction P2. For the labeling with the cleavable ICAT reagent 2 mg of proteins were used from wild-type and transgene S2 and P2. In total 33 SCX fractions for S2 and 30 SCX fractions for P2 were collected, avidin-affinity purified and subsequently loaded on a C18 column for reversed-phase microcapillary liquid chromatography (RP-µLC). An increasing concentration of acetonitrile eluted the peptides from the column. Electrospray ionization generated gas phase ions that were conveyed to linear ion trap (IT) – Fourier Transform Ion Cyclotron Resonance Mass Spectrometer. Whilst performing this measurement in the ICR cell, fragment data can be performed in the IT simultaneously. Full MS scans were measured over the entire mass range (m/z 300 - 2,000). In the first step, the IT accumulated ions. A defined number of ions was then transferred to the ICR cell, where the accurate mass determination took place and a full FT was performed to give a high resolution MS spectrum. Simultaneously, three MS/MS experiments were performed in the IT. The resulting fragments were measured with two detector plates in the IT (NOTE: not high accuracy). Typical base peak chromatograms of SCX fractions and an expanded view of a survey scan over the mass range of m/z 300 – 1100 showed ICAT-labeled peptides of identical sequence eluting from the RP column (Fig. 3.8a). Blown-up extracts of survey scans demonstrate the high resolution and mass accuracy of the LTQ FT-ICR mass analyzer (Fig 3.8b, c). The isotopic distribution of doubly and triply charged precursor ions was resolved and the m/z ratio of each isotope was determined with high accuracy, resulting in peak intervals of 0.5 units for doubly (Fig. 3.8b) and 0.33 units for triply (Fig. 3.8c) charged ions. In addition, the survey scan (Fig. 3.8d (middle)), showing two doubly charged ICAT-pairs of different relative abundance (NOTE: the intensity of one pair is enhanced two-fold) point out the usefulness of atomole sensitivity and high resolution capacity of FT-ICR mass spectrometer for the analysis of complex peptide mixtures with MS. A mass spectrometer with less analytical power would not have resolved the two ICAT-pairs with the corresponding isotopic distribution and would probably not have selected the peak m/z 738.40 for CID as it was done for this particular precursor ion. However, for the purpose of identifying the sequence of the tagged peptide, the peak marked with an asterisk was selected for CID. Database searching with the CID spectrum identified the amino acid sequence: CIEEAIDKLSK, which in turn was unambiguously allocated to glutamine synthetase (Fig. 3.8d).

As opposed to the ICAT experiment with synaptosomes, the XPRESS quantification tool was used to compute the relative quantification of abundance ratios for proteins from the hippocampus (Han et al., 2001) (Fig. 3.8e). Although the ASAPRatio software tool has several advantages over XPRESS, the XPRESS tool has one decisive advantage when analyzing complex peptide mixtures with a highly sensitive, accurate, and high-resolution mass spectrometer. That is, when the light and heavy elution profiles are computed with XPRESS, a user defined value for the mass tolerance can be set. Consequently, by setting a mass tolerance of ± 0.5 units, simultaneously eluting precursor ions with highly similar m/z values but of different amino acid composition can largely be discriminated. Thus, the signals from the 'contaminating' ions are excluded from the SIC. Only signals from the ICAT-pair of interest are taken into account for the computation of the abundance ratio. The ASAPRatio program on the other hand, would reconstruct a SIC by summing up all signals within the range of *m/z* values covering the first three theoretical isotopic peaks of an ion. For a doubly charged ion this would correpsond to a tolerance of ± 1.5 m/z units.

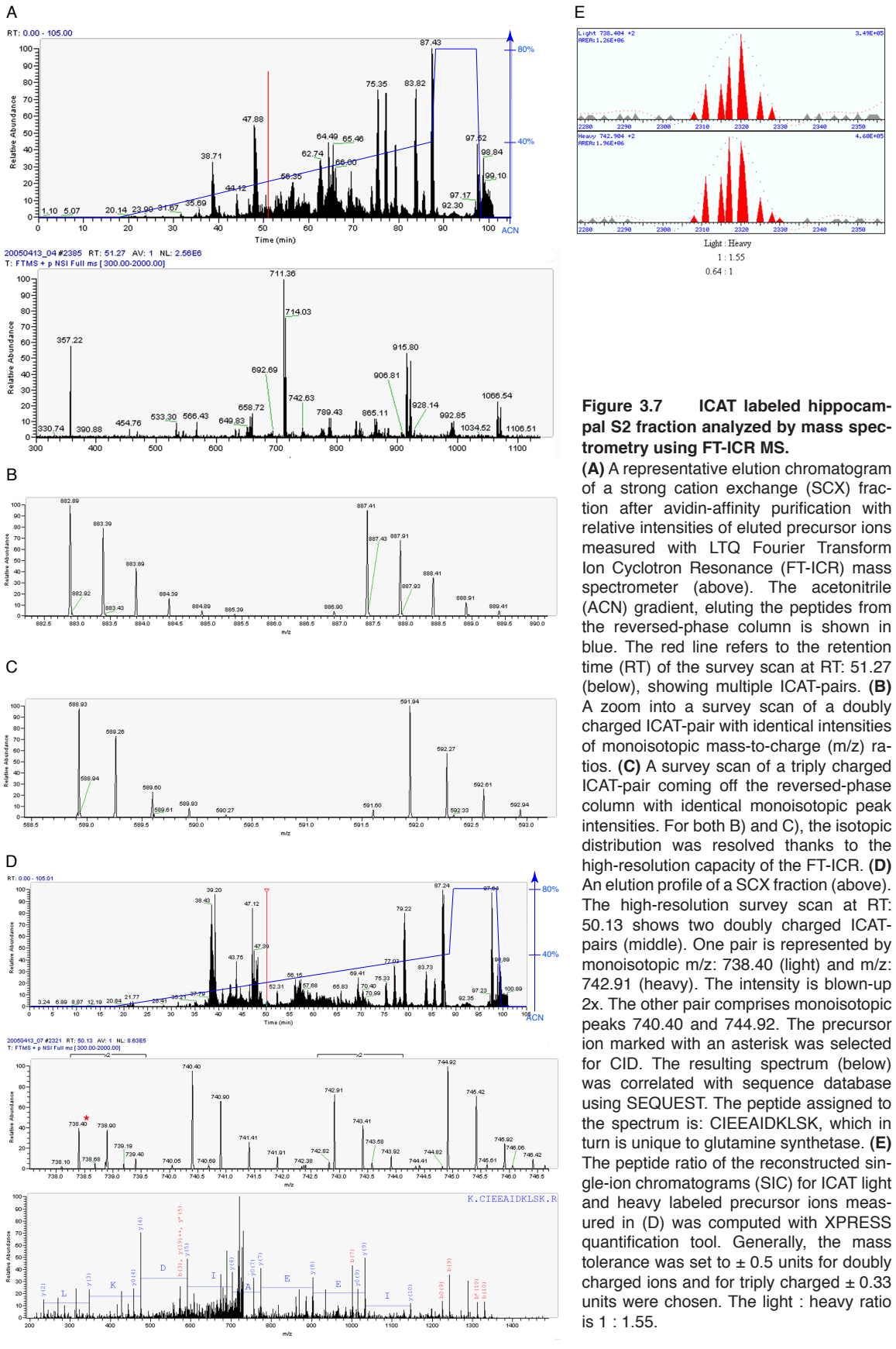

Figure 3.7 ICAT labeled hippocampal S2 fraction analyzed by mass spectrometry using FT-ICR MS.
(A) A representative elution chromatogram of a strong cation exchange (SCX) fraction after avidin-affinity purification with relative intensities of eluted precursor ions measured with LTQ Fourier Transform Ion Cyclotron Resonance (FT-ICR) mass spectrometer (above). The acetonitrile (ACN) gradient, eluting the peptides from the reversed-phase column is shown in blue. The red line refers to the retention time (RT) of the survey scan at RT: 51.27 (below), showing multiple ICAT-pairs. **(B)** A zoom into a survey scan of a doubly charged ICAT-pair with identical intensities of monoisotopic mass-to-charge (m/z) ratios. **(C)** A survey scan of a triply charged ICAT-pair coming off the reversed-phase column with identical monoisotopic peak intensities. For both B) and C), the isotopic distribution was resolved thanks to the high-resolution capacity of the FT-ICR. **(D)** An elution profile of a SCX fraction (above). The high-resolution survey scan at RT: 50.13 shows two doubly charged ICAT-pairs (middle). One pair is represented by monoisotopic m/z: 738.40 (light) and m/z: 742.91 (heavy). The intensity is blown-up 2x. The other pair comprises monoisotopic peaks 740.40 and 744.92. The precursor ion marked with an asterisk was selected for CID. The resulting spectrum (below) was correlated with sequence database using SEQUEST. The peptide assigned to the spectrum is: CIEEAIDKLSK, which in turn is unique to glutamine synthetase. **(E)** The peptide ratio of the reconstructed single-ion chromatograms (SIC) for ICAT light and heavy labeled precursor ions measured in (D) was computed with XPRESS quantification tool. Generally, the mass tolerance was set to ± 0.5 units for doubly charged ions and for triply charged ± 0.33 units were chosen. The light : heavy ratio is 1 : 1.55.

3.3.4.1 Data filtering with Peptide- and ProteinProphet (II)

Equally as with the ICAT experiment with synaptosomes, the peptides and proteins were filtered automatically using Peptide- and ProteinProphet statistical analysis programs (Fig. 3.9). Peptides were filtered using PeptideProphet with an error rate of 5%. In S2 the total estimated number of correctly identified peptides was 14076, 12336 of which passed the filter. The minimal probability threshold (MPT) was computed at 0.58 with a sensitivity of 87.6%. The MPT for ProteinProphet was set to 0.95, resulting in the identification of a total of 1376 correctly and 6 incorrectly assigned proteins. Similarly, the 6523 peptide assignments from P2 were filtered with an error rate of 5%, ending up with an estimated number of correctly identified peptides of 6027 with an MPT of 0.53 and a sensitivity of 92.4%. Subsequently, the peptides were allocated to proteins, which were filtered again, applying an MPT of 0.95 to ProteinProphet, resulting in the correct identification of 883 proteins with an error rate of 0.4%. Sensitivities and false positive identification error rates of protein identifications as a function of minimum computed protein probability for the experiments with S2 and P2 were listed (Fig. 3.9).

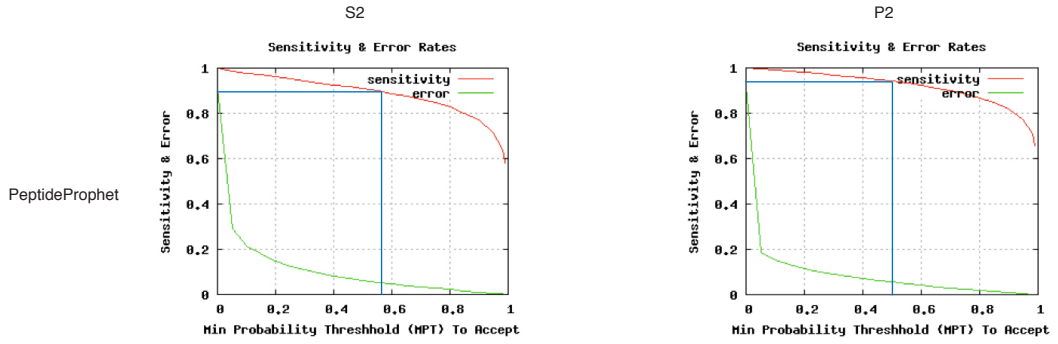

min_prob	sens	err	# corr	# incorr
1.00	0.623	0.000	1032	0
0.99	0.747	0.001	1237	1
0.98	0.790	0.002	1308	3
0.97	0.807	0.003	1336	4
0.96	0.824	0.004	1365	5
0.95	0.831	0.004	1376	6
0.90	0.862	0.007	1428	10
0.80	0.897	0.014	1486	21
0.70	0.921	0.022	1525	34
0.60	0.941	0.032	1558	52
0.50	0.956	0.044	1583	73
0.40	0.969	0.059	1605	101
0.30	0.985	0.085	1631	152
0.20	1.000	0.121	1656	228
0.10	1.000	0.121	1656	228
0.00	1.000	0.729	1656	4455

min_prob	sens	err	# corr	# incorr
1.00	0.625	0.000	654	0
0.99	0.757	0.002	792	2
0.98	0.796	0.003	833	3
0.97	0.815	0.003	853	3
0.96	0.831	0.004	870	3
0.95	0.840	0.004	879	4
0.90	0.875	0.008	916	7
0.80	0.909	0.014	951	14
0.70	0.932	0.022	975	22
0.60	0.949	0.031	993	32
0.50	0.960	0.039	1005	41
0.40	0.973	0.054	1018	58
0.30	0.988	0.078	1034	87
0.20	1.000	0.109	1046	128
0.10	1.000	0.109	1046	128
0.00	1.000	0.544	1046	1248

Figure 3.8 PeptideProphet and ProteinProphet analysis for hippocampus S2 and P2.
Sensitivity and error plots from PeptideProphet. In S2 an estimated number of 14076 peptides were correctly assigned. Within an error rate of 5% the number of correctly identified peptides is reduced to 12336 peptide assignments with a minimal probability threshold (MPT) of 0.58. In P2, totally 6523 correctly identified peptides were estimated. Filtering with an error rate of 5% resulted in an estimated number of correctly identified peptides of 6027 with a MPT of 0.53. ProteinProphet predicted a total number of correct protein entries of 1656 for S2 and 1046 for P2. When a MPT of 0.95 was set, 1382 proteins passed the filter with an error rate of 0.4% for S2 and 883 proteins with an error rate of 0.4% in P2.

3.3.4.2 Visual inspection and comparison of data sets obtained from repeated MS runs

Images obtained from high-throughput MS contain information that remains hidden when looking at a single elution profile at a time. A software tool, MSight, was applied for the 2D representation of liquid chromatography mass spectrometry (LC-MS) runs of hippocampus S2 fractions (Palagi et al., 2005). Four consecutive early SCX fractions (fractions 3 – 6) and two later fractions (fraction 19/20) were analyzed by MSight side-by-side for quality control of the LC-MS performance (Fig 3.10a). The signals represent eluting precursor ions from the RP column detected in the ICR cell. Contaminating compounds were scarcely detected in the sample. On the x-axis the m/z ratio and on the y-axis the time (t) is displayed. Due to comparable patterning among the fractions the analysis of the reconstructed elution profiles indicated that the four early consecutive fractions (fr. 3 - 6) had highly similar peptide composition. In other words, peptides of identical sequence and thus with the same chemical composition were separated in multiple fractions during SCX and behaved similarly during HPLC using a RP column. Consistently, due to discriminative sample composition the 2D images of the two latter fractions (fr. 19, 20) looked completely different as compared to the profiles of fractions 3 – 6, but are very similar themselves. A zoom into the four early SCX fractions showed paired signals that represent co-eluting ICAT-pairs. With increasing fraction number the pairs appeared (red circles) and disappeared (blue circles) indicating that during SCX they were separated according to their ionic strength, and upon elution from the RP column the ICAT peptide of the same sequence behaved the same (Fig. 3.10b). Thus, peptides of identical amino acid composition were fractionated over multiple fractions, depending on their capacity to bind to the SCX column with increasing salt concentration. Furthermore, with increasing fraction number the 2D reconstruction showed an augmented overall ion intensity particularly among the early fractions pointing to the fact that more and more peptides eluted from the RP column. This is due to the fact, that the elution profile of S2 peptides during SCX HPLC showed increased signal intensities with increasing fraction number implying more peptides to be present in later fractions (compare mAU in fractions 3 – 6 of SCX in Fig. 3.5c).

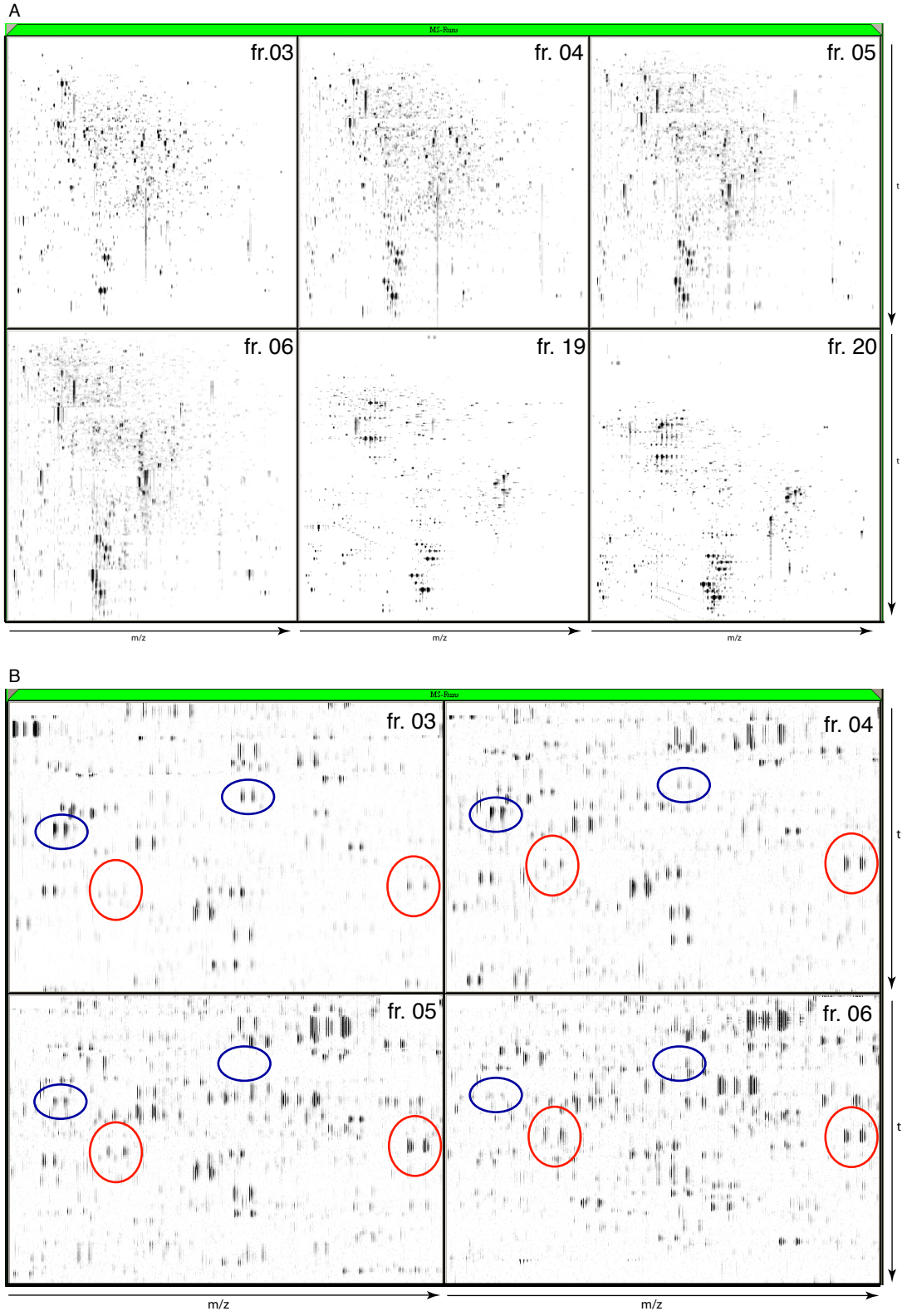

Figure 3.9 Visualization of liquid chromatography mass spectrometry using MSight.
(A) A comparison of 2D representations of datasets from six liquid chromatography mass spectrometry (LC-MS) runs of hippocampus S2 fractions fracionated by strong cation exchange (SCX). MS-runs of four consecutive early (fr.03 - fr.06) and two consecutive late (fr.19, fr.20) SCX fractions are shown. Elution chromatograms have a high degree of overlap in fr.03 -06 and fr.19/20. Convincingly, the overlapping signals are virtually absent comparing e.g. fr.06 with fr.19. **(B)** A zoom into LC-MS runs of fr.03 - fr.06 shows signals that emerge (red circles) and signals that disappear (blue circles). The paired signals represent eluting ICAT-pairs and their isotopic distribution that were fractionated by SCX. X-axis: m/z, Y-axis retention time (t).

3.3.4.3 Computational analysis of peptide identifications

To assess whether our approach resulted in reliable and accurate identifications the data of S2 were further analyzed. Delta mass analysis showed a similar distribution for both the observed masses (m/z) and the calculated masses (Da) of the precursor ions. Generally, the delta masses were below 0.04 Da, which corresponds approximately to the mass accuracy of the FT-ICR. There was a significant correlation between the observed or calculated masses and the delta masses. With increasing observed m/z value of the precursor ion a larger deflection to the calculated mass (delta mass) can be expected (Fig. 3.11a). And with increasing calculated masses the delta masses also increased linearly (Fig. 3.11b), indicting that with the FT-ICR MS the highest mass accuracy can be achieved for ions between m/z 400 – 1200, and for peptides between 1000 – 2500 Da. In nearly 98% of all peptides no missed cleavage site from the trypsin digestion was found (Fig. 3.11c), and only 2.5% of the precursor ions were singly charged (Fig. 3.11d). The majority of the ions were doubly charged (74.5%) or triply charged (23%). The frequency of average peptide length showed two Gaussian distribution with one maximum at 13 and the other at 16 amino acids. Surprisingly, there was a third maximum at 23 amino acids (Fig. 3.11e). Finally, the percentage of amino acid frequency was determined (Fig. 3.11f). In nature, the correlation between observed and expected frequencies of amino acids is highly significant ($r = 0.89$) excluding the outlier arginine. Only the frequency of arginine seems to be a product of natural selection acting on one or more of the arginine codons. Instead of particular amino acids being optimal at a certain position in any given protein, the most important thing determining the frequency of an amino acid is simply the number of codons coding for it. Therefore, S, L, G, A, K, V, T, D, and E are the most frequent amino acids, which was nicely reflected by the histogram. Also the low abundant amino acids in vertebrates, H, M, W, and Y, were rare in our approach. Although in nature, with an observed frequency of 3.3%, cysteine is a relatively rare amino acid, in the ICAT approach it was among the most abundant amino acids (7.3%). This is in nice agreement with the expectation that every peptide identification should bear at least one cysteine. In summary, the computational analysis of the peptide identifications from S2 revealed that the data obtained were in excellent agreement with what was being expected.

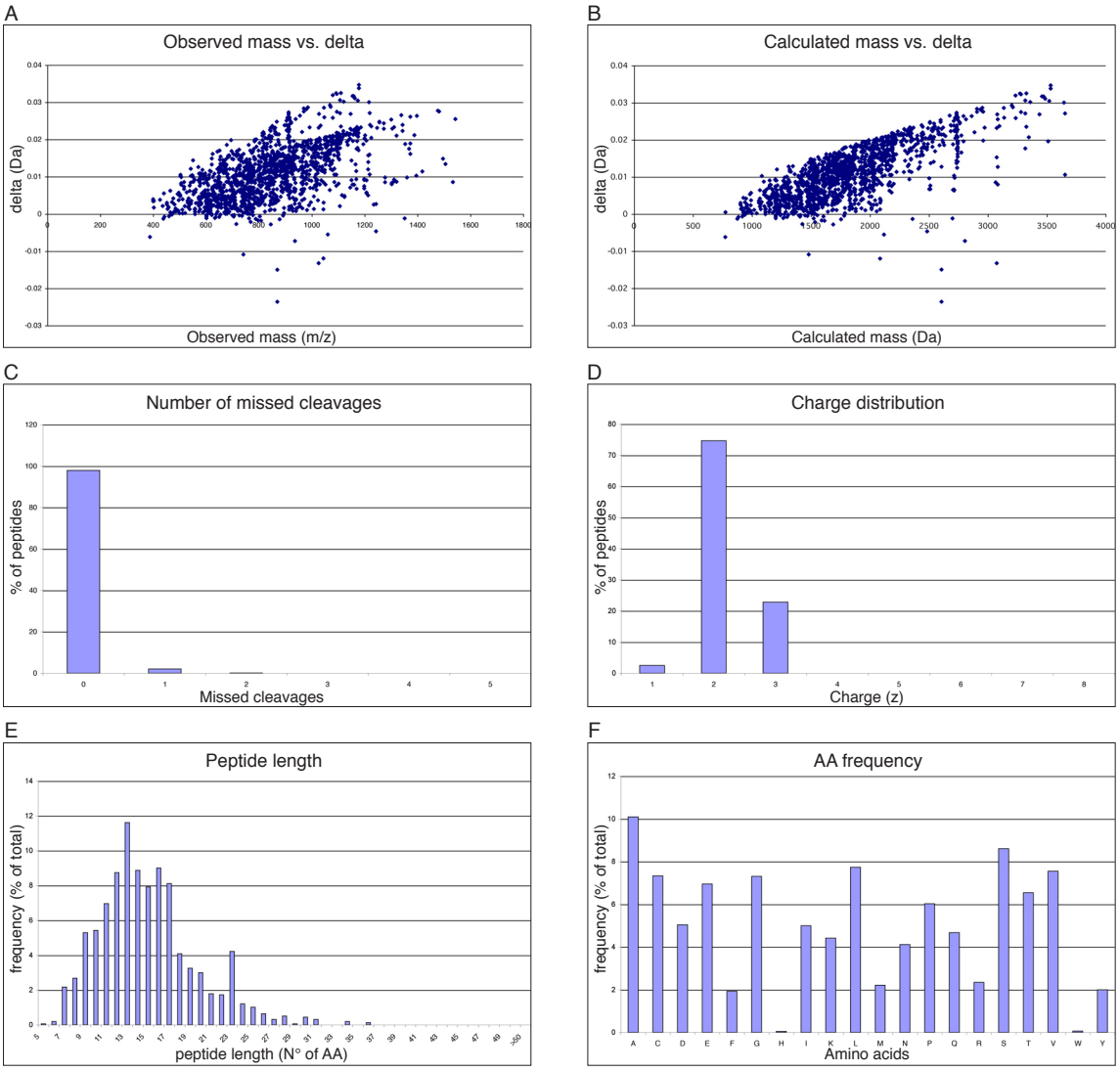

Figure 3.10 MS-data analysis of peptide identifications in S2.
(A) Distribution of observed peptide masses mass-over-charge (m/z) ratio and calculated peptide masses (Da) **(B)** versus delta mass (Da) measured by the mass spectrometer. **(C)** Histogram of percentage of all peptides with missed trypsin cleavage sites and with singly, doubly, or triply charged state **(D)**. **(E)** Histogram of the frequency of peptide length and amino acid (AA) appearance in the dataset **(F)**.

3.3.5 Categorization of total protein identifications from synaptosomes and the hippocampus

As mentioned earlier hundreds and thousands of proteins were identified from synaptosomes and the hippocampus proteome. To get a general idea of what kind of molecules have really been analyzed the complete data sets of P20 synaptosomes and the hippocampus fractions S2 and P2 were subjected to the Gene Ontology (GO) tool GoMiner (Zeeberg et al., 2003). GoMiner is a program package that organizes lists of interesting genes and proteins derived from high-throughput microarray or proteomic experiments for biological interpretation in the context of GO terms. In this report, GoMiner was used to classify protein identifications into 'molecular functions' and 'cellular compartments' (NOTE: one protein can be classified into multiple GO terms, and not every protein was classified due to lacking information). 690 proteins from P20

mice, 1382 from S2 and 883 proteins from P2 were annotated (Fig. 3.12). The synaptosomal proteins were most prominent in 'membrane' 33%, 'mitochondria' 29%, and 'protein complex' 26%. Other highly abundant proteins were those classified to 'ECM' 19% and 'cytoskeleton' 19%, whereas 'cytosol' 10%, 'ribosome' 3%, 'Golgi' 6% and 'ER' 7% proteins were rather seldom. Furthermore, proteins involved in 'transporter activity' constituted 12% of the synaptosomal proteins, 'structural molecules' and 'signal transduction' proteins constituted 5% each. Together, these three categories represent by far the most important molecular functions in synaptosomes. On the other hand, proteins from 'transcription regulator' 0%, 'translation regulator' 1%, 'enzyme regulator' 2% and 'motor activity' 2% are poorly represented in synaptosomes. A high percentage of membrane bound and membrane associated proteins and protein complexes involved in signal transduction and transporter activities are well expected. Moreover, mitochondrial as well as cytoskeletal and other structural constituents such as scaffolding proteins from the postsynaptic density, are important elements of the synapse, while proteins from the protein synthesis machinery, ER and Golgi are less abundant. Altogether this describes very well the composition and function of synaptosomes. Interestingly, a similar distribution was found for P2. 45% of all annotated proteins were classified to 'membrane'. Still 36% were allocated to 'mitochondria'. Prominent terms for P2 also were 'ECM' 19%, 'cytoskeleton' 18%, and 'protein complex' 21%. Components of the 'cytosol' 8%, 'ribosome' 11%, 'Golgi' 9%, and 'ER' 9% were sparsely identified in P2. In contrast to the synaptosomes, the 'nucleus' 16% was more represented. Comparing the isolation protocol for synaptosomes and P2, contaminating nuclei, which were not pelleted during the first centrifugation step ended up in P2 and not in synaptosomes. Unlike the synaptosomes, P2 emerges from S1' and was not further treated and directly analyzed by mass spectrometry. In the isolation protocol for synaptosomes more nuclei were lost when S1' was further centrifuged to get P2', which was subjected to density-gradient centrifugation where finally most of the remaining nuclei were lost. Regarding the 'molecular functions', synaptosomes and P2 also had a lot in common: proteins of the same categories were enriched in P2, such as 'transporter activity' 16%, 'structural constituent' 11%, and 'signal transduction' 9%. Whereas 'transcriptional' 1% and 'translational regulator' 2% as well as 'enzyme regulator' 2% and 'motor activity' 3% were categories with only a few identifications. Striking differences were found in S2. For instance with 24%, the category 'membrane' contained the fewest proteins in S2 among all subcellular fractions analyzed. There was nevertheless a considerable amount of membrane protein because light vesicular membrane structures and membrane-associated proteins were annotated to this category as well. 'ECM' with 13% and 'mitochondrion' with 20% however, were underrepresented in S2 as compared to P2 and synaptosomes, whereas molecules from the 'cytosol' 17% were enriched. Surprisingly, 'nucleus' with 33% contained the most proteins in S2. However, a lot of nuclear proteins are known to translocate between the nucleus and the cytoplasm and consequently an accumulation thereof is plausible. Altogether, the findings speak in favor of the fact that S2 is mainly composed of soluble cytosolic proteins. Consistently, 'transporter activity' 7% and 'signal transduction' 5% were markedly reduced in S2 as compared to P2 and synaptosomes. 'Structural constituents' were, with 7% quite abundant and proteins from 'transcription regulator' 2%, 'translation regulator' 3% and 'enzyme regulator' 5% were more frequent in S2 than in synaptosomes and P2. In all fractions, 1 – 2 % of the proteins were classified as 'unknown'. In summary, the distribution of proteins into 'cellular compartments' and 'molecular function' revealed that synaptosomes and P2 were highly similar, consisting of a lot of molecules that are involved in signal transduction and vesicular transport associated to membranes whereas S2 had a different composition, mainly being constituents of intracellular proteins complexes.

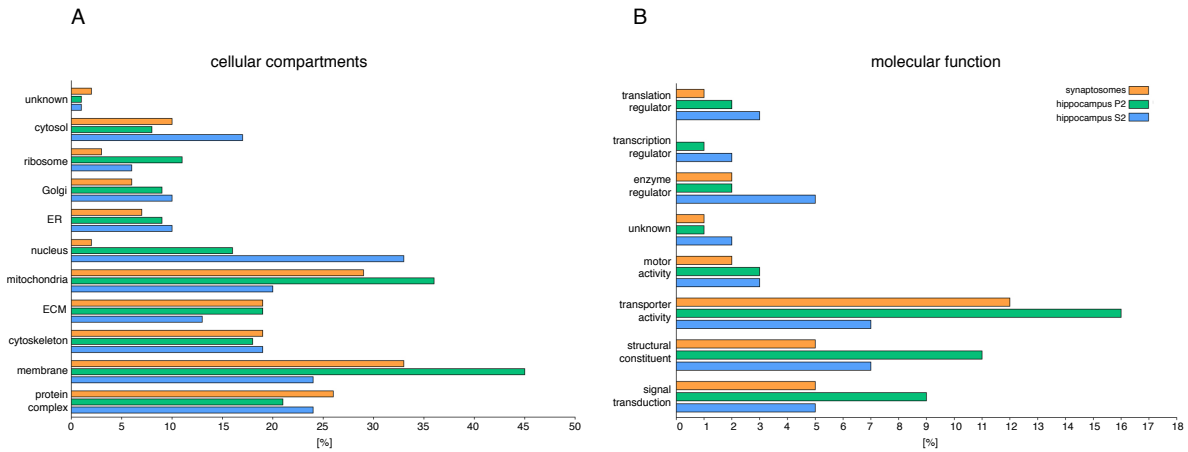

Figure 3.11 Protein identifications from synaptosomes and the hippocampus are annotated to Gene Ontology (GO) terms 'cellular compartment' and 'molecular function'.
(A) Protein datasets from synaptosomes of P20 (orange) and pelletous fraction P2 (green) as well as soluble fraction S2 (blue) from the hippocampus were categorized into GO terms. For all three datasets the distribution of correct protein identifications into 'cellular compartments' and 'molecular functions' are shown in % of the total, e.g. the 'membrane fraction' represents 34% in synaptosomes, 45% in P2, and only 24% in S2, whereas the 'cytosol' is most prominent in S2 (17%). The 'mitochondria' are highly enriched in synaptosomes and P2. Proteins localized to the nucleus are frequently found in S2. **(B)** For the 'molecular function', molecules involved in 'transporter activity' are enriched in synaptosomes (12%) and to a higher extent in P2 (16%). The 'structural constituents' are mainly present in P2 (11%) and S2 (7%), and 'signal transduction' molecules are most abundant in P2 (9%). 'Translational regulators' (3%) and 'enzyme regulators' (2%) are rare but still enriched in S2. Note that one single protein can be annotated to multiple terms.

3.4 Differentially regulated proteins in synaptosomes and the hippocampus

MS/MS peak lists from the raw data of S2 and P2 were converted both to Mascot generic format (MGF) for data files submitted to Mascot and to mzXML files for SEQUEST searches. The MS/MS data from the synaptosomes were database searched with SEQUEST only. All SEQUEST search results were filtered with Peptide- and ProteinProphet and quantified using ASAPRatio and XPRESS software, respectively. Proteins were considered as differentially regulated when their abundance ratio exceeded 20% up- or down regulation in transgenic neurotrypsin-overexpressing mice. Using the ICAT technology 66 proteins from P20 and 81 proteins from P40 synaptosomes were differentially expressed. In the hippocampus 106 proteins from S2 and 67 proteins in P2 were changed.

3.4.1 Neurotrypsin-dependent changes of protein abundance in synaptosomes and the hippocampus proteome

The molecular entities may be perturbed and cellular pathways activated or inhibited due to the neurotrypsin overexpression. In the following sections, selected proteins are presented in the context of their functional categorization (Tables 1 – 7).

Table 1 Regulated proteins in synaptosomes

			SS P20		SS P40	
Accession Number[a]	Protein	Mw (kDa)[b]	protein ratio ± s.d.[c]	No.[d]	protein ratio ± s.d.[c]	No.[d]
	Cytoskeleton, cell adhesion					
P60766	Cdc 42	21.3	1.13 ± 0.18	5	1.59 ± 0.24	2
Q99PT1	Rho GDI alpha	23.4	0.57 ± 0.08	1		
O88643	p21-activated kinase (PAK 1)	60.7	1.55 ± 0.22	2		
O89053	Coronin-1A	51.0	1.48 ± 0.25	6	1.54 ± 0.25	1
P12960	Contactin 1	113.4			1.55 ± 0.16	5
	Synaptic transmission, neurotransmitter uptake, neuroendocrine					
Q9Z2W9	Glutamate receptor 3	100.4	1.77 ± 0.19	4		
P62835	Rap-1A	66.3			1.88 ± 0.17	10
P43006	EAAT2/GLT1	62.0			1.51 ± 0.36	3
P15105	Glutamine synthetase	42.0	0.73 ± 0.04	37		
P63318	PKC-ε	83.6			0.60 ± 0.06	2
Q9Z140	Copine VI (neuronal)	61.8	1.85 ± 0.45	3		
P60202	Myelin proteolipid protein	30.1	1.55 ± 0.13	3	1.29 ± 0.12	3
P16014	Chromogranin B	78.0	1.32 ± 0.38	1	1.83 ± 0.18	1
	Transport, exocytosis, endocytosis					
P28738	Kinesin heavy chain, neuron specific	109.2	1.64 ± 0.58	2	1.74 ± 0.30	1
P62823	Rab3C	25.8	1.05 ± 0.10	2	1.99 ± 0.55	2
O08539	Amphiphysin 2	64.5	1.38 ± 0.33	3	1.52 ± 0.27	4
P17426	Adaptor protein complex AP-2, α1	107.7			1.61 ±0.15	10
	Cell proliferation/differentiation					
P63085	MAPK 1	41.3	1.37 ± 0.29	1	1.66 ± 0.30	1
	Glucose metabolism, tricarboxylic acid cycle, fatty acid metabolism					
P17710	Hexokinase-1	108.3	1.80 ± 0.30	2		
Q9JK42	Pyruvate deyhdrogenase kinase isoform 2	46.1	0.54 ± 0.06	2		
Q9D6R2	Isocitrate deyhdrogenase [NAD] subunit α	39.6			1.65 ± 0.16	5
P14152	Malate dehydrogenase, cyt.	36.3	1.03 ± 0.07	3	1.55 ± 0.13	5
P06151	L-lactate dehydrogenase A chain	36.5	1.02 ± 0.14	4	1.54 ± 0.52	3
Q05816	Fatty acid-binding protein, epidermal	15.0	1.59 ± 0.55	4	1.19 ± 0.11	3
	Varia					
P55264	Adenosine kinase	40.1	0.47 ± 0.04	1	0.10 ± 0.02	1
P35762	CD81	25.8	2.58 ± 0.41	1	2.27 ± 0.33	1
P13861	cAMP-dependent protein kinase type II-α	45.5	1.50 ± 0.22	2	1.22 ± 0.47	2
Q9Z268	RasGAP-activating-like protein 1	89.4			0.56 ±0.08	2
Q60864	Stress-induced-phosphoprotein 1	62.9	1.55 ± 0.12	3	1.67 ± 0.41	2

[a]Primary UniProt accession number. [b]Molecular mass. [c]Average abundance ratio (wt = 1) followed by the standard deviation computed with ASAP Ratio algorithm. [d]Number of different cystein-containing peptides.

Table 2 Regulated proteins in the hippocampus involved in vesicular trafficking, neurotransmitter release, and synaptic plasticity

Accession Number[a]	Protein	Mw (kDa)[b]	protein ratio[c]	No.[d]
	Synaptic vesicle, endocytosis			
P39053	Dynamin 1	97.8	S2: 0.75	S2: 3
Q9WVE8	PACSIN 2	55.8	S2: 0.77	S2: 2
O70439	Syntaxin 7	29.7	P2: 1.23	P2: 1
	Synaptic vesicle, exocytosis			
P62823	Rab3C	25.9	S2: 1.20	S2: 1
Q80UJ7	Rab3-GAP	130.0	S2: 0.82	S2: 4
	Synaptic vesicle, vesicular trafficking			
Q9D0M5	Dynein light chain	10.4	S2: 0.76	S2: 3
P28740	Kinesin-like protein KIF2A	81.0	S2: 1.25	S2: 4
Q8BGN8	Synaptoporin	29.2	S2: 0.72	S2: 2
	Neurotransmission, synaptic plasticity			
P54920	α-SNAP	33.2	S2: 0.70	S2: 1
P28663	ß-SNAP	33.2	S2: 0.63	S2: 5
P46460	Vesicle-fusing protein NSF	82.6	S2: 0.60 P2: 1.17	S2: 5 P2: 8
O08599	Syntaxin-binding protein 1 (Munc18-1)	67.6	S2: 0.84 P2:1.13	S2: 3 P2: 3
P63040	Complexin 1	15.0	S2: 0.71	S2: 1
Q9Z2Q6	Septin 5	42.8	S2: 0.67	S2: 2
P11798	CaMK II α	54.3	S2: 0.85 P2: 0.70	S2: 3 P2: 3
Q9Y2H0	Disks large-associated protein 4 (SAPAP4)	80.5	P2: 1.29	P2: 2
P70175	Disks large homolog 3 (SAP102)	93.5	S2: 1.33	S2: 1
Q9Z140	N-copine	61.8	S2: 0.71 P2: 0.83	S2: 5 P2: 6
	Neuroendocrine, synapse remodelling			
P16014	Chromogranin B	78.0	S2: 0.70	S2: 1
Q62443	Neuronal pentraxin 1	47.1	S2: 0.71	S2: 2
P43006	EAAT2/GLT1	62.0	P2: 0.75	P2: 2

[a]Primary UniProt accession number. [b]Molecular mass. [c]Average abundance ratio (wt =1) computed with XPRESS software. [d]Number of different cystein-containing peptides.

Table 3 **Regulated proteins in the hippocampus involved in cell adhesion, cell migration and cell proliferation**

Accession Number[a]	Protein	Mw (kDa)[b]	protein ratio[c]	No.[d]
	Cell adhesion			
P11627	Neural cell adhesion molecule L1	141.0	S2: 0.79 P2: 1.30	S2: 6 P2: 8
Q810U4	NrCAM	138.5	S2: 0.78	S2: 5
Q60625	ICAM-5	86.9	S2: 0.67	S2: 4
Q99N28	Nectin-like protein 1	42.9	S2: 0.73	S2: 1
Q3TYL3	Opoid-binding cell adhesion molecule (OBCAM)	37.2	S2: 0.56	S2: 3
P12960	Contactin 1	113.3	S2: 0.66	S2: 2
	Neuron migration and differentiation of the nervous system			
Q61361	Brevican	96.0	S2: 0.75	S2: 3
O88809	Doublecortin	40.6	S2: 1.27	S2: 2
O08919	Numb-like protein	64.2	S2: 0.82 P2: 1.32	S2: 2 P2: 1
Q80YX1	Tenascin-C	231.8	S2: 0.75 P2: 1.53	S2: 19 P2: 7
	Cell proliferation			
P34884	Macrophage migration inhibitory factor	12.4	S2: 1.25 P2: 1.42	S2: 2 P2: 2
Q9DCT8	Cysteine-rich protein 2	22.7	S2: 1.30 P2: 1.55	S2: 2 P2: 2
P63085	MAPK 1	41.1	P2: 1.39 S2: 1.20	P2: 1 S2: 3
P20444	PKC-α	76.7	P2: 0.64	P2: 3
P46527	Cyclin-dependent kinase inhibitor 1B	22.2	S2: 0.56	S2: 1

[a]Primary UniProt accession number. [b]Molecular mass. [c]Average abundance ratio (wt =1) computed with XPRESS software. [d]Number of different cystein-containing peptides.

Table 4 Regulated proteins in the hippocampus involved in cytoskeletal rearrangements

Accession Number[a]	Protein	Mw (kDa)[b]	protein ratio[c]	No.[d]
	Microtubule cytoskeleton			
P14873	Microtubule-associated protein 1B (MAP 1B)	270.4	P2: 1.29	P2: 8
O88643	p21-activated kinase (PAK 1)	60.7	S2: 1.27	S2: 1
Q8R5C5	Actin-related protein 1B	42.3	P2: 1.30	P2: 1
Q9ERD7	Tubulin ß-3	50.4	P2: 1.35	P2: 3
Q9D6F9	Tubulin ß-4	49.6	P2: 1.40	P2: 6
	Actin cytoskeleton			
Q9QXS6	Drebrin	77.2	S2: 1.04 P2: 1.46	S2: 9 P2: 6
P63001	Rac1	21.5	S2: 0.92 P2: 1.20	S2: 5 P2: 4
P60766	Cdc42	21.3	S2: 1.38	S2: 2
Q99JY9	Actin-like protein 3	47.2	P2: 1.27	P2: 3
P47754	F-actin caping protein α-2	32.8	S2: 0.83	S2: 3
Q61792	LIM and SH3 domain protein 1	30.0	S2: 1.33 P2: 2.95	S2: 2 P2: 2
Q9CVB6	Actin-related protein 2/3 complex, subunit 2	34.4	S2: 1.31	S2: 1
Q8R5H6	WASP-family protein member 1	61.5	P2: 2.20	P2: 1
O89053	Coronin-1A	50.9	P2: 1.26	P2: 1
	Type III intermediate filament			
P20152	Vimentin	53.6	P2: 0.82	P2: 1

[a]Primary UniProt accession number. [b]Molecular mass. [c]Average abundance ratio (wt =1) computed with XPRESS software. [d]Number of different cystein-containing peptides.

Table 5 Proteins regulated in the hippocampus involved in glycose metabolism and tricarboxylic acid cycle, and lipid metabolism

Accession Number[a]	Protein	Mw (kDa)[b]	protein ratio[c]	No.[d]
	Glycolysis			
P17710	Hexokinase 1	102.4	S2: 0.73	S2: 5
P17182	α-enolase	47.0	S2: 1.25 P2: 1.26	S2: 7 P2: 4
P17183	γ-enolase	47.2	S2: 1.56 P2: 1.32	S2: 2 P2: 1
	Pyruvate dehydrogenase complex			
Q8BKZ9	Pyruvate dehydrogenase protein X component, mitochondrial	54.0	S2: 0.73	S2: 1
P35486	Pyruvate dehydrogenase E1 component α-subunit, mitochondrial	43.2	S2: 0.80 P2: 1.23	S2: 4 P2: 5
Q9D051	Pyruvate dehydrogenase E1 component ß-subunit, mitochondrial	38.9	P2: 1.38	P2: 1
	Tricarboxylic acid cycle			
Q9CZU6	Citrate synthase, mitochondrial	51.7	P2: 1.26	P2: 4
Q99KI0	Aconitate hydratase, mitochondrial	85.5	S2: 0.90 P2: 1.21	S2: 4 P2: 3
O88844	Isocitrate dehydrogenase [NADP] cytoplasmic	46.7	P2: 1.34	P2: 2
P54071	Isocitrate dehydrogenase [NADP], mitochondrial	58.8	S2: 1.24 P2: 1.26	S2: 4 P2: 2
	Glucose metabolism			
Q8CAA7	Phosphoglucomutase-2-like 1	70.3	P2: 1.43	P2: 1
Q05816	Fatty acid-binding protein, epidermal	15.0	S2: 0.77	S2: 3
P47856	Glucosamine-fructose-6-phosphate aminotransferase 1	78.7	S2: 0.77	S2: 2
	Lipid metabolism			
O35678	Monoglyceride lipase	37.5	S2: 0.69	S2: 1
P02772	Alpha-fetoprotein	67.3	S2: 1.52	S2: 3
Q61425	Hydroxyacyl-coenzyme A dehydrogenase, mitochondrial	34.5	P2: 1.31	P2: 1
Q61207	Prosaposin	58.1	S2: 1.44 P2: 1.30	S2: 6 P2: 6
Q9R0Q7	Prostaglandin E synthase 3	18.7	S2: 1.20 P2: 1.33	S2: 3 P2: 3

[a]Primary UniProt accession number. [b]Molecular mass. [c]Average abundance ratio (wt =1) computed with XPRESS software. [d]Number of different cystein-containing peptides.

Table 6 Proteins regulated in the hippocampus involved in various molecular functions

Accession Number[a]	Protein	Mw (kDa)[b]	protein ratio[c]	No.[d]
	Glutamate turnover, detoxification of ammonia			
P26443	Glutamate dehydrogenase 1, mitochondrial	61.2	S2: 0.66 P2: 1.37	S2: 2 P2: 4
P15105	Glutamine synthetase	42.0	S2: 1.40 P2: 0.85	S2: 6 P2: 4
	Apotposis			
P21796	VDAC 1	30.8	P2: 0.70	P2: 2
	Sodium/potassium transport			
Q6PIC6	α3 Na^+/K^+-ATPase	111.7	S2: 0.73 P2: 0.83	S2: 8 P2: 12
P14094	β1 Na^+/K^+-ATPase	35.2	S2: 0.71	S2: 2
P14231	β2 Na^+/K^+-ATPase	33.3	S2: 0.60	S2: 1
	Ubl conjugation pathway, protein folding, transcriptional regulator, splicing activity			
Q7TPH6	Myc-binding protein 2	51.8	S2: 0.78 P2: 1.66	S2: 2 P2: 1
P63038	Heat shock protein 60	61.0	P2: 1.40	P2: 5
Q6ZQ38	Cullin-associated NEDD8-dissociated protein 1	136.3	S2: 1.25	S2: 3
Q6PDM2	Splicing factor arginine/serine rich 1	27.6	S2: 0.58 P2: 2.32	S2: 3 P2: 1
	Protease inhibitor			
O08677	Kiniogen-1	73.1	S2: 1.48	S2: 2

[a]Primary UniProt accession number. [b]Molecular mass. [c]Average abundance ratio (wt =1) computed with XPRESS software. [d]Number of different cystein-containing peptides.

Table 7 Proteins regulated in the hippocampus revealed by 2D gel electrophoresis

			S2	P2
Accession Number[a]	Protein	Mw (kDa)[b]	protein ratio	protein ratio
	Vesicular trafficking			
P50396	Rab GDI 1	51.1	0.58	0
Q9DBG3	AP-2 complex subunit β-1	105.4	0.49	
Q01853	Translational ER ATPase	90.0	0.53	
Q6P8X1	Sorting nexin 6	46.9	0.15	
Q9Z140	N-copine	62.6	1.58	
	Neurite extension, cell proliferation			
Q76MZ3	PP2A, subunit A, 65 kDa regulatory subunit	65.3		0.59
P58389	PP2A, regulatory subunit B'	37.0	1.62	
O08553	Dihydropyrimidinase-related protein 2 (DRP 2)	62.5	0.63	1.56
Q62188	Dihydropyrimidinase-related protein 3 (DRP 3)	62.3	0.56	1.59
P53810	Phsophatidylinositol transfer protein-α	31.9		0.66
Q9R0P9	Ubiquitin cyrboxyl-terminal hydrolase isoenzyme L1	24.8		0.56
O54983	Mu-crystallin homolog	33.5	0.61	0.59
	Cytoskeleon			
Q61166	Microtubule-associated protein RP/EB familiy member 1	30.0	1.75	0.56
P03995	GFAP	49.9	0.64	
P20153	Vimentin	53.6	0.42	
	Glucose metabolism, glycolsis, cell cycle			
Q9DBJ1	Phosphoglycerate mutase 1	28.8		0.20
P17182	α-enolase	47.3	0.58	
Q8CAA7	Phosphoglucomutase 2-like 1	70.3	1.50	
P34022	Ran-specific GAP	23.6		0.48
Q921Q5	Rap1 GDI 1	66.4	1.70	
	Varia			
P55264	Adenosine kinase	40.5	1.60	
Q3TCW4	Neurochondrin	79.0	2.23	

[a]Primary UniProt accession number. [b]Molecular mass. [c]Average abundance ratio (wt=1).

3.4.2 Quantitative proteomic profiling using 2D gel electrophoresis

Despite an increase in overall protein identifications, the four data sets obtained from the ICAT analysis showed a very substantial overlap, indicating that increasing sample diversification alone will not be sufficient to overcome the inherent redundancy of a shotgun approach. Therefore, a different strategy was needed that is capable of adding new protein identifications, especially those which are differentially regulated. To target another set of proteins in the CNS of neurotrypsin-overexpressing mice and thereby assess their expression levels a 2D gel electrophoresis proteomics approach in combination with mass spectrometry (2DE-MS) was chosen. Protein extraction from wild-type and transgenic hippocampus S2 and P2 was followed by 2DE. Spots on the gels were analyzed with ProteomWeaver a platform for quantitative analysis of 2D gels. For both fractions, 2D gels of three wild-type and three transgenic samples were matched and spot intensities were measured. In each case, two protein-spots were compared pairwise on a matrix of 3 x 3 gels and average abundance changes were calculated. In total 626 spots were detected from S2, among which 33 were up regulated and 56 spots were down regulated in transgenic samples. As for P2 in total 343 spots were distinguished. 8 of them were up- and 11 were down regulated (Fig. 3.13). Spots of different average intensities were excised, in-gel digested and protein identifications were determined by matrix-assisted laser desorption/ionization tandem time of flight (MALDI-TOF/TOF) (Fig. 3.14).

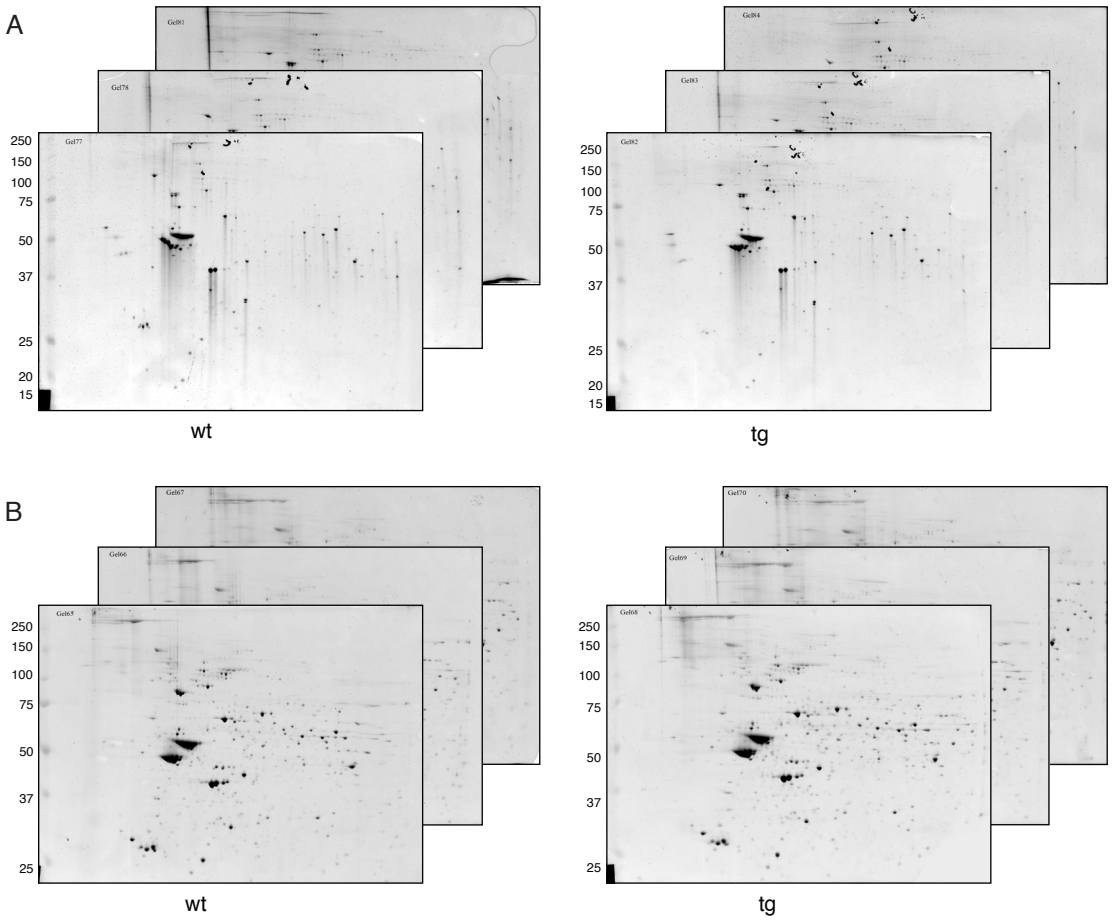

Figure 3.12 Experimental set-up for 2D gel electrophoresis (2DE) to compare differential protein expression in the hippocampus.
(A) Three gels from wild-type (wt) and transgenic (tg) hippocampus P2, and **(B)** three gels from wt and tg hippocampus S2 were prepared and analyzed. For each sample 18 x 24 cm, 10% polyacrylamide 2D gels with linear pH-gradients of 4 - 7 were generated and spot intensities were measured using Proteomweaver. 2D gels were analyzed by pairwise comparison of average spot intensities from wt and tg samples.

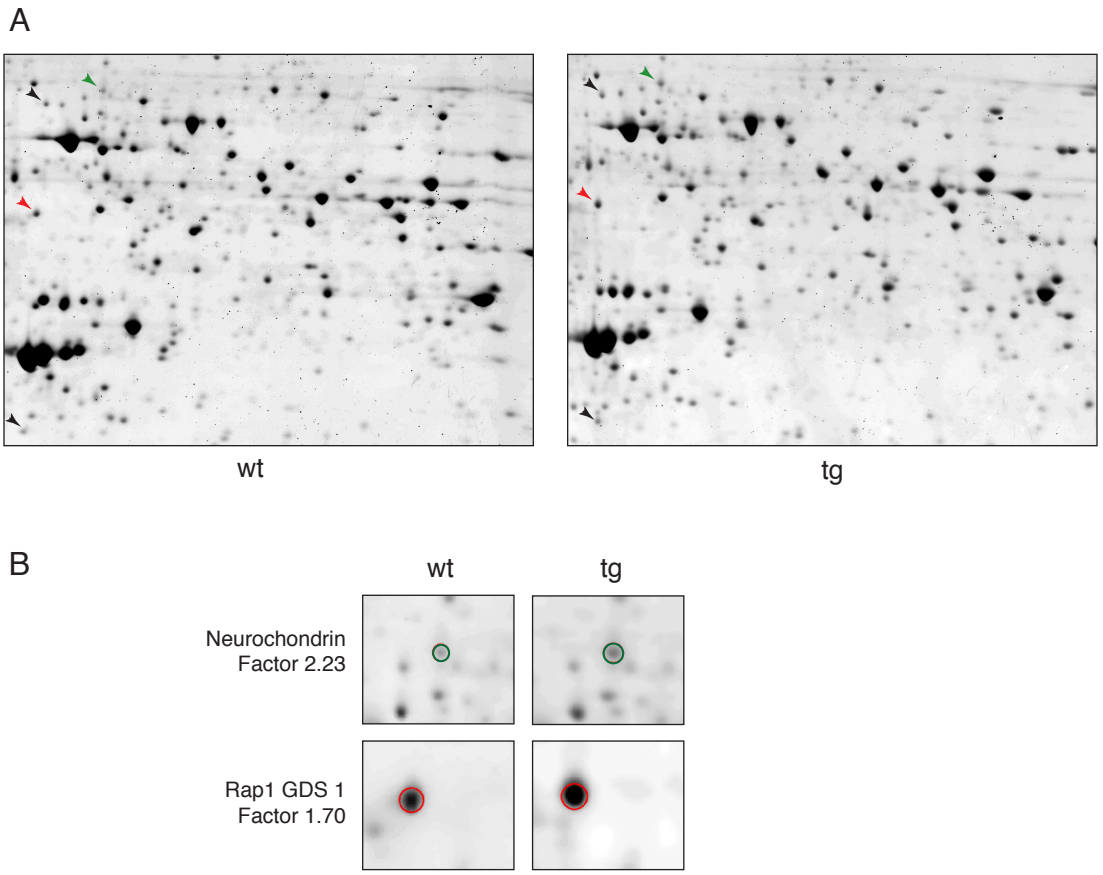

Figure 3.13 Upregulated spots in the hippocampus of neurotrypsin overexpressing mice.
(A) A zoom into 2D gels from wild-type (wt) and transgenic (tg) mice of soluble fraction S2. Arrowheads point to 4 spots with higher intensities in tg as compared to wt. **(B)** A magnification of two color-coded spots from (A) showing higher intensities in the tg samples. The protein identities were revealed by excision and in-gel trypsin digestion of the spots, followed by Matrix-Assisted Laser Desorption/Ionization -Time Of Flight (MALDI-TOF) tandem mass spectrometry. Neurochondrin was upregulated in tg by 2.23x and Rap1, GTP-GDP dissociation stimulator 1 (Rap1 GDI 1) was increased in tg by a factor of 1.70.

3.4.3 Regulatory changes of molecular functions

3.4.3.1 Cytoskeleton reorganization, cell proliferation/differentiation

Cdc42 belongs to the Rho family of Ras like GTPases and was up regulated in the hippocampus S2 and in synaptosomes of young and adult transgenic mice (Table 1 and 4). Interestingly, Rho dissociation inhibitor (GDI) alpha, an inhibitor of Rho family GTPases, was down regulated in synaptosomes. Cdc42 is an important regulator of the actin cytoskeleton. For instance, activated Cdc42 can interact with Wiskott-Aldrich syndrome protein (WASP) that itself activates Arp2/3, which is a nucleation protein complex for F-actin polymers (Yamaguchi et al., 2005). Furthermore, WASP-family protein WAVE plays a critical role downstream of Rac in regulating the actin cytoskeleton required for membrane ruffling (Miki et al., 1998). Both WASP1 and Rac1 expression were induced in transgenic P2 (Table 4). Together with PKCε (down regulated in P40 synaptosomes) and δ, Cdc42 induces neurite outgrowth (Troller and Larsson, 2006). Cdc42 is also involved in axon guidance via PAK1 (Robles et al., 2005) (up regulated in P20

synaptosomes and S2 (Tables 1 and 4)). PAK proteins are critical effectors that link RhoGTPase to cytoskeleton reorganization and regulate a number of processes such as cell proliferation and motility. Recently it was found that PAK 1 has three nuclear localization signals (NLS) that associate with chromatin and thus modulates transcription (Singh et al., 2005). Furthermore, adhesion stimulates direct association of PAK1 with Mitogen-activated protein kinase 1 (MAPK1) and leads to MAPK-dependent PAK1 Thr_{212} phosphorylation (Sundberg-Smith et al., 2005). MAP kinases, also known as extracellular signal-regulated kinases (ERKs), act as integration points for multiple biochemical signals, and are involved in a wide variety of cellular processes such as proliferation, differentiation, transcription regulation and development. The activation of this kinase requires its phosphorylation by upstream kinases. Upon activation, it translocates to the nucleus of stimulated cells, where it phosphorylates nuclear targets, which in turn initiate transcription. MAPK1 was more abundant in transgenic mice overexpressing neurotrypsin in both synaptosomes and the hippocampus (Tables 1 and 3). Drebrin is a cytoplasmic actin-binding protein thought to play a role in the process of neuronal outgrowth. A decrease in drebrin expression in the brain has been implicated as a possible contributing factor in the pathogenesis of AD. Drebrin was up regulated in transgenic hippocampus P2 (Table 4).

3.4.3.2 Cell adhesion

Contactin 1 is a member of the immunoglobulin superfamily. It is a GPI-anchored neuronal membrane protein that functions as a heterophilic cell adhesion molecule, binding to NrCAM and neurofascin. It may play a role in the formation of axon connections in the developing nervous system. Contactin 1 expression was induced in adult transgenic animals by 1.55 but was reduced in S2 by a factor of 0.66 (Tables 1 and 3).

Neural cell adhesion molecule L1 is an axonal glycoprotein that belongs to the immunoglobulin supergene family. The ectodomain consists of several immunoglobulin-like domains and fibronectin-like repeats. It is linked via a single transmembrane sequence to a cytoplasmic domain. L1 plays an important role in nervous system development, including neuronal migration and differentiation. Mice that do not express L1 have defects in axon guidance of the corticospinal tract (Cohen et al., 1998). L1 expression was decreased in S2 but induced in P2 in P10 mice (Table 3).

Neuronal cell adhesion molecule (NrCAM) contains multiple immunoglobulin-like C2-type domains and fibronectin type-III domains. It is involved in neuron-neuron adhesion and promotes directional signaling during axonal outgrowth. Allelic variants of the gene have been associated with autism and addiction. Complex homo- and heterophilic binding and several extracellular ligands of NrCAM have been described, but less is known about intracellular interaction partners. Binding partner to the cytoplasmic terminus of NrCAM is ankyrin G and SAP102 (see later in the text) (Davey et al., 2005). Furthermore, the cytoplasmic C-terminus of NrCAM contains a typical sequence motif for binding to PDZ domains. Specific interactions of the intracellular domain of NrCAM with class I PDZ domains of PSD-95 and SAP97 were demonstrated (Dirks et al., 2006).

Intercellular adhesion molecule-5 (ICAM-5) is a dendritically polarized membrane glycoprotein in telencephalic neurons. ICAM-5 displays two types of adhesion activity, homophilic binding between neurons and heterophilic binding between neurons and leukocytes (Tian et al., 2000). Both immunoglobulin superfamily members NrCAM and ICAM-5, were down regulated in transgenic S2 (Table 3).

3.4.3.3 Synaptic transmission and synaptic plasticity

Glutamate receptors are the predominant excitatory neurotransmitter receptors in the mammalian brain and are activated in a variety of neurophysiologic processes. These receptors are heteromeric protein complexes with multiple subunits, each possessing transmembrane region, and all arranged to form a ligand-gated ion channel. The ionotrophic glutamate receptor 3 (GluR3) belongs to a family of AMPAR and was up regulated in P20 synaptosomes (Table 1). Alternative splicing results in several different isoforms, which may vary in their signal transduction properties. Knockout mice deficient in the expression of both GluR2 and GluR3 are severely impaired in the basal synaptic transmission. However, these mutant mice are competent in establishing several forms of long-lasting synaptic changes in the CA1 of the hippocampus, including LTD and LTP (Meng et al., 2003).

Small GTPase Rap1 plays an important role in the induction of mGluR5-dependent LTD by direct coupling to receptor trafficking machineries to facilitate the loss of synaptic AMPAR (Huang et al., 2004). Negative effects of Rap1 are observed in NMDAR-mediated synaptic transmission in hippocampal pyramidal neurons. This implies a possible role for Rap1 in glutamatergic synaptic transmission. In the context of neurotrypsin overexpression, Rap1 was up regulated by 1.88 in the synaptosomes of P40 transgenic mice (Table 1) as well as Rap1 GDI1 that was also up regulated in S2 by 1.7 as found in 2DE analysis (Table 7).

Protein kinase C (PKC) is a family of serine- and threonine-specific protein kinases that can be activated by Ca^{2+} and second messenger DAG. PKC family members phosphorylate a wide variety of protein targets and are known to be involved in diverse cellular signaling pathways. Each member of the PKC family has a specific expression profile and is believed to play distinct roles in cells. PKCε, down regulated in synaptosomes by 40% (Table 1) has been shown to be involved in many different cellular functions, such as neuron channel activation, apoptosis, cardioprotection from ischemia, heat shock response, as well as insulin exocytosis. Knockout studies in mice suggest that PKCε is important for lipopolysaccharide (LPS)-mediated signaling in activated macrophages and may also play a role in controlling anxiety-like behavior. PKCα, also down regulated in P2 by 35% (Table 3) has been reported to play roles in many different cellular processes, such as cell adhesion, cell transformation, cell cycle checkpoint, and cell volume control.

N-copine contains two copies of C2-domain. The mRNA expression was detected only in brain and was up regulated by stimulation evoking CA3-CA1 LTP. Thus, N-copine may have a role in synaptic plasticity (Nakayama et al., 1998). *In situ* hybridization analysis showed that N-copine mRNA was expressed exclusively in neurons of the hippocampus and in the main and accessory olfactory bulb. In immunohistochemical analyses, N-copine was mainly detected in the cell bodies and dendrites of neurons. In fractionation experiments of brain homogenate, N-copine was associated with the membrane fraction in the presence of Ca^{2+} but not in its absence. Therefore, N-copine may have a role as a Ca^{2+} sensor in postsynaptic events (Nakayama et al., 1999). There is evidence that copines may represent members of universal transduction pathways for Ca^{2+} signaling because it was found that copines are capable of interacting with a wide variety of "target" proteins including MAP/ERK kinase 1 (MEK1), protein phosphatase 5, and the Cdc42-binding kinase. The interaction with copines may result in the recruitment of target proteins to membrane surfaces and regulation of the enzymatic activities of target proteins (Tomsig et al., 2003). N-copine was up regulated in synaptosomes of P20 transgenic animals by 1.85 and down regulated in the hippocampus of P10 transgenic mice (S2: 0.71; P2: 0.83).

The 'SNARE hypothesis' is a model explaining the process of docking and fusion of vesicles to their target membranes. According to this model, membrane proteins from the vesicle (v-SNAREs) and proteins from the target membrane (t-SNAREs) govern the specificity of vesicle targeting and docking through mutual recognition. Once the 2 classes of SNAREs bind to each other, they form a complex that recruits the general elements of the fusion apparatus, namely NSF (N-ethylmaleimide-sensitive factor) and SNAPs (soluble NSF-attachment proteins). Stimulation of NSF ATPase activity by alpha-SNAP is required for SNARE complex disassembly and exocytosis (Barnard et al., 1997). A specific interaction of the GluR2 C-terminal peptide with ATPase NSF and alpha- and beta- SNAPs was found (Osten et al., 1998). The direct interaction suggests a rapid NSF-dependent modulation of AMPAR trafficking and stabilization. Alpha- and gamma-SNAPs are found in a wide range of tissues and act synergistically in intra-Golgi transport. The third SNAP, beta, is brain-specific. Thus, NSF and SNAPs play key roles in vesicular trafficking through the secretory pathway and appear to be general components of the intracellular membrane fusion apparatus (Whiteheart et al., 1993). Both alpha-SNAP and beta-SNAP were down regulated in transgenic S2. NSF protein was also less expressed in S2 by 40% (Table 2). Proteins that bind to cytoplasmic tails of AMPARs control receptor trafficking and thus the strength of postsynaptic responses. Adaptor protein complex 2 (AP-2) associates with a region of GluR2 that overlaps with the NSF binding site. AP-2 is involved specifically in NMDA receptor-induced internalization of AMPAR, and is essential for hippocampal LTD (see 'endocytosis'). NSF function, on the other hand, is needed to maintain synaptic AMPAR responses, but is not directly required for NMDA receptor-mediated internalization and LTD (Lee et al., 2002). Interestingly, NSF is up regulated in P2 by 1.17 (Table 2) and AP-2 alpha 1 subunit is also up regulated in P40 synaptosomes (Table 1 and 3). The AP-2 complex is a heterotetramer consisting of two large adaptins (alpha or beta), a medium adaptin (mu), and a small adaptin (sigma). The complex is part of the protein coat on the cytoplasmic face of coated vesicles, which links clathrin to receptors in vesicles. It was shown to interact with amphiphysin 2 (McMahon et al., 1997). AP-2 complex subunit alpha 1 was found in synaptosomes of adult mice and was up regulated whereas beta 1 subunit was down regulated in S2 demonstrated by 2DE (Tables 1 and 7).

Syntaxin binding protein (Munc18-1) is required for neurotransmitter release and inhibits binding of synaptobrevin and SNAP-25 to syntaxin 1A to modulate SNARE complex formation. During synaptic vesicle exocytosis, Munc18-1 is known to bind tightly to syntaxin-1, but only when syntaxin-1 is in a closed conformation that is incompatible with SNARE complex formation. Munc18-1 also binds tightly to assembled SNARE complexes containing syntaxin-1, suggesting that binding of Munc18-1 to closed syntaxin-1 is a specialization that evolved to meet the strict regulatory requirements of neuronal exocytosis, whereas binding of Munc18-1 to assembled SNARE complexes reflects a general function of proteins involved in executing membrane fusion (Dulubova et al., 2007). Deletion of Munc18-1 in mice leads to a complete loss of neurotransmitter secretion from synaptic vesicles throughout development. However, this does not prevent normal brain assembly, including formation of layered structures, fiber pathways, and morphologically defined synapses (Verhage et al., 2000). However, Munc18-1 was down regulated in S2 by 0.84 and up regulated in P2 by 1.14 (Table 2).

Ca^{2+}/calmodulin-dependent protein kinase II (CaMK II) belongs to the Ser/Thr protein kinase family, and to the Ca^{2+}/calmodulin-dependent protein kinase subfamily. This enzyme is composed of four different chains: alpha, beta, gamma, and delta. The alpha chain is required for hippocampal LTP and spatial learning. In addition to its calcium-calmodulin (CaM)-dependent activity, this protein can undergo autophosphorylation, resulting in CaM-independent activity. LTP and LTD of synaptic function often requires Ca^{2+}-influx via NMDARs and changes in the

autophosphorylation of CaMK II at Thr_{286}. Autophosphorylated CaMK II binds directly to NMDAR subunits, co-localizes with NMDARs in the PSD, and phosphorylates NR2B subunits. Calcium entry through postsynaptic NMDARs and subsequent activation of CaMK II triggers synaptic plasticity in many brain regions. Switching synaptic NMDAR containing NR2B subunits that bind CaMK II with high affinity with those containing NR2A, a subunit with low affinity for CaMK II, dramatically reduces LTP. Thus association between active CaMK II and NR2B is required for different forms of synaptic enhancement (Barria and Malinow, 2005). In particular, although NR2A and NR2B subunits are highly homologous, the sites of their interaction with CaMK II as well as the regulation of this binding differ. It is the CaMK II-dependent phosphorylation of the PDZ1 domain of PSD-95 regulating the signaling transduction pathway downstream of NMDA receptors (Gardoni et al., 2006). CaMK II expression was reduced both in S2 and P2 by 15 and 30%, respectively (Table 2).

NMDARs are targeted to dendrites and anchored at the PSD through interactions with PDZ proteins. However, little is known about how these receptors are sorted from the ER and Golgi apparatus to the synapse. It was found that synapse-associated protein 102 (SAP102) interacts with the PDZ-binding domain of Sec8, a member of the exocyst complex. Interactions between SAP102 and Sec8 are involved in the delivery of NMDARs to the cell surface in neurons. It was suggested that an exocyst-SAP102-NMDAR complex is an important component of NMDAR trafficking (Sans et al., 2003). Humans with mutations in SAP102 show mental retardation. Using SAP102 KO mice, specific impairments in synaptic plasticity were found. This was paralleled by inflexibility and impairment in spatial learning (Cuthbert et al., 2007). Interestingly, SAP102 was up regulated in transgenic S2 by 1.33 (Table 2).

SAPAP 4 is a membrane-associated guanylate kinase found at the PSD in neuronal cells. It is a signaling molecule that can interact with potassium channels and receptors, as well as other signaling molecules. It can interact with PSD-95 and may be involved in clustering PSD-95 in the postsynaptic density region. It may play a role in PSD structure and synaptic function (Takeuchi et al., 1997). SAPAP 4 was up regulated in P2 by 30% (Table 2).

3.4.3.4 Exocytosis

The Ca^{2+}-triggered release of neurotransmitters is mediated by fusion of synaptic vesicles with the plasma membrane. Complexins are two highly conserved cytosolic proteins that modulate neurotransmitter release. *In vitro*, they bind in a 1:1 stoichiometry to the assembled synaptic SNARE complex and modulate neuroexocytosis (Pabst et al., 2002). Besides synaptotagmin 1, fast Ca^{2+}-triggered exocytosis requires complexins. Complexin binding activates SNARE complexes into a metastable state and Ca^{2+}-binding to synaptotagmin 1 triggers fast exocytosis by displacing complexin from metastable SNARE complexes (Tang et al., 2006). Complexins compete with alpha-SNAP for SNARE complex binding. They are enriched in neurons where they co-localize with syntaxin and SNAP-25 (McMahon et al., 1995). Complexin 1 is down regulated in the soluble fraction of the hippocampus by 0.71 (Table 2).

Septin 5, which is predominantly expressed in the nervous system, was associated with membrane fractions, and co-precipitated with synaptic vesicles. It is linked to syntaxin by direct binding via the SNARE interaction domain. This interaction was occluded by the binding of alpha-SNAP, suggesting that septin 5 may regulate the availability of SNARE proteins through its interaction with syntaxin (Beites et al., 2005). Transfection of cells with wild-type septin 5 inhibited secretion, whereas GTPase dominant-negative mutants enhanced secretion. Thus, septins may regulate vesicle dynamics through interactions with syntaxin (Beites et al., 1999). Septin 5 overexpression exerted dopamine-dependent neurotoxicity (Dong et al., 2003). Homozygotic septin 5 null mice

appeared normal with respect to synaptic properties and hippocampal neuron outgrowth, suggesting that septin 5 is not essential for neuronal development or function. Changes in expression of other septins may account for its functional redundancy (Peng et al., 2002). In S2 of neurotrypsin-overexpressing mice septin 5 was down regulated by 0.67 (Table 2).
Rab3C plays a role in intracellular vesicle-mediated transport. It may be involved in Ca^{2+}-dependent exocytosis and neurotransmitter release. Rab3-induced modifications to primed vesicles causes a transient increase in the transduction efficacy of synaptic action potential (Schluter et al., 2006). Rab3C expression was induced both in P40 synaptosomes of transgenic mice by 1.99 and in S2 of the hippocampus by 1.20 (Table 1 and 2). GDP GDI are proteins that regulate the GDP-GTP exchange reaction of members of the Rab family. GDIs slow down the rate of dissociation of GDP from Rab proteins. Rab GDI 1 is expressed primarily in neural and sensory tissues. Mutations in Rab GDI 1 have been linked to X-linked nonspecific mental retardation. Interestingly, 2DE revealed that Rab GDI 1 was down regulated in S2 by 0.58 (Table 7). The cycling between the GDP-bound and GTP-bound forms of Rab small GTPases is also regulated by the action of a GTPase activating proteins (GAPs). Rab3-GAP 1 is a heterodimeric complex consisting of a 130 kDa catalytic subunit and a 150 kDa noncatalytic subunit. It is specifically active on the Rab3 subfamily members (Rab3A, -B, -C, and -D). In hippocampus S2 overexpressing neurotrypsin, the Rab3-specific Rab-GAP 1 catalytic subunit was reduced by 0.82. (Table 2).

3.4.3.5 Endocytosis

Amphiphysin 2 (BIN1) is a putative tumor suppressor that was identified through its interaction with the Myc oncoprotein. Two isoforms are produced by alternative splicing, one of which is mainly expressed in the nerve terminals. Amphiphysin, through its SH3 domain, acts as an adaptor for a series of proteins important for the clathrin-mediated endocytosis, such as dynamin (Wigge and McMahon, 1998). Amphiphysin 2 is not only a regulator of the early steps of endocytosis. It could also play a role at the surface of endocytic vesicles that have just been formed and of the future endosomes, in order to regulate intracellular trafficking. It was up regulated both in synaptosomes of young (1.38) and adult (1.52) transgenic mice (Table 1).
Dynamin 1 is involved in clathrin-mediated endocytosis and other vesicular trafficking processes (Koenig and Ikeda, 1989; Roux et al., 2006). Actin and other cytoskeletal proteins act as binding partners for dynamin 1, which can also self-assemble leading to stimulation of GTPase activity. A long proline-rich stretch present in dynamin 1 specifically recognizes and binds the SH3 domain-containing neuronal protein amphiphysin 2 (Grabs et al., 1997). PACSIN 2 is a ubiquitously expressed isoform of the brain-specific PACSIN 1. PACSIN 2 binds dynamin I, synaptojanin, synapsin I, and N-WASP, a stimulator of Arp2/3 induced actin filament nucleation. In neuroendocrine cells PACSIN 2 co-localizes with dynamin consistent with a role for PACSIN in dynamin-mediated endocytic processes. Furthermore, PACSINs localize to sites of high actin turnover, such as filopodia tips and lamellipodia (Qualmann and Kelly, 2000). It strongly suggests that PACSINs link endocytosis and actin dynamics. Both proteins dynamin 1 and PACSIN 2 were down regulated in S2 transgenic sample by 0.75 and 0.77, respectively (Table 2).
Syntaxin 7 is a component of the SNARE complex crucial for vesicle docking and fusion events with membranes. It mediates the endocytic trafficking from early endosomes to late endosomes and lysosomes. The crystal structure of an endosomal SNARE core complex contained four SNAREs: syntaxin 7, syntaxin 8, vti1b and endobrevin/VAMP-8 were resolved (Antonin et al., 2002). Syntaxin 7 showed an upregulation of 1.23 in transgenic P2 (Table 2).

3.4.3.6 Neuroendocrine, synapse remodeling, and neurotransmitter clearance

Chromogranin B is a tyrosine-sulfated secretory protein found in a wide variety of peptidergic endocrine cells. It functions as a neuroendocrine secretory granule protein, which may be the precursor for other biologically active peptides. It was up regulated in synaptosomes of P20 by 1.32 as well as of P40 mice by 1.83 (Table 1) but down regulated in the hippocampal S2 of P10 transgenic mice by 0.70 (Table 2).

Neuronal pentraxin 1 (NP1) is a protein involved in excitatory synapse remodeling that has recently been shown to mediate neuronal death induced by reduction in neuronal activity in mature neurons (DeGregorio-Rocasolano et al., 2001). Treatment of cortical neurons in culture with Aβ produces a marked increase in NP1 protein that precedes apoptotic neurotoxicity. Silencing NP1 gene expression by RNA interference prevents the loss of synapses, the reduction in neurite outgrowth, and apoptosis evoked by Aβ. Transgenic overexpression of NP1 reproduced the neurotoxic effects of Aβ. Moreover, it was found that NP1 was increased in dystrophic neurites of brains from patients with sporadic late-onset AD. Thus, NP1 is a key factor for the synapse loss, neurite damage, and the apoptotic neuronal death evoked by Aβ (Abad et al., 2006). It was down regulated in S2 by 0.71 (Table 2).

Excitatory amino acid transporter 2 (EAAT2) is specific to astrocytes under normal conditions. Functional studies suggest that up to 95% of all glutamate is cleared from the synaptic cleft by EAAT2 (Zhou and Sutherland, 2004). Loss of EAAT2 has been reported in amyotrophic lateral sclerosis (ALS) and Alzheimer's disease (Masliah et al., 1996; Rothstein et al., 1995). Interestingly, numerous abnormally spliced EAAT2 mRNAs have been identified from the affected areas of ALS patients and the expression of these abnormally spliced RNA species correlated with the loss of EAAT2 protein in ALS (Lin et al., 1998). The loss of functional EAAT2 could lead to the accumulation of extracellular glutamate, resulting in cell death known as excitotoxicity. Furthermore, increased expression of EAAT2 was found in the prefrontal cortex of schizophrenics (Matute et al., 2005). These examples illustrate that under normal conditions, expression and splicing of EAAT2 must be tightly controlled otherwise the clearance of glutamate from the synaptic cleft is disturbed, which has fatal consequences. In the synaptosomes of adult mice overexpressing neurotrypsin, EAAT2 was up regulated (Table 1). In the hippocampus EAAT2 was found in P2. Its expression was down regulated by 0.75 in the transgenic samples (Table 2).

Glutamine is the main source of energy and is involved in cell proliferation, inhibition of apoptosis, and cell signaling (Haberle et al., 2005). Glutamine synthetase (GS) is expressed throughout the body and plays an important role in controlling body pH and in removing ammonia from the circulation. In the CNS, GS is almost exclusively expressed by the glial cells and astrocytes (Grossman et al., 1994). GS serves to convert L-glutamate, the primary amino acid neurotransmitter in the CNS. L-glutamate is converted to glutamine under the consumption of ATP and ammonia. Glutamine diffuses from the astrocytes to the neurons, where it is converted back to L-glutamate by glutaminase, thus re-entering the neurotransmitter pool. If the synthesis of glutamine is blocked, neither uptake nor *de novo* synthesis is sufficient to maintain proper neurotransmission (Laake et al., 1995). The main mechanism for ammonia elimination in the brain is its reaction with glutamate to form glutamine. Acute intoxication with large doses of ammonia leads to rapid death. GS activity and glutamine content in brain are modulated by NMDA receptors and nitric oxide (Kosenko et al., 2003). High extracellular glutamate concentrations have been identified as a likely trigger of epileptic seizures in mesial temporal lobe epilepsy (MTLE). Loss of GS was particularly pronounced in areas of the MTLE hippocampus with astroglial proliferation. Quantitative immunoblotting showed no significant change in the amount of

EAAT2. Therefore, a deficiency in GS in astrocytes is a possible molecular basis for extracellular glutamate accumulation and seizure generation in MTLE (Eid et al., 2004). In the ICAT screen GS was down regulated in the synaptosomes of transgenic mice by 0.73. The expression was also reduced in transgene P2 of the hippocampus by 0.85, but was up regulated in the S2 fraction of neurotrypsin-overexpressing mice by 1.40 (Table 1 and 6).

3.4.3.7 Metabolic processes

Aerobic glycolysis of glucose to pyruvate requires two equivalents of ATP to activate the process, with the subsequent production of four equivalents of ATP and two equivalents of NADH. Thus, conversion of one mole of glucose to two moles of pyruvate is accompanied by the net production of two moles each of ATP and NADH.

Glucose + 2 ADP + 2 NAD^+ + 2 Pi --------> 2 Pyruvate + 2 ATP + 2 NADH + 2 H^+

Hexokinase 1 is the enzyme involved in the first reaction of the glycolysis. It catalyzes the ATP-dependent phosphorylation of glucose that activates the biochemically inert glucose into a labile form capable of being further metabolized. Hexokinase 1 is up regulated in synaptosomes by 1.80 but down regulated in S2 by 0.73 (Tables 1 and 5). Before pyruvate kinase catalyzes the final step of the glycolysis by conserving the high-energy phosphate of phosphoenolpyruvate (PEP) as ATP and thereby producing pyruvate, phosphoglycerate mutase and enolase convert the relatively low energy phosphoacyl-ester of 3-phosphoglycerate in two catalyzed reactions to PEP. While the expression of phosphoglycerate mutase 1 and α-enolase was down regulated in the 2DE experiment (Table 7), two isoforms of enolase, alpha and gamma, were up regulated both in S2 and P2 in ICAT (Table 5).
The bulk of ATP used by many cells to maintain homeostasis is produced by the oxidation of pyruvate in the tricarboxylic acid (TCA) cycle. The fate of pyruvate depends on the cell energy charge. In cells or tissues with a high-energy charge pyruvate is directed toward gluconeogenesis, but when the energy charge is low pyruvate is preferentially oxidized to CO_2 and H_2O in the TCA cycle, with generation of 15 equivalents of ATP per pyruvate. When transported into the mitochondrion, pyruvate encounters two principal metabolizing enzymes: pyruvate carboxylase and pyruvate dehydrogenase (PDH), the first enzyme of the PDH complex. When the energy charge is low coenzyme A (CoA) is not acylated, pyruvate carboxylase is inactive, and pyruvate is preferentially metabolized via the PDH complex and the enzymes of the TCA cycle. Reduced NADH and $FADH_2$ generated during the oxidative reactions can then be used to drive ATP synthesis via oxidative phosphorylation. The PDH complex is comprised of multiple copies of 3 separate enzymes: pyruvate dehydrogenase (20-30 copies), dihydrolipoyl transacetylase (60 copies) and dihydrolipoyl dehydrogenase (6 copies) and 5 different coenzymes. The net result of the reactions of the PDH complex is:

Pyruvate + CoA + NAD^+ ------> CO_2 + acetyl-CoA + NADH + H^+

The reactions of the PDH complex serves to interconnect the metabolic pathways of glycolysis, gluconeogenesis and fatty acid synthesis to the TCA cycle. As a consequence, the activity of the PDH complex is highly regulated by a variety of allosteric effectors and by covalent modification. PDH activity is regulated by its state of phosphorylation, being most active in the dephosphorylated state. Phosphorylation of PDH is catalyzed by a specific PDH kinase. The

activity of the kinase is enhanced when cellular energy charge is high which is reflected by an increase in the level of ATP, NADH and acetyl-CoA. Conversely, an increase in pyruvate strongly inhibits PDH kinase. In the synaptosomes of transgenic mice the PDH kinase isoform 2 is down regulated by 0.54 and components of the PDH complex are down regulated in S2 and up regulated in P2 (Tables 1 and 5).

The first reaction of the TCA cycle is the condensation of the methyl carbon of acetyl-CoA with the keto carbon of oxaloacetate (OAA). When the cellular energy charge increases the rate of flux through the cycle will decline leading to a build-up of citrate. Excess citrate is used to transport acetyl-CoA carbons from the mitochondrion to the cytoplasm where they can be used for fatty acid and cholesterol biosynthesis. Additionally, the increased levels of citrate in the cytoplasm activate the key regulatory enzyme of fatty acid biosynthesis, acetyl-CoA carboxylase. Citrate synthase was up regulated in the hippocampus P2 fraction (Table 5). The isomerization of citrate to isocitrate is catalyzed by aconitase and is the second step in the TCA cycle. Its expression was up regulated in P2 hippocampus fraction (Table 5).

In the third step, isocitrate is oxidatively decarboxylated to α-ketoglutarate by isocitrate dehydrogenase, (IDH). There are two different IDH enzymes. The IDH of the TCA cycle uses NAD^+ as a cofactor, whereas the other IDH uses $NADP^+$ as a cofactor. Unlike the NAD^+-requiring enzyme, which is located only in the mitochondrial matrix, the $NADP^+$-requiring enzyme is found in both the mitochondrial matrix and the cytosol. IDH catalyzes the rate-limiting step, as well as the first NADH-yielding reaction of the TCA cycle. All IDH isoforms found in the ICAT screen were up regulated (Table 1 and 5).

L-malate is the specific substrate for malate dehydrogenase (MDH), the final enzyme of the TCA cycle. The forward reaction of the cycle, the oxidation of malate yields OAA. MDH was up regulated at least in synaptosomes of P40 animals (Table 1).

In addition, lactate dehydrogenase (LDH) catalyzes the interconversion of pyruvate and lactate with concomitant oxidation of NADH. The lactate produced during anaerobic glycolysis diffuses from the tissues and is transported to highly aerobic tissues such as cardiac muscle liver or brain. The lactate is then oxidized to pyruvate in these cells by LDH and the pyruvate is further oxidized in the TCA cycle. If the energy level in these cells is high the carbons of pyruvate will be diverted back to glucose via the gluconeogenesis pathway. Mammalian cells contain two distinct types of LDH subunits, termed M and H. Combinations of these different subunits generates LDH isozymes with different characteristics. The H type subunit predominates in aerobic tissues while the M subunit predominates in anaerobic tissues. The H-type LDH is utilized for oxidizing lactate to pyruvate and the M-type the reverse. In synaptosomes of P40 transgenic mice LDH-M is up regulated (Table 1). Finally, after glycogen phosphorylase has broken off a single glucose molecule from the greater glycogen structure the free glucose has a phosphate group on its 1-carbon. This glucose-1-phosphate isomer cannot be metabolized easily. The enzyme phosphoglucomutase phosphorylates the 6-carbon, while subsequently dephosphorylating the 1-carbon. The result is glucose-6-phosphate, which can now travel down the glycolysis pathway. Phosphoglucomutase also acts in the opposite fashion when a large concentration of glucose-6-phosphate is present. Phosphoglucomutase 2-like 1 expression was increased in S2 of 2DE and P2 of ICAT by 1.5 and 1.43, respectively (Tables 5 and 7).

3.4.3.8 Neuron migration and differentiation of the nervous system

Brevican is the most abundant chondroitin sulfate proteoglycan in the ECM of the adult rat brain. Brevican expression is up regulated coincident with glial cell proliferation and/or motility and during early CNS development and in invasive glioma. An understanding of the molecular interactions that mediate Brevican function is still in its infancy because of the existence of several isoforms, each of which may mediate different functions (Viapiano et al., 2003). It was demonstrated that MMP-1, -2, -3, -7, -8, -10, and -13 and aggrecanase-1 digest brevican in a similar pattern to aggrecan and suggest that they may be responsible for the physiological turnover and pathological degradation of brevican (Nakamura et al., 2000). Expression of brevican was reduced in hippocampal S2 by 0.75 (Table 3).
In the developing cortex, cortical neurons must migrate over long distances to reach the site of their final differentiation. Doublecortin appears to direct neuronal migration by regulating the organization and stability of microtubules (Gleeson et al., 1999). It contains two doublecortin domains, which bind microtubules. A certain proportion of doublecortin interacts with AP-1 and/or AP-2 complex *in vivo* and are consistent with a potential involvement of doublecortin in protein sorting or vesicular trafficking (Friocourt et al., 2001). Doublecortin expression was induced in S2 by 1.27 (Table 3).

3.4.3.9 Apoptosis

Mitochondrial outer membrane permeability is conferred by a family of voltage-dependent anion channels (VDACs), also known as mitochondrial porins. VDACs conduct small molecules and constitute one component of the permeability transition pore that opens in response to apoptotic signals (Shimizu et al., 1999). Mitochondrial porins have significant roles in diverse cellular processes including regulation of mitochondrial ATP and calcium flux. Furthermore, fear conditioning and spatial learning are disrupted in VDAC-deficient mice. Electrophysiological recordings of VDAC-deficient hippocampal slices reveal deficits in long and short-term synaptic plasticity (Weeber et al., 2002). VDACs may also serve as binding sites for kinases, including hexokinase. Mitochondria-bound hexokinase activity was significantly reduced in oxidative muscles (heart and soleus) in vdac1(-/-) mice. Mice lacking both VDAC1 and VDAC3 have reduced exercise capacity together with impaired glucose tolerance. Therefore, there is a link between VDAC1 mediated mitochondria-bound hexokinase activity and the capacity for glucose clearance (Anflous-Pharayra et al., 2007). VDAC1 was reduced in transgenic P2 by 30% (Table 6).

3.4.3.10 Varia

Adenosine kinase (AK) is an abundant enzyme in mammalian tissues, which was strongly down-regulated in both P20 and P40 transgenic animals. The enzyme catalyzes the transfer of the gamma-phosphate from ATP to adenosine, thereby serving as a regulator of concentrations of both extracellular adenosine and intracellular adenine nucleotides. Immunohistochemical analysis of brain sections of mice revealed intense staining for adenosine kinase, mainly in astrocytes, which were more or less evenly distributed throughout the brain, as well as in some neurons, particularly in olfactory bulb, striatum, and brainstem. Adenosine has widespread effects on the cardiovascular, nervous, respiratory, and immune systems and inhibitors of the enzyme could play an important pharmacological role in increasing intravascular adenosine

concentrations and acting as anti-inflammatory agents. Endogenous adenosine in the brain is thought to prevent the development and spread of seizures via a tonic anticonvulsant effect (Gouder et al., 2004). Brain levels of adenosine are primarily regulated by the activity of adenosine kinase. Thus, transient down regulation of AK after acute brain injury protects the brain from seizures and cell death. Conversely, chronic overexpression of AK causes seizures in epilepsy and promotes cell death in epilepsy and stroke (Boison, 2006). AK was down regulated in synaptosomes of transgenic young (0.47) and adult (0.1), whereas 2DE revealed that AK was up regulated in S2 by 60% (Tables 1 and 7)

The Na^+/K^+-ATPase (NKA) belongs to the family of P-type cation transport ATPases. NKA is an integral membrane protein responsible for establishing and maintaining the electrochemical gradients of Na^+ and K^+ ions across the plasma membrane. These gradients are essential for osmoregulation, for sodium-coupled transport of a variety of organic and inorganic molecules, and for electrical excitability of nerve and muscle. This enzyme is composed of two subunits, a large catalytic subunit (alpha) and a smaller glycoprotein subunit (beta). Multiple genes encode the catalytic subunit of NKA. Today three alpha subunits are known in the brain: alpha 1 isoform is found in many cell types, the alpha 2 isoform is predominantly expressed in astrocytes, and the alpha 3 isoform is exclusively expressed in neurons (Shull et al., 1986). Several disorders have been associated with mutations in NKA alpha isoforms (rapid-onset dystonia parkinsonism, familial hemiplegic migraine type-2), as well as reduction in NKA content (depression and Alzheimer's disease), thereby raising the issue of whether haploinsufficiency or altered enzymatic function contribute to disease etiology. Mice heterozygous for the alpha3 isoform displayed spatial learning and memory deficits, increased locomotor activity, and a 40% reduction in hippocampal NMDA receptor expression (Moseley et al., 2007). There is biochemical evidence that agrin binds to the alpha3 subunit of the NKA in CNS neurons. Co-localization with agrin binding sites at synapses supports the hypothesis that the alpha3NKA is a neuronal agrin receptor. A 20 kDa C-terminal agrin fragment that acts as a competitive antagonist depresses action potential frequency, showing that endogenous agrin regulates native alpha3NKA function. Therefore it was hypothesized that agrin regulates activity-dependent processes in neurons (Hilgenberg et al., 2006). α3, β1, and β2 subunits were all down regulated in transgenic S2 and P2 by around 30% (Table 6).

3.4.4 GO annotation of differentially expressed proteins

Because only small differences in protein abundance ratios were found we thought that modulatory changes of neurotrypsin-dependent cellular processes and molecular functions were better to disclose. The question arose whether the regulatory changes were more distinct when the changed proteins were grouped into functional categories. Therefore, the regulated proteins irrespective of their up- or down regulation were brought together and grouped into GO terms. Pie diagrams of 'biological process' in general and more specific of 'transport' and 'metabolic process' highlighted the affected categories (Fig. 3.15). NOTE: not every GO term that changed proteins could possibly be annotated to, was taken into account. Some rare GO terms were ignored. Furthermore, one term does not necessarily reflect 100% of all regulated proteins. And due to manifold functions proteins were allowed being allocated to multiple categories. In the hippocampus changed proteins that are involved in neuronal signal transduction mechanisms such as 'synaptic transmission', 'signal transduction', and 'synaptic plasticity' accounted for 36%. 45% of the differentially regulated proteins were involved in

morphological or functional rearrangements of neuronal cells like 'neurite development', 'cell proliferation and motility', 'axon/neuron guidance' and 'differentiation', while 'adhesion' was composed of 19%. In synapses much more regulated proteins were involved in signal transduction (54%). Less affected were proteins involved in proliferation and differentiation (30%). A comparable amount of candidates played a role in 'adhesion' (16%).
As for the 'metabolic process', 26% were involved in fatty acid/lipid metabolism, whereas in the synaptosomes it was 56%. In the hippocampus the tricarboxylic acid (TCA) cycle was well represented by 35% and in the synaptosomes it was mere 4%. 39% in the hippocampus and 40% in the synaptosomes, were involved in 'glycolysis' and 'glucose and glutamate metabolism'. Comparing the diagrams 'transport' from the hippocampus and the synaptosomes a lot of similarities were found. Together 'endocytosis' and 'exocytosis' represented 44% (hippocampus) and 38% (synaptosomes) of the differentially regulated proteins. 56% and 62% were annotated to vesicle transport mechanisms like 'antero- and retrograde ER-Golgi transport', 'secretory pathway' and 'vesicle mediated transport'. However, the major difference here was the total amount of proteins classified into the GO term 'transport'; whereas only 18 hippocampal proteins fell into this category from the synaptosomes 29 different proteins were involved in 'transport'.

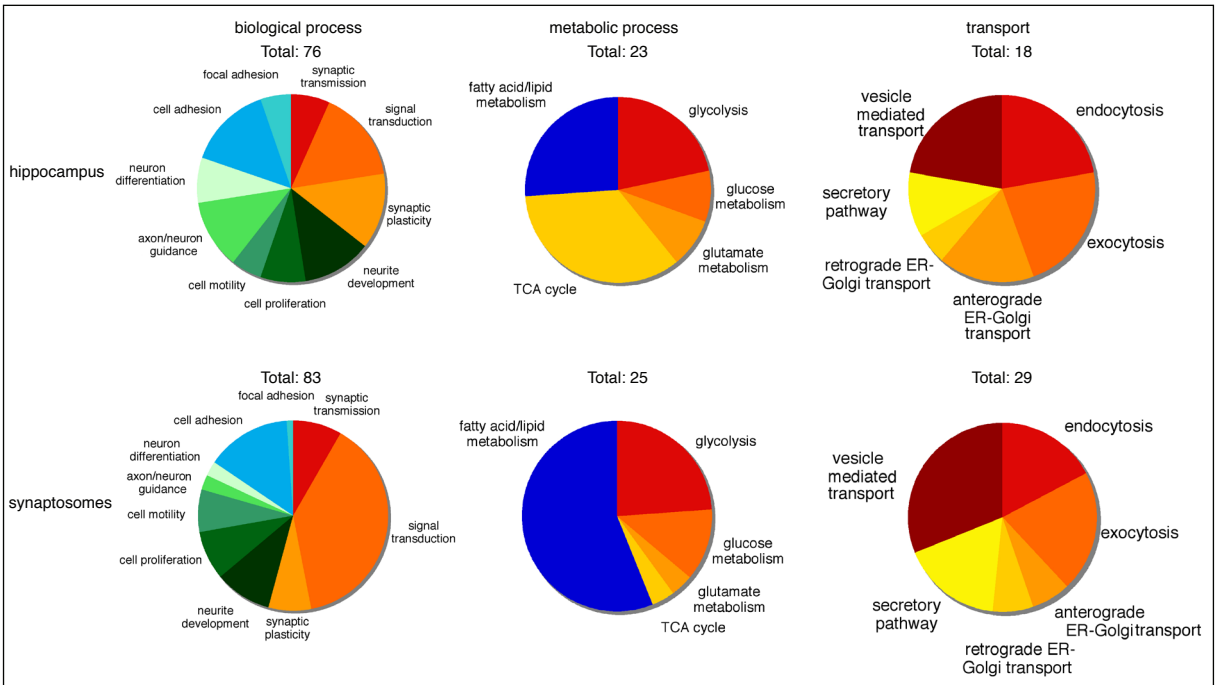

Figure 3.14 Differentially expressed proteins from synaptosomes and the hippocampus are annotated according to Gene Ontology (GO) terms.
Categorization of changed proteins from the hippocampus (S2 and P2 together) and the synaptosomes into GO terms irrespective of up- or downregulation. Highly represented categories imply perturbance of the particular process or function. Relatively a lot of proteins were allocated to 'biological processes' such as signal transduction (in synaptosomes), 'cell adhesion', 'synaptic plasticity and transmission', as well as 'cell proliferation' and 'differentiation', 'neurite development' and 'axon/neuron guidance'. Many proteins were found involved in 'metabolic process' as diverse as 'fatty acid/lipid metabolism', 'tricarboxylic acid cycle' (hippocampus), 'glycolysis' (hippocampus), and 'energy reserve metabolism'. Finally, proteins assigned to 'transport' such as 'endo- and exocytosis' and 'vesicle mediated transport' are also remarkably often changed.

3.5 Verification of candidate proteins

3.5.1 Verification of three candidates found in synaptosomes

Adenosine is a potent modulator of excitatory neurotransmission, especially in seizure-prone regions such as the hippocampal formation. Chronic overexpression of AK causes seizures and promotes cell death in epilepsy and stroke. Whereas transient down regulation of AK after acute brain injury protects the brain from seizures and cell death. The finding that AK is reduced in the synaptosomal preparations of transgenic mice suggested a compensatory mechanism to potentially evoked seizure by neurotrypsin overexpression.

A specific role of TM-agrin in shaping the cytoskeleton of neurites in the developing nervous system (Annies et al., 2006) and the knowledge that PAK1 protein is an important regulator of cytoskeletal dynamics lead to the hypothesis that increased cleavage of agrin by overexpressed neurotrypsin might elicit a signaling pathway implicating PAK1 as a molecular switch. It was further shown that the intracellular level of activated Cdc42 and Rac1 (Parrini et al., 2002) regulates its dimerization. Moreover, PAK1 is believed to act directly on the JNK1 MAP kinase pathway.

Finally, the MAPK/ERK pathway is a signal transduction cascade that couples intracellular responses to the binding of growth factors to cell surface receptors. The pathway has a hierarchical structure starting with the extracellular stimuli activating MAP kinase kinase kinase (MAPKKK), MAP kinas kinase (MAPKK) and MAP kinase (MAPK) that transduces further signals to the nucleus, which then promotes transcription of specific genes. The MAPK signaling pathway is usually activated by growth factors, which might be provided by the excessive production of the C-terminal agrin LG3 domain by neurotrypsin.

In order to confirm the regulatory changes in protein expression of AK, PAK1, and MAPK1, quantitative Western blotting was performed. The abundance ratios of the proteins were assessed by spot densitometry of at least three immunoblots of three independent preparations. PSD-95 was used for normalization. As opposed to the findings from the ICAT proteomic profiling, AK tested in different mouse lines (M494, M491S and S/A785) was either not regulated in P20 synaptosomes or up regulated in synaptosomes of P40 neurotrypsin overexpression mice (Fig. 3.16a and b).

Synaptosomes of P20 M494 mice showed an increased abundance ratio in PAK1 expression in transgenic samples. The outcome with a regulation factor of 1.5 was consistent with the ICAT (Table 1). However, a ratio of 1: 1 was found for PAK1 in synaptosomes of the same age from the other neurotrypsin-overexpressing mouse line M491S (Fig. 3.17a and b).

MAPK 1 showed a ratio of 1.20, 1.37, and 1.66 in the ICAT screen (Tables 1 and 3). Consistently, an increased expression level of 1.22 and 1.25 was also found in P20 synaptosomes of M494 and M491S mice, and yet an abundance ratio of 1.49 was demonstrated in M494 P40. The Western blotting of synaptosomes from the control line f494 with a silent transgene revealed a ratio of 0.79 and 1.15 for P20 and P40, respectively (Fig. 3.17c and d).

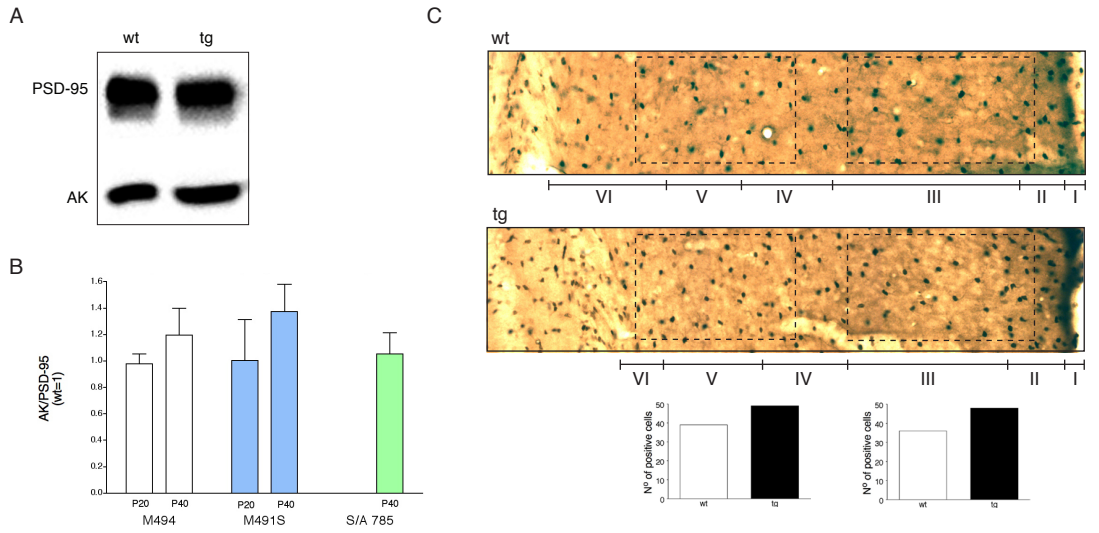

Figure 3.15 Verification of adenosine kinase expression in synaptosomes.
(A) To confirm the MS-data, suggesting a downregulation of adenosine kinase (AK) in synaptosomes of neurotrypsin overexpressing mice (P20: 0.47, P40: 0.10), equal amounts of synaptosomal protein extracts from wild-type (wt) and transgenic (tg) mice were loaded on a SDS-PAGE, immunoblotted with anti-AK antibody and quantified (N=3). PSD-95 was used as a reference protein for normalization. **(B)** A histogram showing slightly increased expression of AK in the tg samples of P40 mice for M494 and M491S. For the S/A 785 mouse line no regulation was found in P40. In P20 mice, AK was equally expressed in both wt and tg. **(C)** Immunohistochemical staining of AK in the neocortex of wt and tg P40 mice. The AK-positive cells in the dashed squares were counted and wt was plotted against tg. In both the deeper and the higher cortical layers more AK-positive cells in tg than in wt were found. Cortical layers I - VI are indicated. Layer VI is shortened in tg animals.

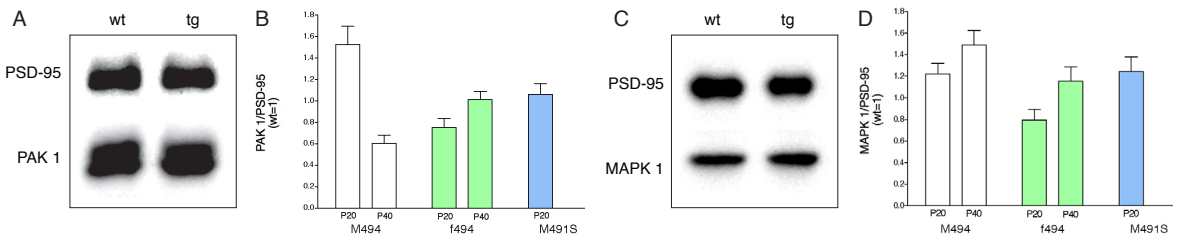

Figure 3.16 Verification of p21-activated kinase (PAK 1) and mitogen-activated protein kinase 1 (MAPK 1) expression in synaptosomes.
(A) To confirm the MS-data, suggesting an upregulation of PAK 1 in synaptosomes of neurotrypsin overexpressing mice (P20: 1.59, P40: 1.04), equal amounts of protein extracts were loaded on a SDS-PAGE. PAK 1 was immunoblotted and quantified in wild-type (wt) and transgenic (tg) mice (N=3). PSD-95 was used as a reference protein for normalization. **(B)** A histogram confirming an increase in the tg samples of P20 M494 and a tremendous decrease in P40 M494 mice. Changes are not detectable in P20 M491S. In tg mice f494 no change for PAK 1 expression was found in P40 and slightly reduced levels were found in P20 animals. **(C)** MAPK 1 showed an upregulation by a factor of 1.66 in the ICAT with P40 synaptosomes, a 1.39 upregulation in P2, and 1.22 upregulation in S2. The protein was immunoblotted and relative quantities were calculated. **(D)** In both, M494 and M491S of P20 synaptosomes, MAPK 1 was slightly stronger in tg samples. In P40 the increase was even stronger, confirming the findings of ICAT. In the control line f494 MAPK 1 expression is at 0.8 in P20 and at 1.18 in P40.

Although the quantitative changes of AK found in the ICAT approach revealed a down regulation in the transgenic samples could not be confirmed by immunoblotting, further efforts have been taken to investigate the expression level in more detail. Because the synaptosomes originated from a pool of whole mouse brains, it was hypothesized that the differential regulation of AK was restricted to well-defined specialized areas of the brain such as the hippocampus, where exogenous neurotrypsin was abundant. Moreover, the 2DE analysis suggested that AK might indeed be up regulated in S2. Therefore, immunohistochemical staining of coronal sections from mouse brains comparing wild-type and transgene were prepared. A punctated somatic, AK-

positive staining was evenly distributed throughout the different layers of the cortex. Interestingly, cortical layer VI was shortened in the transgenic P40 M494 mice as compared to wild-type litter mates. In addition, the number of AK-positive cells was increased in transgenic samples by 25% in layers III and V (Fig. 3.16c). At this point it was unclear whether the staining is glial or neuronal. From the literature it was described that AK is primarily expressed in astrocytes (Gouder et al., 2004). The question, whether the neurotrypsin induced, newly expressing cells were of neuronal or of astroglial origin arose. Therefore, fluorescent immunohistochemistry with double labeling of AK and neuronal or astroglial marker proteins were performed. Double staining of cortical layers I – III with AK and neuronal marker NeuN antibodies confirmed the increased number of AK-positive cells. But firstly, the AK signal did not co-localize with NeuN staining and secondly the number of neuronal cells was equal comparing wild-type and transgene (Fig. 3.18a). A comparable situation was found in layers V and VI where more AK-positive cells were found, but neither an increase in neuronal cells nor co-localization was found (Fig. 3.18b). In contrast, co-localization studies with glial fibrillary acidic protein (GFAP) and AK demonstrated that in the hippocampus and particularly in the dentate gyrus there was a substantial overlap between the two (Fig. 3.19a, b). In the dentate gyrus the protrusions stained with GFAP antibody reaching out of the cell bodies originated by up to 100% from AK-positive cells. Furthermore, there was an increase in both AK- and GFAP-positive staining in the dentate gyrus. However, the AK-positive cells outside of the dentate gyrus rarely co-localized with GFAP. There, neither the number of GFAP-positive nor the number of AK-positive cells seemed to be changed, indicating that the newly AK-positive cells in the dentate gyrus are of astroglial origin (Fig. 3.19a).

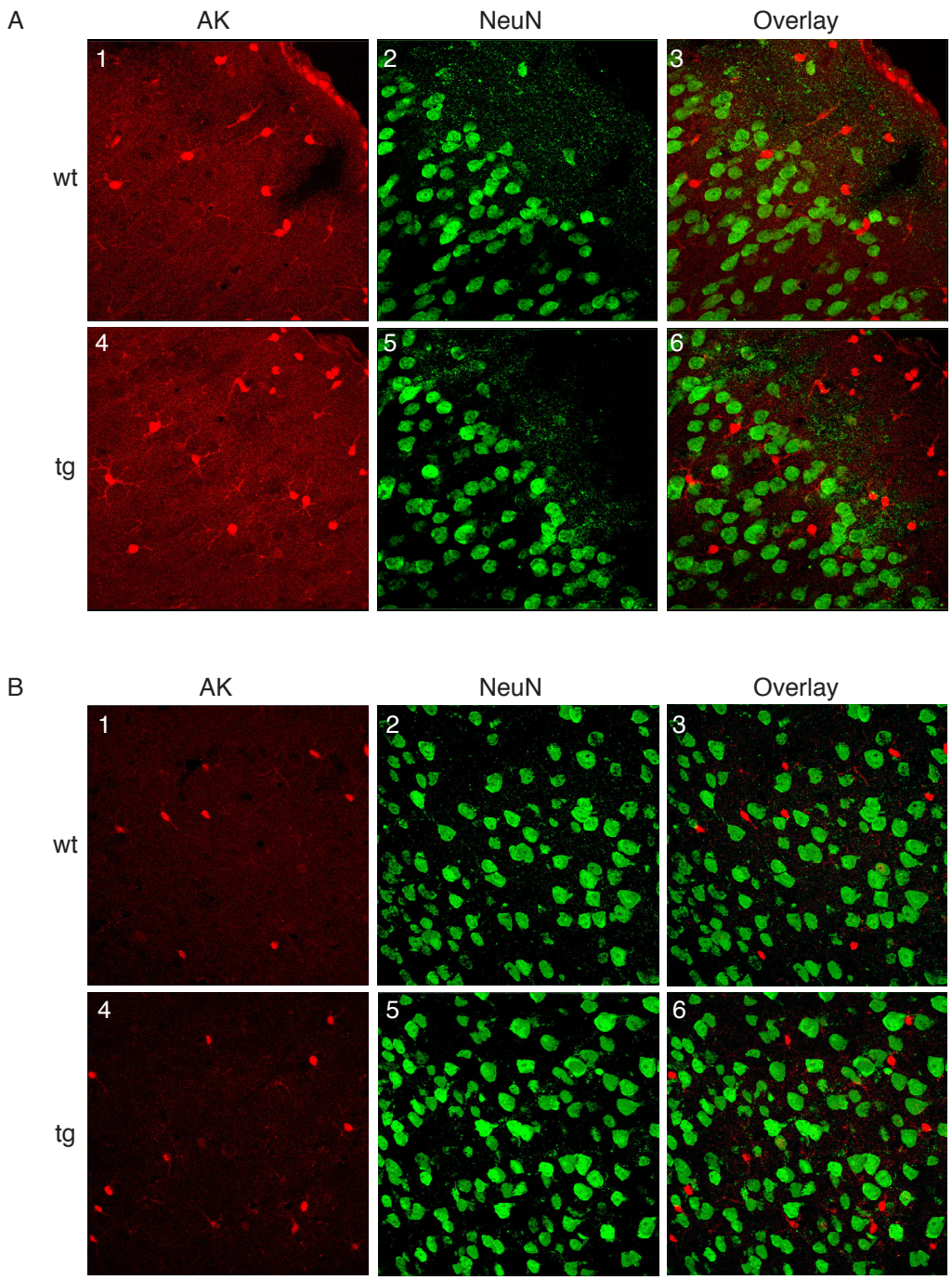

Figure 3.17 Adenosine kinase expression in the cortex.
(A) In cortical layers I - III the adenosine kinase (AK)-positive cells are enriched in the transgenic mice (1 vs. 4), whereas the number of neurons, detected with neuron-specific marker NeuN is unchanged (2 vs. 5). Absolutely no co-localization of the two proteins could be observed (3 and 6). **(B)** There are also more AK-positive cells in cortical layers V and VI (1, 4), and the number of neurons is similar as well (2 vs. 5). Co-localization was not found either (3 and 6).

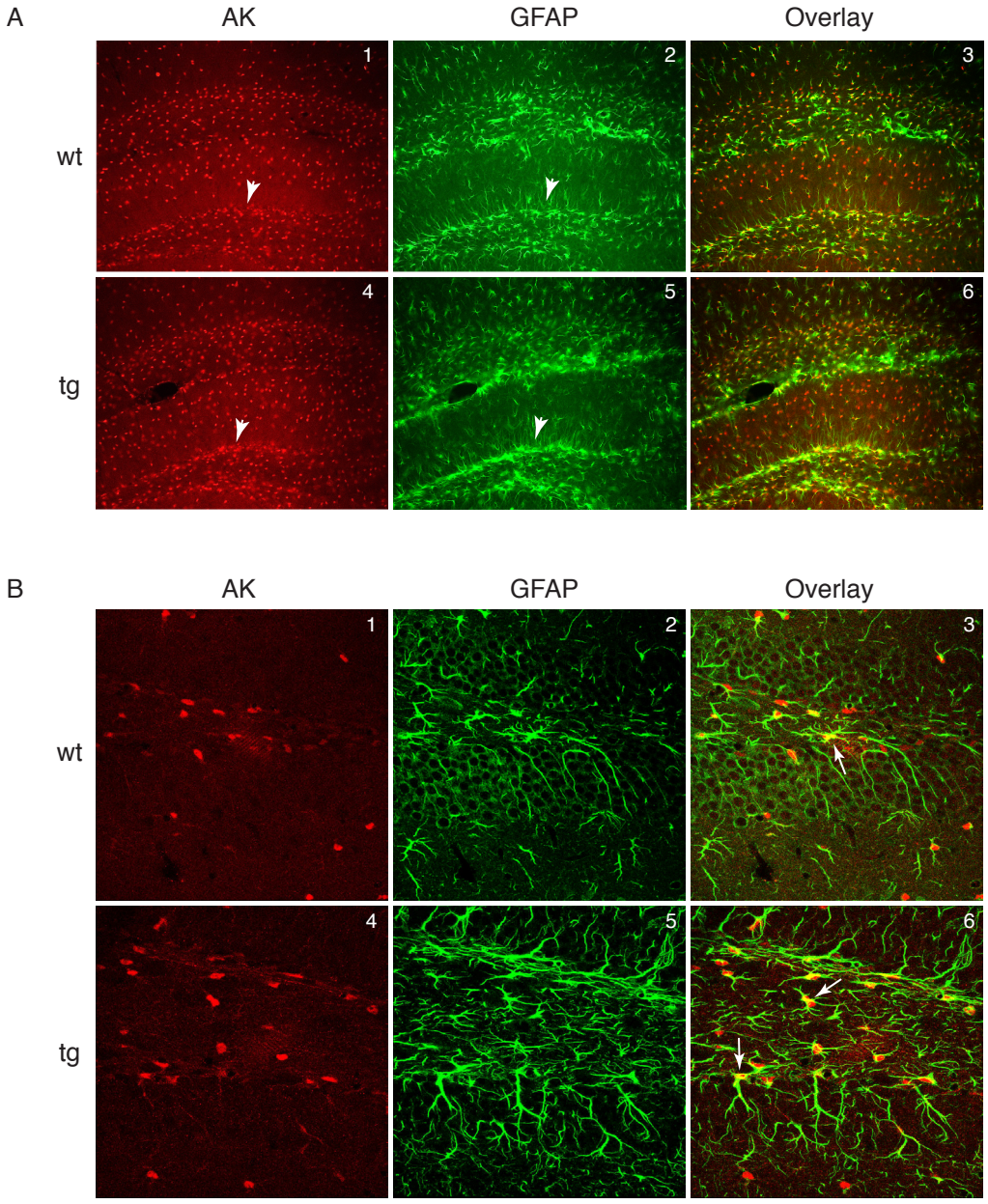

Figure 3.18 Adenosine kinase expression in the hippocampus.
(A) Comparing the hippocampus of wild-type (wt) and transgenic (tg) mice, the number of adenosine kinase (AK)-positive cells as well as glial fibrillary acidic protein (GFAP) positive cells are increased, first of all in the dentate gyrus (arrowheads). Co-localization mainly was found in the dentate gyrus ((3 and 6) **(B)** The number of AK-positive cells is increased in the detnate gyrus of tg mice (1 and 4). The staining for GFAP is stronger in tg dentate gyrus (B2, B5). Co-localization of AK-positive cells with GFAP staining was found mainly within the dentate gyrus. Somatic staining for AK with GFAP-positive protrusions extending from the cell bodies suggests astroglial expression of AK (arrows in 3 and 6).

3.6 Verification of regulated proteins found in the hippocampus

Firstly, in order to ascertain the accurate protein identification and quantification of several candidates by quantitative MS, the tandem mass spectra and SICs were examined. Secondly, the protein of interest was immunoblotted and quantified. Three independent preparations were analyzed each.

3.6.1 Copine VI (N-copine) is a Ca^{2+} sensor in postsynaptic events

N-copine is a molecule from the CNS whose function is poorly understood. It is regulated in an activity dependent manner and may target proteins to membrane surfaces where they can exert their function. Moreover N-copine probably serves as a postsynaptic Ca^{2+} sensor capable to elicit signaling pathways.

SEQUEST identified three out of a total of four identified peptides from N-copine. All four peptides were identified by Mascot search engine. A representative CID spectrum derived from Mascot showed a high coverage of fragmentation peak identification (Fig. 3.20a). The difference of relative intensities between the light and heavy form of the precursor ions became apparent when a zoom in a survey scan was made in such a way that the isotopic distribution was resolved (Fig. 3.20b, left). The relative peak intensities for the light isotopes were significantly higher than those for the heavy-labeled precursor ions. Because this particular peptide was only identified by Mascot no XPRESS ratio was calculated. Instead, the raw data were used to estimate the peptide abundance ratio. Therefore with MSight the elution profiles of the respective ions were reconstructed and displayed in a 3D diagram (Fig. 3.20b, right). Therein, time was taken into account as an additional parameter, showing precise co-elution and confirming reduced signal intensities for the heavy form. The protein identification as well as the quantification of N-copine by MS was convincing, at least for peptides of the C-terminal side (see below). Four peptides were identified with high discriminant scores and a peptide ratio of at least 0.74 or less (Fig. 3.20c). The accepted protein abundance ratio for N-copine in S2 was 0.71 and in P2 it was 0.83. The primary structure of N-copine is composed of 557 amino acids. *In silico* trypsin digestion resulted in 12 theoretical Cys-containing peptides of which 5 are located to the C-terminal half of the protein and 7 to the N-terminal half. Assuming that peptides longer than 25 amino acids are hardly identified by MS, four out of five potential peptides from the C-terminal half of the protein were detected, while none out of four from the N-terminal half remained undetected. A sequence alignment of the four identified peptides with the eight members of the copine family ensured the univocal identification of peptides from N-copine by MS (Fig. 3.20d). Even the highly homologous very N-terminal peptide starting at amino acid 521 could unambiguously be assigned to N-copine because of the monoisotopic mass difference of the two is 27 Da (CVLAEVPR vs. CVLAEVPK). This mass difference can easily be discriminated by FT-ICR MS. Taken together the convincing MS-data and the fact that N-copine may be involved in synaptic plasticity led us to the decision to further investigate the expression level. Consequently Western blot analysis was performed to verify the regulatory changes in N-copine expression (Fig. 3.21, c). The same quantities of protein extracts from wild-type and transgene S2 and P2 were immunoblotted with antibodies against N-terminal half of N-copine, neurofilament 160 (NF 160) and β-actin. Both NF160 and β-actin are regarded as housekeeping proteins in neuronal tissue and are unlikely to be affected by neurotrypsin overexpression. Therefore, they were used as loading controls for normalization. No change was detected for S2 whereas for P2 a down regulation of 10% was verified. The regulatory changes were significant with the normalization

to both NF160 and β-actin (Fig. 3.21b, d).

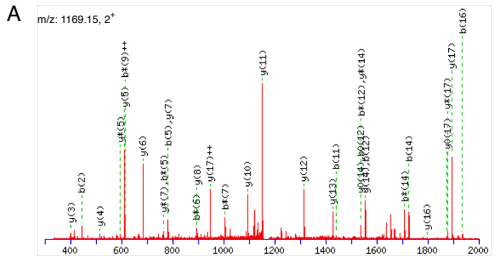

#	b	b++	b*	b*++	b0	b0++	Seq.	y	y++	y*	y*++	y0	y0++	#
1	331.14	166.08					C							19
2	444.23	222.62					L	2007.14	1004.07	1990.11	995.56	1989.13	995.07	18
3	541.28	271.14					P	1894.05	947.53	1877.03	939.02	1876.04	938.53	17
4	669.34	335.17	652.31	326.66			Q	1797.00	899.00	1779.98	890.49	1778.99	890.00	16
5	782.42	391.72	765.40	383.20			I	1668.94	834.98	1651.92	826.46	1650.93	825.97	15
6	910.48	455.74	893.45	447.23			Q	1555.86	778.43	1538.83	769.92	1537.85	769.43	14
7	1023.57	512.29	1006.54	503.77			L	1427.80	714.40	1410.77	705.89	1409.79	705.40	13
8	1186.63	593.82	1169.60	585.30			Y	1314.72	657.86	1297.69	649.35	1296.71	648.86	12
9	1243.65	622.33	1226.62	613.82			G	1151.65	576.33	1134.63	567.82	1133.64	567.32	11
10	1340.70	670.86	1323.68	662.34			P	1094.63	547.82	1077.61	539.31	1076.62	538.81	10
11	1441.75	721.38	1424.72	712.87	1423.74	712.37	T	997.58	499.29	980.55	490.78	979.57	490.29	9
12	1555.79	778.40	1538.77	769.89	1537.78	769.40	N	896.53	448.77	879.50	440.26			8
13	1654.86	827.93	1637.84	819.42	1636.85	818.93	V	782.49	391.75	765.46	383.23			7
14	1725.90	863.45	1708.87	854.94	1707.89	854.45	A	683.42	342.21	666.39	333.70			6
15	1822.95	911.98	1805.93	903.47	1804.94	902.97	P	612.38	306.70	595.36	298.18			5
16	1936.04	968.52	1919.01	960.01	1918.03	959.52	I	515.33	258.17	498.30	249.66			4
17	2049.12	1025.06	2032.09	1016.55	2031.11	1016.06	I	402.25	201.63	385.22	193.11			3
18	2163.16	1082.09	2146.14	1073.57	2145.15	1073.08	N	289.16	145.08	272.14	136.57			2
19							R	175.12	88.06	158.09	79.55			1

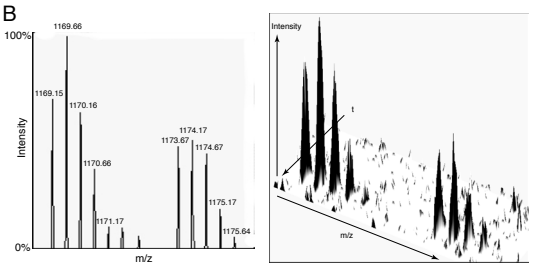

C

Peptide	Mascot	Sequest	XPRESS	Raw	Position
SSGTVVLAQCTVEK	3	2	0.65		278 - 291
SSQSLHCLSPR	3	3	0.67		322 - 332
CLPQIQLYGPTNVAPIINR	2			0.74	400 - 418
CVLEAVPR	1	1	0.67		521 - 528
Copine VI	**4**	**3**	**0.66**	**0.74**	

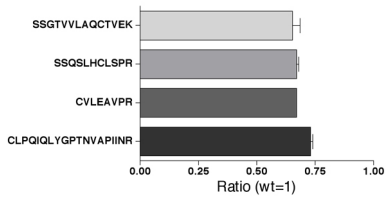

D

Cpne1	256	NSGTVRVKTCRVET	300	SPDSLHYLSPT	378	ALPQVRLYGPTNFAPIINH	499	TVLAEVPT
Cpne2	279	NSGIIILRSCKIHR	323	DPSSLHYINPM	401	CLPHIRFYGPTNFSPIVNH	522	AVLAELPQ
Cpne3	263	NSGVISVKHCEITV	307	SPDSLHYISPN	385	CLPQIRLYGPTNFSPIINH	506	CVLAEIPQ
Cpne4	279	NSGMVILNQCKIHK	323	NSCSLHYIHPY	401	CLPKLQLYGPTNIAPIIQK	522	SVLAEVPN
Cpne5	300	NSGTVTLLSFAVES	344	QSTSLHYMSPY	422	SLRTVQLYGPTNFAPVVTH	545	DVLAEIPD
Cpne6	**278**	**SSGTVVLAQCTVEK**	**322**	**SSQSLHCLSPR**	**400**	**CLPQIQLYGPTNVAPIINR**	**521**	**CVLAEVPR**
Cpne7	278	NSGVVILADLKLHR	322	NSCSLHHINPY	400	CLPKVQLYGPTNVAPIISK	521	CVLAEVPK
Cpne8	281	NSGTVTLLSFLVET	325	QPTSLHYMNPY	405	SLKSVQLYGPTNFAPVINH	526	DVLAEIPE

Figure 3.19 Protein identification and relative quantification of N-copine (copine VI) in the hippocampus by mass spectrometry.

(A) Mascot search result of the CID spectrum from a doubly charged parent ion with mass-to-charge (m/z) ratio of 1169.15 found in soluble fraction S2. The CID series of the y-type ions is nearly complete. Furthermore, all of the y-type ions ending with a proline (y(5), y(10), y(17)) are highly abundant, while the corresponding b-ions (b(3), b(10), b(15)) are completely absent. Notably, the abundance of y(10) is low. This is due to the fact that N-terminal of the proline is a glycine, whose fragmentation on the C-terminal side is often reduced. Thus, even though the bond N-terminal to proline is particularly labile to CID, the cleavage N-terminal to glycine was favored, resulting in a high abundance of y(11). **(B)** Full MS scan at RT: 65.58 of the ICAT-pair of which the parent ion was selected for tandem MS denotes the ICAT light labeled form. A typical isotopic distribution of a doubly charged ion with m/z > 1000 whose second peak, bearing one isotope is most abundant. The peak intensity for the light form is significantly higher than the one for the heavy form (left). The three dimensional single-ion chromatogram (SIC) displays the higher abundance of the light form. Precise co-elution of the light and heavy variant of an ICAT-pair is shown (right). **(C)** Summary table for all four identified peptides allocated to N-copine. The first column of the table shows the amino acid sequence of identified peptides. In the second and third column the frequency of identification with either Mascot or SEQUEST search engines is listed. The fourth and fifth column indicate the peptide abundance ratio calculated either by XPRESS software or deduced from SICs of the raw data. The last column reflects the amino acid positions of the petpide identification in the N-copine primary sequence. The last row in the table is the summary for N-copine identification and quantification. The abundance ratio of each peptide is graphically shown in a histogram (below). Wild-type (wt) is set to 1. The peptides are all downregulated in transgenic by at least a factor of 1.35. **(D)** Sequence alignment of the peptides allocated to N-copine with homologous peptides from other members of the copine family make a unique identification of copine VI clear. Indeed, all of the identified peptides unambiguously affiliate to N-copine. Their amino acid composition varies in such a way that the mass differences can be distinguished in mass spectrometry. Astonishingly, the peptides all lay on the C-terminal halft of the N-copine.

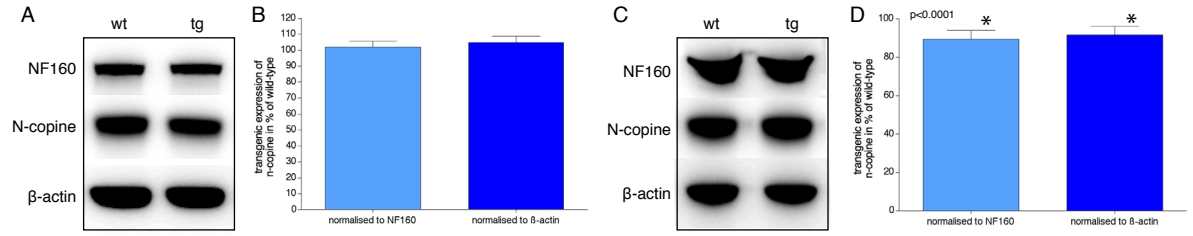

Figure 3.20 Verification of N-copine expression in the hippocampus.
(A) N-copine was immunoblotted and quantified (N=3). Equal amounts of protein extracts from S2 were loaded. Two reference proteins (neurofilament NF 160 and β-actin) were used for normalization. **(B)** No significant downregulation was found in S2. **(C)** Equal amounts of protein extracts from P2 were loaded. The two reference proteins NF 160 and β-actin were used for normalization. **(D)** In P2 a significant downregulation by 10% was found (asterisk) with two-tailed p-value < 0.0001.

3.6.2 Glutamine synthetase is responsible for the conversion of L-glutamate

Despite GS being almost exclusively expressed by glial cells and astrocytes it represents an interesting candidate for a downstream effector of neurotrypsin overexpression in synaptosomes and the hippocampus. It's important function in converting the primary excitatory neurotransmitter L-glutamate to glutamine as well as the possible role of GS in hippocampal epilepsy brings it under the spotlight.

In S2 GS was identified by 6 different peptides all with high reliability. With Mascot search engine five different peptides were identified and with SEQUEST only three were (Fig. 3.22c). Most CID spectra showed a very high coverage of fragmentation peak identification with an almost complete series of y-type ions (Fig. 3.22a). Typically, the y-type ion ending with a proline is most intensive because the N-terminal peptide bond of proline is particularly labile to CID. The extended survey scan of the corresponding ICAT-pair of which the heavy variant was selected for MS/MS (Fig. 3.22a) indicated that the heavy labeled peptide has a higher peak intensity as compared to the light variant (Fig. 3.22b, left). To estimate the abundance ratio of this ICAT-pair the SIC was reconstructed by MSight. It clearly demonstrates that the heavy peptide was more abundant than the light peptide by a factor of 1.53 (Fig. 3.22b, right). This finding was consistent among all peptides allocated to GS, since peptide abundance ratios lay between 1.17 and 1.54 (Fig. 3.22c, d). Thus, the protein abundance ratio in S2 was 1.40. In P2, where GS was also detected the ratio was reversed, namely 0.85. Verification by immunoblot analysis of the data from the ICAT screen revealed only minor aberration in GS expression comparing transgenic with wild-type (Fig. 3.22e). In M494 neurotrypsin-overexpressing mouse line no change of GS expression was found in P2 whereas in S2 a 10% down regulation was found. This is directly opposite to what was predicted by the ICAT. On the other hand, testing M491S a down regulation of 0.83 in P2 was verified while the regulation in S2 was still not reproducible. In the control mouse line S/A785 no change was detected in P2 but in S2 the diminution of 10% was similar to M494.

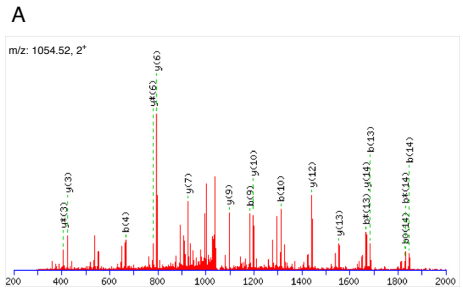

#	b	b++	b*	b*++	b0	b0++	Seq.	y	y++	y*	y*++	y0	y0++	#
1	102.05	51.53			84.04	42.53	T							16
2	441.22	221.11			423.21	212.11	C	2006.96	1003.98	1989.93	995.47	1988.95	994.98	15
3	554.31	277.66			536.29	268.65	L	1667.79	834.40	1650.76	825.89	1649.78	825.39	14
4	667.39	334.20			649.38	325.19	L	1554.71	777.86	1537.68	769.34	1536.70	768.85	13
5	781.43	391.22	764.41	382.71	763.42	382.21	N	1441.62	721.32	1424.60	712.80	1423.61	712.31	12
6	910.47	455.74	893.45	447.23	892.46	446.74	E	1327.58	664.29	1310.55	655.78	1309.57	655.29	11
7	1011.52	506.26	994.50	497.75	993.51	497.26	T	1198.54	599.77	1181.51	591.26	1180.53	590.77	10
8	1068.54	534.78	1051.52	526.26	1050.53	525.77	G	1097.49	549.25	1080.46	540.74	1079.48	540.24	9
9	1183.57	592.29	1166.54	583.78	1165.56	583.28	D	1040.47	520.74	1023.44	512.22	1022.46	511.73	8
10	1312.61	656.81	1295.59	648.30	1294.60	647.81	E	925.44	463.22	908.41	454.71	907.43	454.22	7
11	1409.67	705.34	1392.64	696.82	1391.66	696.33	P	796.40	398.70	779.37	390.19			6
12	1556.73	778.87	1539.71	770.36	1538.72	769.87	F	699.35	350.18	682.32	341.66			5
13	1684.79	842.90	1667.77	834.39	1666.78	833.90	Q	552.28	276.64	535.25	268.13			4
14	1847.86	924.43	1830.83	915.92	1829.85	915.43	Y	424.22	212.61	407.19	204.10			3
15	1975.95	988.48	1958.93	979.97	1957.94	979.47	K	261.16	131.08	244.13	122.57			2
16							N	133.06	67.03	116.03	58.52			1

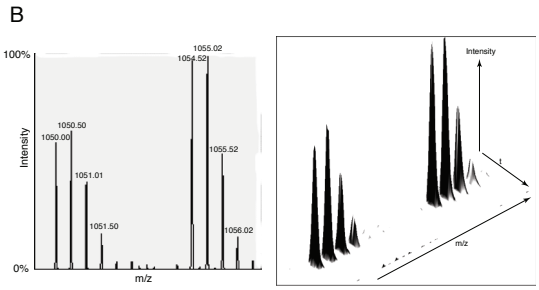

C

Peptide	Mascot	Sequest	XPRESS	Raw	Position
TRTLDCEPK	2	2	1.45		44 - 52
TLDCEPK	4			1.47	46 - 52
ACLYAGVK	2	3	1.17		182 - 189
CIEEAIDK		2	1.54		269 - 276
RPSANCDPYAVTEAIVR	5			1.32	340 - 356
TCLLNETGDEPFQY	5			1.53	357 - 372
Glutamine synthetase	**5**	**3**	**1.39**	**1.44**	

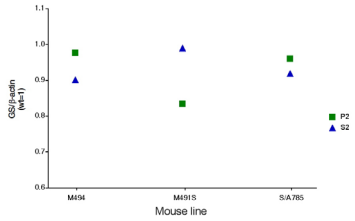

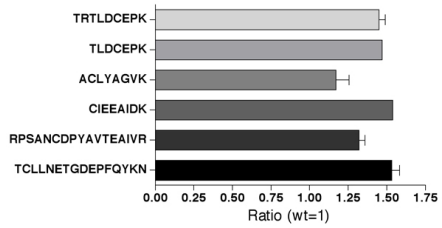

Figure 3.21 Protein identification and relative quantification of glutamine synthetase in the hippocampus by mass spectrometry.
(A) The Mascot search result of the CID spectrum from hippocampus soluble fraction S2 of doubly charged parent ion with mass-to-charge (m/z) ratio: 1054.52. The fragmentation of N-terminal peptide bonds, resulting in a nearly complete series of y-type ions. The y-type ion ending with proline (y(6)) has the most intensive peak while the corresponding b-ion (b(11)) is completely absent. **(B)** Full MS scan of the ICAT-pair, of which the parent ion selected for tandem MS denotes the ICAT heavy labeled form. A typical isotopic distribution of a doubly charged ion with m/z > 1000, where the second peak bearing one isotope is most abundant. The peak intensity for the heavy form is significantly higher than the one for the light form (left). The 3D single-ion chromatogram (SIC) confirms a higher abundance for the heavy form. Precise co-elution of the light and heavy variant of the parent ions is shown (right). **(C)** Summary table of all six peptides allocated to glutamine synthetase (GS). The first column of the table shows the amino acid sequence of peptide identifications. In the second and third columns the frequency of peptide identifications with either Mascot or SEQUEST search engines is listed. The fourth and fifth columns indicate the peptide abundance ratio either calculated with XPRESS software or deduced from SICs of the raw data. The last column reflects the positions of the amino acids for each peptide of GS. Considering the fact that the primary structure of GS is composed of 373 amino acids it is evident that the identified peptides cover fragments evenly disrtibuted over the complete amino acid sequence. The last row in the table is a summary for GS identification and quantification. Totally 6 different peptides were allocated, 5 of them were identified by Mascot and 3 by SEQUEST. Using XPRESS software a computed protein abundance ratio of 1 : 1.39 was calculated. The ratio in P2 was 1 : 0.85. **(D)** The peptide abundance ratios in S2 shown in a histogram. Wild-type (wt) is set to 1. All peptides are equally upregulated in transgenic by at least a factor of 1.17. **(E)** Statistical analysis from Western blot analysis of S2 and P2 fractions from different mouse lines. Antibodies against GS and β-actin were used to quantify the regulatory changes. In P2 no significant change was confirmed, whereas in M491S mice a downregulation of 0.83 is shown. In S2 no change is detected.

3.6.3 Neuron specific alpha3 Na^+/K^+-ATPase is essential for the excitability of nerve cells

The alpha 3NKA isoform is exclusively expressed in neurons. Mutations in NKA alpha isoforms have been associated with multiple disorders involving rapid-onset of dystonia, Parkinsonism, and familial hemiplegic migraine type-2. A reduction in NKA content leads to depression and AD. Moreover, mice heterozygous for the alpha3NKA displayed spatial learning and memory deficits as well as a 40% reduction in hippocampal NMDA receptor expression. Most interestingly, alpha3NKA potentially constitutes a neuronal receptor for agrin. Alpha3NKA was identified in S2 as well as in P2 by mass spectrometry. The CID spectra of the peptides allocated to alpha3NKA had high discriminant score values, reflected with almost complete coverage of fragment peak identification (Fig. 3.23a). SICs of the peptides identified by Mascot were reconstructed with raw data (Fig. 3.23b) and SICs identified by SEQUEST were computed with XPRESS. Peptide ratios from S2 (Fig. 3.23c1) and from P2 (Fig. 3.23c2) were taken together and displayed in bar diagrams. In S2 alpha3NKA was identified by eight different peptides, two of which showed a ratio of nearly one. All others had a reduced abundance ratio of at least 1: 0.75. In P2 even twelve peptides were allocated to alpha3NKA. Here, only one is an outlier, which of all things has one missed cleavage site. Astonishingly, almost every Cys-containing peptide from the N-terminal side of alpha3NKA was found (Fig. 3.23d). Only two unidentified Cys-containing peptides (red) were located N-terminally of the middle of the protein, whereas at least four were missing from the C-terminal half (NOTE: many unidentified peptides are composed of more than 20 amino acids). On the other hand only two identified peptides were localized C-terminally. The two peptides highlighted in blue were identified and quantified in S2 as well as in P2, but unexpectedly they only appeared changed in P2. The peptide further downstream (LIICEQCQR) (green) was down regulated again. Despite this discrepancy it seemed that alpha3NKA was down regulated in transgenic samples and alpha1NKA was not (data not shown). Therefore the two proteins were examined further by Western blot quantification.

First, it was shown that the alpha3NKA was detectable in all but the S2 fraction of the hippocampus (Fig. 3.24a). Thus, the following experiments were performed with the P2 fraction. Second, quantitative immunoblot assays for alpha3- and alpha1NKA from different mouse lines were performed (Fig. 3.24b). Three independent preparations of wild-type and transgenic samples were tested. None of them showed a significant change in NKA expression neither in neurotrypsin-overexpressing animals nor in KO. This is in contradiction to the MS-data, suggesting a down regulation of more than 25% in transgenic S2 and 20% in P2.

A1

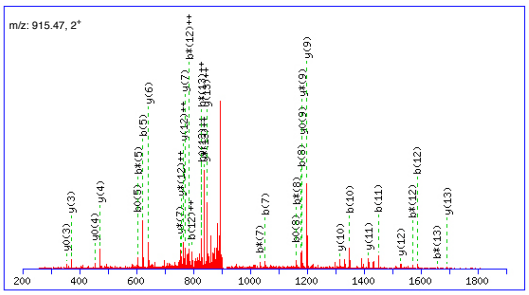

#	b	b++	b*	b*++	b0	b0++	Seq.	y	y++	y*	y*++	y0	y0++	#
1	129.10	65.05	112.08	56.54			K							14
2	292.17	146.59	275.14	138.07			Y	1692.80	846.90	1675.77	838.39	1674.79	837.90	13
3	406.21	203.61	389.18	195.09			N	1529.74	765.37	1512.71	756.86	1511.73	756.37	12
4	507.26	254.13	490.23	245.62	489.25	245.13	T	1415.69	708.35	1398.67	699.84	1397.68	699.35	11
5	622.28	311.65	605.26	303.13	604.27	302.64	D	1314.65	657.83	1297.62	649.31	1296.64	648.82	10
6	952.42	476.71	935.39	468.20	934.41	467.71	C	1199.62	600.31	1182.59	591.80	1181.61	591.31	9
7	1051.49	526.25	1034.46	517.73	1033.48	517.24	V	869.48	435.25	852.46	426.73	851.47	426.24	8
8	1179.55	590.28	1162.52	581.76	1161.54	581.27	Q	770.42	385.71	753.39	377.20	752.40	376.71	7
9	1236.57	618.79	1219.54	610.27	1218.56	609.78	G	642.36	321.68	625.33	313.17	624.35	312.68	6
10	1349.65	675.33	1332.63	666.82	1331.64	666.32	L	585.34	293.17	568.31	284.66	567.32	284.17	5
11	1450.70	725.85	1433.67	717.34	1432.69	716.85	T	472.25	236.63	455.22	228.12	454.24	227.62	4
12	1587.76	794.38	1570.73	785.87	1569.75	785.38	H	371.20	186.11	354.18	177.59	353.19	177.10	3
13	1674.79	837.90	1657.76	829.39	1656.78	828.89	S	234.14	117.58	217.12	109.06	216.13	108.57	2
14							K	147.11	74.06	130.09	65.55			1

A2

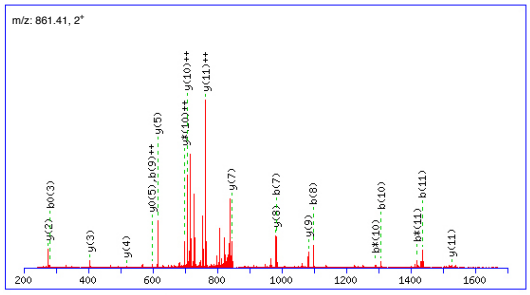

#	b	b++	b*	b*++	b0	b0++	Seq.	y	y++	y*	y*++	y0	y0++	#
1	88.04	44.52			70.03	35.52	S							13
2	185.09	93.05			167.08	84.04	P	1624.74	812.87	1607.71	804.36	1606.73	803.87	12
3	300.12	150.56			282.11	141.56	D	1527.69	764.35	1510.66	755.83	1509.68	755.34	11
4	630.26	315.63			612.24	306.63	C	1412.66	706.83	1395.63	698.32	1394.65	697.83	10
5	731.30	366.16			713.29	357.15	T	1082.52	541.76	1065.50	533.25	1064.51	532.76	9
6	868.36	434.68			850.35	425.68	H	981.47	491.24	964.45	482.73	963.46	482.24	8
7	983.39	492.20			965.38	483.19	D	844.42	422.71	827.39	414.20	826.41	413.71	7
8	1097.43	549.22	1080.41	540.71	1079.42	540.21	N	729.39	365.20	712.36	356.68	711.38	356.19	6
9	1194.48	597.75	1177.46	589.23	1176.47	588.74	P	615.35	308.18	598.32	299.66	597.34	299.17	5
10	1307.57	654.29	1290.54	645.77	1289.56	645.28	L	518.29	259.65	501.27	251.14	500.28	250.64	4
11	1436.61	718.81	1419.58	710.30	1418.60	709.80	E	405.21	203.11	388.18	194.59	387.20	194.10	3
12	1537.66	769.33	1520.63	760.82	1519.65	760.33	T	276.17	138.59	259.14	130.07	258.16	129.58	2
13							R	175.12	88.06	158.09	79.55			1

B1

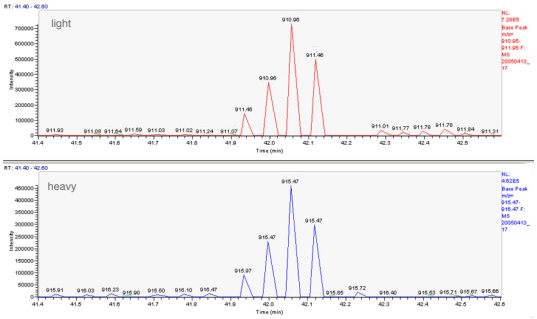

B2

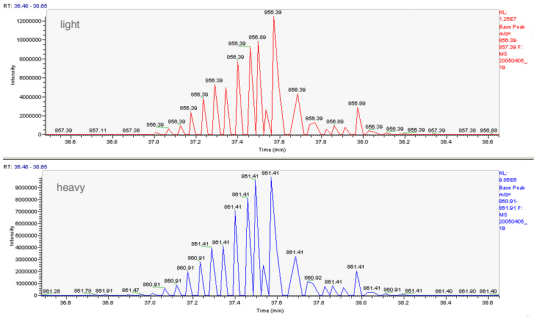

C1

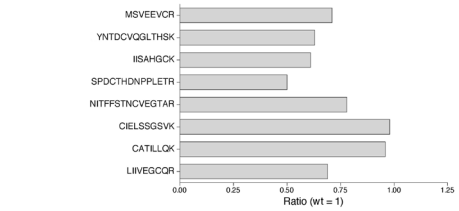

C2

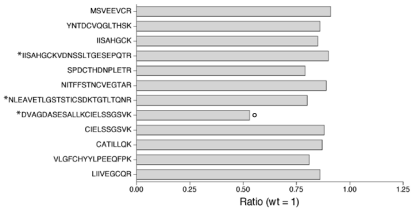

D

```
MGDKKDDKSS PKKSKAKERR DLDDLKKEVA MTEHKMSVEE VCRKYNTDCV QGLTHSKAQE ILARDGPNAL TPPPTTPEWV KFCRQLFGGF SILLWIGAIL
CFLAYGIQAG TEDDPSGDNL YLGIVLAAVV IITGCFSYYQ EAKSSKIMES FKNMVPQQAL VIREGEKMQV NAEEVVVGDL VEIKGGDRVP ADLRIISAHG
CKVDNSSLTG ESEPQTRSPD CTHDNPLETR NITFFSTNCV EGTARGVVVA TGDRTVMGRI ATLASGLEVG KTPIAIEIEH FIQLITGVAV FLGVSFFILS
LILGYTWLEA VIFLIGIIVA NVPEGLLATV TVCLTLTAKR MARKNCLVKN LEAVETLGST STICSDKTGT LTQNRMTVAH MWFDNQIHEA DTTEDQSGTS
FDKSSHTWVA LSHIAGLCNR AVFKGGQDNI PVLKRDVAGD ASESALLKCI ELSSGSVKLM RERNKKVAEI PFNSTNKYQL SIHETEDPND NRYLLVMKGA
PERILDRCAT ILLQGKEQPL DEEMKEAFQN AYLELGGLGE RVLGFCHYYL PEEQFPKGFA FDCDDVNFTT DNLCFVGLMS MIDPPRAAVP DAVGKCRSAG
IKVIMVTGDH PITAKAIAKG VGIISEGNET VEDIAARLNI PVSQVNPRDA KACVIHGTDL KDFTSEQIDE ILQNHTEIVF ARTSPQQKLI IVEGCQRQGA
IVAVTGDGVN DSPALKKADI GVAMGIAGSD VSKQAADMIL LDDNFASIVT GVEEGRLIFD NLKKSIAYTL TSNIPEITPF LLFIMANIPL PLGTITILCI
DLGTDMVPAI SLAYEAAESD IMKRQPRNPR TDKLVNERLI SMAYGQIGMI QALGGFFSYF VILAENGFLP GNLVGIRLNW DDRTVNDLED SYGQQWTYEQ
RKVVEFTCHT AFFVSIVVVQ WADLIICKTR RNSVFQQGMK NKILIFGLFE ETALAAFLSY CPGMDVALRM YPLKPSWWFC AFPYSFLIFV YDEIRKLILR
RNPGGEGRMA RGKGWEGKQR VSTPCASQMC PFFFLFPLSP PCLSLSFQVR LCV
```

Figure 3.22 Protein identification and relative quantification of α3 Na⁺/K⁺-ATPase in the hippocampus by mass spectrometry.

(A) The Mascot search results of CID spectra from doubly charged parent ions with mass-to-charge (m/z) ratios of 915.47 in soluble fraction S2 and in pelletous fraction P2 of 861.41. In both instances the heavy labeled peptide was selected for MS/MS. The fragmentation at the N-terminal peptide bonds, resulting in y-type ions, is in both samples nearly complete. Prolines are either absent in the sequence (A1), or so close to the N-terminus that fragmentation is rare (y(12)). The y(5) ion ending with a proline is clearly present (A2). The corresponding b-type ion (b(9)) is not detected. **(B)** Single-ion chromatograms (SIC) of the parent ions identified in (A) showing precise co-elution of light and heavy labeled peptides. The maximum peak intensity in S2 for light is 7 x 10^5 and for the heavy peptide it is 4.5 x 10^5 (B1). The ICAT-pair identified in P2 has a SIC with maximal peak intensity of 1.2 x 10^7 for light and of 9 x 106 for heavy (B2), resulting in a decreased abundance ratio for the transgenic samples. In fact the ratio of KYNTDCVQGLTHSK is 1 : 0.63 and the ratio of SPDCTHDNPLETR is 1 : 0.79. **(C)** The abundance ratios of all peptides allocated to α3Na⁺/K⁺-ATPase (α3NKA) are displayed in histograms for S2 (C1) and P2 (C2). Strikingly, in S2 most of the ratios are between 0.5 and 0.75 except for the two peptides

CIELSSGSVK and CATILLQGK, which have a ratio of nearly 1 : 1. The average ratio though, is 0.73 (C1). In P2, totally twelve different peptides were allocated to α3NKA with an average ratio of 0.83. Three peptides have one missed cleavage (*), among which one is an outlier (°) showing a peptide ratio of nearly 0.5. **(D)** Allocation of peptide identifications from S2 and P2 to the amino acid sequence of α3NKA (green). Peptides in magenta were found in P2 only. The two peptides with a ratio of 1 : 1 in S2 lie in the middle of the sequence (blue). Notably, there are primarily peptides from the N-terminal half of the protein that were found in the proteomic profiling. The missing Cys-containing peptides (red) from the C-terminus are often very long (> 20 amino acids) and therefore, not very likely being identified by mass spectrometry.

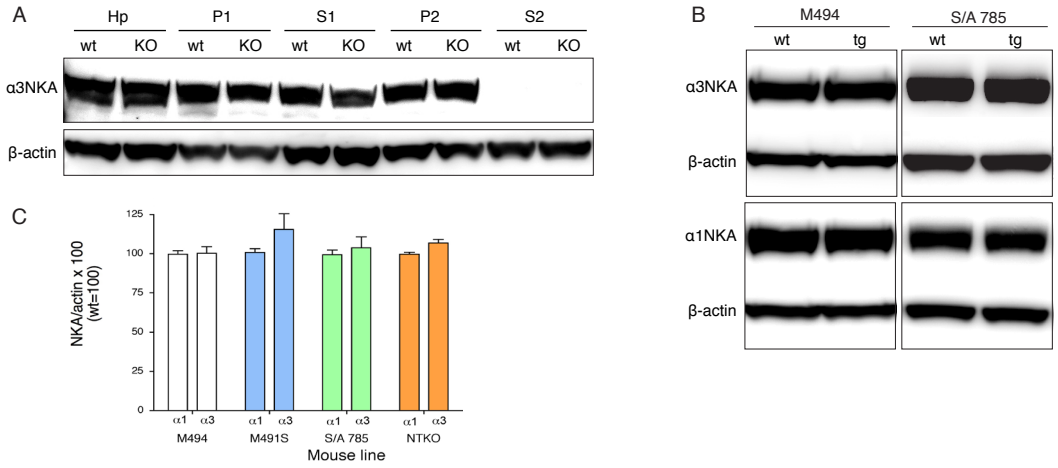

Figure 3.23 Verification of α3 Na^+/K^+-ATPase expression in different mouse lines.
(A) Immunoblotting of α3 Na^+/K^+-ATPase (α3NKA), showing an equal distribution in all hippocampus fractions apart from soluble fraction S2, where it is absent (upper panel). β-actin is shown as a loading control (lower panel). **(B)** To confirm the data from ICAT-MS, suggesting a downregulation of α3NKA by 20% but no change in the expression of α1 Na^+/K^+-ATPase (α1NKA) in the pelletous fraction P2 of transgenic mice, α3NKA and α1NKA were immunoblotted and quantified. Equal amounts of protein extract from wild-type (wt) and neurotrypsin overexpressing mice M494 (tg), as well as S/A 785 (tg) were tested. β-actin was used for normalization. Signal intensities were measured by spot densitometry and relative expression levels were calculated. **(C)** Histogram showing the expression levels of α1NKA and α3NKA from M494, M491S, S/A 785 and neurotrypsin knock-out (NTKO) mice. None of them showed significant changes either in α3NKA or α1NKA expression. Wt was set to 100.

3.6.4 Differential protein expression of various other proteins

The list of protein identifications with deviating abundance ratios comparing wild-type and transgenic samples is by all means manifold and revealing. Therefore, other proteins were tested in order to verify the findings by the ICAT method (Fig. 3.25). One verification was achieved with EAAT2. In the ICAT P2 it was down regulated by 25%. Similarly it was reduced by Western blot quantification. Furthermore, EAAT2 was slightly up regulated in NTKO and not regulated at all in S/A785. For VDAC1 as well, the data from ICAT were confirmed by Western blot. A decreased expression of 10% was found by immunoblot assay in M494 and M491S, while the expression was not changed either in NTKO or S/A 785. Likewise the decreased expression of α-CaMK II by 15 – 30% found with ICAT was confirmed in the hippocampus of M494 transgenic mice, although the reduction was only 5%. Interestingly, the autophosphorylated form, phospho-α-CaMK II was enriched by 10% in transgenic P2 fraction. This analysis provides more evidence that in the neurotrypsin-overexpressing mice differentially expressed proteins were present but the aberrations were little and versatile and thus challenging to prove.

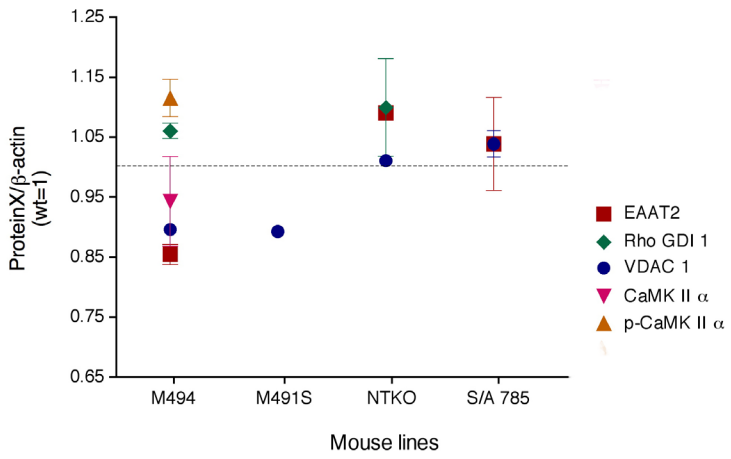

Figure 3.24 Differential protein expression in the hippocampus of neurotrypsin overexpressing mice.
Various proteins with differential regulation found in the ICAT experiments were tested by immunoblot analysis. The immunoblots were carried out for pelletous fractions P2 comparing wild-type (wt) and transgenic (tg) samples. ICAT-MS suggested a downregulation of excitatory amino acid transporter 2 (EAAT2) in P2 of transgenic mice and an upregulation in the synaptosomes of adult transgenic mice. By immunoblot quantification the reduction was confirmed in P2 of M494 .In NTKO, EAAT2 was slightly increased. In the control line S/A785 the transporter protein is basically not regulated. RhoGDP-dissociation inhibitor 1 (Rho GDI 1) was downregulated in the ICAT of synaptosomes from P20 mice, but was slightly increased in P2 of both, M494 and NTKO by immunoblot assay. The ratio for voltage-dependent anion-selective channel protein 1 (VDAC 1) in ICAT-MS was 0.70 in P2 and was also reduced by immunoblot quantification in M494 and M491S, whereas in the NTKO and S/A785 its expression was not changed. Calcium/calmodulin-dependent protein kinase II alpha (α-CaMK II), downregulated in ICAT P2 by 0.70, is slightly reduced in M494. The autophosphorylated form (Thr-286), p-CaMK II α, is upregulated in M494.

4. Discussion

The results of this report support the idea that neurotrypsin is a brain-specific serine peptidase. In synaptosomes and the hippocampus neurotrypsin intrinsically recognizes the proteoglycan agrin and mediates cleavage at two positions. The catalytic activity on agrin was elevated in neurotrypsin-overexpressing mice and completely diminished in neurotrypsin KO mice. Both the 22-kDa C-terminal LG3 domain and the 90-kDa agrin intermediate fragments were enriched in the S2 fractions of hippocampal and synaptosomal preparations. However, the fate of the agrin cleavage products is still vague. In transgenic mice, changes in protein expression of molecules interacting either directly or indirectly with neurotrypsin are subtle. In fact, alterations in protein abundance of more than 1.5-fold were scarcely identified. The proteomic profiling implies that in the transgenic mice cellular processes, such as synaptic plasticity, cytoskeleton reorganization, and exo- and endocytosis are affected, since the majority of the changed proteins are allocated to these functional units. Taken together our findings suggest that neurotrypsin is involved in synaptic transmission and can regulate synapse structure and activity.

4.1 Neurotrypsin – Agrin interaction in synaptosomes and in the hippocampus

Synaptosomes are isolated synapses produced by subcellular fractionation of brain tissue. Morphologically they consist of the complete presynaptic terminal, including mitochondria, synaptic vesicles and portions of the postsynaptic density. Recent proteomic analysis showed that on the molecular level synaptosomes are enriched in proteins associated with synaptic function, including synaptic vesicle exocytosis for neurotransmitter release, vesicle endocytosis for recycling, as well as postsynaptic receptors and scaffolding proteins from the PSD. Moreover, a large number of soluble and membrane-bound molecules serving functions in synaptic signal transduction and metabolism were detected (Schrimpf et al., 2005; Witzmann et al., 2005). Western blot analysis of synaptosomes indicated that neurotrypsin is not particularly enriched in synapses. The neurotrypsin specific substrate agrin however, at least the most susceptible form to neurotrypsin cleavage, was clearly accumulated in wild-type synaptosomes. On the other hand, the agrin cleavage products were almost undetectable in wild-type synaptosomes indicating that they are released from the synaptic cleft. They might either diffuse out of the synaptic junction or be internalized, be it by the pre- or postsynapse, where they might elicit cellular signaling. Furthermore, in transgenic synaptosomes the cleavage products are well detectable. This speaks in favor of the idea that due to the extensive production of agrin fragments, they aggregate in the synaptic cleft and can therefore not be appropriately removed from there. Thus, to shed light on the proteomic changes in neurotrypsin-overexpressing mice, performing a large-scale proteomic approach was tempting. Endogenous neurotrypsin expression as well as the activity of the Thy-1.2 expression cassette decline to baseline after postnatal day 15 (P15). Therefore quantitative proteomic profiling of synaptosomes from P20 and P40 mice was undertaken in order to identify long-term proteomic changes in transgenic animals. Regarding the accurately defined spatial distribution of neurotrypsin expression (Wolfer et al., 2001) and the fact that synaptosomes are usually isolated from whole mouse brains or at least from large brain regions such as the cortex, provoked us to additionally target a specific area of the brain that is involved in processes such as storage of memory and learning. Moreover, we wanted to seek

changes that are temporally and spatially related to endogenous neurotrypsin function. With samples from younger animals we intended to track down short-term effects of overexpressed neurotrypsin on differential protein expression. Therefore in a second approach, hippocampi of P10 mice were dissected and subjected to subcellular fractionation and subsequent proteomic analysis. The hippocampus was homogenized and fractionated to reduce the complexity of the samples. To classify the two fractions, S2 and P2, which were generated as a result of the differential centrifugation, were grouped according to their composition of marker proteins. Accordingly, S2 is regarded as the 'soluble' fraction, consisting mainly of cytosolic proteins including dendritic marker MAP2, NF-160, Golgi-marker β-COP and Grp78. P2 on the other hand is particularly delineated by 'membranous' or 'synaptosome-like' fraction. It mainly contains postsynaptic integral membrane protein GluR 2/3, scaffolding and membrane-associated PSD-95, and presynaptic vesicle glycoprotein synaptophysin. P2 also comprises ER vesicles demonstrated by the presence of Grp78. β-COP and MAP2 were nearly absent, implying that light Golgi vesicles and proteins from dendrites were exclusively present in S2. Moreover, full-length neurotrypsin and the protease domain were heavily enriched in P2. Similar to the synaptosomes the most amenable agrin full-length form to neurotrypsin cleavage was strongest in wild-type P2. Both cleavage products were more pronounced in S2. For all these reasons, we postulate that agrin processing by neurotrypsin also occurs in the hippocampus. Consequently, in order to identify neurotrypsin-dependent changes four different ICAT screens were performed: two with synaptosomes (P20 and P40) and two with P10 hippocampal fractions, S2 and P2. The samples were treated similarly. The major differences were imposed during mass spectrometry and relative quantification. While for the synaptosomes a classical 3D ion trap mass spectrometer was used and the computation of the abundance ratios was performed with ASAPRatio, for the hippocampal fractions a highly sophisticated mass spectrometer combining the most advanced ion trap and Fourier Transform Ion Cyclotron Resonance technologies into a single instrument was used. Furthermore, the protein ratios were calculated using XPRESS software. These adaptations theoretically bring about more accurate protein identifications.

4.2 Quantitative proteomic profiling of a transgenic mouse line

Quantitative mass spectrometry using stable isotope-labeled tagging reagents such as ICAT has emerged as a powerful tool for the identification and relative quantification of proteins in current proteomic studies. In the past years a variety of large-scale quantitative proteomic profiles have been published using ICAT technology. It was (Han et al., 2001), who first presented an approach to the systematic identification and quantification of proteins contained in subcellular fractions. They identified and determined the abundance ratios of 491 microsomal proteins of naïve and *in vitro* - differentiated human myeloid leukemia (HL-60) cells. For most identified proteins, the abundance did not change significantly. Nevertheless, they found that some of the membrane-associated signal transduction proteins and enzymes showed significant changes in their ratios with up to 20-fold variation. An ensuing report described the differences in protein expression comparing the PSDs isolated from rat forebrain and cerebellum (Cheng et al., 2006). PSD protein profiles were determined using the cleavable ICAT strategy and LC-MS/MS. A total of 296 proteins were identified and quantified with 43 proteins exhibiting statistically significant abundance change (with ratios > 6-fold) between forebrain and cerebellum, indicating marked molecular heterogeneity of PSDs between different brain regions.
In this work, the first quantitative proteomic profiling of a transgenic mouse line is presented. We

isolated synaptosomes from whole brain and prepared two subcellular fractions of the isolated hippocampus. Protein profiles were determined using the cleavable ICAT strategy and LC-MS/MS. Altogether, 761 synaptosomal proteins were identified of which 66 had an abundance ratio higher than 1.2 in P20 and 81 in P40 animals. In the hippocampus 1382 protein identifications were made in S2, and 883 proteins in P2. 365 overlapping proteins were identified in both S2 and P2 (Fig. 4.1). Totally 165 proteins were changed in S2 and P2. Data analysis revealed highly reliable protein identifications and quantification. Firstly, the elution profiles of the biochemical fractionation using cation exchange chromatography indicated highly reproducible complexity reduction of resembling samples. Secondly, with a minimal probability of ≥ 0.95 that proteins are present in the sample, a maximum of 0.5% incorrect protein assignments were estimated for all samples analyzed. Yet hundreds of protein identifications with high probability scores were quantitated. Thirdly, abundance ratios were accurately quantified since chromatographic co-elution profiles of ICAT-labeled peptides were observed. Fourthly, 2D reproduction of LC-MS/MS runs revealed that the samples are almost devoid of contaminating compounds and that the separation of peptides eluting from the RP-column was excellent and reproductive. And finally, computational analysis of the peptide identifications of one experiment indicated a nearly complete trypsin digestion of the proteins; only in about 2% of all proteins one missed cleavage site was found. Furthermore, barely 2.5% of all peptides were singly charged, showing that the ionization during ESI was appropriate. The average delta error mass of the observed and calculated ions was within the range of the mass accuracy of the mass analyzer. Furthermore, the distribution of peptide length peaked at 13 amino acids, which is expected and the amino acid frequency suggested an accumulation of cysteines being an indicator for an enrichment of Cys-containing peptides. Taken together, many different proteins were accurately identified from synaptosomes and the hippocampus. Comparing the protein abundance ratios of wild-type and transgenic mice the changes are astonishingly subtle. Interestingly, neither neurotrypsin nor agrin could be identified. The reason for it is as yet unclear. Possibly, the traceable amounts of neurotrypsin even from the overexpressing mice were already lost during sample preparation. From what is known in our group, it is an extremely sticky molecule (unpublished data). Concerning the missing identification of agrin no obvious explanation is given. However, at the time when the database search was performed, entries for mouse mini-agrin and the N-terminal NtA and TM domains were recorded only. Nevertheless, database entries for rat and human full-length agrin, were present and extremely homologous to the recently published mouse sequence. Therefore, the majority of the agrin peptides could still be assigned. Furthermore, both neurotrypsin and agrin had served as meaningful internal standards for quantification. Regarding neurotrypsin because of its overexpression in the transgenic mice leading to a several fold increase in neurotrypsin expression compared to wild-type samples. Regarding agrin due to its increased processing by neurotrypsin and subsequent redistribution of the emerging fragments, which may lead to different quantities comparing wild-type and transgenic fractions, such as S2 or P2.

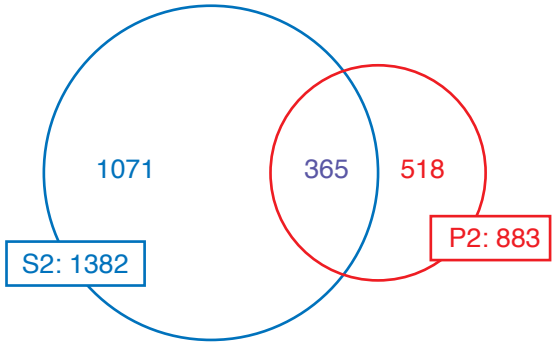

Figure 4.1 Intersection of protein identification comparing S2 and P2.
A total of 1593 hippocampal protein were identified and quantified using the ICAT strategy. 1382 proteins were found in S2 and 887 in P2. Only 365 proteins were present in both fractions.

4.3 Multifaceted neurotrypsin-dependent changes in protein expression

The classification of all protein identifications into GO terms convincingly reflected the major classes of cellular compartments and molecular functions describing each subcellular fraction. A selective attribution of proteins to specific categories was observed. The fact that the 'membrane' and the 'mitochondria' fractions were enriched in P2 as well as in the synaptosomes is absolutely expected. Evidentially the GO terms 'transporter activity', 'structural component', and 'signal transduction' accounted for most of the protein identifications from P2. And, many proteins from S2 were assigned to 'cytosol', 'enzyme regulator', 'structural constituent' and 'nucleus', from which proteins can translocate to the cytoplasma.

GO annotation of regulated proteins showed that, though moderate, specific biological processes are affected by neurotrypsin overexpression. Remarkably a lot of proteins with changed abundance ratios were involved in neuronal signal transduction mechanisms. In particular many of the proteins are involved in SNARE complex assembly or disassembly. Crucial factors for the regulation of SNARE complex formation and exocytosis are NSF proteins, SNAPs, Munc18-1, complexins, and syntaxins all of which are down regulated in the transgenic S2 fraction of the hippocampus by 30 – 40%. Interestingly, NSF ATPase and Munc18-1 were additionally found in P2 where they were up regulated by 10 – 20%. We therefore speculate that a compartmentalization of proteins involved in the regulation of the fusion apparatus is taking place. Conclusively, an accumulation of SNARE fusion proteins associated to the plasma membrane possibly results in a perturbed exocytosis of neurotransmitter and a deregulated synaptic vesicle recycling. Furthermore, a reduced level of adequate protein supply for membrane docking and fusion might inhibit normal neuronal exocytosis. Changed expression levels were also found for dynamin 1 and PACSIN 2 (down regulated by 20%), and amphiphysin 2 (up regulated by 40 – 50%), all of which are involved in endocytosis. This provides another hint for a modified vesicle turnover. Yet another indication for a disruption of synaptic vesicle trafficking is the fact that small GTPases, GDIs, and GAPs are affected. For instance we found more Rab3C protein in synaptosomes and hippocampal S2 of transgenic mice, while Rab GDI 1 and Rab3-GAP 1 levels were reduced, raising the possibility that in the neurotrypsin-overexpressing mouse Rab3C is preferentially found

in the GTP-bound, therefore active, form. Accumulating evidence suggests that Rab3C plays a key role in neurotransmitter release and synaptic plasticity. On top of that a mutation in the GDI1 gene, which reduces binding and recycling of Rab3C, was linked to X-linked mental retardation associated with epileptic seizure (D'Adamo et al., 1998). Not only the exo- and endocytotic machinery was apparently affected, but also components of the postsynaptic density (PSD) like GluR3, SAP102 and SAPAP 4 were up regulated in transgenic by > 30% and α-CaMK II was reduced by up to 30%. Metabotropic GluR3 is a group II mGluR, which prevents the formation of cAMP, by activating G proteins that inhibit the enzyme adenylyl cyclase that forms cAMP from ATP (Chu and Hablitz, 2000). Found on both pre- and postsynaptic membranes, these receptors are involved in presynaptic inhibition and do not appear to affect postsynaptic membrane potentials by themselves (Endoh, 2004). Glutamate receptors in groups II and III reduce the activity of postsynaptic potentials, both excitatory and inhibitory, in the cortex. SAP102 couples the NMDAR to specific plasticity pathways and learning strategies (Cuthbert et al., 2007). Since SAP102 was also more abundant in transgenic S2, NMDAR trafficking might indirectly be linked to neurotrypsin activity. In addition, mutations in the SAP102 gene cause nonsyndromic X-linked mental retardation (Tarpey et al., 2004). In conjunction with neurotransmitter turnover two important molecules were found in the proteomic profiling, both of which are primarily found in astrocytes and for both the abundance was reduced in transgenic samples. Firstly, EAAT2 transmembrane protein clears most of the glutamate from the synaptic cleft. It was down regulated by 25%. Acting as a symporter by cotransporting sodium with L-glutamate and also L- and D-aspartate, EAAT2 is essential for the termination of the postsynaptic action. Secondly, although the quantitative differences could only partially be confirmed, it is glutamine synthetase that catalyzes the conversion from glutamate, transported intracellularly by EAAT2, to glutamine under the consumption of ATP and ammonia. GS serves for two functions in parallel: one is to eliminate the glutamate and provide the glutamine, which can then diffuse from astrocytes to neurons to supply the neurotransmitter pool. The other function is to detoxify ammonia. On the one hand glutamate accumulates in the synaptic cleft and residual glutamate that is still removed is not converted into glutamine efficiently enough. Thus, reduced levels of EAAT2 and GS can consequently lead to epileptic seizure and excitotoxic cell death. On the other hand there is an acute intoxication with ammonia going on leading to rapid cell death.

Nevertheless, critical integration points of multiple signaling pathways, also considered as molecular switches, such as PKC, MAPK and PAK proteins were also affected. Two isozymes of the PKC family were identified and both of them were down regulated by roughly 40%. PKCα, which belongs to the subfamily of the 'conventional' PKC, requiring Ca^{2+}, DAG, and a phospholipid, and PKCε, a 'novel' PKC that is activated without Ca^{2+}. Upon activation, PKCs are translocated to the plasma membrane by RACK proteins (membrane-bound receptor for activated protein kinase C proteins). PKCs are known for their long-term activation: they remain activated after the original activation signal until the Ca^{2+}-wave is gone. This is presumably achieved by the production of diacylglycerol from phosphatidylcholine by phospholipase. Their substrates are myristoylated alanine-rich C-kinase substrate (MARCKS) proteins, MAP kinase, transcription factor inhibitor IκB, calpain, and the epidermal growth factor receptor.

MAPK1 is a widely expressed protein kinase signaling molecule whose abundance was increased by 20 – 40% in samples of transgenic animals. MAPKs are involved in functions including the regulation of meiosis, mitosis, and postmitotic functions in differentiated cells. Many different stimuli, including growth factors, cytokines, virus infection, ligands for heterotrimeric G protein-coupled receptors, and carcinogens, activate the MAPK pathway. In the MAPK pathway, Ras activates c-Raf, followed by MAPK/ERK kinase (MEK) and then MAPK1/2 (Itoh et al., 1993).

Phosphorylation of MAPKs leads to the activation of their kinase activity. Concerning the role of MAPKs in the hippocampus: they have recently been directly implicated in human learning through studies of a human mental retardation syndrome. A role of MAPKs in stabilizing structural changes in dendritic spines has been defined as well. A crucial role for MAPKs in the regulation of local dendritic protein synthesis is emerging. And finally, the importance of MAPK interactions with scaffolding and structural proteins at the synapse is increasingly apparent (Sweatt, 2004).
Also the protein level of PAK1 was elevated in synaptosomes and the hippocampus by 30 – 55%. PAK is a serine-threonine kinase that binds to and is activated by Rho family GTPases. PAK family members have an N-terminal kinase domain and a C-terminal p21 Rac and Cdc42-binding domain. Both p21-Rac and Cdc42 were up regulated in the P2 fraction of the hippocampus as well. The binding of Rho family GTPases results in autophosphorylation and activation of the kinase. PAK family members have been shown to play a role in actin polymerization and cytoskeletal dynamics (Brown et al., 1996). A primary role for dendritic spine defects was strengthened by the recent identification of a set of genes related to mental retardation. These mental retardation genes represent a cluster of proteins in the postsynaptic pathways regulating spine actin assembly and disassembly and spine morphogenesis. One of these proteins is PAK.
Several other proteins whose expression was changed in transgenic mice were involved in the reorganization of the cytoskeleton. Strikingly, most of these were up regulated apart from F-actin capping protein alpha-2 that binds to the barbed end of actin filaments and thereby regulate the growth of the actin filament. The phenomenon of compartmentalization, which was observed for synaptic vesicle proteins, also occurred in other disturbed functional entities such as cell adhesion and cytoskeletal rearrangements. While neural cell adhesion molecules L1, NrCAM, ICAM-5, contactin 1 and others were down regulated in transgenic samples S2, L1 was more abundant in P2 and contactin 1 was increased in synaptosomes. Basically, this speaks in favor of the fact that adhesion, first of all at the synaptic plasma membrane, was increased. Reduced levels of adhesion molecules in S2 however, suggests either that intracellular levels, possibly for the molecules that are about to be secreted, were less abundant or that cell adhesion elsewhere, e.g. extrasynaptic regions, is weakened. For L1 a cytoplasmic domain mutation was found leading to X-linked mental retardation due to impaired neural migration and axonal growth (Thelen et al., 2002).
Such systemic changes in the CNS of transgenic mice also require adaptations in metabolic pathways involved in the chemical conversion of carbohydrates, fats, and proteins into carbon dioxide and water to generate a usable form of energy, e.g. ATP. Consequently, the expression level of several proteins involved in the glycolysis, pyruvate oxidation or the tricarboxylic acid cycle were changed. From the data obtained by the ICAT screen it is yet too speculative to determine whether these individual metabolic reactions are stimulated or suppressed. Further experiments determining the metabolic rate would shed light on changes in the energy conversion in more detail.

Even though the abundance ratios determined by the ICAT experiment were small as compared to some previously published studies (Cheng et al., 2006; Han et al., 2001), there are several other publications presenting a similar range of relative abundance changes of proteins comparing two samples (Moron et al., 2007; Prokai et al., 2005; Zhang et al., 2005a; Zhang et al., 2005b). Likewise, the authors of these studies were partially successful in validating the findings of the ICAT-MS approach. From Hilgenberg's study (Hilgenberg et al., 2006) it is known that binding of a C-terminal agrin fragment to alpha 3NKA induces Ca^{2+}-influx. Others have shown that clustering of agrin can induce filopodia formation (Annies et al., 2006). Based on this and the findings in

our study we hypothesize that neurotrypsin cleavage of agrin elicits Ca^{2+} influx, possibly through alpha3NKA, thereby activating α-CaMK II and MAPK signaling pathways, which in turn could lead to rearrangements of the cytoskeleton. Through this the expression level of Cdc42 , p21-Rac, PAK1 are also affected.
With some exceptions the verification of our candidate proteins by Western blot analysis was often marginal but sufficient. For instance MAPK 1 was repeatedly more abundant in transgenic samples. Similarly, the expression level in P2 of N-copine, EEAT 2, and VDAC 1 was well confirmed. While PAK1 and GS expression was validated in one mouse line only, in the second line overexpressing neurotrypsin the endorsement failed. Merely the validation of the abundance ratios of adenosine kinase and of GS in S2 was contradictory and the amount of protein of alpha3NKA and RhoGDI was unchanged in wild-type and transgenic samples. The reason for this might be due to unspecific antibodies, intrinsic variation of the Western blot technique from *in vivo* protein extracts, or false positives from the ICAT screen. However, the quantification of proteins extracted from animal tissue with differences of about 30 – 50% might be a critical undertaking with Western blotting. Other reasons like the intramolecular location of the epitope from the antibodies used could lead to misinterpretations. E.g. the N-copine-specific antibody used in this study recognizes an epitope in the N-terminus of the protein, whereas in the ICAT-MS regulated peptide identifications were exclusively from the C-terminal end. Whether the abundance changes of the C-terminus were found due to fragmentation of N-copine by neurotrypsin is unlikely, since no putative cleavage site was identified. The fact is that the epitope of the antibody and the changed peptides do not overlap and therefore renders any conclusion about why the confirmation failed difficult.
The overall changes in protein abundance ratios comparing wild-type and neurotrypsin-overexpressing samples were unexpectedly small. Almost no outstanding protein was found with a ratio far above 1 : 2, or vice versa. It might well be that neurotrypsin, like other serine peptidases such as tPA, has multiple molecular functions in different regions of the brain. On account of this we suggest that the effects of the neurotrypsin-dependent changes might be diluted out, analyzing e.g. synaptosomes isolated from whole brain. Therefore, the idea emerged to focus on the proteome of the hippocampus. But compensatory mechanisms might reduce putatively harmful regulatory anomalies in such a way that brings the system back into balance. On the other hand already small variations in protein expression levels sometimes shut the complex biological system up, resulting in disastrous consequences. For example in kainic-acid induced seizure endogenous upregulation of tPA mediates the progression of the seizure spreading (Yepes et al., 2002). Moreover, the tPA-plasmin system has been implicated in neuronal plasticity and degeneration. Expression of catalytically active tPA is transiently induced in CA1 pyramidal neurons but its expression is decreased in the mossy fiber pathway after excitotoxic injury, indicatinig a complex control of tPA protein expression and enzymatic activity in the hippocampus (Salles and Strickland, 2002).

Immunohistochemical analysis of AK expression suggested an increase of AK- positive cells in cortical layers II, III and V. Adenosine is considered to be responsible for seizure arrest. In addition, deficiencies within the adenosine-based neuromodulatory system may contribute to epileptogenesis (Boison, 2005). AK is the key enzyme that controls ambient levels of adenosine. Since adenosine can suppress seizures, an elevated level of AK might contribute to persistent seizure that itself results in neuronal cell death. This in turn might lead to the catastrophic damage of cortical layer VI, which was observed in neurotrypsin-overexpressing mice. Indeed, adolescent transgenic mice suffered from chronic trembling, indicative for epileptogenic

seizures (eye-catching observation while handling with transgenic mice). Although, compared to tPA the specificity of neurotrypsin is probably more confined, neurotrypsin might likewise promote seizure. In case adequate inhibitors fail to restrain its elevated proteolytic activity that had become out of control due to overexpression, a deregulated cascade of proteolytic events and subsequent activation of signaling pathways like α-CaMK II and MAPK could possibly result in abnormal neuronal activity.

4.4 Pros and Cons of two proteomic approaches to investigate brain proteins of a transgenic mice

This study is the first large-scale proteomic analysis of a transgenic mouse line. We could not conclude that a complete proteome of the subcellular fractions was identified and quantified. Indeed, a subset of proteins that lack cysteine residues, very low abundance proteins and very hydrophobic proteins will not be analyzed using this technique. The advantage of multidimensional ICAT analysis is that the complexity of the peptide mixture is reduced and thus analysis of a higher number of unique proteins and associated quantification is achieved for a given time during the automated LC-MS/MS procedure. As the technique selects for peptides that contain free cysteine residues before labeling, it was relatively rare to find posttranslationally modified peptides. However, this lack of posttranslationally modified peptides could be overcome by simply analyzing avidin flow through peptides separately in a MS approach. Nevertheless, from our analysis, it is apparent that ICAT analysis yields maximal information for protein quantification, whereas studies that are targeted toward posttranslational modifications such as protein phosphorylation would require enrichment steps, as has been demonstrated by (Zhou et al., 2001).

As with any screening method, the data obtained by this study are not by themselves sufficient to explain the mechanisms of neurotrypsin-dependent changes in the CNS. The data do, however, implicate new proteins in these processes and suggest that can subsequently be tested by hypothesis-driven research or by further large-scale experiments. The insights gained by the proteomic profiling also do not explain the mechanisms by which protein concentrations in the CNS change. Changes in the rates of synthesis or degradation, the intracellular redistribution of a constant protein pool, or a combination of these factors could lead to the same apparent result. More extensive and repetitive experiments using ICAT protein profiling that include systemic subcellular fractions of brain tissue and additional time-resolved observations would be expected to differentiate the factors underlying the observed changes.

Four independent approaches to measure protein changes in E. coli treated with triclosan, an inhibitor of fatty acid biosynthesis were performed and more than 24'000 peptides were quantitated in an ICAT-MS experiment (Molloy et al., 2005). The results of this study demonstrated that quantitatively, the technique provided good reproducibility, and on average identified more than 450 unique proteins per experiment. However, the method was strongly biased to detect acidic proteins (pI < 7), underrepresented small proteins (<10 kDa) and failed to show clear superiority over 2DE methods in monitoring hydrophobic proteins from cell lysates.

Therefore, we complemented the ICAT-MS approach with the 2DE-MS method, which shows a preference for low Mr proteins and also identifies cysteine-free proteins that were transparent to the ICAT method. Whereas the ICAT-MS method quantifies the sum of the protein species of one gene product, the 2DE-MS method quantifies at the level of resolved protein species,

including posttranslationally modified and processed polypeptides. Our data indicate that different proteomic technologies applied to the same sample may provide additional types of information that contribute to a more complete understanding of the biological system studied. On the other hand, we also conclude that the potential of 2DE-MS for complete proteome analysis is likewise limited and is preferentially used to support quantifications from LC-MS based proteomics through stable isotope coding. Applying this technique alone limits the ability to analyze proteins of medium to low abundance. Due to the large range of protein expression levels as well as to subtle neurotrypsin-dependent changes it would be difficult to sufficiently resolve the perturbations of regulatory changes by 2DE alone.

In conclusion the proteomic profiling of subcellular fractions from the neurotrypsin-overexpressing mouse line provided insight into the complex interaction of a serine peptidases in the brain. Until now, no outstanding change in any of the protein identification was recorded. Two reasons might account for this. Either there is no bigger change than what we have found in our approach or, more strongly affected proteins with higher abundance ratios are not yet identified. It is known from the literature that serine peptidases potentially have different functions and even recognize different substrates depending either on the brain region or on the developmental stage (Samson and Medcalf, 2006). Thus, the effects might be diluted out or be too subtle in such a way that changes are scarcely detectable in a quantitative approach. Furthermore, the proteolytic overactivity might be inhibited by compensatory mechanisms operating in a temporally restricted manner such as an increase in the synthesis of inhibitors. Induction of endogenous inhibitors that limit the glaring damage potentially caused by overexpressed neurotrypsin during the time of active Thy-1.2 promotor might protect the brain from disastrous consequences. Of course technical improvements might as well lead to a more comprehensive proteome analysis. Due to redundant and incomplete database entries, still many uninterpreted good quality CID spectra are left over in shotgun proteomics. With a dynamic spectrum quality assessment and iterative computational analysis of proteomic data we would gain more efficient identifications of posttranslational modifications, sequence polymorphisms, and novel peptides (Nesvizhskii et al., 2006).
In conclusion, minor proteome changes can technically be shown with differential isotope labeling but remain difficult to be verified by independent methods.

5. Material and Methods

5.1 Subcellular fractionation

5.1.1 Isolation of synaptosomes

Synaptosomes were prepared as described by Phelan P. & Gorden-Weeks P.R. (in Turner A.J. and Bachelard H.S., Neurochemistry: A Practical Approach). Briefly, whole mouse brains were dissected and homogenized in a Potter-Elvehjem homogenizer (900 rpm, 12 up-and-down passes) in solution A (5 mM HEPES, 320 mM sucrose, pH 7.4). To remove cell debris and nuclei, the homogenate was centrifuged twice for 5 min at 1000 x g_{max} (Sorvall centrifuge, SS-34 rotor, DuPont Instruments) and the combined supernatants were centrifuged for 20 min at 12 000 x g_{max} (Sorvall centrifuge, SS-34 rotor, DuPont Instruments). The resulting pellet had a colored layer at the bottom of the centrifuge tube, which was mainly composed of mitochondria, whereas the rest of the pellet was white and contained the majority of the synaptosomes. By careful whirl mixing the synaptosomes could be resuspended, whereas the major part of the mitochondrial pellet was left behind. This step was repeated once. The white part of the pellet was resuspended in 2.6 ml solution A in a handheld homogenizer, and layered carefully on top of a Ficoll gradient consisting of 4.8 ml 12% Ficoll overlaid with 4.8 ml 7.5% Ficoll in 13.2 ml centrifuge tubes (Beckman Instruments). After centrifugation at 68 000 x g_{max} (Centrikon ultracentrifuge, SW 41 Ti rotor, Beckman Coulter), for 1 hour, the synaptosomes were enriched as a cream-colored band at the 7.5%/12% Ficoll interface. A myelin layer was floating on top of the gradient and free mitochondria were in the pellet. The synaptosomes were recovered by aspiration, resuspended in Krebs' solution (145 mM NaCl, 5 mM KCl, 1.2 mM $CaCl_2$, 1.3 mM $MgCl_2 \times 6H_2O$, 1.2 mM $NaH_2PO_4 \times 2H_2O$, 10 mM glucose and 20 mM HEPES, pH 7.5) and centrifuged for 20 min at 12 000 x g_{max} (Sorvall centrifuge, SS-34 rotor). The pellet was resuspended in solution A and stored at -80 °C.

5.1.2 Hippocampus fractionation

Mouse hippocampi were dissected and homogenized in a Potter-Elvehjem homogenizer (900 rpm, 12 up-and-down passes) in solution A. To remove cell debris and nuclei, the homogenate was centrifuged twice for 10 min at 3000 x g_{max} (Eppendorf 5417R Microcentrifuge) and the combined supernatants were centrifuged for 45 min at 34 000 x g_{max} (Optima™ TLX Ultracentrifuge and TLA 100.3 rotor, Beckman Coulter). The resulting pellet was resuspended in solution A and termed P2, and the supernatant was collected and termed S2. Except for the ICAT experiment, both fractions were then incubated at 4 °C for 30 min with lysis buffer (20 mM Tris-HCl, pH 7.5, 150 mM NaCl, 1% Triton X-100 and 1x Roche complete Mini, EDTA free protease inhibitor cocktail) and stored at -80 °C until use.

5.2 Isotope-coded Affinity Tag (ICAT)

Between 0.5 and 1 mg proteins extracts from wild-type and transgenic sample were solubilized in 0.1% SDS, 200 mM Tris-HCl pH 8.3, 5 mM EDTA, 6 M urea. To reduce the disulphide bridges, 5

mM TCEP was added and the protein extract was incubated for 30 min at 37 °C. Equal amounts of proteins were labeled with cleavable light (^{12}C) for wild-type and heavy (^{13}C) ICAT reagent (Applied Biosystemss) for transgenic sample. In order to guarantee a complete labeling at least a two fold molar excess of reagent over free sulfhydryl groups was added to the sample for 90 min in the dark at room temperature with gentle agitation. The labeling reaction was quenched with ten fold molar excess of DTT over reagent. The labeled proteins were then combined, diluted down to a final urea concentration of 1 M, and digested with 1 mg trypsin (Promega) per 100 mg protein overnight at 37 °C. To reduce the complexity, the resulting peptide mixture was separated by strong cation exchange chromatography on an Ettan LC system (Amersham Biosciences) using a 2.1 mm x 20 cm Polysulfoethyl A column (PolyLC) at a flow rate of 0.2 ml/min. The buffers used were 5 mM KH_2PO_4 pH 3.0, 25% ACN for buffer A and 5 mM KH_2PO_4 pH 3.0, 400mM KCl, 25% ACN for buffer B. The eluting salt gradient was up to 25% buffer B within 13.2 ml and up to 100% buffer B within 8.8 ml. In total, 62 fractions, 440 µl each, were collected. To neutralise the pH, 100 mM Na_2HPO_4 pH 10 was used. The labeled cysteine-containing peptides were then isolated manually using an avidin affinity column (ICAT cartridge avidin, Applied Biosystems) according to the manufacturer's instructions. After concentration of the avidin purified fractions, the biotin tag was removed by acid cleavage using cleaving reagent (Applied Biosystems) for 2 h at 37 °C. Finally, the peptides were cleaned-up for MS by solid phase extraction using Sep-Pak cartridges (Waters). The samples were concentrated again, dissolved in 15 µl 0.2% acetic acid and stored at -80 °C until use.

5.3 Mass Spectrometry (MS)

5.3.1 Reversed-Phase microcapillary Liquid Chromatography Electrospray Ionization Mass Spectrometry (RP-µLC-ESI-MS)

RP-µLC-ESI-MS was performed coupling a Probot (LC-Packings/Dionex) autosampler system in-line with an LCQ Deca quadrupole IT (ion trap) mass spectrometer (Thermo Finnigan). Samples were automatically injected into a 10 µl loop and loaded onto an analytical column (75 µm x 8 cm column packed in-house with Magic C18 AQ beads 5 µm, 100 Å (Michrom)) prior to the ionization. Peptide mixtures were delivered to the analytical column at a flow rate of 300 nl/min of buffer A (5% ACN, 0.2% formic acid) for 25 min and then eluted using a gradient of buffer B (80% ACN, 0.2% formic acid). 0 – 12%; 6%/min, 12 – 43%; 0.3%/min. Peptide ions were detected in a survey scan from 400 – 2000 a.m.u. followed by 3 MS/MS scans in an automated fashion. Alternatively, for the hippocampus S2 and P2 fraction an LTQ-FT mass spectrometer was used. Nanoflow-LC MS/MS was performed coupling an Agilent 1100 HPLC (Agilent Technologies) to a 7-Tesla LTQ-FT mass spectrometer (Thermo). For peptide LC analytical columns (15 cm X 50 µm) were packed in-house with ReproSil-Pur C18- AQ, 3 µm (Dr. Maisch GmbH). With a flow rate of 150 nl/min, peptides were transferred to the analytical column and eluted in a gradient of acetonitrile (1%/min) in 0.1 M acetic acid. The eluate was sprayed via emitter tips (New Objective), butt-connected to the analytical column. The mass spectrometer operated in data-dependent mode, automatically switching between MS and MS/MS acquisition for the three most abundant peaks in a given spectrum. The full-scan MS spectra were acquired in the Fourier transform-ion cyclotron resonance (FT-ICR) at a target value of 5×10^6 with a resolution of 20,000. The three most intense ions were then isolated for accurate mass measurements by

an FT-ICR-selected ion monitoring scan, which consisted of 10-Da mass range, at a resolution of 50,000. These ions were then fragmented in the linear ion trap.

5.3.2 Matrix-Assisted Laser Desorption/Ionization-Time-Of-Flight Mass Spectrometry (MALDI-TOF MS)

The samples were analyzed on a 4700 Proteomics Analyser MALDI TOF/TOF system (Applied Biosystems), which is equipped with a Nd:YAG laser operating at 200 Hz. All mass spectra were recorded in positive reflector mode, and they were generated by accumulating data from 5000 laser pulses. First, MS spectra were recorded from the standard peptides on each of the six calibration spots, and the default calibration parameters of the instrument were updated. Subsequently, MS spectra were recorded for all sample spots and internally calibrated using signals from autoproteolytic fragments of trypsin if these signals were detectable. Up to four spectral peaks per spot that met the threshold criteria were included in the acquisition list for the MS/MS spectra. Peptide fragmentation was performed at collision energy of 1 kV and a collision gas pressure of approximately 2 x 10^{-7} Torr. Data from 2500 - 5000 laser pulses were summed up for each fragment ion spectrum.

5.3.3 Protein identification and quantification

5.3.3.1 Mascot search engine

For the database searches of MS/MS spectra of ICAT labeled hippocampal peptides collected with the LTQ FT-ICR, the peptide tolerance was set to 10 ppm and the MS/MS tolerance to 0.5 Da. Variable modifications on cysteine residues of the ICAT light and heavy reagents were chosen at 227.126991 and 236.157185, rsp. Oxidation of methionine, N-terminal pyroglutamic acid and N-acetylation were selected as variable modifications. A human-mouse-rat database downloaded from EBI (83028 sequences, release date: September 09, 2006) was used.
GPS (Global Proteome Server) Explorer Software version 3.5 (Applied Biosystemss) was used for submitting MS and MS/MS data for database searching from MALDI TOF-TOF experiments. Mascot version 2.1.0 (Matrix Science, London, UK) was utilized as the search engine (Perkins et al., 1999) and database searching was performed using a mouse protein database downloaded from the European Bioinformatics Institute (EBI) (32849 sequences, release date: March 25, 2006) Typically, the following search settings were used: maximum number of missed cleavages: 1; peptide tolerance: 35 ppm; MS/MS tolerance: 0.2 Da. Carboxyamidomethylation of cysteine was set as fixed modification, and oxidation of methionine was selected as variable modification.

5.3.3.2 SEQUEST search algorithm

The MS/MS spectra from the ESI-MS were used by SEQUEST algorithm (Eng et al., 1994) to search a protein sequence database. To identify the proteins from the synaptosomes, which were all recorded with an LCQ Deca mass spectrometer and proteins from the hippocampus fractions S2 and P2 that were measured with LTQ-FT mass spectrometer a the following settings were applied for SEQUEST analysis: the maximum number of missed cleavages was 1; the peptide tolerance was 3.0 Da; the fragment ion tolerance 1 Da. Different search options were selected

for oxidation of methionine and 9 Da on cysteine, whereas a fixed modification of 227.13 was selected for cysteine residues. As for the identification of hippocampal proteins a human-mouse-rat database downloaded from EBI (83028 sequences, release date: September 09, 2006) was used and the settings were taken as indicated above.

5.3.3.3 Peptide and Protein Probability Assignment

The statistical model PeptideProphet™ was used to assess the validity of peptide assignments from SEQUEST data set (Keller et al., 2002). From each data set, it learns the distribution of search scores and peptide properties among correct and incorrect peptides. Those distributions are used to compute for each result a probability that it is correct. This analysis allows filtering large volumes of MS/MS data with predictable false error rates and sensitivity values. A maximum error rate of 5% was chosen for peptides to pass the filter. Protein identifications were validated, using ProteinProphet™, a statistical model that allows filtering large-scale proteomics data sets with predictable sensitivity and false positive identification error rates. Different peptide identifications allocated to the same protein are combined to estimate the probability that their corresponding protein is present in the sample (Nesvizhskii et al., 2003). A Minimal Probability Threshold (MPT) of 0.95 was chosen for ProteinProphet.

5.3.3.4 Automated Statistical Analysis on Protein Ratio (ASAPRatio)

ASAPRatio calculates the relative abundance of proteins and the corresponding confidence intervals from ICAT-type LC ESI-MS data (Li et al., 2003). First, the software reconstructs single ion chromatogram (SIC) of a peptide and its partner, subtracts background noise from each chromatogram, and calculates light: heavy ratio, in one charge state. Second, the ratios of the same peptide in different charge states are averaged and weighted by the corresponding intensity to obtain the peptide light: heavy ratio and its error. Subsequently, all unique peptides identifications for a given protein are collected; their ratios and errors calculated, and the relative protein abundance ratio and the confidence interval are computed, applying statistics for weighted samples. A by-product of the software is to identify outlier peptides that may be misidentified or, more interestingly, may bear unidentified post-translational modifications (PTM).

5.3.3.5 XPRESS software

The XPRESS software automates protein expression calculations by accurately quantifying the relative abundance of ICAT-labeled peptides from their chromatographic co-elution profile. Starting with the peptide identification, XPRESS reconstructs the light and heavy peptide elution profiles of the precursor ions and determines the area of each peptide peak and calculates the protein abundance ratio based on these areas (Han et al., 2001). Furthermore, the program provides a graphical, interactive interface to the results. Averages plus standard deviations are calculated for each protein expression value when multiple peptide measurements are available. As opposed to ASAPRatio the mass tolerance is displayed and can be adjusted according to the mass accuracy of the mass spectrometer used. Accordingly, the mass tolerance was set to ± 0.5 units when using FT-ICR.

5.4 2D Gel Electrophoresis

5.4.1 First Dimension: Isoelectric Focusing (IEF)

IEF was performed using Immobiline Dry Strip pH 4 – 7, 24 cm. The strips were rehydrated in the Reswelling Tray (Amersham Biosciences) for 20 hours in 450 µl of rehydration buffer (7 M urea, 2 M thiourea, 4% (w/v) CHAPS, 0.5% (v/v) IPG Buffer pH 4-7 (Amersham Biosciences), 1.2% (v/v) DeStreak Reagent (Amersham Biosciences), 0.002% bromphenol blue). 150 µg of protein was precipitated and interfering substances (salt, detergent) were removed with the 2D Clean-Up Kit (Amersham Biosciences). The proteins were dissolved in 50 µl of solubilization buffer (7 M urea, 2 M thiourea, 40 mM DTT, 4% (w/v) CHAPS, 2% IPG Buffer pH 4-7) and cup-loaded onto the strips. For the first dimension the Ettan™ IPGphor™ IEF System (Amersham Biosciences) was used with the following focusing steps: Step 1: 500 V, 1 min, gradient; Step 2: 500 V, 4 hours, step-and-hold; Step 3: 4000 V, 1.5 hours, gradient; Step 4: 8000 V, 45 kVh, step-and-hold. After the IEF the strips were frozen at -80 °C until use.

5.4.2 Second Dimension: SDS-PAGE

In-house casted 10% gels containing 10% acrylamide, 0.32% methylenebisacrylamide, 0.375 M Tris/HCl (pH 8.8), 5% glycerol, 0.1% SDS, 0.05% ammonium persulfate, 0.0005% TEMED were casted in the Ettan Dalt II Gel Caster System (Amersham Biosciences). The Immobiline Dry Strips were first equilibrated for 15 min in SDS-equilibration buffer (25 mM Tris-base, 192 mM glycine, 01% (w/v) SDS) with 2% (w/v) DTT, followed by a 15 min equilibration in SDS-equilibration buffer containing 2.5% (w/v) iodacetamide, before placed on top of the gels. The Ettan Dalt II System (Amersham Biosciences) was used to run the gels in SDS-electrophoresis buffer containing 25 mM Tris-HCl pH 8.3, 192 mM glycine, 0.1% SDS with constant power of 2.5 W/gel for 30 min for a start followed by 12 W/gel for 3 – 4 hours to separate the proteins in the second dimension. The gels were fixed in 30% EtOH and 10% acetic acid overnight and washed three times 30 min in 20% EtOH. Ruthenium II tris (bathophenantroline disulfonate) (RuBP) was added to stain the gels as described by Lamanda et al., 2004 (Lamanda et al., 2004). The 2D gels were scanned using the Typhoon 9400 Variable Mode Imager (Molecular Dynamics) and Proteomeweaver software was used to analyze the gels.

5.4.3 2D Gel Analysis software

High-resolution images were analyzed using Proteomweaver v3.0 (Definiens). Gel images were converted into 8-bit TIF files and processed with Proteomweaver software, which allowed spot detection, gel matching, quantification, and statistical analysis. Different analysis sets were used for pairwise comparison of two protein-spots on the gels. The entire signal on each gel was normalized before the detection of spot boundaries and calculation of the intensity ratio for each spot pair was performed. Average abundance changes were calculated from regulation factors. Student's *t* test was used for statistical analysis. Quality assurance statistics, which calculates the reliability of the regulation factor, indicated that a regulation factor for S2 is suitable at 1.7 and for P2 it was above 2. Only spots with at least 1.5-fold change in intensity ($P \leq 0.05$) and a coefficient of variation of less than 25% after normalization were considered as differentially expressed.

5.4.4 Spot Excision, Digestion and Spotting on MALDI target plate

Protein spots from the 2D gels were excised with the GelPix Spot Picking Robot (Genetix). Before it, the gels were imaged using an on-board camera. The image was matched with pre-selected spots from analysis sets using Proteomweaver. In this way a user defined protein target excision list was generated. The protein spots were picked with an eight channel excision head. The gel slices were transferred to a V-shaped 96-well plate (Greiner) and stored in H_2O at -20 °C. In-gel digestion, extraction, and purification of peptides with subsequent spotting onto MALDI target plates was performed using the fully automated Genesis ProTeam 150 Platform (TECAN). The robot was configured with eight liquid handling tips. Four nanopipetting tips were used to prepare excised gel samples for proteolytic digestion and four adaptor tips picked up ZipTips µ-C18 (Millipore) pipette tips in order to desalt peptide mixtures and to spot them onto MALDI target plates. In brief: The storage solution was removed and replaced by 80% ACN. After 10 min, the ACN was removed and evaporated for additional 10 min. The dehydrated gel slices were incubated in 6.7 µg/µl sequence grade modified Trypsin (Promega) dissolved in 5 mM Tris-HCl, pH 8.3 for 3 hours. The proteolysis was stopped by adding 1% TFA. The tryptic peptides were purified and spotted onto MALDI target plates as follows: First, the ZipTips were pre-wetted with 80% ACN, 0.02% TFA and washed two times with 0.1% TFA. Second, the peptides were bound to the ZipTips by aspirating and dispensing the sample 5 – 7 cycles and washed again. Third, the peptides were spotted onto the target plate with MALDI matrix solution, containing 4 mg/ml α-CCA in 65% ACN, 0.035% TFA. Finally, the samples were analyzed using 4700 Protoemics Analyser MALDI-TOF/TOF.

5.5 Antibodies

Polyclonal goat antibody G87 was generated against the protease domain of mouse neurotrypsin. G93 was raised against the full-length protein of mouse neurotrypsin. The R132 polyclonal rabbit antibody was raised against the 80 kDa cleaved agrin fragment and R139 was generated against the very C-terminal LG3 domain of rat agrin. G92 was produced using the same antigen but immunization was performed in a goat instead of a rabbit. All antibodies were affinity purified. A polyclonal antibody against adenosine kinase was a kind gift of Dr. D. Boison (Department of Pharmacology, University of Zurich). Monoclonal antibodies against α-CaMK II, clone 6G9 (ab2725), Na^+/K^+-ATPase-α3, clone XVIF9-G10 (ab2826) and polyclonal antibodies against Glutamine Synthetase (ab16802), Kinesin Heavy Chain 2 (ab3475) and PKC-γ (ab4144) were all purchased from Abcam. The monoclonal antibody against phospho-α-CaMK II (pThr286), clone 22B1 (MA-1-047) was from Affinity BioReagents. Monoclonal antibodies against CD81, clone Eat1 (559516), N-Copine (611588), Glutamate Receptor 2/3, clone 6C4 (556341), Complexin 2, (610728), PSD-95 (610495), Rab3 (610379), and α-/ß-SNAP (611898) were all from BD Biosciences Pharmingen. Monoclonal antibodies against MAP-2, clone AP20 (MAB3418), Synaptophysin, clone SY38 (MAB5258), NeuN (MAB377) and GFAP (MAB360) were from Chemicon. Polyclonal antibodies against Rho GDI (sc-360), PKC-ε (sc-214), Tenascin-C (sc-20932), VDAC1 (sc-8828), MAP-1A (sc-8969), EAAT2/GLT-1 (sc-7760), PAK-1 (sc-882), Grp-78 (sc-1050) were from Santa Cruz Biotechnology, Inc. Monoclonal antibodies agains ß-actin, clone AC-74 (A5316) and ß-COP (G6160) were from Sigma. The monoclonal antibody against Na^+/K^+-ATPase-α1, clone C464.6 (05-369), and polyclonal antibodies against MAPK2 (06-333), phospho-MAPK1/2 (07-467), and PP2A, A subunit (07-250) were from Upstate. And monoclonal antibody

against Neurofilament-160 (NF-M), clone RMO-270 (13-0700) was from Zymed Laboratories Inc.

5.6 Gel electrophoresis and immunoblotting

5.6.1 SDS-PAGE

Protein samples were boiled for 5 min in reducing SDS-PAGE loading buffer and electrophoretically separated on 7.5%, 10% or 12% polyacrylamide containing 0.1% SDS with constant current of 25 mA/gel (Laemmli, 1970).

5.6.2 NuPAGE 4 – 12% Bis-Tris and 10 – 20% Tricine Gel

Protein samples were dissolved in NuPAGE® LDS Sample Buffer or Novex® Tricine SDS Sample Buffer (Invitrogen) and incubated at 70 °C for 10 min or 85 °C for 2 min, respectively. The samples were loaded onto NuPAGE® 4-12% Bis-Tris or 10-20% Tricine Gels (Invitrogen) and separated at 40 mA/gel.

5.6.3 Immunoblotting

Proteins resolved by gel electrophoresis were transferred to either nitrocellulose (Schleicher & Schuell) or PVDF (Millipore) membranes. For semi-dry Western blotting the proteins were transferred at constant voltage of 24 V for 1 hour in a BioRad Trans-Blot semi-dry power supply or the transfer was done at 30 V constant overnight in a Criterion™ Blotter (BioRad) for wet blotting. The nitrocellulose membranes were blocked for 1 hour in PBS containing 1% Western Blocking Reagent (Roche) and the PVDF membranes were rinsed in MetOH and let air-dry for blocking. Primary antibodies were incubated at room temperature for 2 hours or at 4 °C overnight, diluted in PBS and 0.4% Western Blocking Reagent as indicated below. After washing, secondary antibodies conjugated to HRP were added for 45 min at room temperature as follows: anti-goat-HRP (1:30,000), anti-rabbit-HRP (1:20,000) and anti-mouse-HRP (1:20,000). Finally, the blots were developed with chemiluminescent substrate Chemiglow (Witec AG, Littau, Switzerland; Alpha Innotech) and recorded digitally on LAS-300 Luminscent Image Analyzer (Fujifilm).

Antiobody dilutions

Name	**Preparation**	**Dilution**
G87	affinity-purified	0.005 mg/ml
G93	affinity-purified	0.005 mg/ml
R132	serum (2nd boost)	1:3000
R139	serumm (2nd boost)	1:1000
anti-ß-actin	ascites fluid	1:10000
anti-ADK	affinity-purified	1:3000
anti-ß-COP	ascites fluid	1:10000
anti-α-CaMK II	IgG_1	1:4000
anti-p-α-CaMK II	IgG_1	1:2000
anti-EAAT2/GLT-1	IgG_1	1:1000
anti-GFAP	IgG_1	1:2000

anti-GluR2	IgG_{2a}	1:1000
anti-Glutamine Synthetase	IgG_1	1:2000
anti-Grp-78	IgG_1	1:1000
anti-MAPK2	IgG_1	1:2000
anti-p-MAPK1/2	IgG_1	1:2000
anti-Na^+/K^+-ATPase-α1	ascites fluid	1:3000
anti-Na^+/K^+-ATPase-α3	IgG_1	1:5000
anti-N-Copine	IgG_1	1:2000
anti-Neurofilament	IgG_{2a}	1:2000
anti-PAK-1	IgG_1	1:2000
anti-PSD-95	IgG_1	1:2000
anti-Rho GDI	IgG_1	1:1000
anti-Synaptophysin	IgG_1	1:10000
anti-VDAC1	IgG_1	1:1000

5.7 Cleavage of agrin by co-expression with neurotrypsin in HeLa cells

For expression ot neurotrypsin, the coding region of full-length human neurotrypsin (CAA04816) was inserted into pcDNA3.1 vector (Invitrogen). Catalytically inactive neurotrypsin (S/A) was generated by mutating Ser_{825} to Ala by means of overlapping extension PCR. For expression of membrane-bound full-length agrin, the coding sequence ranging from Met_1 to Pro_{1959} of rat agrin (P25304, splice variant y4z8) was inserted into pcDNA3.1. HeLa cells were cultured to 60 . 80% confluency in 12-well culture plates (Corning) with DMEM supplemented with 10% FCS (Biochrom). Polyethylenimine (PEI) was used as transfection reagent as described in (Baldi et al., 2005). The transfection mixture was removed 4 – 6 h after transfection by washing once with PBS. After 48 h in DMEM without FCS the medium was harvested and the cells were lysed in 150 mM NaCl, 0.5 mM EDTA, 10% glycerol, 1% Triton-X-100 in 20mM Tris-HCl, pH 7,4. For the analysis of the cleavage products supernatants and cell lysates were separated on a 4 – 12% NuPAGE gel (Invitrogen) and analysed by immunodetection.

5.8 Immunohistochemistry

Animals were fixed by transcardiac perfusion using a perfusion pump. Freshly prepared fixative containing 4% PFA in Na^+ phosphate buffer, pH 7.4, and 15% saturated picric acid was used to ensure preservation of the tissue and good antibody penetration. The brain was dissected out and postifxed in the same fixative for 1 hour or overnight at 4 °C. Cryoprotection was done in ice-cold PBS with 10% (v/v) DMSO for 3 hours at 4 °C. The tissue was embedded in Tissue-Tek® O.C.T.™ Compound (Bayer) and was shock frozen in isopenthan and stored at -20 °C until use. Sectioning from frozen blocks was cut with LEICA CM3050 S sliding microtome at 40 µm. The tissue sections were either stained with immunoperoxidase (VECTASTAIN Elite ABC Kit VECTOR Laboratories) method or with immunofluorescence.

In brief, for immunoperoxidase staining the sections were blocked in Tris-Triton (0.05%) pH 7.4 with 20% normal goat serum (NGS), 0.2% Triton X-100 for 1 hour and incubated with the primary

antibody diluted in Tris-Triton with 2% NGS and 0.1% Triton X-100 overnight. The next day, the sections were washed in TBS and biotinylated secondary antibodies were allowed to bind for 2 hours (Elite ABC Kit). After another wash step the ABC solution (Elite ABC Kit) containing avidin DH and biotinylated HRP H reagents was added for 1 hour, washed again, and then the sections were conditioned to pH 7.6 in 50 mM Tris buffer before the incubation with substrate solution DAB (0.5 mg/ml in TB, pH 7.6) for 30 min at dark. The reaction was catalyzed with 0.5% H_2O_2 until the sections had the appropriate color and stopped by transferring them into TB for two times 5 min and further into PBS before mounting the sections onto gelatinized glass slides. For dehydration they were shortly incubated in increasing vol.-% of EtOH (50, 70, 96 and 100%) followed by Xylene for 30 min before coverslipped with EUKITT mounting medium (Fluka).
For immunofluorescence staining the sections were blocked in TBS pH 7.4 with 20% FCS, 0.2% Triton X-100 for 1 hour and incubated overnight with the primary antibody diluted in TBS with 2% FCS and 0.1% Triton X-100, washed and incubated with the Cy3 or FITC labeled secondary antibody for 2 hours. After another washing step the sections were mounted using the Vectashield mounting medium (Vector Laboratories). The staining was either visualized under the epifluorescent microscope LEITZ DMRXE (Leica) or by confocal microscopy using a LEICA SP1 confocal microscope at the Center for Microscopy and Image Analysis, University of Zurich.

5.9 Generation of transgenic mouse lines overexpressing neurotrypsin

Endogenous expression of neurotrypsin was mainly localized to specific brain regions involved in learning and memory. It was also found that neurotrypsin is tightly regulated during postnatal development of the nervous system and its expression is reduced for the maintenance of the nervous system during adulthood (Gschwend et al., 1997; Wolfer et al., 2001). The intriguing expression pattern and the finding that neurotrypsin is a CNS specific serine peptidase suggests an important molecular function in processes such as synapse formation, elimination and synaptic plasticity. To shed light on the proteolytic and non-proteolytic activity of neurotrypsin transgenic mouse lines overexpressing neurotrypsin under the control of the brain specific Thy-1.2 expression cassette were generated. The Thy-1.2 expression cassette drives strong constitutive expression of transgenes specifically in neurons of transgenic mice (Caroni, 1997). Transgene expression begins at P6 - 10, at a time when it can affect activity-dependent rearrangements of synaptic connections and neuron-glia interactions during the late phase of nervous system development. The Thy-1.2 activity peaks at P12, with a subsequent sharp decline. The promotor activity remains relatively low thereafter (Radrizzani et al., 1995). These properties of the Thy-1.2 promotor can be exploited to study the effects of neurotrypsin during late phase nervous system development and in the adult with the added possibility that different combinations of expressing and non-expressing neurons in transgenic animals derived from different founder lines can be analyzed. An expression construct including a floxed STOP cassette followed by the cDNA of human neurotrypsin (hNT) was ligated into the *Xho*I site of the promotor region, resulting in a dormant hNT expression cassette under the control of the Thy-1.2 promotor (Fig. 5.1a). Removal of the STOP cassette can be used to activate the hNT transgene expression. This was achieved by crossing CMV-Cre with hNT (transgene494) transgenic mice. In the resulting double transgenic animals the Cre-recombinase removes the STOP cassette. Subsequent crossing with another hNT-CMV-Cre double transgenic mouse might occasionally result in a constitutively hNT overexpressing mouse line where the transgene has gone germline. In these

mice, termed Muslick 494 (M494), hNT expression is solely under the control of the Thy-1.2 promotor (Fig. 5.1b). Transgenic mice derived from different founder lines, carrying the same expression constructs, called Muslick 491 (M491) strong expressor, or M491S, were also used in this report. Furthermore, two control lines were used. First, a transgenic mouse line still bearing the STOP cassette since it was not crossed with a CMV-Cre transgenic mouse, resulting in a transgenic mouse line with a dormant hNT transgene (floxed 494, or f494). Second, a mouse line overexpressing a proteolytically inactive form of mouse neurotrypsin, where the active serine of the catalytic triad was mutated to an alanine (S/A 785). Finally, a neurotrypsin knock-out (KO) mouse was used to check for protein expression levels (Zurlinden et al., submitted). Prior to use, all of the animals were tested for the presence of the transgene or the absence of the neurotrypsin gene by PCR using specific primers.

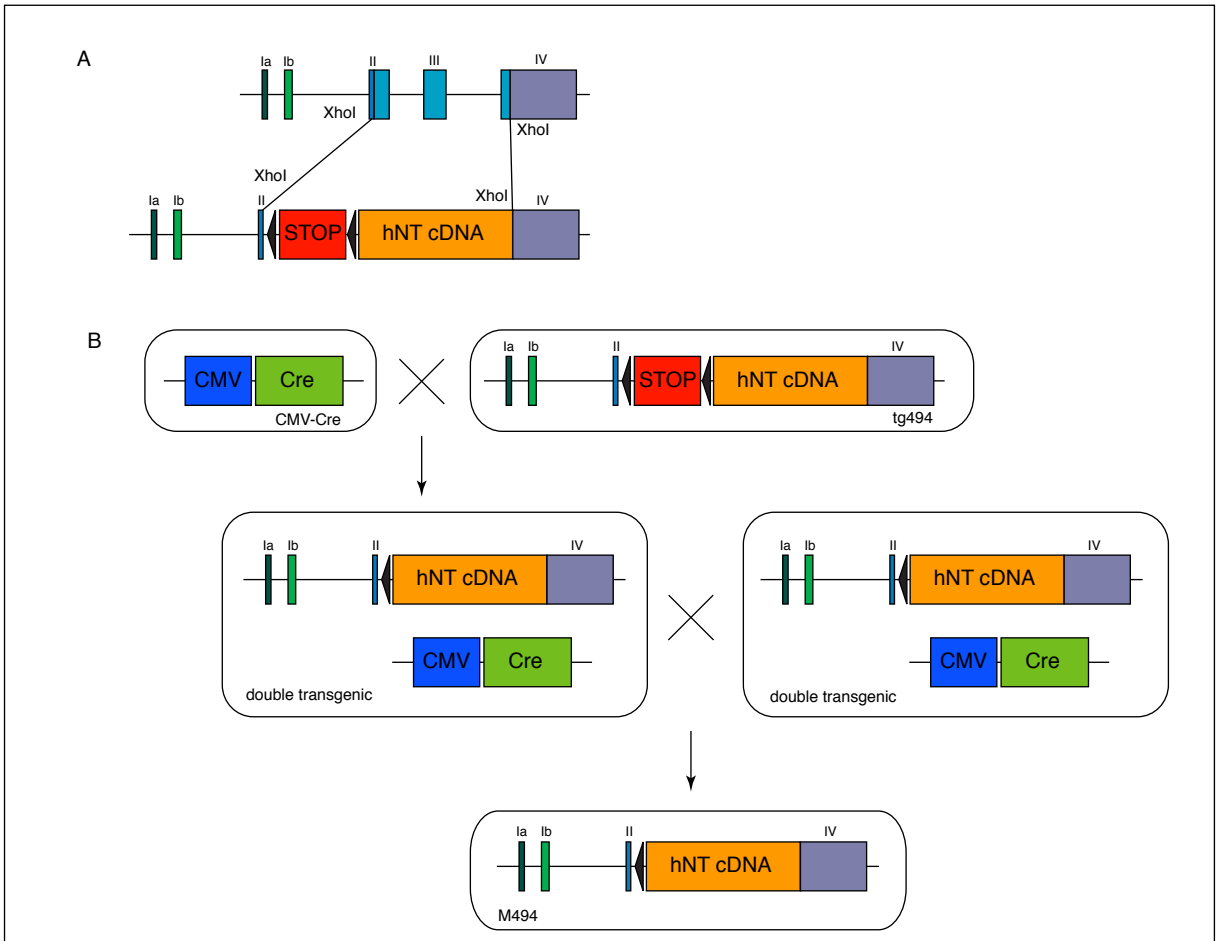

Figure 5.1 Generation of a constitutively human neurotrypsin overexpressing mouse line.
(A) The mouse Thy-1.2 expression cassette is used to drive strong constitutive expression of transgenes specifically in neurons. The floxed STOP cassette followed by the human neurotrypsin (hNT) cDNA is cloned into the XhoI site of Thy-1.2 expression cassette. For injection into mouse pronuclei EcoRI and PvuI sites, flanking the basic construct can be used to recover the 6.5 kb of the expression cassette plus transgene, resulting in a transgenic mouse line with a dormant hNT transgene. **(B)** Double transgenic mice are generated by crossing CMV-Cre and silent hNT transgenic mice (tg494). The Cre recombinase removes the STOP cassette and activates hNT expression. The subsequent crossing of two double transgenic mice may result in a constitutively hNT overexpressing mouse line under the control of the Thy-1.2 promotor. This coincidentally can occur when the Cre recombinase removes the STOP cassette in the germline to give rise to Muslick 494 (M494).

5.10 Polymerase Chain Reaction (PCR)

5.10.1 PCR genotyping

Genomic DNA was extracted with alkaline lysis from tail biopsies of offspring from hNT overexpressing mice crossed with wild-type Black/6 mice. 300 µl alkaline lysis reagent (25 mM NaOH; 0.2 mM Na-EDTA, pH 12.0) added to 0.5 cm tail biopsies and lysed for 45 min at 96°C. To stop the reaction 300 µl neutralizing reagent (400 mM Tris-HCl, pH 5.0) were added. 1µl extraction mixture was used for 20 µl reaction mix. For all PCR reactions the following reaction mix was prepared: 1x Buffer (Applied Biosystems), 0.25 mM dNTPs (Applied Biosystems), 1.5 mM $MgCl_2$ (Sigma) and 0.1 µl Taq-Polymerase (5 U/µl) (Applied Biosystems), 0.5 µM forward primer and 0.5 µM reverse primer. The primer sequences and the PCR program for each mouse line is indicated below (for all but NTKO TAG was used as a positive control for PCR amplification, PCR products of NTKOF01 and NTKOR02 indicated NTKO and of NTKOF01 and NTKOR03 indicated wild-type allel:

M494, M491S and f494

hNTSIIfor	5'-GCAATGTGCCAGATTCAGCAG-3'
Thy1back	5'-CCCATGTTCTGAGATATTGGAAG-3'
TAG83for	5'-GGAGGAGAGAGACCCCGTGAAA-3'
TAG82back	5'-ACACGAAGTGACGCCCAATCCGT-3'
PCR program:	1x (3', 95°C), 40x (45'', 95°C; 45'' 63°C; 60'', 72°C), 1x (5' 72°C)

S/A 785

mNTIIfor	5'-CAATGTGCCAGACTAAGCACC-3'
Thy1back	5'-CCCATGTTCTGAGATATTGGAAG-3'
TAG83for	5'-GGAGGAGAGAGACCCCGTGAAA-3'
TAG82back	5'-ACACGAAGTGACGCCCAATCCGT-3'
PCR program:	1x (3', 95°C), 40x (45'', 95°C; 45'' 56°C; 60'', 72°C), 1x (5' 72°C)

NTKO

NTKOF01	5'-CAGAGCTCCTGGCGCTCATC-3'
NTKOR02	5'-GGAAGACAATAGCAGGCATGCTG-3'
NTKOR03	5'-CTCGCAGCTCAGCCCAACTG-3'
PCR program:	1x (3', 95°C), 40x (45'', 95°C; 45'' 61°C; 60'', 72°C), 1x (5' 72°C)

5.10.2 Real-time PCR

Real-time PCR was performed to discriminate between heterozygous and homozygous transgenic mice. PCR amplifications were measured using the Applied Biosystems 7500 Fast Real-Time PCR System. The primers and TaqMan® probes were all designed with Primer Express 2.0 software (Applied Biosystems). The sequences of the primers and probes used for the amplicons of human NT were: forward primer: 5'-CAGTGGAAGTATATGCAAGTGGAGTT-3', reverse primer: 5'-GGTTTGTTTTGCTATTCCTTTTCCT-3', TaqMan® probe: 5'-VIC-TCATTTGTCACCAGCTGCAGCTG GG-TAMRA-3', and of murine Tubulin -3 were: forward primer: 5'-TGCGGAAAGAGTGTGAGAATTG-3' and reverse primer: 5'-TCACGCACCTTGCTGA TGA-3', TaqMan® probe: 5'-FAM-

AGGGCTTCCAGCTGACACACTCA-TAMRA-3'. The real-time PCR was conducted in 10 µl reaction volume containing 100 ng template genomic DNA, 1x TaqMan® Fast Universal PCR Master Mix No AmpErase® UNG (Applied Biosystems), 900 nM each, forward and reverse primer, and 200 nM TaqMan® probes. PCR cycling conditions were as follows: 1 cycle at 95°C for 10 min, followed by 40 cycles at 95°C for 15 s and 58 °C for 1 min. The results were analysed on Applied Biosystems 7500 Real Time PCR system using Relative Quantitation (RQ) gene expression analysis software.

6. References

Abad, M.A., M. Enguita, N. DeGregorio-Rocasolano, I. Ferrer, and R. Trullas. 2006. Neuronal pentraxin 1 contributes to the neuronal damage evoked by amyloid-beta and is overexpressed in dystrophic neurites in Alzheimer's brain. *J Neurosci*. 26:12735-47.

Adachi, J., C. Kumar, Y. Zhang, J.V. Olsen, and M. Mann. 2006. The human urinary proteome contains more than 1500 proteins, including a large proportion of membrane proteins. *Genome Biol*. 7:R80.

Anflous-Pharayra, K., Z.J. Cai, and W.J. Craigen. 2007. VDAC1 serves as a mitochondrial binding site for hexokinase in oxidative muscles. *Biochim Biophys Acta*. 1767:136-42.

Annies, M., G. Bittcher, R. Ramseger, J. Loschinger, S. Woll, E. Porten, C. Abraham, M.A. Ruegg, and S. Kroger. 2006. Clustering transmembrane-agrin induces filopodia-like processes on axons and dendrites. *Mol Cell Neurosci*. 31:515-24.

Antonin, W., D. Fasshauer, S. Becker, R. Jahn, and T.R. Schneider. 2002. Crystal structure of the endosomal SNARE complex reveals common structural principles of all SNAREs. *Nat Struct Biol*. 9:107-11.

Baldi, L., N. Muller, S. Picasso, R. Jacquet, P. Girard, H.P. Thanh, E. Derow, and F.M. Wurm. 2005. Transient gene expression in suspension HEK-293 cells: application to large-scale protein production. *Biotechnol Prog*. 21:148-53.

Baldwin, M.A. 2004. Protein identification by mass spectrometry: issues to be considered. *Mol Cell Proteomics*. 3:1-9.

Barnard, R.J., A. Morgan, and R.D. Burgoyne. 1997. Stimulation of NSF ATPase activity by alpha-SNAP is required for SNARE complex disassembly and exocytosis. *J Cell Biol*. 139:875-83.

Barria, A., and R. Malinow. 2005. NMDA receptor subunit composition controls synaptic plasticity by regulating binding to CaMKII. *Neuron*. 48:289-301.

Beites, C.L., K.A. Campbell, and W.S. Trimble. 2005. The septin Sept5/CDCrel-1 competes with alpha-SNAP for binding to the SNARE complex. *Biochem J*. 385:347-53.

Beites, C.L., H. Xie, R. Bowser, and W.S. Trimble. 1999. The septin CDCrel-1 binds syntaxin and inhibits exocytosis. *Nat Neurosci*. 2:434-9.

Bezakova, G., J.P. Helm, M. Francolini, and T. Lomo. 2001. Effects of purified recombinant neural and muscle agrin on skeletal muscle fibers in vivo. *J Cell Biol*. 153:1441-52.

Boison, D. 2005. Adenosine and epilepsy: from therapeutic rationale to new therapeutic strategies. *Neuroscientist*. 11:25-36.

Boison, D. 2006. Adenosine kinase, epilepsy and stroke: mechanisms and therapies. *Trends Pharmacol Sci*. 27:652-8.

Bose, C.M., D. Qiu, A. Bergamaschi, B. Gravante, M. Bossi, A. Villa, F. Rupp, and A. Malgaroli. 2000. Agrin controls synaptic differentiation in hippocampal neurons. *J Neurosci*. 20:9086-95.

Bowe, M.A., K.A. Deyst, J.D. Leszyk, and J.R. Fallon. 1994. Identification and purification of an agrin receptor from Torpedo postsynaptic membranes: a heteromeric complex related to the dystroglycans. *Neuron*. 12:1173-80.

Brass, L.F., S. Pizarro, M. Ahuja, E. Belmonte, N. Blanchard, J.M. Stadel, and J.A. Hoxie. 1994. Changes in the structure and function of the human thrombin receptor during receptor activation, internalization, and recycling. *J Biol Chem*. 269:2943-52.

Braun, M.C., L. Li, B. Ke, W.P. Dubinsky, M.C. Pickering, and J.Y. Chang. 2006. Proteomic profiling of urinary protein excretion in the factor H-deficient mouse. *Am J Nephrol*. 26:127-35.

Brown, J.L., L. Stowers, M. Baer, J. Trejo, S. Coughlin, and J. Chant. 1996. Human Ste20 homologue hPAK1 links GTPases to the JNK MAP kinase pathway. *Curr Biol*. 6:598-605.

Brunner, E., C.H. Ahrens, S. Mohanty, H. Baetschmann, S. Loevenich, F. Potthast, E.W. Deutsch, C. Panse, U. de Lichtenberg, O. Rinner, H. Lee, P.G. Pedrioli, J. Malmstrom, K. Koehler, S. Schrimpf, J. Krijgsveld, F. Kregenow, A.J. Heck, E. Hafen, R. Schlapbach, and R. Aebersold. 2007. A high-quality catalog of the Drosophila melanogaster proteome. *Nat Biotechnol*. 25:576-83.

Burgess, R.W., Q.T. Nguyen, Y.J. Son, J.W. Lichtman, and J.R. Sanes. 1999. Alternatively spliced isoforms of nerve- and muscle-derived agrin: their roles at the neuromuscular

junction. *Neuron*. 23:33-44.
Burgess, R.W., W.C. Skarnes, and J.R. Sanes. 2000. Agrin isoforms with distinct amino termini: differential expression, localization, and function. *J Cell Biol*. 151:41-52.
Campanelli, J.T., S.L. Roberds, K.P. Campbell, and R.H. Scheller. 1994. A role for dystrophin-associated glycoproteins and utrophin in agrin-induced AChR clustering. *Cell*. 77:663-74.
Caroni, P. 1997. Overexpression of growth-associated proteins in the neurons of adult transgenic mice. *J Neurosci Methods*. 71:3-9.
Centonze, D., M. Napolitano, E. Saulle, P. Gubellini, B. Picconi, A. Martorana, A. Pisani, A. Gulino, G. Bernardi, and P. Calabresi. 2002. Tissue plasminogen activator is required for corticostriatal long-term potentiation. *Eur J Neurosci*. 16:713-21.
Chen, Z.L., and S. Strickland. 1997. Neuronal death in the hippocampus is promoted by plasmin-catalyzed degradation of laminin. *Cell*. 91:917-25.
Chen, Z.L., S. Yoshida, K. Kato, Y. Momota, J. Suzuki, T. Tanaka, J. Ito, H. Nishino, S. Aimoto, H. Kiyama, and et al. 1995. Expression and activity-dependent changes of a novel limbic-serine protease gene in the hippocampus. *J Neurosci*. 15:5088-97.
Cheng, D., C.C. Hoogenraad, J. Rush, E. Ramm, M.A. Schlager, D.M. Duong, P. Xu, S.R. Wijayawardana, J. Hanfelt, T. Nakagawa, M. Sheng, and J. Peng. 2006. Relative and absolute quantification of postsynaptic density proteome isolated from rat forebrain and cerebellum. *Mol Cell Proteomics*. 5:1158-70.
Chu, Z., and J.J. Hablitz. 2000. Quisqualate induces an inward current via mGluR activation in neocortical pyramidal neurons. *Brain Res*. 879:88-92.
Cohen, N.R., J.S. Taylor, L.B. Scott, R.W. Guillery, P. Soriano, and A.J. Furley. 1998. Errors in corticospinal axon guidance in mice lacking the neural cell adhesion molecule L1. *Curr Biol*. 8:26-33.
Comisarow, M.B., and A.G. Marshall. 1996. The early development of Fourier transform ion cyclotron resonance (FT-ICR) spectroscopy. *J Mass Spectrom*. 31:581-5.
Conrads, T.P., H.J. Issaq, and T.D. Veenstra. 2002. New tools for quantitative phosphoproteome analysis. *Biochem Biophys Res Commun*. 290:885-90.
Cote, P.D., H. Moukhles, M. Lindenbaum, and S. Carbonetto. 1999. Chimaeric mice deficient in dystroglycans develop muscular dystrophy and have disrupted myoneural synapses. *Nat Genet*. 23:338-42.
Cuthbert, P.C., L.E. Stanford, M.P. Coba, J.A. Ainge, A.E. Fink, P. Opazo, J.Y. Delgado, N.H. Komiyama, T.J. O'Dell, and S.G. Grant. 2007. Synapse-associated protein 102/dlgh3 couples the NMDA receptor to specific plasticity pathways and learning strategies. *J Neurosci*. 27:2673-82.
D'Adamo, P., A. Menegon, C. Lo Nigro, M. Grasso, M. Gulisano, F. Tamanini, T. Bienvenu, A.K. Gedeon, B. Oostra, S.K. Wu, A. Tandon, F. Valtorta, W.E. Balch, J. Chelly, and D. Toniolo. 1998. Mutations in GDI1 are responsible for X-linked non-specific mental retardation. *Nat Genet*. 19:134-9.
Davey, F., M. Hill, J. Falk, N. Sans, and F.J. Gunn-Moore. 2005. Synapse associated protein 102 is a novel binding partner to the cytoplasmic terminus of neurone-glial related cell adhesion molecule. *J Neurochem*. 94:1243-53.
Davies, B., I.R. Kearns, J. Ure, C.H. Davies, and R. Lathe. 2001. Loss of hippocampal serine protease BSP1/neuropsin predisposes to global seizure activity. *J Neurosci*. 21:6993-7000.
Davis-Salinas, J., S.M. Saporito-Irwin, F.M. Donovan, D.D. Cunningham, and W.E. Van Nostrand. 1994. Thrombin receptor activation induces secretion and nonamyloidogenic processing of amyloid beta-protein precursor. *J Biol Chem*. 269:22623-7.
DeChiara, T.M., D.C. Bowen, D.M. Valenzuela, M.V. Simmons, W.T. Poueymirou, S. Thomas, E. Kinetz, D.L. Compton, E. Rojas, J.S. Park, C. Smith, P.S. DiStefano, D.J. Glass, S.J. Burden, and G.D. Yancopoulos. 1996. The receptor tyrosine kinase MuSK is required for neuromuscular junction formation in vivo. *Cell*. 85:501-12.
DeGregorio-Rocasolano, N., T. Gasull, and R. Trullas. 2001. Overexpression of neuronal pentraxin 1 is involved in neuronal death evoked by low K(+) in cerebellar granule cells. *J Biol Chem*. 276:796-803.
del Zoppo, G.J., S. Wagner, and M. Tagaya. 1997. Trends and future developments in the pharmacological treatment of acute ischaemic stroke. *Drugs*. 54:9-38.
Dihanich, M., M. Kaser, E. Reinhard, D. Cunningham, and D. Monard. 1991. Prothrombin mRNA

is expressed by cells of the nervous system. *Neuron*. 6:575-81.

Dirks, P., U. Thomas, and D. Montag. 2006. The cytoplasmic domain of NrCAM binds to PDZ domains of synapse-associated proteins SAP90/PSD95 and SAP97. *Eur J Neurosci*. 24:25-31.

Dong, Y.N., E.A. Waxman, and D.R. Lynch. 2004. Interactions of postsynaptic density-95 and the NMDA receptor 2 subunit control calpain-mediated cleavage of the NMDA receptor. *J Neurosci*. 24:11035-45.

Dong, Z., B. Ferger, J.C. Paterna, D. Vogel, S. Furler, M. Osinde, J. Feldon, and H. Bueler. 2003. Dopamine-dependent neurodegeneration in rats induced by viral vector-mediated overexpression of the parkin target protein, CDCrel-1. *Proc Natl Acad Sci U S A*. 100:12438-43.

Donovan, F.M., and D.D. Cunningham. 1998. Signaling pathways involved in thrombin-induced cell protection. *J Biol Chem*. 273:12746-52.

Donovan, F.M., C.J. Pike, C.W. Cotman, and D.D. Cunningham. 1997. Thrombin induces apoptosis in cultured neurons and astrocytes via a pathway requiring tyrosine kinase and RhoA activities. *J Neurosci*. 17:5316-26.

Dulubova, I., M. Khvotchev, S. Liu, I. Huryeva, T.C. Sudhof, and J. Rizo. 2007. Munc18-1 binds directly to the neuronal SNARE complex. *Proc Natl Acad Sci U S A*. 104:2697-702.

Ehrenreich, H., T. Costa, K.A. Clouse, R.M. Pluta, Y. Ogino, J.E. Coligan, and P.R. Burd. 1993. Thrombin is a regulator of astrocytic endothelin-1. *Brain Res*. 600:201-7.

Eid, T., M.J. Thomas, D.D. Spencer, E. Runden-Pran, J.C. Lai, G.V. Malthankar, J.H. Kim, N.C. Danbolt, O.P. Ottersen, and N.C. de Lanerolle. 2004. Loss of glutamine synthetase in the human epileptogenic hippocampus: possible mechanism for raised extracellular glutamate in mesial temporal lobe epilepsy. *Lancet*. 363:28-37.

Endoh, T. 2004. Characterization of modulatory effects of postsynaptic metabotropic glutamate receptors on calcium currents in rat nucleus tractus solitarius. *Brain Res*. 1024:212-24.

Eng, J.K., A.L. McCormack, and J.R.I. Yates. 1994. An approach to correlate tandem mass spectral data of peptides with amino acid sequences in a protein database. *J. Am Soc Mass Spectrom*. 5:976 - 989.

Fenn, J.B., M. Mann, C.K. Meng, S.F. Wong, and C.M. Whitehouse. 1989. Electrospray ionization for mass spectrometry of large biomolecules. *Science*. 246:64-71.

Fernandez-Monreal, M., J.P. Lopez-Atalaya, K. Benchenane, M. Cacquevel, F. Dulin, J.P. Le Caer, J. Rossier, A.C. Jarrige, E.T. Mackenzie, N. Colloc'h, C. Ali, and D. Vivien. 2004. Arginine 260 of the amino-terminal domain of NR1 subunit is critical for tissue-type plasminogen activator-mediated enhancement of N-methyl-D-aspartate receptor signaling. *J Biol Chem*. 279:50850-6.

Ferreira, A. 1999. Abnormal synapse formation in agrin-depleted hippocampal neurons. *J Cell Sci*. 112 (Pt 24):4729-38.

Friocourt, G., P. Chafey, P. Billuart, A. Koulakoff, M.C. Vinet, B.T. Schaar, S.K. McConnell, F. Francis, and J. Chelly. 2001. Doublecortin interacts with mu subunits of clathrin adaptor complexes in the developing nervous system. *Mol Cell Neurosci*. 18:307-19.

Gardoni, F., F. Polli, F. Cattabeni, and M. Di Luca. 2006. Calcium-calmodulin-dependent protein kinase II phosphorylation modulates PSD-95 binding to NMDA receptors. *Eur J Neurosci*. 24:2694-704.

Gautam, M., P.G. Noakes, L. Moscoso, F. Rupp, R.H. Scheller, J.P. Merlie, and J.R. Sanes. 1996. Defective neuromuscular synaptogenesis in agrin-deficient mutant mice. *Cell*. 85:525-35.

Gebbink, M.F., O. Kranenburg, M. Poland, F.P. van Horck, B. Houssa, and W.H. Moolenaar. 1997. Identification of a novel, putative Rho-specific GDP/GTP exchange factor and a RhoA-binding protein: control of neuronal morphology. *J Cell Biol*. 137:1603-13.

Gee, S.H., F. Montanaro, M.H. Lindenbaum, and S. Carbonetto. 1994. Dystroglycan-alpha, a dystrophin-associated glycoprotein, is a functional agrin receptor. *Cell*. 77:675-86.

Gesemann, M., V. Cavalli, A.J. Denzer, A. Brancaccio, B. Schumacher, and M.A. Ruegg. 1996. Alternative splicing of agrin alters its binding to heparin, dystroglycan, and the putative agrin receptor. *Neuron*. 16:755-67.

Gesemann, M., A.J. Denzer, and M.A. Ruegg. 1995. Acetylcholine receptor-aggregating activity of agrin isoforms and mapping of the active site. *J Cell Biol*. 128:625-36.

Gingras, J., and M. Ferns. 2001. Expression and localization of agrin during sympathetic synapse formation in vitro. *J Neurobiol*. 48:228-42.

Gingras, J., S. Rassadi, E. Cooper, and M. Ferns. 2002. Agrin plays an organizing role in the formation of sympathetic synapses. *J Cell Biol*. 158:1109-18.

Gingrich, M.B., C.E. Junge, P. Lyuboslavsky, and S.F. Traynelis. 2000. Potentiation of NMDA receptor function by the serine protease thrombin. *J Neurosci*. 20:4582-95.

Glass, D.J., D.C. Bowen, T.N. Stitt, C. Radziejewski, J. Bruno, T.E. Ryan, D.R. Gies, S. Shah, K. Mattsson, S.J. Burden, P.S. DiStefano, D.M. Valenzuela, T.M. DeChiara, and G.D. Yancopoulos. 1996. Agrin acts via a MuSK receptor complex. *Cell*. 85:513-23.

Gleeson, J.G., P.T. Lin, L.A. Flanagan, and C.A. Walsh. 1999. Doublecortin is a microtubule-associated protein and is expressed widely by migrating neurons. *Neuron*. 23:257-71.

Goretzki, L., C.R. Lombardo, and W.B. Stallcup. 2000. Binding of the NG2 proteoglycan to kringle domains modulates the functional properties of angiostatin and plasmin(ogen). *J Biol Chem*. 275:28625-33.

Gouder, N., L. Scheurer, J.M. Fritschy, and D. Boison. 2004. Overexpression of adenosine kinase in epileptic hippocampus contributes to epileptogenesis. *J Neurosci*. 24:692-701.

Grabham, P., and D.D. Cunningham. 1995. Thrombin receptor activation stimulates astrocyte proliferation and reversal of stellation by distinct pathways: involvement of tyrosine phosphorylation. *J Neurochem*. 64:583-91.

Grabs, D., V.I. Slepnev, Z. Songyang, C. David, M. Lynch, L.C. Cantley, and P. De Camilli. 1997. The SH3 domain of amphiphysin binds the proline-rich domain of dynamin at a single site that defines a new SH3 binding consensus sequence. *J Biol Chem*. 272:13419-25.

Grady, R.M., H. Zhou, J.M. Cunningham, M.D. Henry, K.P. Campbell, and J.R. Sanes. 2000. Maturation and maintenance of the neuromuscular synapse: genetic evidence for roles of the dystrophin--glycoprotein complex. *Neuron*. 25:279-93.

Graf, L., A. Jancso, L. Szilagyi, G. Hegyi, K. Pinter, G. Naray-Szabo, J. Hepp, K. Medzihradszky, and W.J. Rutter. 1988. Electrostatic complementarity within the substrate-binding pocket of trypsin. *Proc Natl Acad Sci U S A*. 85:4961-5.

Greenbaum, D., K.F. Medzihradszky, A. Burlingame, and M. Bogyo. 2000. Epoxide electrophiles as activity-dependent cysteine protease profiling and discovery tools. *Chem Biol*. 7:569-81.

Grossman, R., L.E. Fox, R. Gorovits, I. Ben-Dror, S. Reisfeld, and L. Vardimon. 1994. Molecular basis for differential expression of glutamine synthetase in retina glia and neurons. *Brain Res Mol Brain Res*. 21:312-20.

Gschwend, T.P., S.R. Krueger, S.V. Kozlov, D.P. Wolfer, and P. Sonderegger. 1997. Neurotrypsin, a novel multidomain serine protease expressed in the nervous system. *Mol Cell Neurosci*. 9:207-19.

Gualandris, A., T.E. Jones, S. Strickland, and S.E. Tsirka. 1996. Membrane depolarization induces calcium-dependent secretion of tissue plasminogen activator. *J Neurosci*. 16:2220-5.

Guttmann, R.P., D.L. Baker, K.M. Seifert, A.S. Cohen, D.A. Coulter, and D.R. Lynch. 2001. Specific proteolysis of the NR2 subunit at multiple sites by calpain. *J Neurochem*. 78:1083-93.

Gygi, S.P., D.K. Han, A.C. Gingras, N. Sonenberg, and R. Aebersold. 1999a. Protein analysis by mass spectrometry and sequence database searching: tools for cancer research in the post-genomic era. *Electrophoresis*. 20:310-9.

Gygi, S.P., B. Rist, S.A. Gerber, F. Turecek, M.H. Gelb, and R. Aebersold. 1999b. Quantitative analysis of complex protein mixtures using isotope-coded affinity tags. *Nat Biotechnol*. 17:994-9.

Gygi, S.P., Y. Rochon, B.R. Franza, and R. Aebersold. 1999c. Correlation between protein and mRNA abundance in yeast. *Mol Cell Biol*. 19:1720-30.

Haberle, J., B. Gorg, F. Rutsch, E. Schmidt, A. Toutain, J.F. Benoist, A. Gelot, A.L. Suc, W. Hohne, F. Schliess, D. Haussinger, and H.G. Koch. 2005. Congenital glutamine deficiency with glutamine synthetase mutations. *N Engl J Med*. 353:1926-33.

Hacke, W., M. Kaste, C. Fieschi, D. Toni, E. Lesaffre, R. von Kummer, G. Boysen, E. Bluhmki, G. Hoxter, M.H. Mahagne, and et al. 1995. Intravenous thrombolysis with recombinant tissue plasminogen activator for acute hemispheric stroke. The European Cooperative Acute Stroke Study (ECASS). *Jama*. 274:1017-25.

Han, D.K., J. Eng, H. Zhou, and R. Aebersold. 2001. Quantitative profiling of differentiation-induced microsomal proteins using isotope-coded affinity tags and mass spectrometry. *Nat Biotechnol*. 19:946-51.

Hedstrom, L. 1996. Trypsin: a case study in the structural determinants of enzyme specificity. *Biol Chem*. 377:465-70.

Hedstrom, L. 2002. Serine protease mechanism and specificity. *Chem Rev*. 102:4501-24.

Hedstrom, L., L. Szilagyi, and W.J. Rutter. 1992. Converting trypsin to chymotrypsin: the role of surface loops. *Science*. 255:1249-53.

Herbst, R., E. Avetisova, and S.J. Burden. 2002. Restoration of synapse formation in Musk mutant mice expressing a Musk/Trk chimeric receptor. *Development*. 129:5449-60.

Hilgenberg, L.G., C.L. Hoover, and M.A. Smith. 1999. Evidence of an agrin receptor in cortical neurons. *J Neurosci*. 19:7384-93.

Hilgenberg, L.G., and M.A. Smith. 2004. Agrin signaling in cortical neurons is mediated by a tyrosine kinase-dependent increase in intracellular Ca2+ that engages both CaMKII and MAPK signal pathways. *J Neurobiol*. 61:289-300.

Hilgenberg, L.G., H. Su, H. Gu, D.K. O'Dowd, and M.A. Smith. 2006. Alpha3Na+/K+-ATPase is a neuronal receptor for agrin. *Cell*. 125:359-69.

Hollenberg, M.D., and S.J. Compton. 2002. International Union of Pharmacology. XXVIII. Proteinase-activated receptors. *Pharmacol Rev*. 54:203-17.

Hopf, C., and W. Hoch. 1996. Agrin binding to alpha-dystroglycan. Domains of agrin necessary to induce acetylcholine receptor clustering are overlapping but not identical to the alpha-dystroglycan-binding region. *J Biol Chem*. 271:5231-6.

Hrabetova, S., and T.C. Sacktor. 1996. Bidirectional regulation of protein kinase M zeta in the maintenance of long-term potentiation and long-term depression. *J Neurosci*. 16:5324-33.

Huang, C.C., J.L. You, M.Y. Wu, and K.S. Hsu. 2004. Rap1-induced p38 mitogen-activated protein kinase activation facilitates AMPA receptor trafficking via the GDI.Rab5 complex. Potential role in (S)-3,5-dihydroxyphenylglycene-induced long term depression. *J Biol Chem*. 279:12286-92.

Huang, Y.Y., M.E. Bach, H.P. Lipp, M. Zhuo, D.P. Wolfer, R.D. Hawkins, L. Schoonjans, E.R. Kandel, J.M. Godfraind, R. Mulligan, D. Collen, and P. Carmeliet. 1996. Mice lacking the gene encoding tissue-type plasminogen activator show a selective interference with late-phase long-term potentiation in both Schaffer collateral and mossy fiber pathways. *Proc Natl Acad Sci U S A*. 93:8699-704.

Husi, H., M.A. Ward, J.S. Choudhary, W.P. Blackstock, and S.G. Grant. 2000. Proteomic analysis of NMDA receptor-adhesion protein signaling complexes. *Nat Neurosci*. 3:661-9.

Ip, F.C., D.G. Glass, D.R. Gies, J. Cheung, K.O. Lai, A.K. Fu, G.D. Yancopoulos, and N.Y. Ip. 2000. Cloning and characterization of muscle-specific kinase in chicken. *Mol Cell Neurosci*. 16:661-73.

Ishii, K., J. Chen, M. Ishii, W.J. Koch, N.J. Freedman, R.J. Lefkowitz, and S.R. Coughlin. 1994. Inhibition of thrombin receptor signaling by a G-protein coupled receptor kinase. Functional specificity among G-protein coupled receptor kinases. *J Biol Chem*. 269:1125-30.

Itoh, T., K. Kaibuchi, T. Masuda, T. Yamamoto, Y. Matsuura, A. Maeda, K. Shimizu, and Y. Takai. 1993. A protein factor for ras p21-dependent activation of mitogen-activated protein (MAP) kinase through MAP kinase kinase. *Proc Natl Acad Sci U S A*. 90:975-9.

Jacobson, C., P.D. Cote, S.G. Rossi, R.L. Rotundo, and S. Carbonetto. 2001. The dystroglycan complex is necessary for stabilization of acetylcholine receptor clusters at neuromuscular junctions and formation of the synaptic basement membrane. *J Cell Biol*. 152:435-50.

Jalink, K., and W.H. Moolenaar. 1992. Thrombin receptor activation causes rapid neural cell rounding and neurite retraction independent of classic second messengers. *J Cell Biol*. 118:411-9.

Johnson, R.S., S.A. Martin, K. Biemann, J.T. Stults, and J.T. Watson. 1987. Novel fragmentation process of peptides by collision-induced decomposition in a tandem mass spectrometer: differentiation of leucine and isoleucine. *Anal Chem*. 59:2621-5.

Jones, G., T. Meier, M. Lichtsteiner, V. Witzemann, B. Sakmann, and H.R. Brenner. 1997. Induction by agrin of ectopic and functional postsynaptic-like membrane in innervated muscle. *Proc Natl Acad Sci U S A*. 94:2654-9.

Karas, M., and F. Hillenkamp. 1988. Laser desorption ionization of proteins with molecular masses exceeding 10,000 daltons. *Anal Chem*. 60:2299-301.

Katz, B.A., R. Mackman, C. Luong, K. Radika, A. Martelli, P.A. Sprengeler, J. Wang, H. Chan, and L. Wong. 2000. Structural basis for selectivity of a small molecule, S1-binding, submicromolar inhibitor of urokinase-type plasminogen activator. *Chem Biol*. 7:299-312.

Keller, A., A.I. Nesvizhskii, E. Kolker, and R. Aebersold. 2002. Empirical statistical model to estimate the accuracy of peptide identifications made by MS/MS and database search. *Anal Chem*. 74:5383-92.

Kinder, D.H., M.S. Berger, B.A. Mueller, and J.R. Silber. 1993. Urokinase plasminogen activator is elevated in human astrocytic gliomas relative to normal adjacent brain. *Oncol Res*. 5:409-14.

Kingston, I.B., M.J. Castro, and S. Anderson. 1995. In vitro stimulation of tissue-type plasminogen activator by Alzheimer amyloid beta-peptide analogues. *Nat Med*. 1:138-42.

Koenig, J.H., and K. Ikeda. 1989. Disappearance and reformation of synaptic vesicle membrane upon transmitter release observed under reversible blockage of membrane retrieval. *J Neurosci*. 9:3844-60.

Komai, S., T. Matsuyama, K. Matsumoto, K. Kato, M. Kobayashi, K. Imamura, S. Yoshida, S. Ugawa, and S. Shiosaka. 2000. Neuropsin regulates an early phase of schaffer-collateral long-term potentiation in the murine hippocampus. *Eur J Neurosci*. 12:1479-86.

Kosenko, E., M. Llansola, C. Montoliu, P. Monfort, R. Rodrigo, M. Hernandez-Viadel, S. Erceg, A.M. Sanchez-Perez, and V. Felipo. 2003. Glutamine synthetase activity and glutamine content in brain: modulation by NMDA receptors and nitric oxide. *Neurochem Int*. 43:493-9.

Kvajo, M., H. Albrecht, M. Meins, U. Hengst, E. Troncoso, S. Lefort, J.Z. Kiss, C.C. Petersen, and D. Monard. 2004. Regulation of brain proteolytic activity is necessary for the in vivo function of NMDA receptors. *J Neurosci*. 24:9734-43.

Laake, J.H., T.A. Slyngstad, F.M. Haug, and O.P. Ottersen. 1995. Glutamine from glial cells is essential for the maintenance of the nerve terminal pool of glutamate: immunogold evidence from hippocampal slice cultures. *J Neurochem*. 65:871-81.

Laemmli, U.K. 1970. Cleavage of structural proteins during the assembly of the head of bacteriophage T4. *Nature*. 227:680-5.

Lamanda, A., A. Zahn, D. Roder, and H. Langen. 2004. Improved Ruthenium II tris (bathophenantroline disulfonate) staining and destaining protocol for a better signal-to-background ratio and improved baseline resolution. *Proteomics*. 4:599-608.

Landau, B.J., H.C. Kwaan, E.N. Verrusio, and S.S. Brem. 1994. Elevated levels of urokinase-type plasminogen activator and plasminogen activator inhibitor type-1 in malignant human brain tumors. *Cancer Res*. 54:1105-8.

Ledesma, M.D., J.S. Da Silva, K. Crassaerts, A. Delacourte, B. De Strooper, and C.G. Dotti. 2000. Brain plasmin enhances APP alpha-cleavage and Abeta degradation and is reduced in Alzheimer's disease brains. *EMBO Rep*. 1:530-5.

Lee, S.H., L. Liu, Y.T. Wang, and M. Sheng. 2002. Clathrin adaptor AP2 and NSF interact with overlapping sites of GluR2 and play distinct roles in AMPA receptor trafficking and hippocampal LTD. *Neuron*. 36:661-74.

Levicar, N., R.K. Nuttall, and T.T. Lah. 2003. Proteases in brain tumour progression. *Acta Neurochir (Wien)*. 145:825-38.

Li, X.J., H. Zhang, J.A. Ranish, and R. Aebersold. 2003. Automated statistical analysis of protein abundance ratios from data generated by stable-isotope dilution and tandem mass spectrometry. *Anal Chem*. 75:6648-57.

Li, Z., L.G. Hilgenberg, D.K. O'Dowd, and M.A. Smith. 1999. Formation of functional synaptic connections between cultured cortical neurons from agrin-deficient mice. *J*

Neurobiol. 39:547-57.

Lijnen, H.R. 2001. Plasmin and matrix metalloproteinases in vascular remodeling. *Thromb Haemost*. 86:324-33.

Lin, C.L., L.A. Bristol, L. Jin, M. Dykes-Hoberg, T. Crawford, L. Clawson, and J.D. Rothstein. 1998. Aberrant RNA processing in a neurodegenerative disease: the cause for absent EAAT2, a glutamate transporter, in amyotrophic lateral sclerosis. *Neuron*. 20:589-602.

Link, A.J., J. Eng, D.M. Schieltz, E. Carmack, G.J. Mize, D.R. Morris, B.M. Garvik, and J.R. Yates, 3rd. 1999. Direct analysis of protein complexes using mass spectrometry. *Nat Biotechnol*. 17:676-82.

Link, A.J., L.G. Hays, E.B. Carmack, and J.R. Yates, 3rd. 1997. Identifying the major proteome components of Haemophilus influenzae type-strain NCTC 8143. *Electrophoresis*. 18:1314-34.

Liot, G., K. Benchenane, F. Leveille, J.P. Lopez-Atalaya, M. Fernandez-Monreal, A. Ruocco, E.T. Mackenzie, A. Buisson, C. Ali, and D. Vivien. 2004. 2,7-Bis-(4-amidinobenzylidene)-cycloheptan-1-one dihydrochloride, tPA stop, prevents tPA-enhanced excitotoxicity both in vitro and in vivo. *J Cereb Blood Flow Metab*. 24:1153-9.

Liu, D., T. Cheng, H. Guo, J.A. Fernandez, J.H. Griffin, X. Song, and B.V. Zlokovic. 2004. Tissue plasminogen activator neurovascular toxicity is controlled by activated protein C. *Nat Med*. 10:1379-83.

Liu, Y., J. Dore, and X. Chen. 2007. Calcium influx through L-type channels generates protein kinase M to induce burst firing of dopamine cells in the rat ventral tegmental area. *J Biol Chem*.

Liu, Y., M.P. Patricelli, and B.F. Cravatt. 1999. Activity-based protein profiling: the serine hydrolases. *Proc Natl Acad Sci U S A*. 96:14694-9.

Lu, X., M. Wyszynski, M. Sheng, and M. Baudry. 2001. Proteolysis of glutamate receptor-interacting protein by calpain in rat brain: implications for synaptic plasticity. *J Neurochem*. 77:1553-60.

Lynch, G., and M. Baudry. 1984. The biochemistry of memory: a new and specific hypothesis. *Science*. 224:1057-63.

Macfarlane, S.R., M.J. Seatter, T. Kanke, G.D. Hunter, and R. Plevin. 2001. Proteinase-activated receptors. *Pharmacol Rev*. 53:245-82.

Majumdar, M., T.M. Seasholtz, D. Goldstein, P. de Lanerolle, and J.H. Brown. 1998. Requirement for Rho-mediated myosin light chain phosphorylation in thrombin-stimulated cell rounding and its dissociation from mitogenesis. *J Biol Chem*. 273:10099-106.

Makarova, A., I. Mikhailenko, T.H. Bugge, K. List, D.A. Lawrence, and D.K. Strickland. 2003. The low density lipoprotein receptor-related protein modulates protease activity in the brain by mediating the cellular internalization of both neuroserpin and neuroserpin-tissue-type plasminogen activator complexes. *J Biol Chem*. 278:50250-8.

March, R.E. 2000. Quadrupole ion trap mass spectrometry: a view at the turn of the century. *International Journal of Mass Spectrometry*. 200:285 - 312.

Marler, J.R., and L.B. Goldstein. 2003. Medicine. Stroke--tPA and the clinic. *Science*. 301:1677.

Masliah, E., M. Alford, R. DeTeresa, M. Mallory, and L. Hansen. 1996. Deficient glutamate transport is associated with neurodegeneration in Alzheimer's disease. *Ann Neurol*. 40:759-66.

Matsumoto-Miyai, K., A. Ninomiya, H. Yamasaki, H. Tamura, Y. Nakamura, and S. Shiosaka. 2003. NMDA-dependent proteolysis of presynaptic adhesion molecule L1 in the hippocampus by neuropsin. *J Neurosci*. 23:7727-36.

Matute, C., M. Melone, A. Vallejo-Illarramendi, and F. Conti. 2005. Increased expression of the astrocytic glutamate transporter GLT-1 in the prefrontal cortex of schizophrenics. *Glia*. 49:451-5.

Matys, T., and S. Strickland. 2003. Tissue plasminogen activator and NMDA receptor cleavage. *Nat Med*. 9:371-2; author reply 372-3.

Mawuenyega, K.G., H. Kaji, Y. Yamuchi, T. Shinkawa, H. Saito, M. Taoka, N. Takahashi, and T. Isobe. 2003. Large-scale identification of Caenorhabditis elegans proteins by multidimensional liquid chromatography-tandem mass spectrometry. *J Proteome Res*. 2:23-35.

May, P., A. Rohlmann, H.H. Bock, K. Zurhove, J.D. Marth, E.D. Schomburg, J.L. Noebels, U. Beffert, J.D. Sweatt, E.J. Weeber, and J. Herz. 2004. Neuronal LRP1 functionally associates with postsynaptic proteins and is required for normal motor function in mice. *Mol Cell Biol*. 24:8872-83.

McCroskery, S., A. Chaudhry, L. Lin, and M.P. Daniels. 2006. Transmembrane agrin regulates filopodia in rat hippocampal neurons in culture. *Mol Cell Neurosci*. 33:15-28.

McMahon, H.T., M. Missler, C. Li, and T.C. Sudhof. 1995. Complexins: cytosolic proteins that regulate SNAP receptor function. *Cell*. 83:111-9.

McMahon, H.T., P. Wigge, and C. Smith. 1997. Clathrin interacts specifically with amphiphysin and is displaced by dynamin. *FEBS Lett*. 413:319-22.

Mechtersheimer, S., P. Gutwein, N. Agmon-Levin, A. Stoeck, M. Oleszewski, S. Riedle, R. Postina, F. Fahrenholz, M. Fogel, V. Lemmon, and P. Altevogt. 2001. Ectodomain shedding of L1 adhesion molecule promotes cell migration by autocrine binding to integrins. *J Cell Biol*. 155:661-73.

Medina, M.G., M.D. Ledesma, J.E. Dominguez, M. Medina, D. Zafra, F. Alameda, C.G. Dotti, and P. Navarro. 2005. Tissue plasminogen activator mediates amyloid-induced neurotoxicity via Erk1/2 activation. *Embo J*. 24:1706-16.

Meiri, N., T. Masos, K. Rosenblum, R. Miskin, and Y. Dudai. 1994. Overexpression of urokinase-type plasminogen activator in transgenic mice is correlated with impaired learning. *Proc Natl Acad Sci U S A*. 91:3196-200.

Melchor, J.P., R. Pawlak, and S. Strickland. 2003. The tissue plasminogen activator-plasminogen proteolytic cascade accelerates amyloid-beta (Abeta) degradation and inhibits Abeta-induced neurodegeneration. *J Neurosci*. 23:8867-71.

Meng, Y., Y. Zhang, and Z. Jia. 2003. Synaptic transmission and plasticity in the absence of AMPA glutamate receptor GluR2 and GluR3. *Neuron*. 39:163-76.

Miki, H., S. Suetsugu, and T. Takenawa. 1998. WAVE, a novel WASP-family protein involved in actin reorganization induced by Rac. *Embo J*. 17:6932-41.

Mirgorodskaya, O.A., Y.P. Kozmin, M.I. Titov, R. Korner, C.P. Sonksen, and P. Roepstorff. 2000. Quantitation of peptides and proteins by matrix-assisted laser desorption/ionization mass spectrometry using (18)O-labeled internal standards. *Rapid Commun Mass Spectrom*. 14:1226-32.

Mohan, P.M., S.K. Chintala, S. Mohanam, C.L. Gladson, E.S. Kim, Z.L. Gokaslan, S.S. Lakka, J.A. Roth, B. Fang, R. Sawaya, A.P. Kyritsis, and J.S. Rao. 1999. Adenovirus-mediated delivery of antisense gene to urokinase-type plasminogen activator receptor suppresses glioma invasion and tumor growth. *Cancer Res*. 59:3369-73.

Mohanam, S., N. Chandrasekar, N. Yanamandra, S. Khawar, F. Mirza, D.H. Dinh, W.C. Olivero, and J.S. Rao. 2002. Modulation of invasive properties of human glioblastoma cells stably expressing amino-terminal fragment of urokinase-type plasminogen activator. *Oncogene*. 21:7824-30.

Mohanam, S., R.E. Sawaya, M. Yamamoto, J.M. Bruner, G.L. Nicholson, and J.S. Rao. 1994. Proteolysis and invasiveness of brain tumors: role of urokinase-type plasminogen activator receptor. *J Neurooncol*. 22:153-60.

Molinari, F., M. Rio, V. Meskenaite, F. Encha-Razavi, J. Auge, D. Bacq, S. Briault, M. Vekemans, A. Munnich, T. Attie-Bitach, P. Sonderegger, and L. Colleaux. 2002. Truncating neurotrypsin mutation in autosomal recessive nonsyndromic mental retardation. *Science*. 298:1779-81.

Moller, T., U.K. Hanisch, and B.R. Ransom. 2000. Thrombin-induced activation of cultured rodent microglia. *J Neurochem*. 75:1539-47.

Molloy, M.P., S. Donohoe, E.E. Brzezinski, G.W. Kilby, T.I. Stevenson, J.D. Baker, D.R. Goodlett, and D.A. Gage. 2005. Large-scale evaluation of quantitative reproducibility and proteome coverage using acid cleavable isotope coded affinity tag mass spectrometry for proteomic profiling. *Proteomics*. 5:1204-8.

Moron, J.A., N.S. Abul-Husn, R. Rozenfeld, G. Dolios, R. Wang, and L.A. Devi. 2007. Morphine administration alters the profile of hippocampal postsynaptic density-associated proteins: a proteomics study focusing on endocytic proteins. *Mol Cell Proteomics*. 6:29-42.

Moseley, A.E., M.T. Williams, T.L. Schaefer, C.S. Bohanan, J.C. Neumann, M.M. Behbehani, C.V. Vorhees, and J.B. Lingrel. 2007. Deficiency in Na,K-ATPase alpha isoform genes

alters spatial learning, motor activity, and anxiety in mice. *J Neurosci*. 27:616-26.
Munchbach, M., M. Quadroni, G. Miotto, and P. James. 2000. Quantitation and facilitated de novo sequencing of proteins by isotopic N-terminal labeling of peptides with a fragmentation-directing moiety. *Anal Chem*. 72:4047-57.
Nagai, T., K. Yamada, M. Yoshimura, K. Ishikawa, Y. Miyamoto, K. Hashimoto, Y. Noda, A. Nitta, and T. Nabeshima. 2004. The tissue plasminogen activator-plasmin system participates in the rewarding effect of morphine by regulating dopamine release. *Proc Natl Acad Sci U S A*. 101:3650-5.
Nakamura, H., Y. Fujii, I. Inoki, K. Sugimoto, K. Tanzawa, H. Matsuki, R. Miura, Y. Yamaguchi, and Y. Okada. 2000. Brevican is degraded by matrix metalloproteinases and aggrecanase-1 (ADAMTS4) at different sites. *J Biol Chem*. 275:38885-90.
Nakayama, T., T. Yaoi, and G. Kuwajima. 1999. Localization and subcellular distribution of N-copine in mouse brain. *J Neurochem*. 72:373-9.
Nakayama, T., T. Yaoi, M. Yasui, and G. Kuwajima. 1998. N-copine: a novel two C2-domain-containing protein with neuronal activity-regulated expression. *FEBS Lett*. 428:80-4.
Nesvizhskii, A.I., A. Keller, E. Kolker, and R. Aebersold. 2003. A statistical model for identifying proteins by tandem mass spectrometry. *Anal Chem*. 75:4646-58.
Nesvizhskii, A.I., F.F. Roos, J. Grossmann, M. Vogelzang, J.S. Eddes, W. Gruissem, S. Baginsky, and R. Aebersold. 2006. Dynamic spectrum quality assessment and iterative computational analysis of shotgun proteomic data: toward more efficient identification of post-translational modifications, sequence polymorphisms, and novel peptides. *Mol Cell Proteomics*. 5:652-70.
Neumann, F.R., G. Bittcher, M. Annies, B. Schumacher, S. Kroger, and M.A. Ruegg. 2001. An alternative amino-terminus expressed in the central nervous system converts agrin to a type II transmembrane protein. *Mol Cell Neurosci*. 17:208-25.
Neveu, I., F. Jehan, M. Jandrot-Perrus, D. Wion, and P. Brachet. 1993. Enhancement of the synthesis and secretion of nerve growth factor in primary cultures of glial cells by proteases: a possible involvement of thrombin. *J Neurochem*. 60:858-67.
Nicole, O., F. Docagne, C. Ali, I. Margaill, P. Carmeliet, E.T. MacKenzie, D. Vivien, and A. Buisson. 2001. The proteolytic activity of tissue-plasminogen activator enhances NMDA receptor-mediated signaling. *Nat Med*. 7:59-64.
Nitkin, R.M., M.A. Smith, C. Magill, J.R. Fallon, Y.M. Yao, B.G. Wallace, and U.J. McMahan. 1987. Identification of agrin, a synaptic organizing protein from Torpedo electric organ. *J Cell Biol*. 105:2471-8.
O'Connor, L.T., J.C. Lauterborn, C.M. Gall, and M.A. Smith. 1994. Localization and alternative splicing of agrin mRNA in adult rat brain: transcripts encoding isoforms that aggregate acetylcholine receptors are not restricted to cholinergic regions. *J Neurosci*. 14:1141-52.
Oda, Y., T. Nagasu, and B.T. Chait. 2001. Enrichment analysis of phosphorylated proteins as a tool for probing the phosphoproteome. *Nat Biotechnol*. 19:379-82.
Oka, T., T. Hakoshima, M. Itakura, S. Yamamori, M. Takahashi, Y. Hashimoto, S. Shiosaka, and K. Kato. 2002. Role of loop structures of neuropsin in the activity of serine protease and regulated secretion. *J Biol Chem*. 277:14724-30.
Ong, S.E., B. Blagoev, I. Kratchmarova, D.B. Kristensen, H. Steen, A. Pandey, and M. Mann. 2002. Stable isotope labeling by amino acids in cell culture, SILAC, as a simple and accurate approach to expression proteomics. *Mol Cell Proteomics*. 1:376-86.
Osten, P., S. Srivastava, G.J. Inman, F.S. Vilim, L. Khatri, L.M. Lee, B.A. States, S. Einheber, T.A. Milner, P.I. Hanson, and E.B. Ziff. 1998. The AMPA receptor GluR2 C terminus can mediate a reversible, ATP-dependent interaction with NSF and alpha- and beta-SNAPs. *Neuron*. 21:99-110.
Pabst, S., M. Margittai, D. Vainius, R. Langen, R. Jahn, and D. Fasshauer. 2002. Rapid and selective binding to the synaptic SNARE complex suggests a modulatory role of complexins in neuroexocytosis. *J Biol Chem*. 277:7838-48.
Pai, K.S., and D.D. Cunningham. 2002. Geldanamycin specifically modulates thrombin-mediated morphological changes in mouse neuroblasts. *J Neurochem*. 80:715-8.
Pai, K.S., V.B. Mahajan, A. Lau, and D.D. Cunningham. 2001. Thrombin receptor signaling to cytoskeleton requires Hsp90. *J Biol Chem*. 276:32642-7.

Palagi, P.M., D. Walther, M. Quadroni, S. Catherinet, J. Burgess, C.G. Zimmermann-Ivol, J.C. Sanchez, P.A. Binz, D.F. Hochstrasser, and R.D. Appel. 2005. MSight: an image analysis software for liquid chromatography-mass spectrometry. *Proteomics*. 5:2381-4.

Pan, S., D. Zhu, J.F. Quinn, E.R. Peskind, T.J. Montine, B. Lin, D.R. Goodlett, G. Taylor, J. Eng, and J. Zhang. 2007. A combined dataset of human cerebrospinal fluid proteins identified by multi-dimensional chromatography and tandem mass spectrometry. *Proteomics*. 7:469-73.

Parrini, M.C., M. Lei, S.C. Harrison, and B.J. Mayer. 2002. Pak1 kinase homodimers are autoinhibited in trans and dissociated upon activation by Cdc42 and Rac1. *Mol Cell*. 9:73-83.

Pawlak, R., J.P. Melchor, T. Matys, A.E. Skrzypiec, and S. Strickland. 2005a. Ethanol-withdrawal seizures are controlled by tissue plasminogen activator via modulation of NR2B-containing NMDA receptors. *Proc Natl Acad Sci U S A*. 102:443-8.

Pawlak, R., B.S. Rao, J.P. Melchor, S. Chattarji, B. McEwen, and S. Strickland. 2005b. Tissue plasminogen activator and plasminogen mediate stress-induced decline of neuronal and cognitive functions in the mouse hippocampus. *Proc Natl Acad Sci U S A*. 102:18201-6.

Peng, J., M.J. Kim, D. Cheng, D.M. Duong, S.P. Gygi, and M. Sheng. 2004. Semiquantitative proteomic analysis of rat forebrain postsynaptic density fractions by mass spectrometry. *J Biol Chem*. 279:21003-11.

Peng, X.R., Z. Jia, Y. Zhang, J. Ware, and W.S. Trimble. 2002. The septin CDCrel-1 is dispensable for normal development and neurotransmitter release. *Mol Cell Biol*. 22:378-87.

Perkins, D.N., D.J. Pappin, D.M. Creasy, and J.S. Cottrell. 1999. Probability-based protein identification by searching sequence databases using mass spectrometry data. *Electrophoresis*. 20:3551-67.

Proba, K., T.P. Gschwend, and P. Sonderegger. 1998. Cloning and sequencing of the cDNA encoding human neurotrypsin. *Biochim Biophys Acta*. 1396:143-7.

Prokai, L., A.D. Zharikova, and S.M. Stevens, Jr. 2005. Effect of chronic morphine exposure on the synaptic plasma-membrane subproteome of rats: a quantitative protein profiling study based on isotope-coded affinity tags and liquid chromatography/mass spectrometry. *J Mass Spectrom*. 40:169-75.

Qian, Z., M.E. Gilbert, M.A. Colicos, E.R. Kandel, and D. Kuhl. 1993. Tissue-plasminogen activator is induced as an immediate-early gene during seizure, kindling and long-term potentiation. *Nature*. 361:453-7.

Qiu, Z., K.A. Crutcher, B.T. Hyman, and G.W. Rebeck. 2003. ApoE isoforms affect neuronal N-methyl-D-aspartate calcium responses and toxicity via receptor-mediated processes. *Neuroscience*. 122:291-303.

Qualmann, B., and R.B. Kelly. 2000. Syndapin isoforms participate in receptor-mediated endocytosis and actin organization. *J Cell Biol*. 148:1047-62.

Radrizzani, M., H. Carminatti, O.H. Pivetta, and V.P. Idoyaga Vargas. 1995. Developmental regulation of Thy 1.2 rate of synthesis in the mouse cerebellum. *J Neurosci Res*. 42:220-7.

Ranish, J.A., E.C. Yi, D.M. Leslie, S.O. Purvine, D.R. Goodlett, J. Eng, and R. Aebersold. 2003. The study of macromolecular complexes by quantitative proteomics. *Nat Genet*. 33:349-55.

Rawlings, N.D., F.R. Morton, and A.J. Barrett. 2006. MEROPS: the peptidase database. *Nucleic Acids Res*. 34:D270-2.

Reif, R., S. Sales, S. Hettwer, B. Dreier, C. Giesler, J. Woelfel, D. Luescher, A. Zurlinden, A. Stephan, S. Ahmed, A. Baici, B. Ledermann, B. Kunz, P. Sonderegger. 2007 Specific cleavage of agrin by neurotrypsin, a synaptic protease linked to mental retardation. *FASEB J*.

Reuning, U., S. Sperl, C. Kopitz, H. Kessler, A. Kruger, M. Schmitt, and V. Magdolen. 2003. Urokinase-type plasminogen activator (uPA) and its receptor (uPAR): development of antagonists of uPA/uPAR interaction and their effects in vitro and in vivo. *Curr Pharm Des*. 9:1529-43.

Robles, E., S. Woo, and T.M. Gomez. 2005. Src-dependent tyrosine phosphorylation at the tips of growth cone filopodia promotes extension. *J Neurosci*. 25:7669-81.

Roepstorff, P., and J. Fohlman. 1984. Proposal for a common nomenclature for sequence ions in

mass spectra of peptides. *Biomed Mass Spectrom*. 11:601.
Roldan, A.L., M.V. Cubellis, M.T. Masucci, N. Behrendt, L.R. Lund, K. Dano, E. Appella, and F. Blasi. 1990. Cloning and expression of the receptor for human urokinase plasminogen activator, a central molecule in cell surface, plasmin dependent proteolysis. *Embo J*. 9:467-74.
Rothstein, J.D., M. Van Kammen, A.I. Levey, L.J. Martin, and R.W. Kuncl. 1995. Selective loss of glial glutamate transporter GLT-1 in amyotrophic lateral sclerosis. *Ann Neurol*. 38:73-84.
Roux, A., K. Uyhazi, A. Frost, and P. De Camilli. 2006. GTP-dependent twisting of dynamin implicates constriction and tension in membrane fission. *Nature*. 441:528-31.
Rydel, T.J., A. Tulinsky, W. Bode, and R. Huber. 1991. Refined structure of the hirudin-thrombin complex. *J Mol Biol*. 221:583-601.
Salles, F.J., and S. Strickland. 2002. Localization and regulation of the tissue plasminogen activator-plasmin system in the hippocampus. *J Neurosci*. 22:2125-34.
Samson, A.L., and R.L. Medcalf. 2006. Tissue-type plasminogen activator: a multifaceted modulator of neurotransmission and synaptic plasticity. *Neuron*. 50:673-8.
Sans, N., K. Prybylowski, R.S. Petralia, K. Chang, Y.X. Wang, C. Racca, S. Vicini, and R.J. Wenthold. 2003. NMDA receptor trafficking through an interaction between PDZ proteins and the exocyst complex. *Nat Cell Biol*. 5:520-30.
Schluter, O.M., J. Basu, T.C. Sudhof, and C. Rosenmund. 2006. Rab3 superprimes synaptic vesicles for release: implications for short-term synaptic plasticity. *J Neurosci*. 26:1239-46.
Schmidt, F., B. Dahlmann, K. Janek, A. Kloss, M. Wacker, R. Ackermann, B. Thiede, and P.R. Jungblut. 2006. Comprehensive quantitative proteome analysis of 20S proteasome subtypes from rat liver by isotope coded affinity tag and 2-D gel-based approaches. *Proteomics*. 6:4622-32.
Schmitt, M., N. Harbeck, C. Thomssen, O. Wilhelm, V. Magdolen, U. Reuning, K. Ulm, H. Hofler, F. Janicke, and H. Graeff. 1997. Clinical impact of the plasminogen activation system in tumor invasion and metastasis: prognostic relevance and target for therapy. *Thromb Haemost*. 78:285-96.
Schrimpf, S.P., V. Meskenaite, E. Brunner, D. Rutishauser, P. Walther, J. Eng, R. Aebersold, and P. Sonderegger. 2005. Proteomic analysis of synaptosomes using isotope-coded affinity tags and mass spectrometry. *Proteomics*. 5:2531-41.
Seeds, N.W., B.L. Williams, and P.C. Bickford. 1995. Tissue plasminogen activator induction in Purkinje neurons after cerebellar motor learning. *Science*. 270:1992-4.
Selkoe, D.J. 2001. Clearing the brain's amyloid cobwebs. *Neuron*. 32:177-80.
Serpinskaya, A.S., G. Feng, J.R. Sanes, and A.M. Craig. 1999. Synapse formation by hippocampal neurons from agrin-deficient mice. *Dev Biol*. 205:65-78.
Shimizu, C., S. Yoshida, M. Shibata, K. Kato, Y. Momota, K. Matsumoto, T. Shiosaka, R. Midorikawa, T. Kamachi, A. Kawabe, and S. Shiosaka. 1998. Characterization of recombinant and brain neuropsin, a plasticity-related serine protease. *J Biol Chem*. 273:11189-96.
Shimizu, S., M. Narita, and Y. Tsujimoto. 1999. Bcl-2 family proteins regulate the release of apoptogenic cytochrome c by the mitochondrial channel VDAC. *Nature*. 399:483-7.
Shull, G.E., J. Greeb, and J.B. Lingrel. 1986. Molecular cloning of three distinct forms of the Na+,K+-ATPase alpha-subunit from rat brain. *Biochemistry*. 25:8125-32.
Siconolfi, L.B., and N.W. Seeds. 2003. Mice lacking tissue plasminogen activator and urokinase plasminogen activator genes show attenuated matrix metalloproteases activity after sciatic nerve crush. *J Neurosci Res*. 74:430-4.
Singh, R.R., C. Song, Z. Yang, and R. Kumar. 2005. Nuclear localization and chromatin targets of p21-activated kinase 1. *J Biol Chem*. 280:18130-7.
Smirnova, I.V., S.X. Zhang, B.A. Citron, P.M. Arnold, and B.W. Festoff. 1998. Thrombin is an extracellular signal that activates intracellular death protease pathways inducing apoptosis in model motor neurons. *J Neurobiol*. 36:64-80.
Smolka, M.B., H. Zhou, S. Purkayastha, and R. Aebersold. 2001. Optimization of the isotope-coded affinity tag-labeling procedure for quantitative proteome analysis. *Anal Biochem*. 297:25-31.
Steitz, T.A., R. Henderson, and D.M. Blow. 1969. Structure of crystalline alpha-chymotrypsin. 3.

Crystallographic studies of substrates and inhibitors bound to the active site of alpha-chymotrypsin. *J Mol Biol*. 46:337-48.

Stevens, S.M., Jr., A.D. Zharikova, and L. Prokai. 2003. Proteomic analysis of the synaptic plasma membrane fraction isolated from rat forebrain. *Brain Res Mol Brain Res*. 117:116-28.

Striggow, F., M. Riek, J. Breder, P. Henrich-Noack, K.G. Reymann, and G. Reiser. 2000. The protease thrombin is an endogenous mediator of hippocampal neuroprotection against ischemia at low concentrations but causes degeneration at high concentrations. *Proc Natl Acad Sci U S A*. 97:2264-9.

Striggow, F., M. Riek-Burchardt, A. Kiesel, W. Schmidt, P. Henrich-Noack, J. Breder, M. Krug, K.G. Reymann, and G. Reiser. 2001. Four different types of protease-activated receptors are widely expressed in the brain and are up-regulated in hippocampus by severe ischemia. *Eur J Neurosci*. 14:595-608.

Sugiyama, J., D.C. Bowen, and Z.W. Hall. 1994. Dystroglycan binds nerve and muscle agrin. *Neuron*. 13:103-15.

Sundberg-Smith, L.J., J.T. Doherty, C.P. Mack, and J.M. Taylor. 2005. Adhesion stimulates direct PAK1/ERK2 association and leads to ERK-dependent PAK1 Thr212 phosphorylation. *J Biol Chem*. 280:2055-64.

Suo, Z., M. Wu, S. Ameenuddin, H.E. Anderson, J.E. Zoloty, B.A. Citron, P. Andrade-Gordon, and B.W. Festoff. 2002. Participation of protease-activated receptor-1 in thrombin-induced microglial activation. *J Neurochem*. 80:655-66.

Sweatt, J.D. 2004. Mitogen-activated protein kinases in synaptic plasticity and memory. *Curr Opin Neurobiol*. 14:311-7.

Syrovets, T., and T. Simmet. 2004. Novel aspects and new roles for the serine protease plasmin. *Cell Mol Life Sci*. 61:873-85.

Takeuchi, M., Y. Hata, K. Hirao, A. Toyoda, M. Irie, and Y. Takai. 1997. SAPAPs. A family of PSD-95/SAP90-associated proteins localized at postsynaptic density. *J Biol Chem*. 272:11943-51.

Tang, J., A. Maximov, O.H. Shin, H. Dai, J. Rizo, and T.C. Sudhof. 2006. A complexin/synaptotagmin 1 switch controls fast synaptic vesicle exocytosis. *Cell*. 126:1175-87.

Tarpey, P., J. Parnau, M. Blow, H. Woffendin, G. Bignell, C. Cox, J. Cox, H. Davies, S. Edkins, S. Holden, A. Korny, U. Mallya, J. Moon, S. O'Meara, A. Parker, P. Stephens, C. Stevens, J. Teague, A. Donnelly, M. Mangelsdorf, J. Mulley, M. Partington, G. Turner, R. Stevenson, C. Schwartz, I. Young, D. Easton, M. Bobrow, P.A. Futreal, M.R. Stratton, J. Gecz, R. Wooster, and F.L. Raymond. 2004. Mutations in the DLG3 gene cause nonsyndromic X-linked mental retardation. *Am J Hum Genet*. 75:318-24.

Thelen, K., V. Kedar, A.K. Panicker, R.S. Schmid, B.R. Midkiff, and P.F. Maness. 2002. The neural cell adhesion molecule L1 potentiates integrin-dependent cell migration to extracellular matrix proteins. *J Neurosci*. 22:4918-31.

Tian, L., H. Nyman, P. Kilgannon, Y. Yoshihara, K. Mori, L.C. Andersson, S. Kaukinen, H. Rauvala, W.M. Gallatin, and C.G. Gahmberg. 2000. Intercellular adhesion molecule-5 induces dendritic outgrowth by homophilic adhesion. *J Cell Biol*. 150:243-52.

Tomsig, J.L., S.L. Snyder, and C.E. Creutz. 2003. Identification of targets for calcium signaling through the copine family of proteins. Characterization of a coiled-coil copine-binding motif. *J Biol Chem*. 278:10048-54.

Troller, U., and C. Larsson. 2006. Cdc42 is involved in PKCepsilon- and delta-induced neurite outgrowth and stress fibre dismantling. *Biochem Biophys Res Commun*. 349:91-8.

Tsen, G., W. Halfter, S. Kroger, and G.J. Cole. 1995. Agrin is a heparan sulfate proteoglycan. *J Biol Chem*. 270:3392-9.

Tsirka, S.E., A. Gualandris, D.G. Amaral, and S. Strickland. 1995. Excitotoxin-induced neuronal degeneration and seizure are mediated by tissue plasminogen activator. *Nature*. 377:340-4.

Tsirka, S.E., A.D. Rogove, T.H. Bugge, J.L. Degen, and S. Strickland. 1997. An extracellular proteolytic cascade promotes neuronal degeneration in the mouse hippocampus. *J Neurosci*. 17:543-52.

Tucker, H.M., M. Kihiko, J.N. Caldwell, S. Wright, T. Kawarabayashi, D. Price, D. Walker, S. Scheff, J.P. McGillis, R.E. Rydel, and S. Estus. 2000. The plasmin system is induced by and

degrades amyloid-beta aggregates. *J Neurosci*. 20:3937-46.
Turnell, A.S., D.P. Brant, G.R. Brown, M. Finney, P.H. Gallimore, C.J. Kirk, T.R. Pagliuca, C.J. Campbell, R.H. Michell, and R.J. Grand. 1995. Regulation of neurite outgrowth from differentiated human neuroepithelial cells: a comparison of the activities of prothrombin and thrombin. *Biochem J*. 308 (Pt 3):965-73.
Turner AJ, B.M., Phelan P, Gordon-Weeks PR. 1997. Isolation of synaptosomes, growth cones, and their subcellular components. *Oxford Unversity Press*.
Tzarfaty-Majar, V., R. Lopez-Alemany, Y. Feinstein, L. Gombau, O. Goldshmidt, E. Soriano, P. Munoz-Canoves, and A. Klar. 2001. Plasmin-mediated release of the guidance molecule F-spondin from the extracellular matrix. *J Biol Chem*. 276:28233-41.
Ubl, J.J., and G. Reiser. 2000. A novel proteolytic mechanism for termination of the CA2+ signalling evoked by proteinase-activated receptor-1 (PAR-1) in rat astrocytes. *Adv Exp Med Biol*. 477:323-9.
Ubl, J.J., M. Sergeeva, and G. Reiser. 2000. Desensitisation of protease-activated receptor-1 (PAR-1) in rat astrocytes: evidence for a novel mechanism for terminating Ca2+ signalling evoked by the tethered ligand. *J Physiol*. 525 Pt 2:319-30.
Vajda, T., and T. Szabo. 1976. Specificity of trypsin and alpha-chymotrypsin towards neutral substrates. *Acta Biochim Biophys Acad Sci Hung*. 11:287-94.
Vassalli, J.D., A.P. Sappino, and D. Belin. 1991. The plasminogen activator/plasmin system. *J Clin Invest*. 88:1067-72.
Venekei, I., L. Szilagyi, L. Graf, and W.J. Rutter. 1996. Attempts to convert chymotrypsin to trypsin. *FEBS Lett*. 383:143-7.
Verhage, M., A.S. Maia, J.J. Plomp, A.B. Brussaard, J.H. Heeroma, H. Vermeer, R.F. Toonen, R.E. Hammer, T.K. van den Berg, M. Missler, H.J. Geuze, and T.C. Sudhof. 2000. Synaptic assembly of the brain in the absence of neurotransmitter secretion. *Science*. 287:864-9.
Viapiano, M.S., R.T. Matthews, and S. Hockfield. 2003. A novel membrane-associated glycovariant of BEHAB/brevican is up-regulated during rat brain development and in a rat model of invasive glioma. *J Biol Chem*. 278:33239-47.
Walikonis, R.S., O.N. Jensen, M. Mann, D.W. Provance, Jr., J.A. Mercer, and M.B. Kennedy. 2000. Identification of proteins in the postsynaptic density fraction by mass spectrometry. *J Neurosci*. 20:4069-80.
Wang, H., and G. Reiser. 2003. The role of the Ca2+-sensitive tyrosine kinase Pyk2 and Src in thrombin signalling in rat astrocytes. *J Neurochem*. 84:1349-57.
Wang, H., J.J. Ubl, and G. Reiser. 2002a. Four subtypes of protease-activated receptors, co-expressed in rat astrocytes, evoke different physiological signaling. *Glia*. 37:53-63.
Wang, H., J.J. Ubl, R. Stricker, and G. Reiser. 2002b. Thrombin (PAR-1)-induced proliferation in astrocytes via MAPK involves multiple signaling pathways. *Am J Physiol Cell Physiol*. 283:C1351-64.
Wang, Y., W. Luo, and G. Reiser. 2007. Proteinase-activated receptor-1 and -2 induce the release of chemokine GRO/CINC-1 from rat astrocytes via differential activation of JNK isoforms, evoking multiple protective pathways in brain. *Biochem J*. 401:65-78.
Wang, Y., W. Luo, R. Stricker, and G. Reiser. 2006. Protease-activated receptor-1 protects rat astrocytes from apoptotic cell death via JNK-mediated release of the chemokine GRO/CINC-1. *J Neurochem*. 98:1046-60.
Wang, Y.F., S.E. Tsirka, S. Strickland, P.E. Stieg, S.G. Soriano, and S.A. Lipton. 1998. Tissue plasminogen activator (tPA) increases neuronal damage after focal cerebral ischemia in wild-type and tPA-deficient mice. *Nat Med*. 4:228-31.
Wardlaw, J.M., C.P. Warlow, and C. Counsell. 1997. Systematic review of evidence on thrombolytic therapy for acute ischaemic stroke. *Lancet*. 350:607-14.
Washburn, M.P., D. Wolters, and J.R. Yates, 3rd. 2001. Large-scale analysis of the yeast proteome by multidimensional protein identification technology. *Nat Biotechnol*. 19:242-7.
Weeber, E.J., M. Levy, M.J. Sampson, K. Anflous, D.L. Armstrong, S.E. Brown, J.D. Sweatt, and W.J. Craigen. 2002. The role of mitochondrial porins and the permeability transition pore in learning and synaptic plasticity. *J Biol Chem*. 277:18891-7.
Whiteheart, S.W., I.C. Griff, M. Brunner, D.O. Clary, T. Mayer, S.A. Buhrow, and J.E. Rothman. 1993. SNAP family of NSF attachment proteins includes a brain-specific isoform.

Nature. 362:353-5.

Wigge, P., and H.T. McMahon. 1998. The amphiphysin family of proteins and their role in endocytosis at the synapse. *Trends Neurosci*. 21:339-44.

Witzmann, F.A., R.J. Arnold, F. Bai, P. Hrncirova, M.W. Kimpel, Y.S. Mechref, W.J. McBride, M.V. Novotny, N.M. Pedrick, H.N. Ringham, and J.R. Simon. 2005. A proteomic survey of rat cerebral cortical synaptosomes. *Proteomics*. 5:2177-201.

Wolfer, D.P., R. Lang, P. Cinelli, R. Madani, and P. Sonderegger. 2001. Multiple roles of neurotrypsin in tissue morphogenesis and nervous system development suggested by the mRNA expression pattern. *Mol Cell Neurosci*. 18:407-33.

Wu, Y.P., C.J. Siao, W. Lu, T.C. Sung, M.A. Frohman, P. Milev, T.H. Bugge, J.L. Degen, J.M. Levine, R.U. Margolis, and S.E. Tsirka. 2000. The tissue plasminogen activator (tPA)/plasmin extracellular proteolytic system regulates seizure-induced hippocampal mossy fiber outgrowth through a proteoglycan substrate. *J Cell Biol*. 148:1295-304.

Xi, G., Y. Hua, R.F. Keep, H.K. Duong, and J.T. Hoff. 2001. Activation of p44/42 mitogen activated protein kinases in thrombin-induced brain tolerance. *Brain Res*. 895:153-9.

Xi, G., R.F. Keep, Y. Hua, J. Xiang, and J.T. Hoff. 1999. Attenuation of thrombin-induced brain edema by cerebral thrombin preconditioning. *Stroke*. 30:1247-55.

Xu, H.L., and B. Su. 2005. Genetic evidence of a strong functional constraint of neurotrypsin during primate evolution. *Cytogenet Genome Res*. 108:303-9.

Xu, W.F., H. Andersen, T.E. Whitmore, S.R. Presnell, D.P. Yee, A. Ching, T. Gilbert, E.W. Davie, and D.C. Foster. 1998. Cloning and characterization of human protease-activated receptor 4. *Proc Natl Acad Sci U S A*. 95:6642-6.

Yamaguchi, H., M. Lorenz, S. Kempiak, C. Sarmiento, S. Coniglio, M. Symons, J. Segall, R. Eddy, H. Miki, T. Takenawa, and J. Condeelis. 2005. Molecular mechanisms of invadopodium formation: the role of the N-WASP-Arp2/3 complex pathway and cofilin. *J Cell Biol*. 168:441-52.

Yang, H., J. Henkin, K.H. Kim, and J. Greer. 1990. Selective inhibition of urokinase by substituted phenylguanidines: quantitative structure-activity relationship analyses. *J Med Chem*. 33:2956-61.

Yao, X., A. Freas, J. Ramirez, P.A. Demirev, and C. Fenselau. 2001. Proteolytic 18O labeling for comparative proteomics: model studies with two serotypes of adenovirus. *Anal Chem*. 73:2836-42.

Yates, J.R., 3rd, A. Gilchrist, K.E. Howell, and J.J. Bergeron. 2005. Proteomics of organelles and large cellular structures. *Nat Rev Mol Cell Biol*. 6:702-14.

Yepes, M., M. Sandkvist, T.A. Coleman, E. Moore, J.Y. Wu, D. Mitola, T.H. Bugge, and D.A. Lawrence. 2002. Regulation of seizure spreading by neuroserpin and tissue-type plasminogen activator is plasminogen-independent. *J Clin Invest*. 109:1571-8.

Yepes, M., M. Sandkvist, M.K. Wong, T.A. Coleman, E. Smith, S.L. Cohan, and D.A. Lawrence. 2000. Neuroserpin reduces cerebral infarct volume and protects neurons from ischemia-induced apoptosis. *Blood*. 96:569-76.

Yoshida, S., M. Taniguchi, A. Hirata, and S. Shiosaka. 1998. Sequence analysis and expression of human neuropsin cDNA and gene. *Gene*. 213:9-16.

Yuan, X., and D.M. Desiderio. 2005. Proteomics analysis of human cerebrospinal fluid. *J Chromatogr B Analyt Technol Biomed Life Sci*. 815:179-89.

Zeeberg, B.R., W. Feng, G. Wang, M.D. Wang, A.T. Fojo, M. Sunshine, S. Narasimhan, D.W. Kane, W.C. Reinhold, S. Lababidi, K.J. Bussey, J. Riss, J.C. Barrett, and J.N. Weinstein. 2003. GoMiner: a resource for biological interpretation of genomic and proteomic data. *Genome Biol*. 4:R28.

Zeslawska, E., A. Schweinitz, A. Karcher, P. Sondermann, S. Sperl, J. Sturzebecher, and U. Jacob. 2000. Crystals of the urokinase type plasminogen activator variant beta(c)-uPAin complex with small molecule inhibitors open the way towards structure-based drug design. *J Mol Biol*. 301:465-75.

Zhang, H., X.J. Li, D.B. Martin, and R. Aebersold. 2003. Identification and quantification of N-linked glycoproteins using hydrazide chemistry, stable isotope labeling and mass spectrometry. *Nat Biotechnol*. 21:660-6.

Zhang, J., D.R. Goodlett, E.R. Peskind, J.F. Quinn, Y. Zhou, Q. Wang, C. Pan, E. Yi, J. Eng, R.H. Aebersold, and T.J. Montine. 2005a. Quantitative proteomic analysis of age-related changes in human cerebrospinal fluid. *Neurobiol Aging*. 26:207-27.

Acknowledgments

First of all I want to thank Prof. Peter Sonderegger for providing me with the opportunity to accomplish the doctoral thesis in his group, for his constant support and advice during my thesis.

I particularly thank Bertrand Gerrits, Frank Potthast and Bernd Roschitzki from the Functional Genomics Center Zurich (FGCZ) for their great collaboration and technical support for the ICAT project.

Next I want to thank Prof. Ruedi Aebersold for the collaboration during this project. Without his work we would never have managed to conduct this work.

I also thank Ralph Schlappbach, the Managing Director of the FGCZ, for giving me the opportunity to perform many experiments with the stat-of-the-art instruments at the FGCZ.

I thank Sabine Schrimpf and Beat Kunz for the introduction into the lab and for their help during the beginning of my thesis and I also thank Dorothea Rutishauser for the introduction into the art of mass spectrometry.

Thanks go to Mike Scott and Peter Gehrig from the FGCZ for their valuable advices regarding the 2DE and MALDI-TOF analysis.

Thanks also go to Jean-Claude Tomassina and Stephan Klauser for the technical and computer support.

I would like to thank all members of Peter Sonderegger's lab for their constructive discussion, assistance and advice, especially Alexander Ludwig, Martin Steuble, Jens Wölfel and Alexander Stephan who became great friends inside and outside of the lab.

And last but not least, I am grateful to my better half Anna Ludi, my family and my friends who shared with me the moments of victory and fall during the whole time of my doctoral study.

Curriculum vitae

Pascal Walther, geboren in Bern, Schweiz, am 28. Oktober 1975

1982 - 1991	Primar- und Sekundarschule in Spiegel b. Bern, Schweiz
1991 - 1995	Wirtschaftsgymnasium Lerbermatt in Köniz, Schweiz
1995 - 1998	Studium der Biologie, Spezialisierung auf medizinische Mikrobiologie, Naturwissenschaftliche Fakultät der Universität Bern, Schweiz
1998 - 1999	Masterarbeit unter der Leitung von Prof. R. Friis am Departement Klinische Forschung an der Universität Bern. Titel der Arbeit: "*Expression eines mutmasslichen Sieben-Transmembranen-Rezeptors aus der Familie der Frizzled Rezeptoren*".
Dezember 1999	Abschluss als Diplom-Biologe
2000 - 2002	Sales und Marketing Manager bei Frimorfo AG
2002 - 2007	Doktorand am Biochemischen Institut der Universität Zürich unter der Leitung von Prof. Peter Sonderegger. Dissertation mit dem Titel: "*Identifikation von Neurotrypsin abhängigen Veränderungen im Proteom der Synapsen und im Hippocampus*".